Real-time power system impedance estimation for DG applications

Using PV-inverter based harmonic injection method

Prepared by:

Aleksa Knezevic

KNZALE001

Department of Electrical Engineering
University of Cape Town

Prepared for:

Dr. David Oyedokun

Department of Electrical Engineering
University of Cape Town

March 2017

Submitted to the Department of Electrical Engineering at the University of Cape Town in partial fulfilment of the academic requirements for a Master of Science degree in Electrical Engineering.

Declaration

1. **I know that plagiarism is wrong. Plagiarism is to use another's work and pretend that it is one's own.**
2. **I have used the IEEE convention for citation and referencing. Each contribution to, and quotation in, this final year project report from the work(s) of other people, has been attributed and has been cited and referenced.**
3. **This final year project report is my own work.**
4. **I have not allowed, and will not allow, anyone to copy my work with the intention of passing it off as their own work or part thereof**

Name: Aleksa Knezevic

Signature: Signed by candidate **Date:** 13 March 2017

Acknowledgements

First and foremost, I would like to acknowledge the continued support and guidance of my supervisor, Dr David Oyedokun. I thank you for giving me the opportunity to work with you on such a novel, challenging project. You provided me with enough independence to enjoy my work, whilst also ensuring that there was structure to it all. Your faith in my abilities has motivated me greatly.

I would like to acknowledge Mr Stanley Adams, Senior Engineer at MLT, for his technical assistance that made testing possible at a high level of efficiency. Thank you for the time you spent with me and the many things I learned from working with you.

Dr Bernard Bekker, CEO of MLT Inverters, I thank you for accommodating me at MLT and helping facilitate my research. Furthermore, I would like to thank the staff of MLT Inverters in general for their cooperation and friendliness. I enjoyed working with you.

Mr Chris Wozniak, your assistance in the Machines Lab with equipment and facilitation of my testing was invaluable. I thank you for this. The Machines Lab staff also deserves recognition for their efficiency and helpfulness throughout.

I would also like to thank professors Michel Malengret and Trevor Gaunt for trusting me enough to involve me in the overarching project that this work relates to.

Finally, the support of my family and friends was immeasurable. Your faith in me kept me going when things became truly difficult.

Abstract

On-line power system (PS) Thévenin equivalent impedance (TEI) estimation involves the reduction of the PS's complex circuit into a simple form that provides valuable insight into its state and behaviour. It finds application in numerous areas such as voltage stability monitoring and islanding detection. In the context of distributed generation (DG), on-line TEI estimation can be easily implemented in existing hardware to add functionality and improve the operation of power converters – the key components of DG systems.

Two distinct methods of on-line PS TEI estimation exist. The passive method involves only measurement of voltage and current, whereas the active method involves injection of current into the PS and measurement of the response. This work is focused on the active method.

Through a review of the available literature, limitations of past work are highlighted. It is shown that the nature of current injection varies greatly in different works and that evaluation of implementation performance is generally not thorough. Little consideration has been made of the effect of injection current level and frequency on the performance of on-line TEI estimation. Furthermore, the behaviour of the grid and its impact has not been thoroughly investigated.

In this work, the active method is implemented in a three-phase PV-inverter and thoroughly tested in terms of its TEI estimation accuracy. Dependence of said accuracy on parameters such as the level of injected current and its frequency is shown to be high through tests performed on the live PS at two locations. These parameters are optimised such that TEI accuracy is maximised and the performance of the device is shown to be good compared to calibration equipment. The accuracy of PS TEI tracking is evaluated and quantified. Considerations are also made of the device's hardware limitations and their effect. A process by which a device's TEI estimation accuracy can be thoroughly evaluated is developed through this work.

The behaviour of the PS's TEI is also investigated over long periods and characterised. It is found that the TEI remains steady around an average level in both test locations, with a low standard deviation. Consistency in results is found to be high between the two tests.

Table of contents

List of abbreviations

Abbreviations:

A/D	Analog to digital conversion
AC	Alternating current
AGC	Automatic governor control
AM	Amplitude modulation
ASF	Active shunt filter
CB	Circuit breaker
CFL	Compact fluorescent lamp
COM	Component object model
CWT	Continuous wavelet transform
DC	Direct current
DFT	Discrete Fourier transform
DG	Distributed generation
DKE	Deutsche Kommission Elektrotechnik
DQ	Direct-quadrature
EHV	Extra high voltage
FFT	Fast Fourier transform
HV	High voltage
IB	Inductor bank
IEC	International Electrotechnical Commission
IEEE	Institute for Electric and Electronics Engineers
LF	Low frequency
LSB	Lower sideband
LV	Low voltage
MM	Multimeter
MV	Medium voltage
NLL	Non-linear load
PC	Personal computer
PCC	Point of common connection
PI	Proportional-integral
PLL	Phase locked loop
PMU	Phasor measurement unit
PS	Power system
PV	Photovoltaic
RB	Resistor bank
RLS	Recursive least squares
RMS	Root-mean-square
SCC	Short-circuit current
SCL	Series compensated line
SG	Signal generator
SNR	Signal-to-noise ratio
STATCOM	Static synchronous compensator

TE	Thévenin equivalent
TEI	Thévenin equivalent impedance
THD	Total harmonic distortion
UCT	University of Cape Town
UHV	Ultra high voltage
UK	United Kingdom
US	United States (of America)
USB	Universal serial bus/Upper sideband
VSI	Voltage stability indicator

Important variables/parameters:

$\mathbf{Z_{th\,R}}$, $\mathbf{R_{th\,R}}$, $\mathbf{X_{th\,R}}$	Thévenin equivalent impedance, resistance and reactance of power system **red** phase
$\mathbf{Z_{th\,Y}}$, $\mathbf{R_{th\,Y}}$, $\mathbf{X_{th\,Y}}$	Thévenin equivalent impedance, resistance and reactance of power system **yellow** phase
$\mathbf{Z_{th\,B}}$, $\mathbf{R_{th\,B}}$, $\mathbf{X_{th\,B}}$	Thévenin equivalent impedance, resistance and reactance of power system **blue** phase
$\mathbf{\lvert I_{inj} \rvert}$	RMS injection current magnitude setpoint for inverter
$\mathbf{f_m}$	Modulation frequency setpoint for inverter

List of figures

List of Illustrations

List of Tables

1. Introduction

1.1 Overview

The largest and (arguably) most complex circuit in the world is the power system (PS). Understanding its state and behaviour is a crucial yet typically difficult task, requiring complex analysis using sophisticated software and a large quantity of design/measurement information.

Thévenin's theorem states that any complex circuit made up of linear elements can be simplified into a simple equivalent circuit characterised by two parameters – a series voltage source and impedance [1]. Once simplified, analysis of the complex circuit can be done more easily. This theorem can be applied to the PS itself [2-7], providing insight into its state and behaviour from a particular point of the network. In the case of the PS, the Thévenin equivalent impedance (TEI) is the parameter of interest (rather than voltage). Due to the dynamic nature of the PS, the TEI is most useful when obtained in real-time through on-line estimation[1].

On-line determination of the TEI of the PS has many applications, including but not limited to, real-time voltage stability monitoring[6, 8-17], fault location[18, 19] and anti-islanding detection[20-23]. With the advent of DG and increasing demand on the PS, the aforementioned applications are becoming increasingly important. As a result, on-line TEI estimation shows promise in addressing some of the major issues related to DG and its effects on the transmission system. This is especially due to the fact that on-line TEI estimation can be easily implemented in existing hardware typically present in all DG systems[2, 23-28].

The two distinct methods for on-line TEI estimation are the active and passive methods [2, 27]. Each has seen a significant degree of study and provides different advantages and disadvantages. In this thesis, a literature review of both methods is done, looking at the most prominent past results and commenting on limitations and potential for further research. This thesis focuses on the active method, which has commonly been implemented using power converter hardware and involves injection of current into the PS. A multitude of injection schemes are used by authors to achieve TEI estimation using this method [2, 20, 27, 29-33] and little justification is provided regarding the nature of the current injection and its potential effects. Furthermore, there is a lack of understanding of the typical behaviour of the TEI parameter in general.

The effect of variation of two principal injection parameters - frequency and magnitude of injection current – on the effectiveness of TEI estimation using a PV inverter is presented in this dissertation. This is done through testing of a practical PV-inverter based implementation of a steady-state active method utilising dual harmonic injection. The evaluation of effectiveness is intended to be very thorough, with the aim of ensuring that accuracy and practical viability of TEI estimation is maximised with this device. As a result, a structured practical approach to evaluation of the TEI estimation accuracy is developed. Hardware limitations are investigated and considered. The time variation of the TEI at separate locations is also investigated and presented in this dissertation, based on results from two test locations. This allows for some insight regarding the expected level and behaviour of this parameter at the LV distribution level.

[1] 'On-line' refers to the condition that the estimation is based from measurements taken directly from the PS whilst it is energised.

1.2 Hypothesis

It is hypothesised that TEI estimation accuracy is affected by injection current characteristics such as frequency and magnitude of injection and that said accuracy can be optimised through careful selection of these characteristics. Changes in the PS topology and loading manifest themselves in the measured TEI.

1.3 Research Questions

1. What methods are available for Thévenin equivalent impedance determination?
2. What is a typical value of the Thévenin equivalent impedance of the South African PS?
3. How does the Thévenin equivalent impedance of the PS vary over time?
4. Can variations in the Thévenin equivalent impedance be linked to specific PS behaviours?
5. How accurate is the measurement of the Thévenin equivalent impedance of the PS?
6. What effect does the magnitude of the current injected have on the obtained Thévenin equivalent impedance and its accuracy?
7. What effect does the frequency of the current injected have on the obtained Thévenin equivalent impedance and its accuracy?

Further questions that are specific to the equipment and process are:

8. How should we evaluate the equipment effectiveness?
9. What are the limitations of the equipment?
10. How do we handle such limitations?
11. How can the equipment be improved?

1.4 Aim and objectives

The aim of this work is to further the understanding of how effective TEI estimation can be practically implemented, evaluated and optimised within the context of DG.

The primary objective of this work is to provide definite answers to research questions 1, 5, 6 and 7, to the highest level of detail possible through experimental investigation. The secondary objectives are to provide answers to the remaining research questions.

1.5 Background to testing

As part of a joint project involving the University of Cape Town (UCT) and MLT inverters, prototype inverter equipment (hereafter 'the device') was designed and developed that is capable of three-phase power system (PS) Thévenin equivalent impedance (TEI) estimation. The details of exactly how this is accomplished are discussed later.

This device was set up and connected to the national PS in two separate locations. It underwent several stages of testing spanning from June 2016 to February 2017. These stages of testing and their results form the core content of this thesis.

1.6 Scope and Limitations

This work is restricted in scope to practical implementation and evaluation of TEI estimation effectiveness of a harmonic injection TEI estimation method within a PV inverter. Investigation of the dependence of estimation accuracy on the following parameters is considered: injection frequency and injection magnitude. The range of values considered is limited by the inverter equipment available.

The effect of location of injection is also considered to a limited degree. Only two separate locations are investigated due to constraints of time and facilities.

Estimation effectiveness is evaluated using two separate methods – measurement of known impedance changes and use of an oscilloscope to manually perform TEI estimation.

1.7 Report layout

- Chapter 1 is the Introduction
- Chapter 2 is the Theoretical Background required to understand the work
- Chapters 3 is the Literature Review, concerned with pertinent work relating to the subject
- Chapter 4 presents the Methodology employed in each separate phase of testing

12. Chapters 5, 6 and 7 contain the Results and discussion of stages 1, 2 and 3 respectively.
13. Chapter 6 deals with testing and results.
14. Chapters 8 contains the Conclusions and Recommendations for further work.
15. Chapter 9 is the list of references.
16. Chapter 10 is the appendix.

1.8 Novel contributions

The novel contributions arising from this work are:

- TEI measurement accuracy is shown to be dependent on the magnitude and frequency of injection current in the context of the PV-inverter based active TEI estimation method. The dependence is presented for the full range of current magnitude and frequency that the available equipment can reliably provide.
- PS TEI parameters are measured over long periods of several hours at separate locations and compared.
- A method by which PS TEI measurement accuracy of a practical device is thoroughly evaluated over a specific impedance range is developed.
- Current output limitations of the specific PV-inverter device used are investigated.

2. Theoretical background

2.1 The Power System

2.1.1 Introduction

A basic understanding of the power system (PS) is crucial to this thesis. The concepts, layout and equipment involved are discussed here in brief.

i. Coupled generation and distribution

The electric PS is large, dynamic and complex. It is a system made up of many interconnected components. Understanding its operation and behaviour beyond the basics is not an easy task. The first concept that one should grasp is that the PS connects generation and loads together. At any given time, the power being generated by steam pressure, or by falling water, or other means, is simultaneously being utilised to do things like illuminate households, extract aluminium and run electronic equipment. Some portion of it does not do useful work, but is lost to the environment in the heating of cables or the 'hum' of a transformer.

ii. Automobile metaphor

We can use an automobile as a metaphor to better understand the PS. An automobile engine's power must be used by the wheels as its generated – with some being lost as heat and sound. An automobile's wheels are not directly connected to the engine. The transmission allows the engine to operate at its ideal range of speed despite the variation in speed of the wheels. Like an automobile, the PS has an engine ('generation' unit) a transmission ('transmission' unit) and wheels ('load' unit).

As within an automobile, whose engine requires fuel, the PS generators (e.g. coal, raised water etc.) exercise a mechanism to convert the fuel's energy into the required form (e.g. a turbine connected to a generator). The automobile's transmission is made up of a gearbox (transformers) which changes the speed (voltage) of the engine before it reaches the driveshaft (transmission lines). The driveshaft, in turn, delivers power to the wheels (loads). In this case, our automobile is four-wheel drive and there are differentials and a transfer case (distribution level) that ensure the different wheels (loads) receive power at the right speed (voltage). The automobile's alternator and battery, coupled to the driveshaft, can be conceived of as a PS load at a high voltage level; in this case with energy storage, such as the pumped-storage facility This could be a pumped-storage facility such as the one here at Palmiet, in South Africa [34]. However, if the PS was an automobile, it would be a vehicle that only operated in a certain narrow speed range (voltage). There would also be no brakes.

iii. Structure

Beyond the top-down generation, transmission and distribution levels, there are a lot of links and connections in the network at each stage. These levels are becoming less distinct than they were in the past (discussed in subsection 2.1.4). Another approach to classifying the system is by voltage level, which ranges from low voltage (LV, <1000 V) to ultra-high voltage (UHV, >230 000V, up to 765 kV in South Africa) [35, 36].

Loads are not limited to the distribution level, as there are intermediate loads – large consumers such as factories or mines are more suited to receiving power at a higher voltage level and hence can be connected at this level at their own substations.

2.1.2 Typical Power System

A typical PS is made up of a number of interconnected components, such as:

- Generators
- Transmission lines
- Protection equipment
- Capacitors and reactors
- Power electronics
- Loads

The manner in which these devices are interconnected is dependent on the topology of the PS. It is difficult to categorise the topology of a real PS. It is best described as being a mixture of a number of different categories of topology, resulting in a 'partial mesh'. This description is intentionally vague, as there is great variability in the topologies of real power PSs. This is because the PS is an evolving system. As time passes, more equipment is installed and new nodes and branches added to the topology. Its evolution is driven by a number of interrelated factors including [37]:

- Size and location of demand
- Forecasted growth of demand
- Availability and location of primary energy supply
- Geography between supply and demand
- Quality of supply
- Regulations
- Available funding

As an example of the layout of a typical PS, a 30-bus IEEE test network is shown in Figure 1. It is representative of the PS within the Midwestern USA in 1961. It gives a view of what the MV/HV (medium voltage/high voltage) level topology of a PS may look like. Large equipment such as motors, generators and transformers are indicated on the diagram.

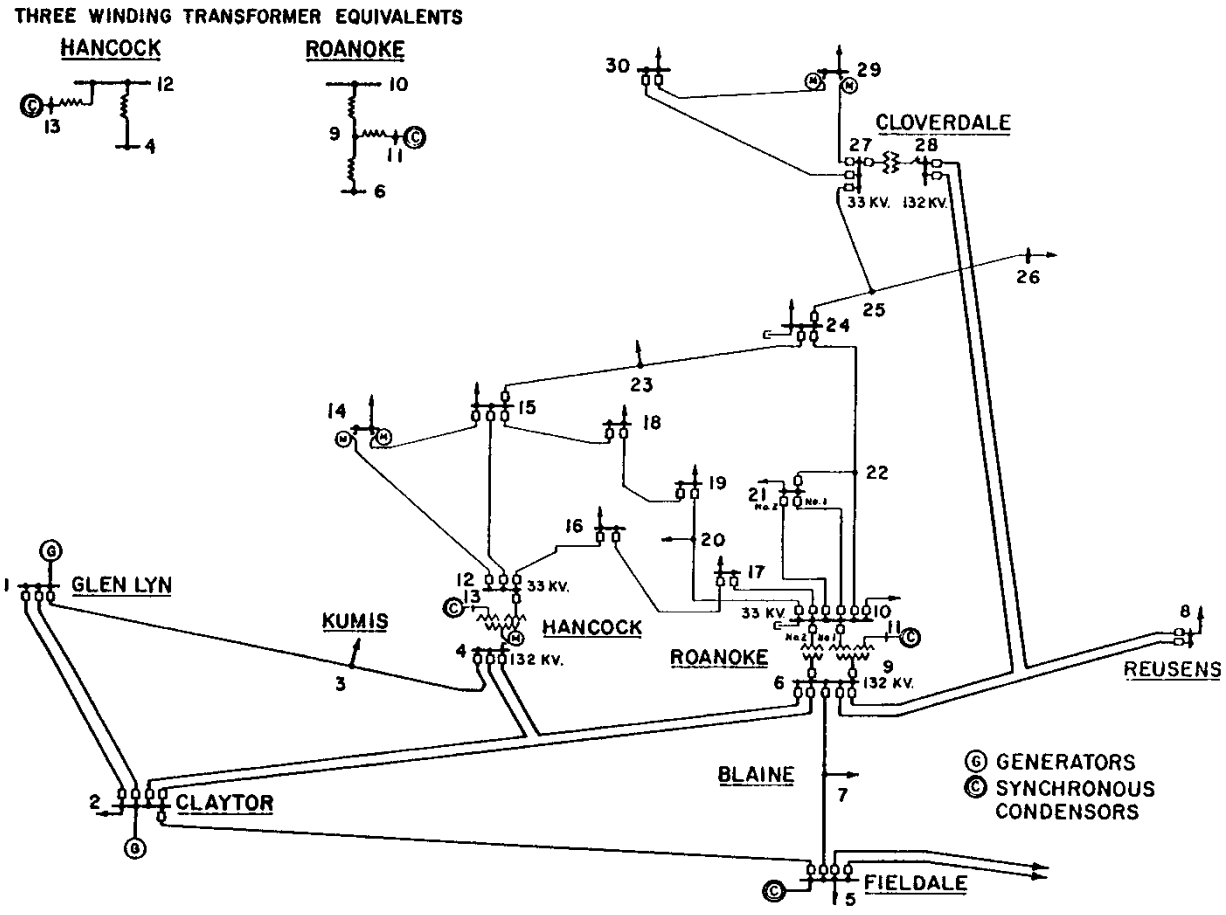

Figure 1: IEEE 30 Bus Test Case

The typical PS is a three-phase system, meaning that power is transmitted over three separate conductors. Each carries a sine wave voltage that is designed to be 120° out of phase of the other two. In this way, the sum of currents resulting from this type of connection tends to zero, and the neutral conductor which completes the circuit can be made relatively smaller and more economical. In South Africa, the convention is that the phases are labelled in order of rotation: Red, Yellow and Blue phases (R, Y, B). This convention is upheld throughout this thesis.

2.1.3 Behaviour

The PS is large, non-linear and dynamic [38]. During the PS's operation there will be periodic variations in certain parameters such as the voltage of the lines and its frequency. Whilst these

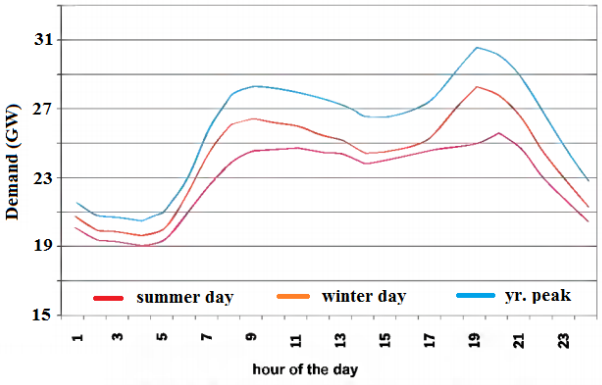

Figure 2: Typical daily load profile – South Africa, 2001 [39]

Figure 3: Variation in frequency of the UK PS over an hour (30/08/16 – 11:07, from [40])

typically remain within certain limits (e.g. f: 50 Hz ±1%, V: 230V ±5%) there are also cases of infrequent, more extreme behaviour such as when a fault occurs on one of the lines. Loading of the system is also variable.

Loading on the PS varies on a daily, monthly and yearly basis. This is one of the causes of the variation in parameters such as voltage and frequency. Typical daily load variation, known as a load profile, is shown in Figure 2. The loading at each part of the network is different. The load profile is an aggregate of the demand on the entire national PS in South Africa in 2001 for a typical weekday.

The PS's frequency will also vary continuously as generation attempts to match loading. The system is designed to operate close to its nominal frequency (50 Hz in South Africa and UK) and hence the frequency deviation is kept to a maximum of about 1.25 Hz [41]. A sample of the typical variation of frequency over an hour in the UK PS is shown in Figure 3.

The voltage also varies during the day, with PS design done according to a 10% voltage deviation limit [41] at the residential level. Of course, these are rare events in which the voltage or frequency exceeds these limits. Harmonic content – the level and quantity of harmonic frequencies in the grid voltage – will also vary over time in an unpredictable way. The voltage and phase differences between lines may also vary over time, although normally by only a small amount. Asymmetrical loading on the three lines is usually the cause of this.

Infrequent behaviour includes but is not limited to faults, voltage flicker, voltage unbalances, transient overvoltages and increased harmonics. Such events are not described in any more detail in this thesis, due to their diversity, complexity and rarity of occurrence.

2.1.4 The changing nature of the power system

When we talk about the future of the PS, two issues are of most concern. The first is the world's rising demand for electrical energy [42]. PS's are already operating under heavily loaded conditions [43]. As the world's population increases and technology improves, more and more people are gaining access to electricity. At the same time, it is expected that demand previously provided for by unclean, inefficient energy sources will naturally be shifted onto the PS [44] in an attempt to improve efficiency and reduce environmental impact. There is no better example for this than electric vehicles, which are nearing widespread deployment. Considering the massive energy needs of the transport sector alone (almost 30% of total energy consumption in the USA [45]), this is expected to place significant added strain on the PS. Furthermore, limited investment into the transmission system over many years leaves ageing infrastructure operating much closer to its limits than designed [11, 46-48]. Thus, delivering to the power needs of the future under the current paradigm will not only be a challenge in terms of creating additional generating capacity, it will also require upgrading of the transmission system. For this to be accommodated, significant investment is required.

The second issue is Distributed generation (DG), which is quickly nearing proliferation [25, 49, 50]. DG refers to generation capacity connected at the distribution level of the PS. This capacity would typically be from a renewable energy resource, such as solar photovoltaic (PV) or wind. The device that converts and injects power from these sources into the grid is known as a power converter. A worldwide trend toward deregulation of the electricity sector, the need for more generation capacity, environmental concerns and the falling cost of solar PV power, are some of the driving forces behind the growth of DG [44]. This is seen as a natural evolution in the nature of the PS, driven by changing needs. As a result, the number of power converter devices connected to the PS, injecting power from

solar and wind sources, is rapidly increasing [23, 50-52]. Whilst this added generation capacity provides clean energy and potentially reduces losses, it is also very disruptive[44]. One of the core assumptions in the PS's design - that the primary substation is the sole source of power and short-circuit capacity – is no longer valid [53]. Hence DG is set to cause a paradigm shift.

The integration of DG into the PS poses a major engineering challenge. Despite strong public support for DG, its integration must be thoroughly planned to avoid serious risks. If care is not taken, many common concerns such as power quality and overloading of equipment are expected to become more prevalent [44]. Furthermore, issues such as islanding detection [53] arise and protection systems are likely to become less effective. In countries with high DG penetration such as Denmark, Germany and Spain, this has already caused operational problems for the PS [54]. Overloading of feeders and transformers, increased risk of overvoltages, higher levels of power quality disturbances and incorrect operation of protection are all potential consequences. It becomes obvious that any research in power engineering that decreases the likelihood or severity of these consequences is of value.

Moving away from a system of centralised, unidirectional power flow, the need for effective monitoring and control at the distribution level also increases [24]. With DG, ownership and operation of generation systems become dispersed. The flow of power in the distribution and transmission systems is altered and it becomes very difficult to predict how the PS will behave, and intervene where necessary. If such DG systems are to be operated and controlled locally, knowledge of the network state and the potential impact of actions like injecting more reactive power or disconnecting from the grid, become invaluable. Co-ordination between these systems is also expected on some level and sharing of information would allow for better decision making.

2.2 Thévenin's theorem

2.2.1 Introduction

Thévenin's theorem (also known as the Thévenin equivalent theorem) is a useful means of reducing complex circuits into simpler forms. It finds application in numerous areas and is especially useful to electrical engineers. The theorem states that, given any circuit made up of linear passive and/or active elements, any two terminals of that network may be replaced by a voltage source and series impedance that is the equivalent of the rest of the network[1]. This circuit is called the Thévenin equivalent (TE) circuit. This way, we can reduce a complex network into a simple voltage and impedance combination for analysis.

2.2.2 The circuit and its parameters

The TE circuit is simply made up of a voltage source V_{th} and series impedance $Z_{th.}$ V_{th} and Z_{th}. These are hereafter referred to as the TE voltage and impedance parameters, respectively. The TE circuit is shown in Figure 4.

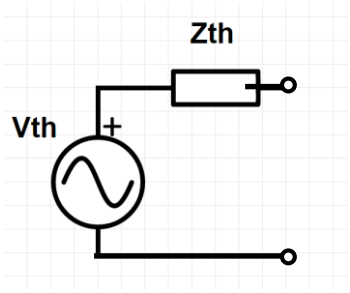

Figure 4: Thévenin equivalent circuit*

2.2.3 Example of complex circuit simplification

An example is presented below for better understanding of the theorem that is of such critical importance in this work:

Given the network shown in Figure 5, we can take any two terminals of the network and 'look' into them, find their TE parameters (voltage and impedance) and form the TE circuit. We choose terminals A and B:

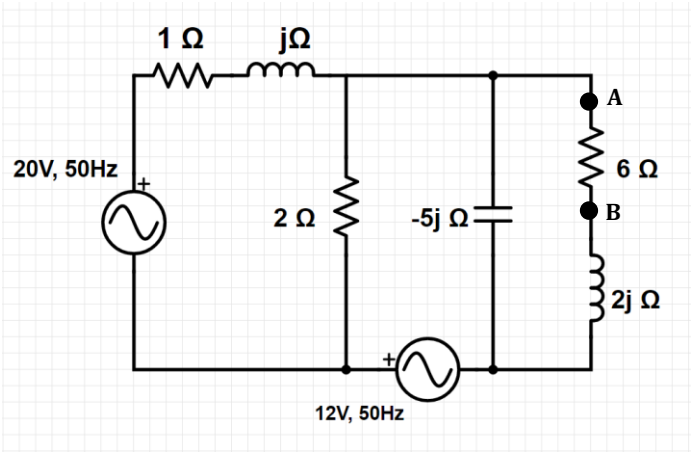

Figure 5: AC Network example – complex circuit*

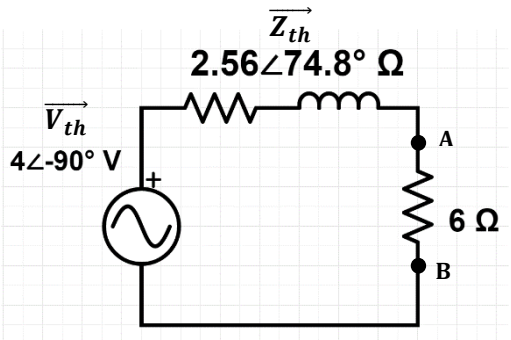

Figure 6: AC Network example – Thévenin equivalent circuit*

*Circuits drawn using tool from http://www.digikey.com/schemeit/

The Thévenin equivalent impedance is given by the impedance between the terminals when all voltage sources are short circuited and current sources open circuited. The Thévenin equivalent voltage is given by the voltage across the terminals when the terminals are open-circuited. The calculations involved are shown in brief below:

Using KVL in leftmost loop of Figure 5, with AB open circuited:

$$V_{th} = V_{ab} = 20V - I(1+j)\Omega + 12, \qquad I = \frac{20V}{(3+j)\Omega}$$

$$=> V_{th} = (4\angle -90°)\text{V}$$

Shorting the voltage sources and taking impedance between A and B:

$$Z_{th} = 2j + (-5j) \,||\, 2 \,||(1+j)$$

$$=> Z_{th} = (2.56\angle 74.8°)\Omega$$

In the case where we do not have a schematic of the circuit we can resort to short-circuiting terminals A and B and measuring the current that results. In this way, we can obtain Z_{th} from:

$$Z_{th} = \frac{V_{th}}{I_{SC}} = R_{th} + jX_{th} \qquad (2.1)$$

From the point of view of the 6 Ω load between terminals A and B, the circuits in Figure 5 and Figure 6 are absolutely identical. That is to say exactly the same voltage and current would be provided by both circuits, regardless of the load placed between A and B. This theorem can be applied to both AC and DC circuits.

2.2.4 The power system as the complex circuit

Consider attempting to find the TEI of the PS. Take the case where we want to find the PS's parameters from the Reusens bus in Figure 1. If the schematic provides all of the parameters of each component in the system, such as line impedances, we can easily obtain the parameters analytically or through simulation. It is beneficial to have a detailed schematic of the PS around the point of interest but simply relying on the schematic limits the potential of the approach. We cannot do real – time monitoring of the TEI and we must rely totally on the accuracy of the schematic. In many cases, especially at the LV level, we do not know the state of the surrounding network and no schematic can give an accurate value of the PS impedance.

Another point to keep in mind is that the PS is dynamic. Its nature is constantly changing depending on loading and other factors such as daily voltage fluctuation. Hence, we cannot expect one set of TE parameters to remain valid over the entire operating range of the PS, or over long periods of time [11]. Hence, the need for on-line real-time TEI estimation arises. At the LV level, it is expected that load variations will have a significant effect on the estimated TEI because singular changes in loading have a large effect. At the higher voltage levels, load changes should have less of an effect due to the law of large numbers. The typical daily voltage, frequency and harmonic content variations are not expected to affect the TEI of the PS.

If we do not wish to depend on an accurate schematic, applying Thévenin's theorem to the PS becomes more difficult. We must be mindful of a number of issues that prevent the theory from being applied directly. At the LV level of the PS, where DG will be most prevalent, we cannot rely on a schematic. Although V_{th} is easily obtained by measuring voltage across the open circuit, it would be quite unwise to short-circuit the terminals (as the theory requires) for us to obtain Z_{th}. A different approach must be taken for determining the PS's impedance in a reasonable way.

Finally, the PS is unlike the circuit used in Figure 5 as it contains non-linear loads in the form of power electronic components and compact fluorescent lamps. Thus, linearizing it must be done carefully and may not be useful in certain situations. The PS's overall impedance characteristics are expected to be mostly linear, as it is dominated by passive elements. Most of the equipment listed in subsection 2.1.2, such as transformers, have an equivalent circuit made up of passive elements. If the case arises where non-linear circuit elements are dominan, linearity may only be a good approximation at the small-signal level.

The layout, equipment and loading of the PS determine the Thévenin equivalent impedance seen at a given point. Consider taking and attempting to determine the TEI from that point. Understanding the effects of transformers, power electronics and loads and their placement on the Thévenin equivalent circuit's parameters would be of much use. However, this would require simulation and analytical work that is beyond the scope of this thesis. Hence, it is enough that we have only a basic understanding that these factors have influence on our results.

2.3 Motivation for and applications of on-line power system Thévenin equivalent impedance parameters determination

2.3.1 Introduction

PS TEI estimation is becoming an increasingly valuable tool which shows promise of easy implementation in existing equipment. Its numerous applications are discussed here along with some examples of successful results in each application.

2.3.2 Motivation in context of distributed generation (DG)

With the increasing prevalence of DG, concerns related to voltage stability, protection system operation, islanding detection and the lack of centralised control over the PS are present. TEI estimation can be implemented easily within DG hardware (discussed later) and used to address some of these issues. Along with this, better monitoring and control over the state of the grid can be obtained and the potential for wide area measurement exists.

2.3.3 Voltage stability monitoring

Voltage instability is a serious concern for electric power utilities, leading to major blackouts [55] and/or damage of equipment if not identified in a timely manner and dealt with [6]. This concern has grown with the ever-increasing loading of the PS [43]. An attractive method to monitoring of the stability of PS voltage is through measurement of the TEI of the PS, due to its simplicity and feasibility [38].

i. TEI as an indicator of stability

The point of voltage instability is linked to be the point of maximal power transfer to the load[6]. Maximal power transfer occurs when the PS TEI is equal to the load impedance (proven true for constant power loads [8, 9]). The TE approach, supported with other stability information such as generator reactive power limits, has been developed to work with more complex load models in [10]. In [10], a voltage stability indicator (VSI) is developed which is essentially load impedance divided by PS TEI. Hence, voltage instability occurs when this indicator falls to 1.0 p.u.

Most voltage stability analysis methods treat the problem as a static phenomenon, relying on load-flow solutions using the Jacobian method or continuation power flow method and PV curves [43]. If on-line TEI estimation is done through a wide area measurement system then a more robust, dynamic system is possible.

ii. Past results

In [11], the author presents the full theory behind use of the TEI as a voltage stability indicator and develops a method based on measuring the voltage magnitude, active and reactive components of load power at a bus. Load flow simulations are used to support the validity of the theory used. The method used is simple enough for on-line application.

In [10], a simulation is performed on the IEEE 39 bus system in which phasor information at load and generator buses, together with generator reactive power limits, is used to determine the voltage stability margin using TEI parameters and thereby accurately predict voltage collapse. A plot of the VSI

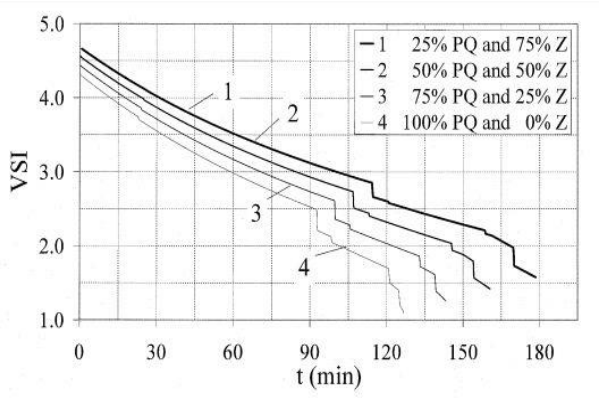

Figure 7: VSI variation with increasing load in [10]

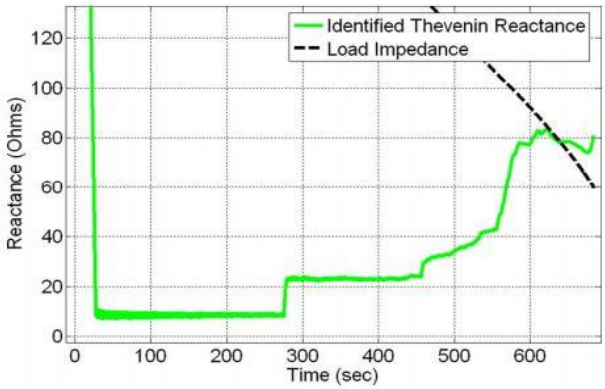

Figure 8: Simulation of RLS TE algorithm on Italian PS in [6]

is shown in Figure 7. This paper considers only one case, with the assumption of linearly increasing loading for all loads. The author concludes that the TEI approach is not a replacement of existing voltage stability monitoring tools such as those based on reactive power availability. The author suggests this tool should be "added on top of the existing control schemes to give them an extra quality" [10]

In [6], a recursive least squares (RLS) algorithm is used to obtain the TE parameters from phasor measurements, specifically at the EHV (Extra high voltage) level of the PS. The algorithm is simulated on a detailed model of the Italian PS and is shown to react predictably to the operation of over-excitation limiters and satisfactorily detect impending voltage instability "in terms of reliability, robustness and speed". The calculated TE reactance of the PS from simulation is shown in Figure 8. The point of instability occurs at the crossing of the two graphs (when the impedances match). The use of the reactance rather than the impedance is due to the application being at the HV level. This means that resistance is negligible and $Z_{th} \approx jX_{th}$. One of the concerns related to this application of TE parameter determination is the uncertainty and sensitivity in the measurement of the PS's parameters[6].

Numerous other authors have also produced results on TEI estimation in this application [12-14, 16, 17, 56].

2.3.4 Fault location

Accurate and fast fault location has always been a goal for PS engineers as it reduces maintenance and power restoration times [18, 48] on long transmission lines, thereby improving PS availability and reliability.

i. Past results

In [18], a fault location algorithm for series compensated lines (SCLs) – typically the longest lines and most difficult for fault location – is developed based on on-line TEI estimation. It utilises a passive TEI estimation method (discussed later in subsection 2.4) using existing hardware. The system is adaptive and does not rely on any data provided by the utility – direct measurements are used. According to

the author, this is the approach's main advantage over others, making it effective regardless of the deterioration of the line impedance. This deterioration is attributed to factors such as conductor sag and temperature. Thorough simulations on a 400 kV SCL is done. Variation in fault type, fault location, fault resistance, fault inception angle, pre-fault loading and compensation degree are simulated and the effects on performance of the method are investigated. The accuracy of fault location is found to be less than 1% in almost all cases and it is shown that other methods drop to low accuracies where the line parameters provided by the utility are significantly off.

Similar work is presented in [19], where single, parallel and teed lines are considered. Similar results are observed regarding the accuracy of the TEI method and its independence from fault characteristics.

2.3.5 Islanding detection

i. Introduction

Islanding, in the context of DG, is the problem of the continued operation of a power injecting device such as an inverter after the connection to the PS has been lost [26]. Islanding can be both unintentional (e.g. caused by a fault) and intentional (e.g. during maintenance services) [20].

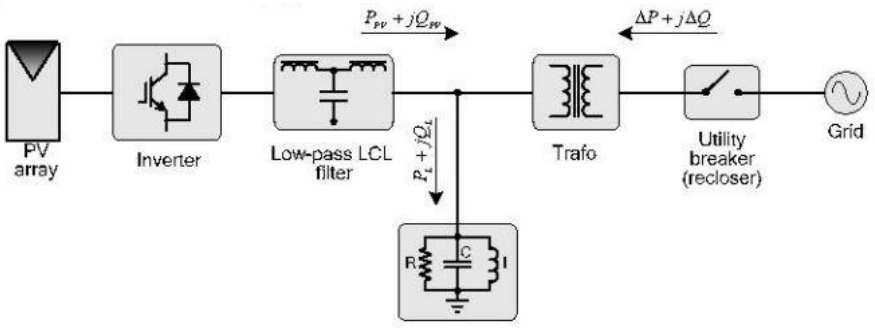

Figure 9: Islanding phenomenon (taken from [2])

Islanding can cause damage to equipment and pose risks for utility workers who are attempting to work on a line believed to be de-energised [20, 26, 28]. When a DG is islanded the topology of the system it is connected to changes, and hence, the TEI of the PS as seen from the DG also changes significantly [20, 22]. Hence, islanding detection is possible through on-line TEI estimation and analysis of the behaviour of the TEI parameters.

Although continued provision of power during islanding theoretically increases power availability, safe and controlled operation of ad-hoc islands has yet to become a reality beyond the local facility level [53].

ii. Standards and requirements

There are a number of anti-islanding requirements concerning the detection of a PS impedance increase in a certain minimum time. The three most relevant bodies developing international standards are the IEEE in USA, IEC in Switzerland and DKE in Germany. EN503 301-1 is a European standard which states that inverters must be able to detect a 0.5Ω change in PS impedance and cease operation within 5 seconds[27, 29]. This kind of requirement makes it clear that real-time, accurate determination of the TEI of the PS is of importance in the context of inverters used in DG applications [3].

Other standards include the VDE 0126-1-1 and IEEE1574 (2 seconds, impedance not specified). The need for harmonisation of such standards on a worldwide scale is considered urgent [57]. Such standards are very important in general, as they affect the PV inverter markets and thereby also further development of inverter technology.

iii. Past results

In [20], a passive method using existing harmonics in the PS to estimate its TEI is employed for islanding detection. The author discusses limitations in existing schemes, such as the existence of a non-detection zone in which these schemes fail, usually due to the presence of a local load whose resonance matches the PS frequency. Simulation results show the scheme has potential to reduce the non-detection zone.

In [22] a similar passive method is used, with robust performance according to simulations. Practical testing shows effective islanding detection is achieved within 0.25 s of islanding, even in the case where other methods such as over/under voltage and over/under frequency monitoring are not able to detect islanding. A discussion in greater detail is provided in subsection 3.1.1iv.

In [23], the author presents a failure mechanism for the popular, existing islanding detection approaches in the case of multi-DG systems and proposes a new TEI estimation-based method that does not share this mechanism.

2.3.6 Adaptive tuning of converter current controller

i. Introduction

Equipment such as PV inverters and power quality compensators (e.g. STATCOMs) base their performance on effective current control. Achieving effective current control can be challenging, especially in the case of an inverter with a LCL filter at its output. For effective current control the PS's impedance must be known and taken into consideration [2, 3, 25, 49]. In designing a power converter, manufacturers must make compromises between producing a device with high control dynamics, or a device that is stable for many PS impedance conditions [58].

In the case of a 'weak network' with a high PS impedance, the current controller may also be prone to instability [2]. Since the PS's impedance can change (e.g. due to a faulted feeder) and especially in the case of high DG penetration [2], real-time TEI measurement could allow for adaptive optimisation such as adjustment of gains or rearrangement of poles and zeroes [3, 24]. Thereby, the performance of such devices under dynamic conditions can be improved [2, 15, 59] without compromising stability.

In the German VDN medium-voltage requirements, the limits to current injection are dependent on the PS impedance as seen from the PCC [60]. This is done to limit supply voltage distortion and emphasises the importance of PS TEI estimation in the context of DG current control [58].

ii. Past results

In [7], an adaptive current controller tuning scheme is developed for voltage source power converters, using the PS's TEI to improve performance. Essentially, a PS impedance change would cause the input LCL filter's resonance frequency to change. Active damping is used to ensure robust stability, maintain good setpoint tracking and performance in the converter. The scheme is simulated on a 500 kW wind turbine and also tested practically on a smaller scale. It is shown to be effective in improving the controller's performance under varying PS impedance conditions.

In [3] a gain scheduling method is suggested for on-line adjustment of current controller parameters, based on the PS TEI.

In [25] it is proposed that the response of the LCL filter itself is used to estimate grid impedance, rather than vice versa. This concept is developed to some degree and the main issues are discussed.

2.3.7 Improvement of filter performance

i. Introduction

The issue of harmonic currents and their negative effects is well known. Harmonics are drawn by non-linear loads (NLLs) such as compact fluorescent lamps (CFL's), computers and power electronic loads [61]. This type of load is becoming increasingly common in the PS (e.g. power converters). The negative effects of these currents are numerous and significant – voltage distortion, increased losses in transformers and motors, interference with sensitive equipment and false operation of protection systems [31]. The mitigation of this and general improvement of power quality are of great interest to PS engineers [52].

Filters are often used to reduce the harmful effects of harmonics on the PS. They prevent harmonics from penetrating deeper into the PS [62] by acting as a sink. Two types of filter exist:

1. **Passive filters** are designed to work under specific conditions outside of which problems can occur, such as high voltage distortion, resonance of certain harmonics [30].
2. **Active filters** adapt to changes in system conditions and are thus more versatile. Various control schemes exist, such as derivative capacitor voltage feedback (DCVF) or lead network [63].

Both passive and active filter stability is strongly dependent on the PS impedance [31]. Hence, much like in the current controller application, knowledge of the system's TEI is a requirement for effective performance [31, 64]. This is either to inform passive filter design or to inform the adaptive tuning of active filters. Furthermore, voltage source converters contain a LCL filter at their output intended to perform harmonic damping, which can be actively tuned [63]. This filter has a high impact on the inverter's operational stability.

Another potential way of reducing the harmful effects of non-linear loads involves redistribution of loads within a network to avoid low power quality in sensitive areas [31]. In this case, knowledge of the impedance structure of the network can again be used.

ii. Past results

In [63], the authors consider a proportional capacitor voltage feed-forward scheme (an active filter control scheme) and analyse its robustness under large PS impedance variations. Considerations are made for the interaction between the active filter and the current controller, as well as their dynamics. The authors' results show that the value of the grid inductance has a significant effect on the inverter's stability through practical testing of a 3 kW, 220 V, 50 Hz inverter prototype.

In [58], a control concept is proposed that uses PS TEI measurement to tune the converter's filter, thereby allowing for compensation of harmonics and voltage unbalances. This is done for PWM converters with medium-low switching frequencies. The approach combines this feature with that of

adaptive current controller tuning. The results of PS TEI estimation (discussed in detail in subsection 0) are used for on-line active filter control.

In [52], on-line PS TEI estimation is used to improve the performance of an active shunt filter (ASF). Essentially, both knowledge of the real-time PS TEI at harmonic frequencies and the line voltage are required to calculate the reference currents that the ASF should provide to counteract the harmonics due to NLLs. Experimental results show effective cancellation of harmonics, significantly improving the power quality. When the TEI input was forcibly caused to stop updating, the ASF current control deteriorated and the system was tripped.

In [58], power quality and harmonic mitigation is improved through adaptive tuning of a medium-low frequency (2.5 Hz) switching converter, informed by TEI estimates provided by a separate device. Results are verified in a 22 kVA laboratory setup using a voltage source converter with a LCL filter connected to the live PS. The converter is able to perform as an active filter and contribute to the PS stability.

2.3.8 Power system modelling and simulation

The accuracy and effectiveness of simulation of the PS is directly dependent on the accuracy of the model used. The TEI can be used to measure parameters of lines and other equipment within the PS directly, thereby, taking into account practical effects the equipment may be experiencing that may be time varying or dependent on other factors. This could improve accuracy of wiring, fuse and circuit breaker calculations, as well as in the design of filters and reactive power compensators [65, 66].

The accurate knowledge of the parameters of a transmission line "is of vital importance in power system operations and planning, such as state estimation, transient stability… and is used as the basis for protective relay settings." [4] The traditional approach would be that these parameters are calculated from estimates and geometries of the line, however, these do not take into account the practical case in which there are conductor sag and temperature variations.[4] In the context of Ps's operating close to their design limits and with DG, the ability to accurately know the parameters of a transmission line is valuable.

i. Past results

Past results in this application are discussed in subsection 3.1.1iii.

2.3.9 Combined benefits

As a result of the numerous applications discussed in this section, implementation of on-line TEI estimation has the potential for easy implementation of a number of complementary applications on a single piece of equipment [33]. For example, if TEI estimation is implemented in PMUs on either side of a transmission line for fault location (as in subsection 2.3.4i), the line's parameters are also determined in real time. In the case of a power converter based implementation, voltage stability monitoring, islanding detection and adaptive current controller tuning can all become added functions [2] based on the measured TEI and its behaviour, with no other components or significant software burden added. The end result is that the power converter becomes a smarter device, easing the transition toward DG and encouraging its proliferation.

2.4 Passive (load change) approach to determining the power system Thévenin equivalent impedance parameters

2.4.1 Introduction

The load change approach is arguably the most well-known and widely researched [67]. This is mainly due to the fact that its implementation is very straightforward. It is done without affecting the PS itself – there is no injection of current or other perturbation involved. It is based solely on measurement, hence, it is commonly referred to as the passive method. It can be implemented using existing measurement hardware, most commonly Phasor Measurement Units (PMUs). These devices are used extensively by utilities and PS operators. Their use at the distribution level may also become more prominent with the advent of DG. The method can also be implemented in a power converter. As a result there is potential for widespread real-time TEI measurement as well as on-line monitoring using these devices.

2.4.2 Theory

Consider a load connected to the PS, under measurement. The circuit is separated into two halves to each side of the measurement point (PS side and load side), as shown in Figure 10. The measurement point is that from which values of the voltage and current phasors are obtained using a PMU or similar device.

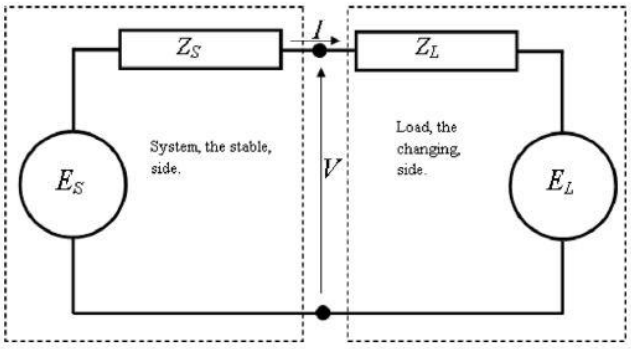

Figure 10: Simplified circuit under consideration, common in literature (taken from [5])

Each side of the circuit is represented by a single load and voltage source combination. That is to say: the left side is the PS TE circuit and the right side is the load TE circuit.
If the load-side impedance is changed (e.g. a heater is switched on) it is possible to calculate the PS TEI (Z_s) based on the change in voltage and current seen at the measurement point before and after the load impedance change:

At any given time t_1, the voltage, current and load impedance are V_1, I_1 and Z_{l1}:

$$E_s - E_L = I_1(Z_s + Z_{L1}) \qquad (2.2)$$

Similarly, at a later time t_2:

$$E_s - E_L = I_2(Z_s + Z_{L2}) \qquad (2.3)$$

Taking (2.2) – (2.3):

$$I_1(Z_s + Z_{L1}) = I_2(Z_s + Z_{L2}) \qquad (2.4)$$

Substituting $Z_{L1} = \frac{V_1 - E_L}{I_1}$:

$$I_1\left(Z_s + \frac{V_1 - E_L}{I_1}\right) = I_2\left(Z_s + \frac{V_2 - E_L}{I_2}\right) \qquad (2.5)$$

$$I_1 Z_s + V_1 - E_L = I_2 Z_s + V_2 - E_L$$

$$Z_s(I_1 - I_2) = V_2 - V_1$$

$$\boxed{Z_s = \frac{V_2 - V_1}{I_1 - I_2} \qquad (2.6)}$$

Equation 2.6 is true if and only if:

1. The PS's TE parameters (Es, Zs) remain unchanged
2. The PS-side and load-side voltage sources (Es, El) have not changed

Thus, through application of equation 2.6 to measurements taken of simultaneous voltage and current, given that there is variation in the load, the TEI of the PS can be determined.

2.4.3 Challenges related to practical implementation

As mentioned earlier, the passive method to TEI parameter estimation has undergone significant study. The PMU-based implementation requires only that measurements of the V and I phasors are measured and that equation 2.6 is solved with this data. Alternatively, on-line monitoring schemes have been suggested which employ real-time computation of the TEI. Application of the above theory to the real, dynamic PS that exists today reveals a number of challenges that require consideration.

i. Power system's impedance is not constant

Firstly, it must be acknowledged that the PS's impedance is constantly changing [49]. However, one of the requirements in the theory presented earlier (subsection 2.4.2) is that the change in the PS's TEI is negligible between two sampling points. The high sampling frequency of typical PMUs (≈3 kHz [68]) means that the time between consecutive samples is about 0.33 ms. Compared to the time taken for one 50 Hz cycle (20 ms) this is very fast. Hence this assumption would seem reasonable. The time constants of generator governors, excitation systems and on-load tap changers are also much greater than the time between two consecutive samples [69, 70]. The general consensus in literature is that the PS can be assumed to remain stationary.

In [5] a new method is developed specifically to take into account possible system-side changes that occur within a very short period (3 sample periods). One possible source for such system-side changes is described as "arduous weather conditions causing multiple transient and permanent loss of generation and transmission capacity". The important findings summarized by the author are:

1. The calculated TE parameters according to equation 2.6 are the parameters of the side (PS or load) that remains stable (undergoes significantly less variation) during measurement.
2. The sign of the calculated parameters indicates to which side the parameters belong.
3. If Es or Zs vary, error is introduced into the calculated parameters
4. This error becomes very large when both sides exhibit changes of the same order of magnitude

The above findings aid in the understanding of the possible phenomena that may present themselves in collected TEI data from PMUs.

ii. Load side must change

Whilst we need a steady PS side for an accurate value of TEI to be extracted, the opposite must occur to the load impedance (Z_L). That is to say, it must experience a significant change in a short time[6].

This is a critical requirement of the theory. If not, there is no change in the phasor measurements. The minimum change in impedance required for accurate results has not been investigated in literature. To be as specific as possible, the load change must cause a change in voltage and current that is large compared to the uncertainty in voltage and current measurement of the PMU.

According to Ciobotaru et al., the passive method's dependence on load changes (which they termed "background distortion of voltage") is undesirable because in numerous cases it has "neither the amplitude nor the repetition rate to be properly measured. This will not be interesting for implementing it in a PV inverter." [3].

iii. Power system's frequency is not constant

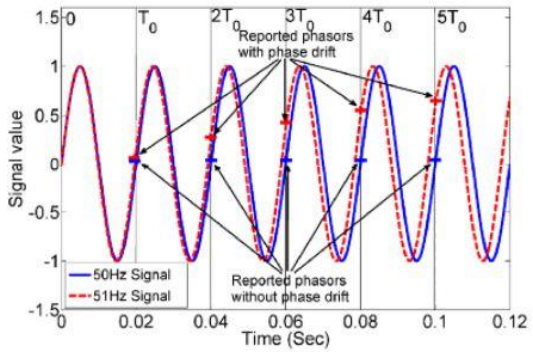

Figure 11: Phase drift phenomenon (from [70])

As discussed in 2.1.3, the PS's frequency varies continuously. The problem this causes is that the PMU sampling frequency and the system frequency are not in sync, causing what is known as phase angle drift[69]. This is essentially the incorrect representation of the phase angle of the measured voltage (see Figure 11). It is shown that a very small frequency change can cause a large drift in phase angle measurements[69] and this must be taken into account for accurate TEI calculation. Several approaches are available which have shown good performance.
In [69] three consecutive measurements are synchronised by triangulation, based on the condition that the three measurements must provide the same impedance with a certain phase correction.

In [70], phase drift is corrected using an algorithm that measures the rate of change of system frequency for every cycle.

iv. Noise and measurement error

The presence of noise and measurement error in phasors obtained by a PMU is problematic, as it can compromise the estimation of the impedance. In [4], it is stated that "the parameters identified are very sensitive to noise and errors in PMU measurements, which are difficult to quantify and can be uncertain under different system operating/loading condition.". It is an especially large concern due to the fact that, if the load does not change significantly, the task effectively becomes accurate measurement of a very small change in voltage and current[6]. According to [4], this is the most difficult obstacle to overcome in implementing this approach.

In [69], the resulting error in impedance due to measurement error is defined:
Given that the voltage and current magnitude are V_m and I_m, the errors in the PMU for each of these are u_v and u_i respectively. Similarly phase errors are σ_v and σ_i such that measured voltage and current phasors are:

$$V_m = V(1 + u_v)\angle(\delta + \sigma_v) \quad (2.7)$$

$$I_m = I(1 + u_i)\angle(\varphi + \sigma_i) \quad (2.8)$$

Then the errors in the impedance magnitude and angle are:

$$|Z|_{error} = \frac{1 + u_v}{1 + u_i} \quad (2.9)$$

$$\angle Z_{error} = \sigma_v - \sigma_i \quad (2.10)$$

In order to overcome noise and measurement error, the precision and noise immunity of measurement equipment should be sufficiently high. This is difficult to achieve without use of dedicated hardware. Another option is that many samples are used [69] (rather than the minimum of 2) and a curve-fitting technique is applied, such as RLS [11]. The disadvantages of the use of these techniques are that they slow the estimation process and can potentially cause short-term events to become overlooked due to averaging [5], as well as adding to computational burden.

v. Difficulty in verifying results

The nature of the TEI of the PS is that it is a representation and simplification of a very large system that is dynamic. There is no other way to know the true value of the TEI accurately than through the active and passive methods in this section, which involve some sort of voltage/current change followed by measurement.

Use of a test circuit is possible. With such a system, impedance components can be individually measured to a high accuracy, and with the topology known, the real impedance of the test system can be known accurately. However, this is very different from being connected to the PS. There is no presence of harmonics and distortion typical of the real PS and the level to which the test circuit is representative of the grid is very limited, due to the grid's complex nature. Hence this verification technique is limited.

A good thing to do would be to apply two different approaches, such as a passive and an active one, to the same system at the same point of connection. This would allow for comparison and greater confidence in the results obtained. However, this is rarely done.

Other options available for comparison are design data and simulations based on parameters from the PS's schematics. However, in many situations these parameters may not be so close to the actual values. Lines sag and insulation deteriorates over time [4], affecting the impedance of lines. As discussed in subsection 2.1.3, the loading of the system changes over time. On a larger scale, the load behaviour can be statistically predicted to a high accuracy. At the distribution level – the level at which DG is most prevalent – unpredictable local load behaviour may have a significant influence. Furthermore, noise and measurement error is generally ignored in these approaches. Hence, it is doubtful that basic simulation results and design data can provide more than a general approximation of the actual case, only giving us an idea of the order of magnitude that can be expected for the parameters.

2.5 Active (harmonic injection) approach to determining the power system Thévenin equivalent impedance parameters

2.5.1 Introduction

The active method involves injection of an uncommon voltage or current harmonic into the PS, usually with a power conversion device such as an inverter. Uncommon refers to the fact that there should be no existing component at that frequency. The product of this injection is a voltage or current response in the PS at that same harmonic frequency, which must be measured for TEI parameter estimation. This approach provides control over the signal-to-noise ratio (SNR), unlike the passive one [49]. Since the injection into the PS requires power and may disturb the PS, it is done periodically. The approach is well-suited to DG applications due to the fact that it can be implemented in an inverter [33], requiring only some software modification. Furthermore, the anti-islanding requirements enforced by some countries[2], mean that PS TEI tracking is already a requirement in many such devices.

2.5.2 Sub-methods: Steady-state and transient [27]

There are two sub-methods within the active method – steady-state and transient. The steady-state sub-method involves injection of a periodic waveform (e.g. sine wave), typically containing one or two frequencies. This restricts measurement of impedance information to only those distinct frequencies. The transient sub-method involves injection of a wideband signal, usually a short current spike. Thus, if the wideband response is measured, the impedance of the PS can be found over a range of frequencies simultaneously. One benefit of the transient sub-method is that it is well suited to obtaining fast results [3, 25]. However, the spreading of signal power over a range of frequencies means that the SNR is lower and the measurements more susceptible to noise [30] for the latter sub-method. Furthermore, it requires high performance "A/D (analog to digital conversion) devices and must also use special numerical techniques to eliminate noise and random errors" which make it somewhat unsuitable for implementation in non-dedicated hardware such as a PV inverter [3].

2.5.3 Theory

The theory is almost identical for the two sub-methods. Normally, two sets of measurements of voltage and current are required. These measurements are at the chosen injection frequency. These are: just before harmonic injection and during harmonic injection. In the same way as before, if V1, I1 and V2, I2 are the phasor measurements before and after injection respectively, equation 2.11 gives the PS impedance. In this case, the measurement point is the point of common connection (PCC) where the inverter and PS are connected. Current is injected here towards Es.

$$Z_{th} = \frac{V_2 - V_1}{I_2 - I_1} \qquad (2.11)$$

If we have the case where there is no existing component at the frequency we intend to inject current, we have $V_1 = 0$ and $I_1 = 0$. Thus, only one set of measurements is needed – that during injection. Equation 2.11 becomes:

$$Z_{th} = \frac{V}{I} \qquad (2.12)$$

If a method is applied consisting of multiple harmonic injections, there is the added advantage that the phase angle information is then not required in the calculation. Equation 2.12 can be used with voltage and current magnitudes only to extract the TEI magnitude for two different harmonics, then by assuming that the reactive inductance varies linearly with frequency, calculate the Thévenin inductance and interpolate the value of Z_{th} at the desired frequency (usually 50 Hz). This can be done as follows:

Given two harmonic frequencies, for example 40 Hz and 60 Hz, at which current is injected:

$$|Z_{th\ 40Hz}| = \frac{|V_{40Hz}|}{|I_{40Hz}|}$$
$$|Z_{th\ 60Hz}| = \frac{|V_{60Hz}|}{|I_{60Hz}|}$$

Then:

$$|Z_{th\ 40Hz}|^2 = R_{th}^2 + X_{th\ 40Hz}^2 = R_{th}^2 + \omega^2 {L_{th}}^2 = R_{th}^2 + (80\pi)^2 {L_{th}}^2 \qquad (2.13)$$
$$|Z_{th\ 60Hz}|^2 = R_{th}^2 + (120\pi)^2 {L_{th}}^2 \qquad (2.14)$$

Simultaneously solving equations 2.13 and 2.14 provides R_{th} and L_{th}, thereby, Z_{th} at any frequency, given that resistance is constant and reactance is linear (supported by [30]). It should be noted that this assumes that the PS's impedance-frequency curve is linear. This is only expected to be true over small frequency intervals.

In the case of a transient method, we have a wideband input and a wideband response. The wideband response must be analysed through a DFT and hence may produce impedance information for a large range of frequencies.

In the case of a steady-state method, measurement of the voltage response at a specific harmonic can be done in a few ways, including by a differential method, filtering, or by discrete Fourier transform (DFT).

2.5.4 Challenges related to practical implementation

i. Power system's impedance is not constant

Similarly to the passive method, the active method must also take into consideration the dynamic nature of the PS. For injection to give an accurate result for the TEI, the injection and measurement period must be short enough that the PS can be assumed to remain stationary over its duration.

ii. Limitations of available technology [27]

The most attractive way to implement this approach is through existing hardware such as PV inverters or similar devices in an on-line context. This enforces several limitations on the method as a result of the hardware used and its non-dedicated nature. Implementing real-time computation that is fast and reliable is constrained by limited A/D conversion accuracy, fixed-point numerical calculation and a low computational complexity requirement [27]. DFT's are especially computationally demanding. Hence, for a real-time implementation, the algorithms used should be simple and fast.

iii. Power system may be unbalanced

In the most common case where we wish to find the parameters of each line in a three phase PS, we can apply symmetric voltages to each phase and they will cancel out at the point of interconnection of the phases. This way, we can theoretically determine the TE parameters for each line by treating each line in a similar way. However, in the case of an unbalanced PS, in which the loading and thereby the impedance of each line is not equal, we have to take another approach. This approach is developed in [29]. If we are able to control the current injected into each line and fix that to be equal despite unequal impedances, the issue is resolved. However, when there is no neutral wire such as in a three-phase three-wire system, we cannot measure phase voltages (the neutral point can shift) and thus the TEI parameters are unlikely to be accurate[29]. At the LV level, three-phase three-wire systems are not common – these systems are used mostly where unbalance is low such as bulk power, high voltage transmission. Hence, this would not really a problem when considering a DG context. Nonetheless, in [29] dual harmonic injection is used with a novel algorithm and proven theoretically to be able to

overcome the shifting neutral issue, providing an accurate TEI for each line. However, the testing was only done in a static impedance case and thus, does not look at performance under real-world PS conditions.

iv. Distortion of power system

The added distortion in the PS due to injected harmonic current is a drawback to the approach and care must be taken to ensure that it is not excessive and does not violate quality of supply requirements [66]. Generally, injection of harmonic currents causes an increase in the total harmonic distortion (THD) of the PS [49]. A compromise must be made between sufficiently disturbing the system for accurate measurement and interfering with the operation of network equipment [65]. Hence, the size and frequency of the current injections (both how often injection is done and of the waveform itself) must be chosen wisely.

v. Difficulty in verifying results

The same difficulties described in 2.4.3v are also present in the case of the active method.

vi. Interference between devices

If the context is widened to a widespread implementation of active TEI estimation hardware, the problem of interference arises [23, 25]. Quite simply, if two or more devices both inject a signal at the same time, their signals will interfere with each other, causing an incorrect impedance estimate. This issue has been addressed in only a limited capacity in literature, although several points are worth noting. The probability of interference is reduced if the duration of injection is minimized[25]. Furthermore, the frequency domain can be divided into separate channels. Essentially, the same principles as those in the field of Telecommunications with regards to a shared medium can be applied.

2.6 Photovoltaic inverters

2.6.1 Introduction

Photovoltaic (PV) inverters, in basic terms, are power converters specifically designed to operate with PV solar panels in converting their DC (direct current) output to the appropriate AC (alternating current) voltages and frequency at which the PS operates. As indicated in the previous section, power converters such as PV inverters can be used for TEI estimation.

This section is devoted to these devices, as the practical testing of much of this thesis is focused on such a device, specifically, its implementation as a TEI sensing device. Hence, a basic understanding of the makeup and complexities of the PV inverter is important. Only the relevant specific schematic is discussed, as present in the device used in testing later on.

Modern PV inverters are complex devices, mainly due to the development and requirement of additional features beyond simply converting from DC to AC. There are numerous technologies to choose from and several categories of device, depending on application and size. The driving factor in the technology of PV inverters is efficiency, mainly due to the high costs associated with solar energy [50]. Many manufacturers offer efficiencies of above 97% in their devices [50].

2.6.2 Typical functions

Beyond DC to AC conversion, a typical PV inverter is able to perform maximum power point tracking, anti-islanding, PS synchronisation and data logging[50]. These should be understood to some degree as TEI estimation is yet another function that must be implemented on the shared hardware.

2.6.3 Structure of full bridge inverter

The device used in this investigation is comprised of the following components:

1. Voltage and current transformers (instrument transformers)

   These are used to bring PS voltage and injection currents down to measureable levels
2. A/D converter

   This is used to quantize outputs from the instrument transformers and convert them to digital format so that they may be read by the microprocessor
3. Microprocessor

   The brain of the inverter, used to control injection, synchronisation and all other functions of the device. It can also receive remote commands in certain cases.
4. Boost transformer

   This is used to step-up the voltage to the PS-level.
5. Input LCL filter

   This is used to filter out harmonic content in the PS that may interfere with the operation of the inverter.
6. H-bridge

   This simple circuit is used to provide a way for actual inversion of the output voltage, through the process of insulated gate bipolar transistor (IGBT) switching, producing an alternating output.
7. Phase locked loop (PLL)

   This circuit is used to synchronise to the supply frequency.

The main circuit performing the task of delivering power is shown in Figure 12.

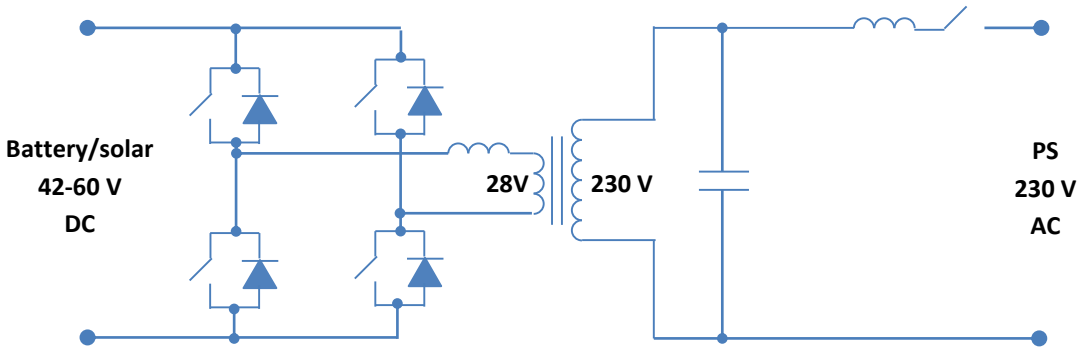

Figure 12: Full bridge voltage source inverter circuit diagram

2.6.4 How it works

The DC connection to a battery or PV panels delivers a constant voltage input and power source. This is applied to the H-bridge, made up of four MOSFETs. The switching of the MOSFETs is done with a unipolar scheme at the PS frequency, set by the PLL. This causes the LV side of the transformer in Figure 12 to pass through the sequence 0V, 28V, 0V, -28V repeatedly. This induces an alternating voltage at a higher level to appear at the HV side, which is connected to the grid through the LCL filter. Through pulse width modulated (PWM) control of the switching at a high frequency, a near-pure sine wave can be delivered. Sensors attached to the HV side monitor the output, sending information to the microprocessor. A proportional-integral controller is used to control the output current to the required sine wave target shape.

3. Literature review

3.1 Passive method

3.1.1 Past results

i. Abdelkader et al.

In [5], simulations are performed using a 30 bus IEEE test system. The authors also take an analytical approach to the effects of system-side changes (discussed in subsection 2.4.3i). The TEI estimation is performed at each load bus. The values obtained at all buses had a standard deviation of less than 1%[5], suggesting very high accuracy. When system-side changes were implemented (switching operations, increasing loads at all buses), the results were as predicted by the theory. The TEI estimation algorithm was also tested on real PMU measurements collected from the Northern Ireland Power System. It was found that the TEI parameters varied in distinct manners at the periods when automatic governor control (AGC) actions, unsuccessful circuit breaker (CB) reclosure attempts and tripping of lines occurred. Furthermore, the TEI values obtained were in agreement with short circuit current (SCC) level data from a nearby substation and were in the range of 4 ohms.

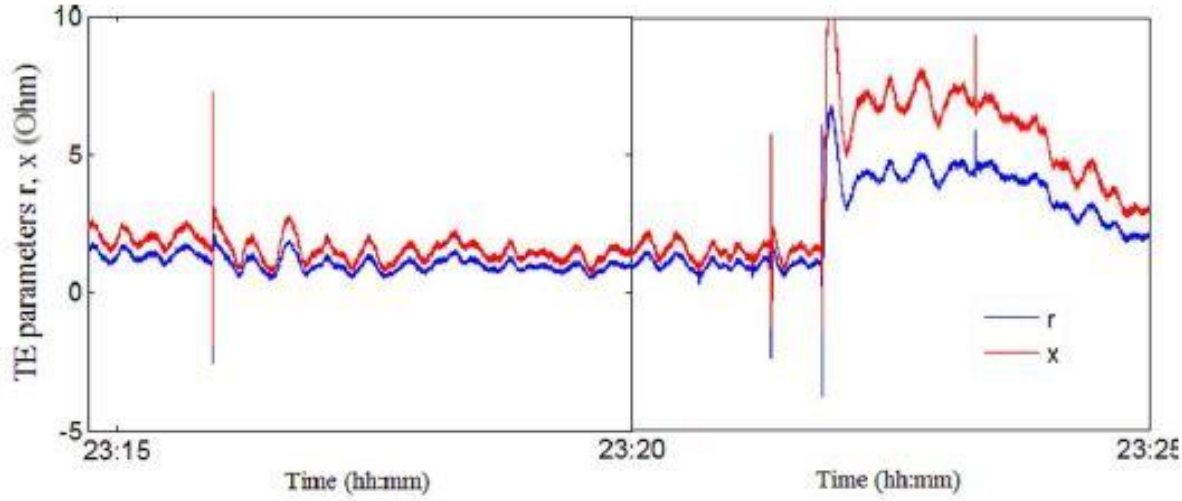

Figure 13: TEI of Northern Ireland PS during arduous weather conditions (taken from [5])

From 23:14 – 23:21 – believed to be due to AGC operation causing system-side changes
Spikes during above interval – caused by unsuccessful CB reclosure attempt of tripped circuit
Spike at 23:22 – tripping of second circuit of parallel transmission line, commencement of run back scheme of generating station.

The same author performed similar tests in [69] earlier on a set of data from the same PS but in this case, under normal system operation. The results were as predicted by the theory.

These results show that the PMU-based implementation is successful in detecting system-side events, as seen by the measurement's distinct reactions to each change. Losing a line meant that the impedance increased abruptly as expected, and also returned to its prior state afterward. Furthermore, the level of the parameters has been verified with real SCC data. However, the size of the change in the parameters was not verified although this could also have been done with similar SCC data. Hence, the dynamic performance is not certain.

ii. Alinejad et al.

In [70], another PMU-based implementation is investigated, in this case not on the distribution/load level but rather at a generator terminal. It is simulated on the New England 39 – bus network model,

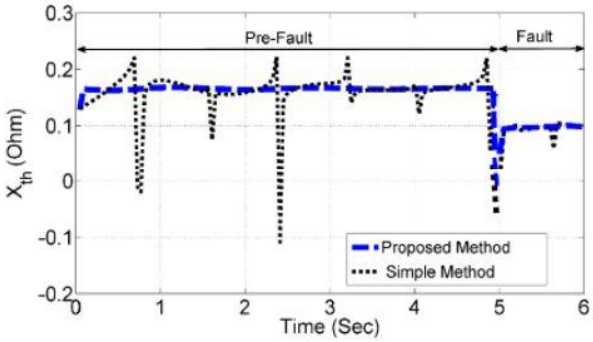

Figure 14: Sustained TEI accuracy in case of simulated fault (from [70])

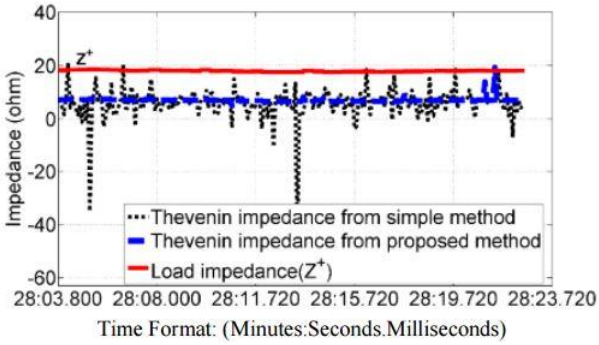

Figure 15: Calculated TEI from raw PMU data collected from Iranian 400 kV substation (from [70])

using DigSILENT software. Several cases are tested. It is shown that when the PS is perfectly steady-state (unchanging), we get identical consecutive phasor measurements from the PMU and the measured impedance tends to the load impedance, as expected according to the theory in subsection 2.4.3i. Small load variations are incurred throughout the network in order to be able to obtain the PS's impedance (also to introduce phase drift) and the result obtained is close to that known to be correct at that bus (0.186Ω) according to load-flow simulation. A three phase fault is applied, dropping the impedance of the PS to the theoretically known value of 0.098Ω and the results show effective TEI determination (see Figure 14). Finally, practical testing of the implementation is done on raw PMU data from a functional Iranian 400 kV substation. The results show that the calculated TEI closely matches the known value ("obtained from the offline load flow and short circuit calculation studies performed on the transmission system developed in DigSILENT software in Iran PS Management Company") of 7.2 Ω, as seen in Figure 15.

The simulation results give further validation that the PMU-based approach's theory is correct. The effectiveness of TEI estimation is seen to be high, however, the context of this result should be kept in mind. The simulations were carried out without consideration of the potential size of noise and measurement error, which can decrease the SNR. The size of the changes in the loading effected in the PS simulation was varied and the method was effective even for load changes considered to be 'small' (steps of 0.05 p.u. loading at a single bus). The impedance results are low for the buses simulated, which is expected. They are lower than the substation data from the previous author, which is lower than the results from the 400 kV substation quoted here. This 400 kV result is one of few results found in literature for PMU implementation at the EHV level. The author notes that the changes in loading do not influence the TEI calculated and explains this as being due to the very low impedance of the transmission system at this level, compared to the high impedance of the load.

The method used is also shown to overcome the issue of phase drift.

iii. Zhou et al.

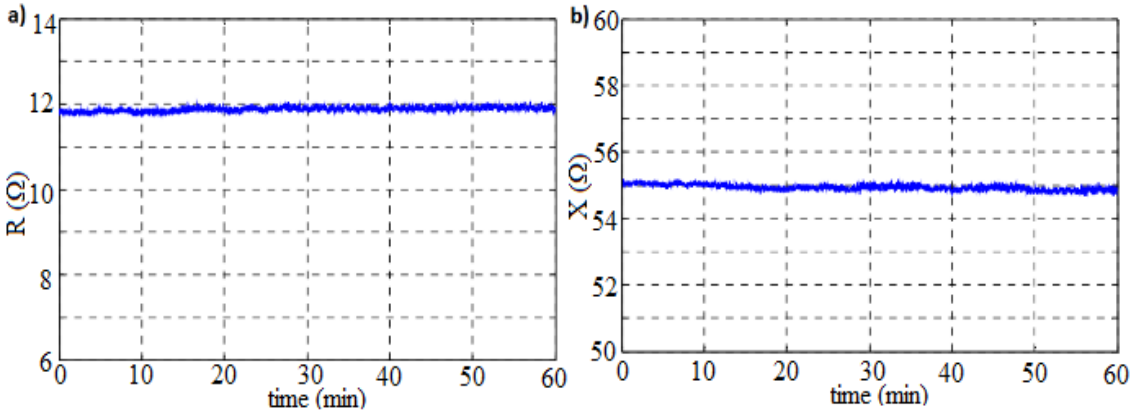

Figure 16: a) Resistance and b) Reactance obtained for CSG transmission line over 60 min period (Taken from [4])

In [4], TEI estimation is intended for validation, update and improvement of network parameters such as line impedances in the China Southern Power Grid Company. Practical implementation at the level of a 525 kV transmission line is done and the obtained impedance found to be within 8 % of the value in the company's database. Figure 16 shows some of their results. In this paper, the authors also propose the use of a credibility metric to give more confidence in results.

The variation in resistance and reactance is found to be very small, as expected at such a high voltage level without nearby loads. It is observed that the reactance was measured to be the largest portion of the line's impedance, both being of the order of tens of ohms. This is greater than that found in the work of Alinejad et al., as is expected by the fact that lines at the HV level are generally very long.

The closeness of the obtained result to the value in the database shows that the approach has been employed effectively. The discrepancy is an indication of the potential improvement in the line's recorded parameters with this approach (assuming no unseen errors are present in the data obtained).

iv. Liu et al.

In [22], the authors propose a passive islanding detection method using the PS TEI, implemented on an inverter-based DG. Despite not being a PMU-based implementation, the approach is still passive. It should be known that passive methods can just as easily be implemented within inverter hardware, which contains much of the same functionality as that of a PMU.

The passive nature of the method means that it does not interfere with the DG control system and thereby can be combined with other islanding detection algorithms (e.g. rate of change of frequency) to improve detection performance. The paper considers the worst case islanding condition where under/over voltage/frequency methods would not detect islanding.

The method is developed based on comparing the measured TEI magnitude to a reference - the TEI for which an islanding condition is present. This is done using an FFT at frequencies where dominant harmonics are existent in the PS, as these are subject to large changes when islanding occurs.

Simulations are done in order to investigate the robustness of the method in a typical LV distribution network. Cases of capacitor bank switching, large load change, other DGs switching on/off and NLL switching are considered, all of which are identified as normal operation (not islanding) by the method

(see NOR1 -5 in Figure 17 a). Worst case islanding is detected effectively (see ISL1-5 in Figure 17 a).

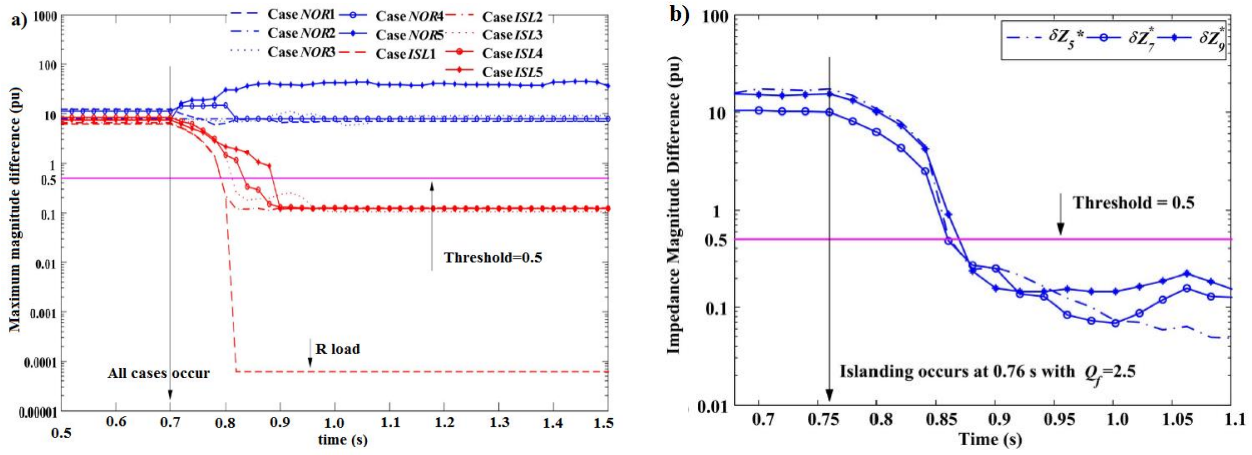

Figure 17: a) Simulation results for different cases, NOR – not islanding condition, ISL – islanding condition, from [22]

b) Experimental results: Detection of islanding condition, from [22]

Experimental validation is also done using a 3 kW single phase PV inverter connected to the PS. An islanding detection device (RLC local load) is used to mimic the worst case islanding condition. Figure 17 shows the variation in an index; this index is the difference between measured impedance at the chosen harmonic and the reference value of that harmonic under islanding condition. Clearly, when islanding occurs the indexes fall to a low value below the 0.5 p.u. threshold for all chosen harmonics. As a result, the method instructs the DG to disconnect itself within 0.25 s, whilst OV/OF and UF/OF methods would not detect islanding condition at all. A sensitivity analysis is done that shows avoidance of false alarm situations and the method is fast enough to satisfy IEEE Std. 1547.

3.1.2 Summary, limitations and implications of past results

The passive method is shown to be easily implemented in PMU hardware and utilised in almost all of the practical applications discussed in subsection 2.3. The results show that, for all the results presented, the TEI values obtained closely match the expected values according to load flow results and design data. However, results from practical implementation of the method are limited and the effects of noise and measurement error are marked as a serious concern for the effectiveness of this method.

The ability of the PMU to provide a TEI estimate is based entirely on the requirement that the load-side changes whilst the grid-side remains the same. However, there is almost no information available regarding how large of a load change is required to overcome noise and measurement error and how often such changes can be expected to occur. Furthermore, very little information is available regarding the frequency and size of system-side changes that can typically be expected. Thereby, their potential effect on the PMU-method is not certain. This is an area in which further study would be greatly beneficial. Despite these drawbacks, results such as those in subsection 3.1.1iii show promise. One adaptation of this method that should be somewhat less susceptible to these effects is that of subsection iv for islanding detection.

The inability to control the precision of measurement is one drawback of the method. This method may be better suited to applications in which high precision is not crucial – such as islanding detection or PS modelling and simulation. The advantages of this method such as its passive nature mean that it can also be implemented in inverter hardware without interfering with normal device operation.

Unlike the method discussed in the next section, the passive method does not require injection of power, which is favourable.

In terms of the TEI of the PS and its behaviour, it was found the PS TEI varies significantly depending on the voltage level of the grid. At transmission level, it is expected to be of the order of several or tens of ohms and at the distribution level it should be less than an ohm. Significant variations in the TEI of the grid have not been seen outside of abnormal behaviour (e.g. fault occurs). Almost no tests have been found where TEI estimation was done over extended time periods to investigate how the PS TEI behaves (maximum found was 1 hour in subsection 3.1.1iii).

3.2 Active method

3.2.1 Past results by authors

i. M. Ciobotaru et al.

M. Ciobotaru et al. in [2] focus on an on-line impedance estimation method for single-phase systems (e.g. PV systems). This method uses both single (500 Hz) and double (400 Hz and 600 Hz) periodic

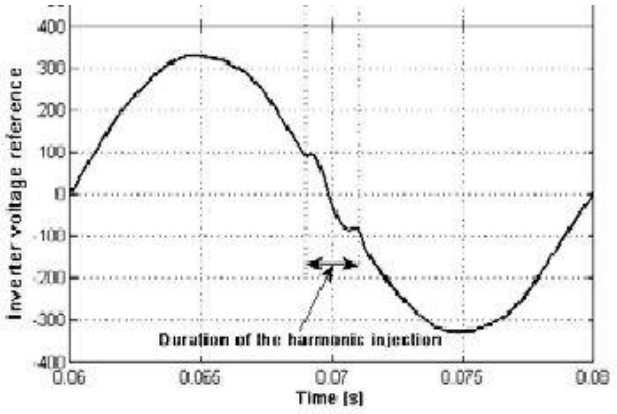

Figure 18: 500 Hz harmonic component added to 50 Hz nominal for injection

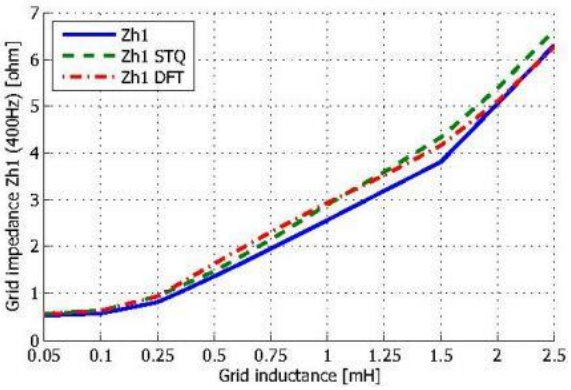

Figure 19: Results from simulation, increasing Zth Blue: actual Zth | Green, Red: calculated Zth 400 Hz case

harmonic injection. The approach taken to injection is to add one cycle of the harmonic component centred at the zero-crossing of the 50 Hz component, as shown in Figure 18. This choice is motivated by the desire to not greatly affect the active power produced by the inverter.

The frequencies chosen for the injection current are somewhat arbitrary. It is argued that a lower frequency "can interact with the resonance of the current controller in the case of the proportional resonant current controller with harmonics compensation is used" and that a higher frequency "can be near the PS resonance frequency" but no specific limits or further justification is provided. Furthermore, linearization of the PS impedance is done based on the 400 and 600 Hz results, much greater than the operating frequency of the grid which may not provide accurate results at 50 Hz.

Two approaches to extracting the measurements of voltage and current are used and compared. In one, a DFT is used, in another the 50 Hz component is subtracted from the received waveform and the magnitude of the remaining harmonic component is simply measured. Both appear to work equally well.

The method is simulated and shows the ability to track changes in PS impedance accurately when the PS resistance and inductance are changed, for both the 400 and 600 Hz injections. An extract of the results is shown in Figure 19. It must be noted that almost no information is provided regarding how the PS is modelled for the simulations, limiting the pertinence of the results greatly.

ii. W. Cai et al.

In [29], a dual harmonic injection method is developed that is able to work under unbalanced PS conditions. The authors argue that the non-characteristic currents injected are small and do not contribute significantly to THD. These currents are shown in Figure 20. Their method is tested in a laboratory setup in which they use series resistors (of the order of 1 Ω) and inductors (50 mH) to act as their three-phase three-wire PS. Their chosen injection frequencies are 75 Hz and 125 Hz, and it is

shown that their method effectively measures the impedance placed in the lines, even when the impedances are unbalanced.

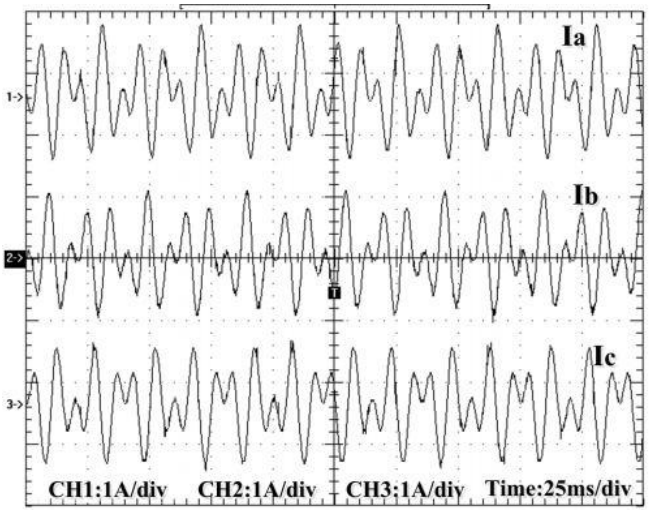

Figure 20: Injection current from [29], made up of 75 Hz, 125 Hz components

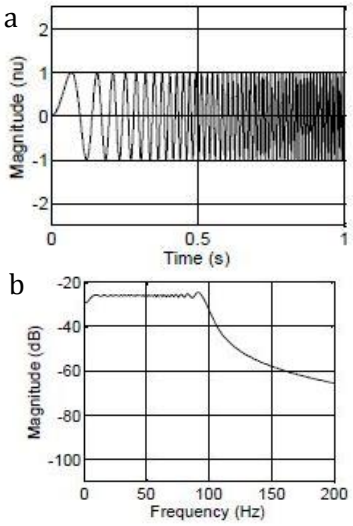

Figure 21: Chirp signal used in [30] (a) Time domain, (b) DFT

The nature of the injection current used is usually vastly different between any two given papers, as is the case between this paper and that by M. Ciobotaru et al. preceding it. In the case of steady-state injection, the frequencies and magnitudes of currents injected are quite arbitrarily chosen, as is the case here. The commonly used justification is that it is a 'non-characteristic' frequency (the possibilities are endless). Thus, values chosen by authors differ by orders of magnitude.

iii. L. Asiminoaei et al.

In [27], a steady-state active method is implemented using a PV inverter for the purpose of islanding detection. The method is straightforward – a non-characteristic harmonic current is injected into the PS and the voltage response at that frequency is extracted through a simple DFT process, shown in Figure 22 below. This is practically done by adding a voltage harmonic to the reference voltage of the inverter, then using the inverter's sensor inputs of current and voltage for the calculations.

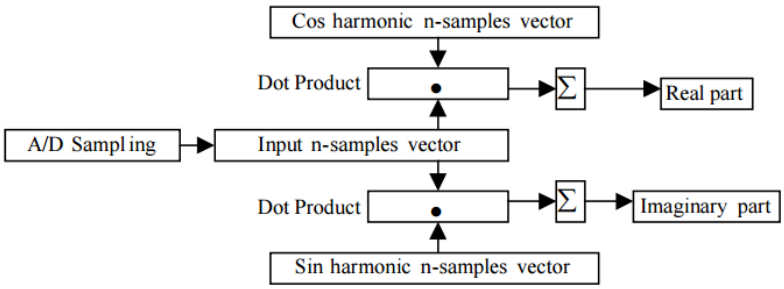

Figure 22: DFT process diagram for voltage response extraction in [27]

Clearly, the DFT process is optimised for computational efficiency, as the processing is constrained by the hardware of the inverter. The author uses a running sum to further increase computation speed.

The author states the need to minimize the duration of harmonic injection so as to "limit the total current harmonic distortion". It is further argued that multiple inverters can all run on the same network with time division multiplexing. The approach is practically tested, in single harmonic injection format. The harmonic is a 75 Hz, 1.5 A amplitude sinusoid with a duration of 40 ms (2 cycles of fundamental). A 3 kW inverter is used for the injection. A "PS tester" (UNILAP100) is used to produce the time-domain and frequency domain images in Figure 23 and Figure 24 below, showing the effects of the injection.

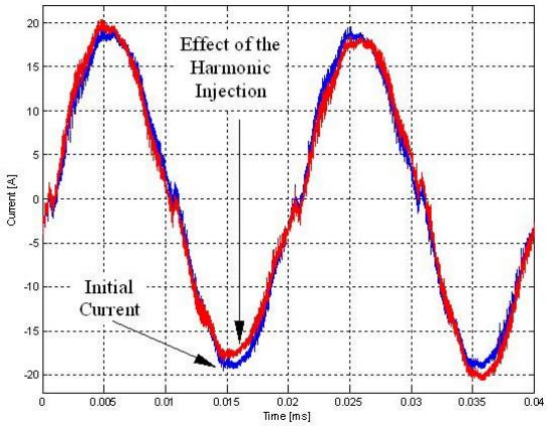

Figure 23: Current waveforms before and after harmonic injection (from [27])

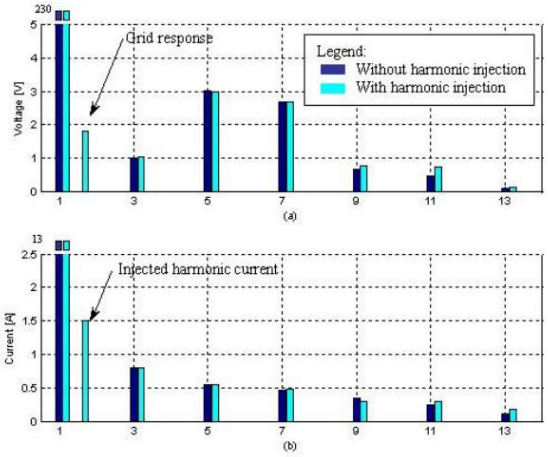

Figure 24: Voltage and current harmonics before and after harmonic injection (from [27])

Since only a single harmonic is injected and the algorithm used does not measure the phase angle, only the magnitude of the impedance is obtained. The final result for the obtained TEI is 1.27 Ω, close to that found by the "PS tester" – 1.2 Ω. Unfortunately this is the only check that is used to verify accuracy of the estimation process.

The author also goes one step further to investigate how the injection repetition ratio affects the THD. This ratio is effectively a 'duty cycle' of the injection. In choosing this ratio, there must be a compromise between how recent the value of the TEI is and how much the THD is raised. The value of 1/14 is settled upon causing 2% THD increase providing a "good balance". The process by which this value is chosen is by no means thorough – only two other values are considered. The choice of the repetition ratio is an important step and any future investigation should consider more closely factors such as how quickly the PS impedance can change as well as how much THD increase is acceptable before choosing repetition ratio.

Post-processing is implemented to filter out "random errors and A/D flickering" present in the impedance estimation. Use of a low pass filter/moving average is suggested.

iv. Z. Shen et al.

In [30], the authors set out to determine TEI with use of a transient method. A chirp (swept-sine) injection signal is used. One of the main advantages of this approach is that it provides a fast way of practically determining the TEI, not just at a single frequency, but for a wide range of frequencies. The context of the paper is system stability analysis. The paper uses direct-quadrature (DQ) coordinates in its analysis, performing a DFT to obtain measurements. A linear chirp is used, moving from 0 Hz to 100 Hz in one second. The waveform is shown in Figure 21, together with its DFT. Simulink simulation of the technique show accurate performance in determining static TEI in the presence of noise over the chosen frequency band.

The technique is tested experimentally, connected to a lab power supply. A frequency sweep is done between two adjacent harmonics of the fundamental. The results are compared to those from a

sinusoidal injection (steady-state) sweep algorithm done on the same system and are seen to match closely.

The authors, in their review of other papers, state that "the perturbation signal level used in these papers is large, which may excite the non-linear response of the circuit" [30]. The question of how linear or non-linear the PS's response can be expected to be has not been addressed in literature.

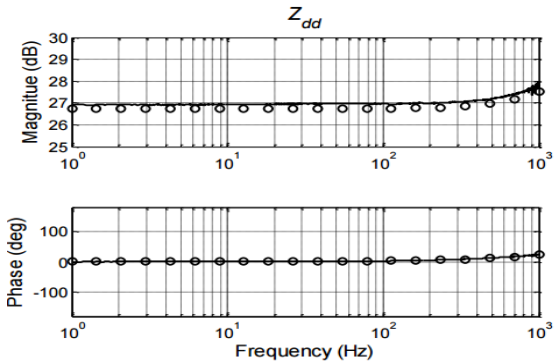

Figure 25: Comparison of TEI of live PS obtained through chirp signal injection and using Agilent impedance analyser (– : chirp, ○ : analyser) from [30]

v. B. Palethorpe et al.

In [31], the authors propose a transient method for obtaining the TEI of the PS. In this case, it is intended to be used in an embedded system in an active shunt filter (ASF). The proposed approach is attractive – the ASF reference currents are to be set using only the voltage at the PCC and the estimated PS impedance. Thereby, all of the inputs are available from the unit itself. As with other work discussed in this section, on-line operation is the aim.

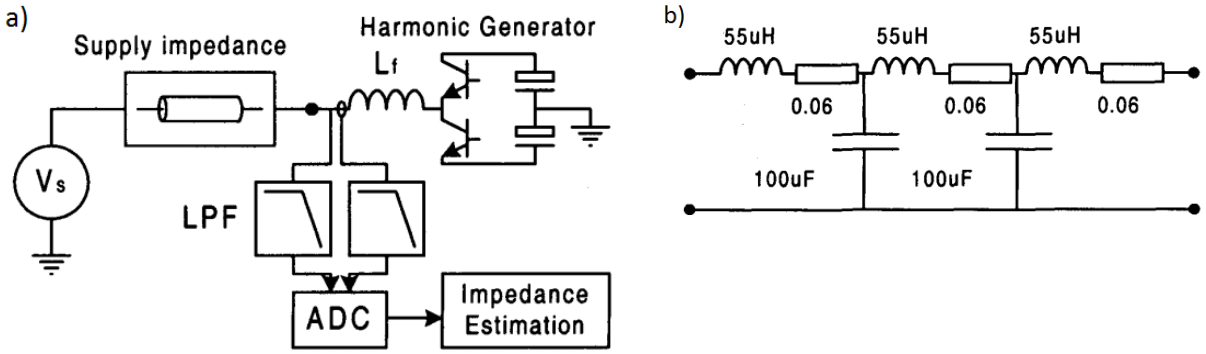

Figure 26: a) Simulation model b) supply impedance model from [31]

Simulation of the method is done. The impulse is generated through switching and lasts 625μs, with amplitude approx. 60-100 A. The frequency range of interest is 0-2 kHz. The voltage and current are both low pass filtered (2.4 kHz Butterworth) before being processed further. The supply voltage waveform is removed by a differential method – 160 ms before and 160 ms after injection are compared and the 'before' waveform subtracted from the 'after'. This also removes the existing harmonics in the supply from our considerations. A simple model is also used for the PS – three cascaded circuits of the series R, L and shunt C combination. The time-domain waveforms of voltage are shown in Figure 27.

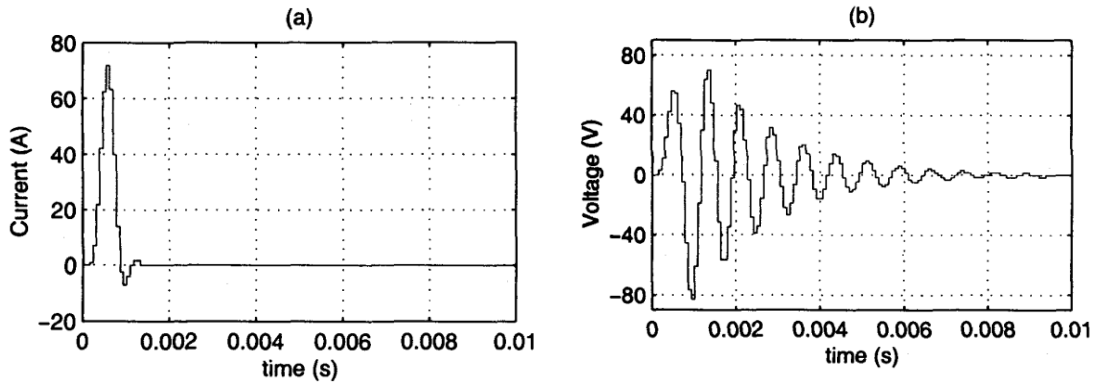

Figure 27: a) Current waveform b) Voltage waveform for injection in [31]

The magnitude and phase plots of the PS impedance obtained were shown to match very closely to the analytical values for the impedance model used.

The differential approach used significantly extends the duration of the measurement and risks the possibility of a PS change during this interval. It is also less effective in the case of a significant frequency drift.

The authors also consider the effects of non-linear loads to a limited degree. Specifically, an instantaneous impedance change which could be caused by switching of a power electronic load is modelled. The switching action 'interrupts' the voltage response, causing the impedance estimation to be inaccurate. In order to overcome this issue, the Prony method is utilised and the impedance of the PS can be found in each separate switching state (depending on during which state the current is injected). However, the computational requirements of this method are expected to be too high for on-line estimation.

In further work by similar authors [62], the use of steady-state injection (and thus, limitation to only a few frequency-impedance results) is seen to be inferior to transient injection because of the non-linear nature of the system. That is to say, it is much better to obtain a frequency/impedance curve and then investigate what level of linearity exists, than to assume linearity from measurements at only one or two frequencies.

Another interesting point raised is that "interharmonic impedance values are not generally affected by NLLs". That is to say, the harmonics caused by NLLs can only take set frequencies and between these frequencies there is no effect – the impedance can be extracted without complication.

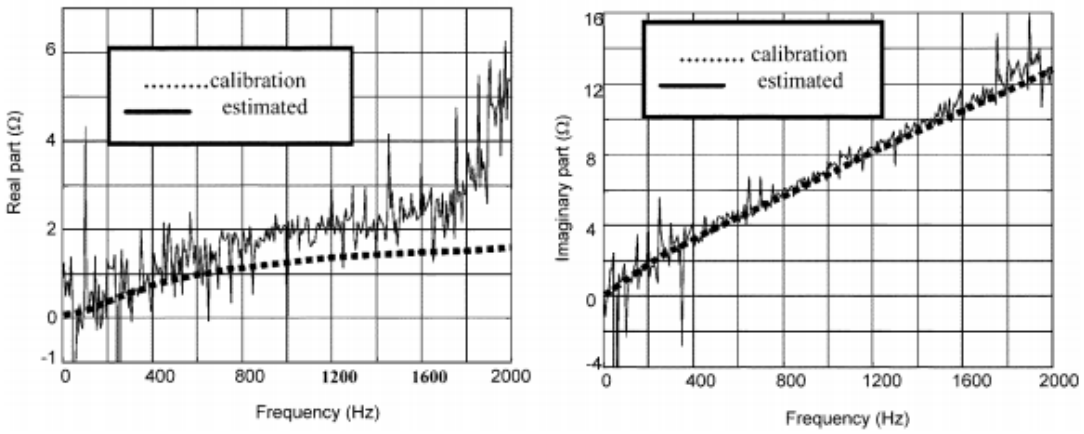

Figure 28: Transient active impedance estimation results (taken from [31])

The authors present the results of a larger-scale test using a 45 kW ASF, connected to the PS through an autotransformer. The setup is similar to the simulations discussed earlier. In this case the impulse lasts 500 µs. Like before, 160 ms of data before and after injection are needed to remove the supply's impact. The impedance expected to be obtained is the combination of that of the autotransformer used in series with the actual laboratory supply impedance – another transformer. For comparison, this was also independently measured using a steady-state method, repeated at a number of frequencies. The results of both methods match quite closely, with some discontinuities at the harmonic frequencies. This is due to the presence of background harmonic voltages that interfere with the method. The results are shown in Figure 28.

A 'worst-case' circuit is used in testing – a large inductor in series that attenuates high frequency currents – and nonetheless the performance of the impedance estimation is still good even with low SNR.

vi. Yazdkhasti et al.

In [20], the authors propose a scheme for TEI based islanding detection. The results of this work have already been discussed in subsection 2.3.4i. The scheme is somewhat difficult to categorise. Essentially, it involves estimation of PS TEI using voltage and current harmonic magnitudes. These magnitudes are determined through DFT calculations. However, the authors propose that existing harmonics measured at the PCC can be used to measure TEI, removing the need for injection. While this is theoretically possible, any existing harmonics must in fact be injected or drawn by the power converter itself. Hence, the method is effectively an active method. Furthermore, no information is given regarding which harmonics are expected to be normally present, whether they are of sufficient magnitude for measurement and their expected variation with time. Although the authors present some limited test-circuit results, this method is clearly still far from practical implementation.

vii. Authors considering THD

One author investigates voltage distortion caused by injection and its effects on THD. Specifically, the effect of the repetition ratio on THD is investigated [27], which is a commonly overlooked aspect. In [32], a Luenberger observer is used to inform the system of when a PS impedance change is detected and only then is estimation done. Thereby, current injection is done much less often, causing lower PS distortion. In fact, the approach used in [32] is similar to that done by M. Ciobotaru et al., as it is an intermittent pulse injected at the zero crossings as well. In this case, it is applied to all three phases (see Figure 29).

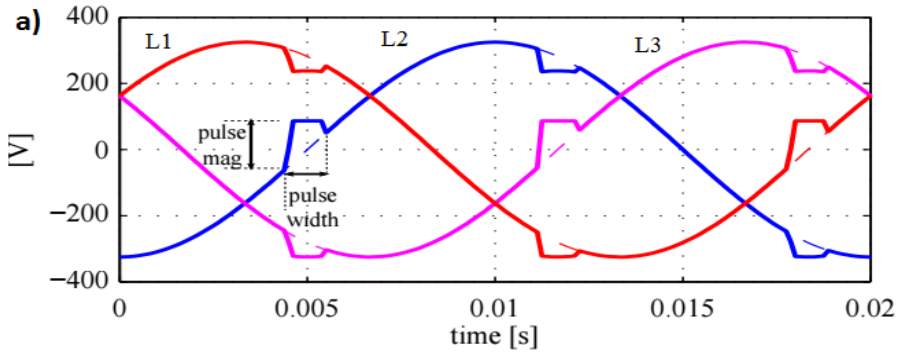

Figure 29: 3-phase zero-crossing injection done in [32]

viii. Sumner et al.

In [33], the authors present an 'ultra-fast' impedance estimation technique based in a PV inverter with ASF. It is done using a transient active method. The injection is performed using the ASF filter, resulting in a 1 ms, 20 A peak current spike.

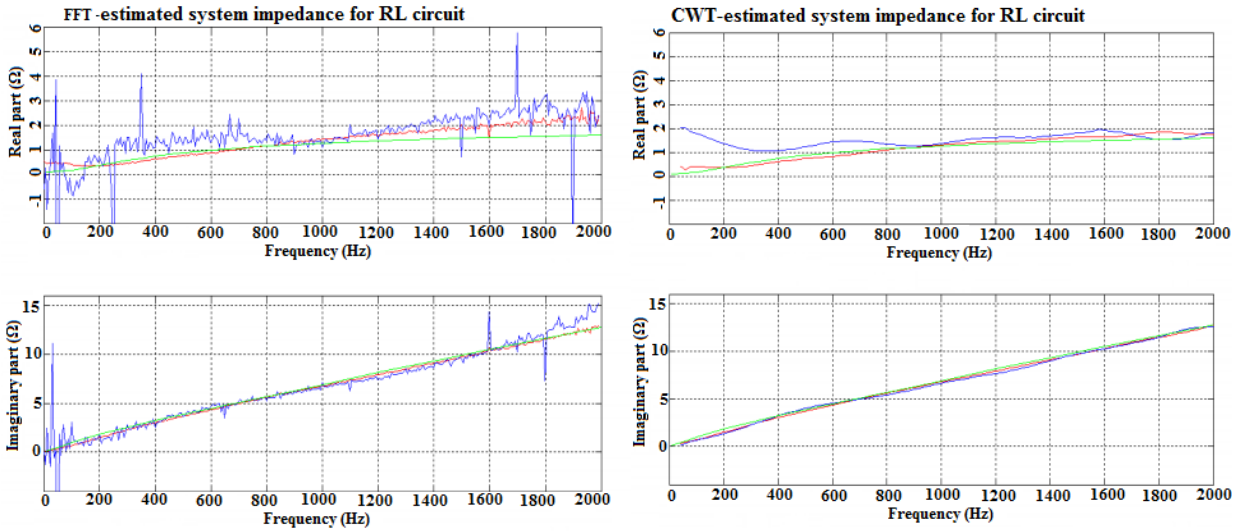

Figure 30: DFT (left) and CWT (right) estimated system impedance from [33]
Blue – FFT or CWT w/ PS connected, Red – FFT or CWT w/PS disconnected, Green – calibration equipment w/PS disconnected

The paper builds on the work presented in [31] by reducing the data capture period from 160 ms to about 20 ms. This is done through use of a continuous wavelet transform (CWT) rather than a DFT, to determine the PS impedance every half cycle of 50 Hz. Figure 30 shows a comparison of the practical TEI estimates of the PS (via isolation transformer connection) using DFT, CWT and calibration equipment for a range of 0-2 kHz. This is only one case of a number of connection circuit configurations used in the paper. Clearly, the CWT method provides results comparable to the slower DFT method, which are also smoother. With the supply disconnected, the calibration results can be compared to that of the DFT and CWT approaches, in which case the CWT approach's error is significantly lower. The performance at low frequency is also much better. The authors do not explain why the case of calibration equipment measuring impedance *with the PS connected* was not included.

The authors highlight the significant contribution that this improved TEI estimation method is expected to have on protection and islanding of DG systems, harmonic compensation equipment (including active filters) and power converter control and potentially voltage support using power converters. The results of the PS TEI estimation produced were applied in on-line active filter control.

3.2.2 Summary, limitations and implications of past results

The results and findings discussed in this section give a good, broad view of the state of the literature on this topic. We see that the active method, although simple in its theory, sees a great deal of variability in its implementation.

Most authors have used power converters in their implementations, with the exception of Palethorpe et al in [31]. These devices are clearly capable of performing TEI estimation in an on-line context.

Almost every implementation is different in terms of the nature of the current injection. For the steady-state sub method authors used:

- 400, 500 and 600 Hz at about 6 A RMS in [2], injecting one cycle at zero-crossings of fundamental, single and dual harmonic
- 75 and 125 Hz at 3 A in [29], continuously injected, dual harmonic
- 75 Hz at 1.5 A in [27], single harmonic, continuously injected

In the case of transient methods, there is overlap between frequencies investigated due to its wideband nature and the current magnitude used is much greater than the steady-state methods due to the need to spread signal power over a wide band of frequencies.

- 0-100 Hz in [30], injection current magnitude not specified, 1 s duration
- 0-2 kHz in [31], 60-100 A peak current spike, 625 μs duration
- 0-2 kHz in [33], 20 A peak current spike, 1 ms duration
-

The details of the injection current, such as which harmonics to inject, how often to inject them and how to measure the response, are clearly not agreed upon by the literature – many different variations are available. In terms of injection frequency, the only guidelines provided are that the frequency of injection is not an existing harmonic frequency, is not too close to the fundamental frequency and is not at the PS's resonance frequency. In terms of the current magnitude, there is a compromise to be made between SNR and disruption of power quality. However, only one author was found that attempted to investigate this relationship [27].

The type of waveform to inject (in the case of transient sub-method) or what magnitude and frequency to use (in the case of steady-state sub-method), are not defined. Furthermore, little to no evidence is provided of the degree of effectiveness of each TEI estimation implementation. Each implementation, if at all tested practically, is usually validated by simply comparing the static design information of the connected circuit to the measurements obtained. It is common for no consideration to be given of the dynamics of a real PS – one whose impedance may change over time considerably and in unexpected ways. Simulations are not made thorough enough to prove that the implementations are robust in a practical sense. These are among the greatest limitations in the work reviewed.

The question of what degree of nonlinearity exists in the PS and how this affects the pertinence of the measured TEI parameters has not been addressed in the literature.

The transient injection methods provide insight into the impedance – frequency relationship. From the results seen, the relationship is considerably linear over the range of 0-1 kHz. As was the case in subsection 3.1.2, there is almost no discussion of how the PS's TEI is expected to vary over time.

4. Methodology

4.1 Setup – Stage 1

4.1.1 Testing overview

The testing of the three-phase PV-inverter based TEI estimation device was separated into several independent tests, each designed to produce results for analysis of a specific aspect of interest and to answer specific research questions. They are:

1. Long sensing test:
   - performed to obtain typical values of the TEI of the PS (Z_{th}) and to produce data regarding how this impedance behaves over a long time period.

2. Changing phases test:
   - performed to check that the operation of the device is uniform and consistent across the three phase modules of the inverter

3. Injection current analysis:
   - performed to verify that the injection current produced by the inverter is as expected.

4. Temperature effects test:
   - performed to investigate variation of resistor bank resistance due to heating effect of injected current. This is in anticipation of resistor bank switching.

5. Variation of injection current ($|I_{inj}|$) test:
   - performed to investigate the relationship between the magnitude of injected current and the determined TE resistance (R_{th}). The accuracy of determined TEI is tested for each magnitude level for comparison.

6. Variation of modulation frequency (f_m) test:
   - performed to investigate the effect of changing the frequency of injected harmonics on the determined TE resistance (R_{th}). The accuracy of determined TEI is tested for each frequency level for comparison.

The results of each separate test described above are contained in Chapter 5.

4.1.2 Equipment

- Prototype Thévenin sensing equipment consisting of:
    - Inverter 1 (Sensing/ “the device”) – 24 kVA Powerstar inverter set to inject a 50 Hz current modulated at 12.5 Hz (variable) on all phases, measure voltage changes, calculate the Thévenin equivalent resistance and reactance and communicate it to external device.
    - Inverter 2 (Injecting) – 24 kVA Powerstar inverter that can inject current from the battery bank into the PS. Current magnitude in each phase can be varied independently and set via communication to an external device (Logging PC in this case).
    - Inverter 3 (Charging) – 24 kVA Powerstar inverter set to charge battery bank continually from PS supply.
    - Battery bank – 900 Ah, 48 V
- Yokogawa 2755 Wheatstone Bridge
- Yokogawa WT1800 Precision Power Analyser
- Desktop PC, fitted with:
    - 2 Channel USB to COM converter and cables
- 4 x steel strapping resistor bank
    - Each made up of 5 resistors with connectors, total series resistance approximately 0.15 Ω each
- 6 x 45 A CB’s

4.1.3 *Diagram*

The setup in the Machines Lab is illustrated by the diagram in Figure 31 below:

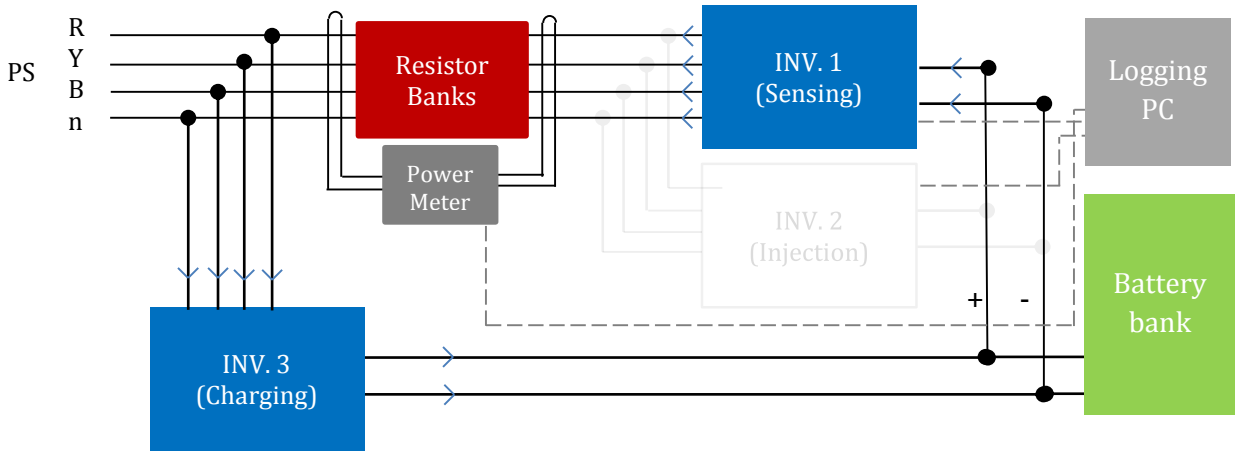

Figure 31: General inverter setup

Inverters 1, 3 and the battery bank form the 'equipment' referred to earlier and together enable the TEI determination. The injection inverter (2, greyed-out) delivers power to the PS in a novel way, based on information provided by the sensing inverter (1). The functionality of inverter 2 is not of interest. As a result, it is turned OFF and plays no part in the testing. Inverter 3 is placed before the resistor banks so that the charging current does not contribute to losses in the resistor banks or significantly affect the Thévenin parameter sensing of Inverter 1.

4.1.4 *Inverters*

i. General

The three-phase sensing inverter is essentially made up of three independent single-phase inverters. These modules each work with one of three phases of the PS as input and are hence intended to operate in a symmetrical manner. The inverter senses the PS's parameters (Z_{th}, R_{th} and X_{th} for each phase and neutral) and logs a sample point every 10 seconds. The first five seconds are spent injecting symmetric currents on each phase that cancel at the common point and measuring the voltage response on each phase, thereby, determining $R_{th\,R}$, $R_{th\,Y}$ and $R_{th\,B}$ (R_{th} of red, yellow and blue lines). The next five seconds are used to determine the neutral $R_{th\,n}$. This is done by injecting current only on the red line; effectively measuring the series combination of $R_{th\,R}$ and R_n. $R_{th\,R}$ is then simply subtracted from this value to give R_n.

The sensing inverter is unlike a standard inverter product that is available on the market, only in that its software has been modified for the TEI estimation application.

The device has a user interface for some functions and parameter variation and can also be communicated to via debug port. This is useful for changing parameters quickly during a test, such as the RMS of injected current. A second port, Modbus protocol, is connected to the laptop for logging purposes. Custom software on the laptop instructs the device during logging, culminating in a .csv file output with raw data of the Thévenin parameters, as well as timestamps, at the end of each test.

The charging inverter simply keeps the battery bank charged, which provides a source of power for the sensing inverter's injection. Through comparison of measured TEI before and after connection of charging inverter to the grid, it was found that the use of this inverter did not have a noticeable effect

on the measured TEI. This is despite the fact that it is an added load in parallel with the PS, hence it appears that the inverter's equivalent impedance is high compared to the grid.

ii. Hardware

The hardware of the device used for TEI estimation was described in subsection 2.6.3 and 2.6.4.

iii. Software

The process by which the inverter obtains the TEI of the grid is through a patented method involving dual harmonic injection, done in the direct-quadrature (DQ) domain. It is essentially an amplitude modulation (AM) method, much like that used in AM radio technology. In fact, it is very similar to that presented in subsection 3.2.1iii. In understanding the process we begin by considering a single phase only.

Modulation

The inverter's target for the D component of the injection current is normally a constant RMS value, set according to the level of power to be injected into the grid at the grid frequency. We use $\left|\mathrm{I_{inj}}\right|$ to denote this target, the PS frequency is f and t is the time in seconds. Hence, the inverter will attempt to output a current of the form:

$$I = \sqrt{2}\left|\mathrm{I_{inj}}\right| \sin(2\Omega f t) \qquad (3.1)$$

Hence, when $\left|\mathrm{I_{inj}}\right|$ is set to 1 A, the inverter injects current of 1 A RMS at the PS frequency. Up until this point, we have been describing normal PV-inverter operation.

Now, for dual harmonic injection by the AM method, the A target is simply multiplied by a low frequency sinusoid. Note that this 10 Hz signal is not synchronised to any other signal. We call this low frequency the modulating frequency, f_m. The LF signal is of the form:

$$\sin(2\Omega f_m t) \qquad (3.2)$$

Hence, the new current will be (3.1) x (3.2):

$$I = \sqrt{2}\left|\mathrm{I_{inj}}\right| \sin(2\Omega f t)\sin(2\Omega f_m t) \qquad (3.3)$$

The same modulating (LF) signal is applied to the three phases of the inverter. In order for the proportional-integral (PI) controller to track the requested output signal well, the gains must be changed. This is because the 10 Hz envelope causes the current to experience more rapid changes than would be experienced with just a steady magnitude 50 Hz signal. Hence, the PI controller gains are increased appropriately to obtain a smooth output.

Demodulation

The demodulation process resulting in extraction of TEI parameter data is under patent review hence it is not provided. They may later become available in an additional section - 'Appendix N'.

4.1.5 Resistor banks

The resistor banks play a key role in the testing process. The purpose of the resistor banks is to effect a change in the TEI of the PS by changing the series resistance in each line. Then, by comparing the measured changes in resistance to our known resistance, we can evaluate the accuracy and precision of the Thévenin parameter measurement. Having a separate resistor bank in each line allows us to independently change the line's TEI and investigate unbalanced conditions.

The resistor banks are simply a bank of series resistors placed into each line (including neutral) with switches (CB's are used) within them allowing us to vary the line's Thévenin resistance (R_{th}) parameter. The circuit diagram of a resistor bank is very simple, as shown in Figure 2.

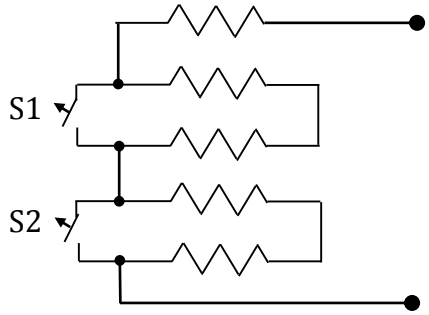

Figure 32: Resistor bank circuit diagram

Switch position		Resistor Bank Resistance (mΩ)
S1	S2	Rbank
ON	ON	≈50 (low)
OFF	ON	≈100 (med)
ON	OFF	≈100 (med)
OFF	OFF	≈150 (high)

Table 1: Resistance possibilities of bank

The approximate value of the resistance states of a given bank, including leads and all connections is shown in Table 1. Actual resistance states of each bank's resistors as measured using the Yokogawa wheatstone bridge are provided in Appendix A. In this stage of testing RB_1, RB_2... RB_4 refer to the separate resistor banks and typically RB_1 will be used in the red line, RB_2 in yellow … and RB_4 in the neutral (see Figure 33).

4.1.6 Power Analyser Setup

A Yokogawa WT1800 power spectrum analyser is used to log data regarding phase currents, voltage across the resistor banks, their resistance, power losses within them and the total power lost over the four banks. It is connected as shown in Figure 33 below:

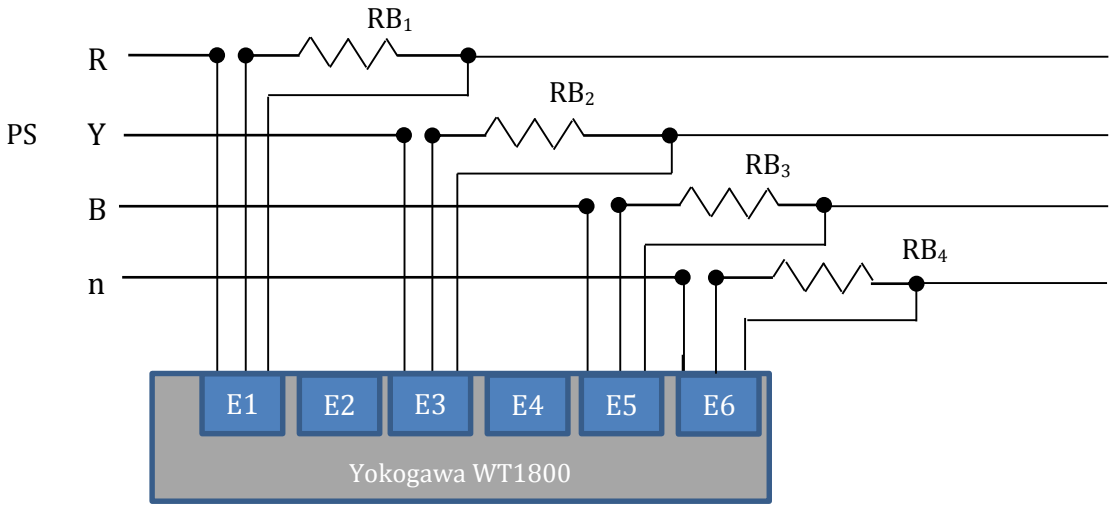

Figure 33: Yokogawa power analyser connection diagram

The connections in Figure 33 are unchanged from the proof of concept test. In the current case, power lost in the resistors is not a concern but we are able to extract line current waveforms, which are of interest.

4.1.7 *Photographs of setup*

Figure 34 and Figure 35 below show photographs of the setup used for testing, as described earlier. In Figure 34 the three inverters are clearly visible with the MLT logo, from left to right: Inverter 1 (charging), Inverter 3 (injection), Inverter 2 (sensing). In the background are the battery banks, covered with a wooden panel. The Yokogawa Power Spectrum Analyser sits on the table, along with all four resistance banks.

Figure 34: General setup photograph, excluding logging PC

Figure 35 below shows a wider view of the testing setup. The logging PC is shown on the far left and some of the connections between the devices are seen under the table.

Figure 35: General setup photograph, including logging PC

4.2 Setup – Stage 2

4.2.1 Testing overview

The testing of the device was separated into several independent tests. Some may appear to investigate the same property or simply be a repeat of the tests done before. In these cases, this is done in order to give a clearer picture of some subtle phenomena identified previously, as well as to compare and verify results from the previous stage.

The tests address different areas of interest. A brief outline is given below each test's name.
They are:

1. Power system voltage analysis:
    - Performed to measure PS voltage at MLT and its behaviour in order to understand its potential effect on the inverter's operation. Also allows us to see the voltage components resulting from injected current.
2. Injection current analysis:
    - Performed to measure inverter current waveforms for different requested magnitudes and frequencies, so as to see whether waveforms are as expected and identify any distortion so as to anticipate its effects on results.
3. Steady-state (constant impedance) measurement performance of ports:
    - Essentially involves measuring the same phase with different inverter ports to compare parameters obtained.
    - Done to compare with previous results and to understand/correct for the influence of differences between the separate inverter's modules on results, if possible.
4. Dynamic (impedance change) measurement performance of ports:
    - First look at inverter's ability to measure known resistance and reactance changes on each line.
    - Done to understand and correct for influence of separate inverter modules on results.
5. Long sensing test:
    - This test is performed to obtain typical values of the Thévenin equivalent impedance of the PS and to produce data regarding how this impedance behaves over a long time period.
6. Variation of injection current magnitude ($|I_{inj}|$) test:
    - This test is performed to investigate the relationship between the magnitude of injected current and the determined TEI. The accuracy of determined TEI is tested for each magnitude level for comparison.
7. Variation of modulation frequency (f_m) test:
    - This test is performed to investigate the effect of changing f_m of injected current on the determined TEI. The accuracy of determined TEI is tested for each frequency level for comparison.

The results of each separate test described above are contained in Chapter 6.

4.2.2 Equipment

i. Equipment common with previous testing stage

- Prototype Thévenin sensing equipment consisting of:
    - Inverter 1 (Sensing/ “the device”) – 24 kVA Powerstar inverter set to inject a 50 Hz current modulated at 12.5 Hz (variable) on all phases, measure voltage changes, calculate the Thévenin equivalent resistance and reactance and communicate it to external device.
    - Inverter 3 (Charging) – 24 kVA Powerstar inverter set to charge battery bank continually from the PS supply.
    - Battery bank – 900 Ah, 48 V
- 4 x steel strapping resistor bank
    - Each made up of 5 resistors with connectors, total series resistance approx. 0.15 Ω each
- 6 x 45 A Circuit breakers (CB's)

ii. Equipment not used previously

- Agilent MSO-X 3014A Mixed Signal Oscilloscope, along with:
    - 3 x Agilent N2791A 25 MHz Differential probe
    - 3 x Keysight 1146B 100 kHz/100 A Clamp-on current probe
    - USB Flash drive (for saving results)
- Toptronic T48 Digital Multimeter
- 2 x Isotech IDM72 Digital Multimeter
- Laptop PC, fitted with:
    - 2 Channel USB to COM converter and cables
- 4 x inductor banks (designed for MPPTs)
    - Each made up of 2 inductors, all inductors approx. 0.101 mH each
- 6 x 45 A Circuit breakers (CB's)
- Digital Vernier calipers

4.2.3 *Diagram*

The setup at MLT's premises is illustrated by Figure 36 below:

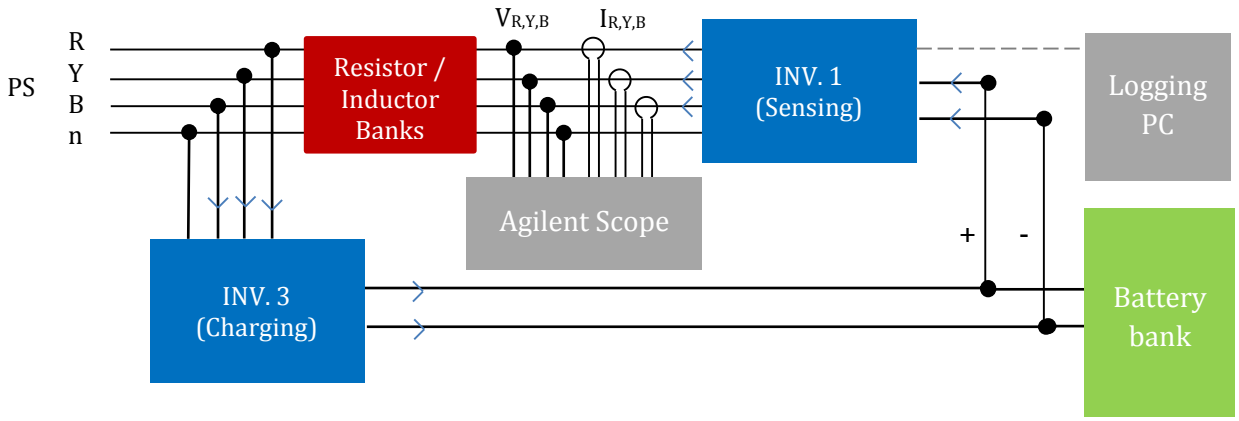

Figure 36: General inverter setup

It is similar to that shown in subsection 4.1.3.

Again, Inverters 1, 3 and the battery bank form the 'equipment' referred to earlier and together enable the TEI determination. The inverter's software is unchanged and hence the process by which the TE parameters are obtained is also the same.

4.2.4 *Resistor banks*

The resistor banks are the same as those involved in the previous stage of testing. They have been described in section 4.1.5.

There is a possibility that during storage or transportation between the two testing locations a connection was loosened or moved. Thus, the resistor bank's resistance needs to be verified before further use. It is extremely important that our resistance measurement is accurate, as all the tests involving resistance change measurement by the Thévenin device will be compared to these.

As a check, all connections were verified to be tight and proper, after which the resistance of the banks was measured using a new method involving multimeters and a signal generator, due to unavailability of the Wheatstone bridge. The details and results of this can be found in Appendix H.

4.2.5 *Inductor banks*

The inductor banks used were originally intended for use in maximum power point trackers (MPPTs), a commonly used device in solar PV installations. An image of one bank is shown in Figure 37 below:

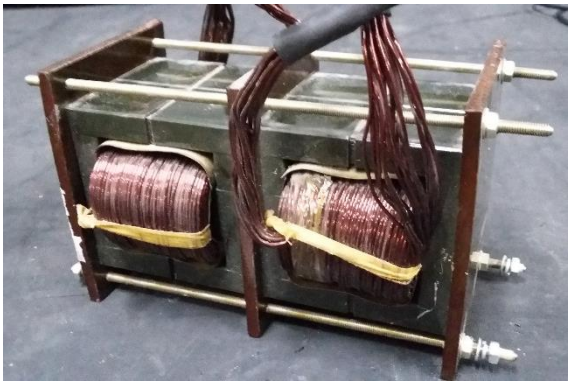

Figure 37: Photograph of Inductor bank

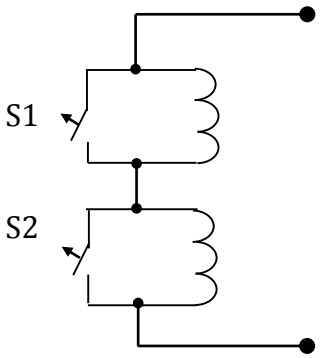

Figure 38: Inductor bank wiring diagram

Each inductor's inductance and resistance were 0.1 mH and 3.3 mΩ. Each inductor bank contains two inductors. Their detailed specifications and measured inductance (obtained using T48 DMM) are shown in Appendix I.

The inductor banks were wired with short lengths of additional cable so that the circuit breakers could be used to switch between a) both inductors in the line, b) one shorted out or c) both shorted out. The circuit diagram is shown above in Figure 38. This allows switching of line reactance, as was done with resistor banks in the previous stage of testing. In this setup, each inductor bank gives a potential for two steps of 31.4 mΩ reactance each, as well as 3.3 mΩ resistance. We cannot avoid adding/removing a small amount of resistance to the line when switching the inductor bank as it is an inherent property of the winding. The modular nature of the inductor banks allowed us to easily put several in series to have a larger range of reactance variation, if needed.

4.2.6 *Oscilloscope Setup*

i. General

The oscilloscope's setup is shown in Figure 36, although that representation is somewhat conceptual. The actual oscilloscope has only 4 input channels, hence, 3 phase current and voltage cannot be measured simultaneously. Unlike the Yokogawa WT1800 used in the previous testing stage, this oscilloscope cannot log data continuously. Data collected from the oscilloscope is the data that appears on the oscilloscope's screen and hence is limited by the window size of the oscilloscope. Waveforms are saved as either .png image files of the oscilloscope's current display or as .csv files of the raw data currently being displayed by the oscilloscope. Results were saved to USB and then transferred onto the laptop for analysis.

ii. Sampling rate

Another fact to note about the oscilloscope is that its sampling rate is not something that can be set. The oscilloscope instead assigns a sampling rate based on the window size chosen (the period of data collected) and the size of its memory. Since it is intended that waveforms collected by the oscilloscope be closely analysed, a high resolution was required. It was decided that at least 20 samples per cycle (50 Hz) is required and therefore the sampling rate must remain above 1 kHz.

iii. Calculations/FFTs

The oscilloscope's math functions were also used during this investigation. Parameters such as standard deviation and average RMS can be taken over many window periods, allowing us to characterise the steady-state behaviour of the line voltage. An example of the oscilloscope's visual output in this function is shown in Figure 39 below.

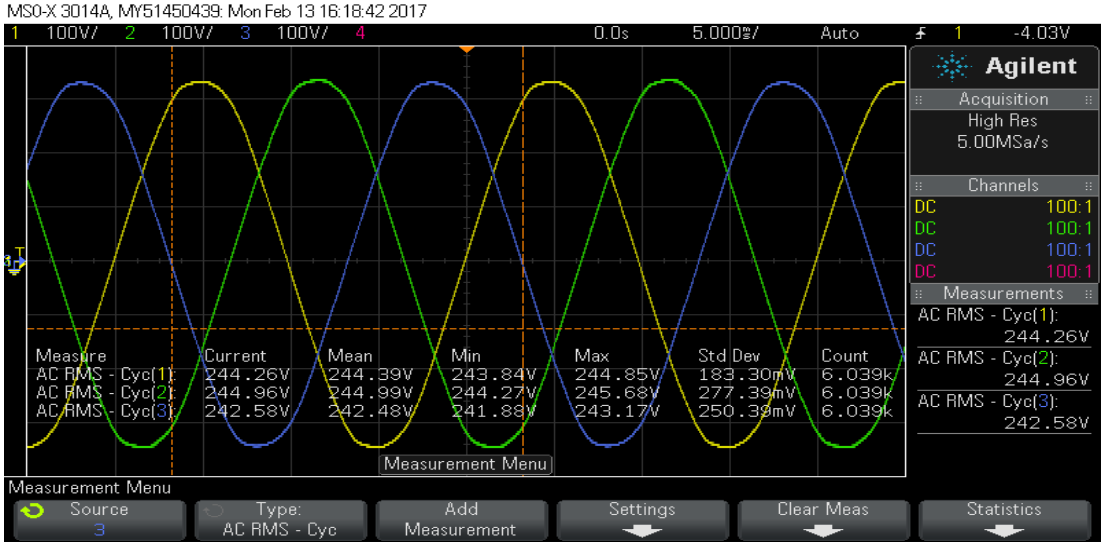

Figure 39: Oscilloscope's measure function – measuring RMS voltages

Several FFT's were taken using the oscilloscope's math function. In all of these a Hanning window was used by default, as well as a V RMS vertical scale (rather than Decibels). The FFT resolution is, like the sampling rate, based on the chosen window size. The same window size is used throughout the FFTs displayed in this report (2 s) thus all FFTs have the same resolution of 238 mHz. An example of the oscilloscope's visual output in this function is shown in Figure 40 below.

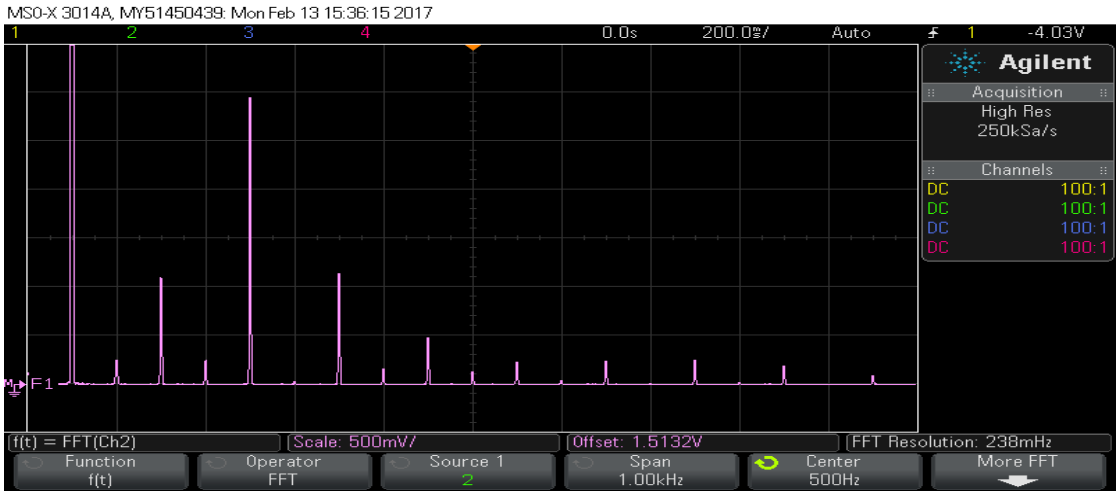

Figure 40: Oscilloscope's FFT function – viewing voltage harmonics

4.2.7 *Photographs of setup*

Figure 41 and Figure 42 below show photographs of the setup used for testing, as described earlier. In Figure 4 from left to right: Logging PC, Inductor banks, Agilent oscilloscope and current clamps, a resistor bank and on the far right the Thévenin sensing inverter. Above the Agilent oscilloscope is the three phase PS socket that the sensing inverter is injecting into. The battery banks lie beneath the table and the battery charging inverter is to the left, not visible. It is connected to a separate PS socket. Figure 42 shows the resistor and inductor banks and their wiring more closely.

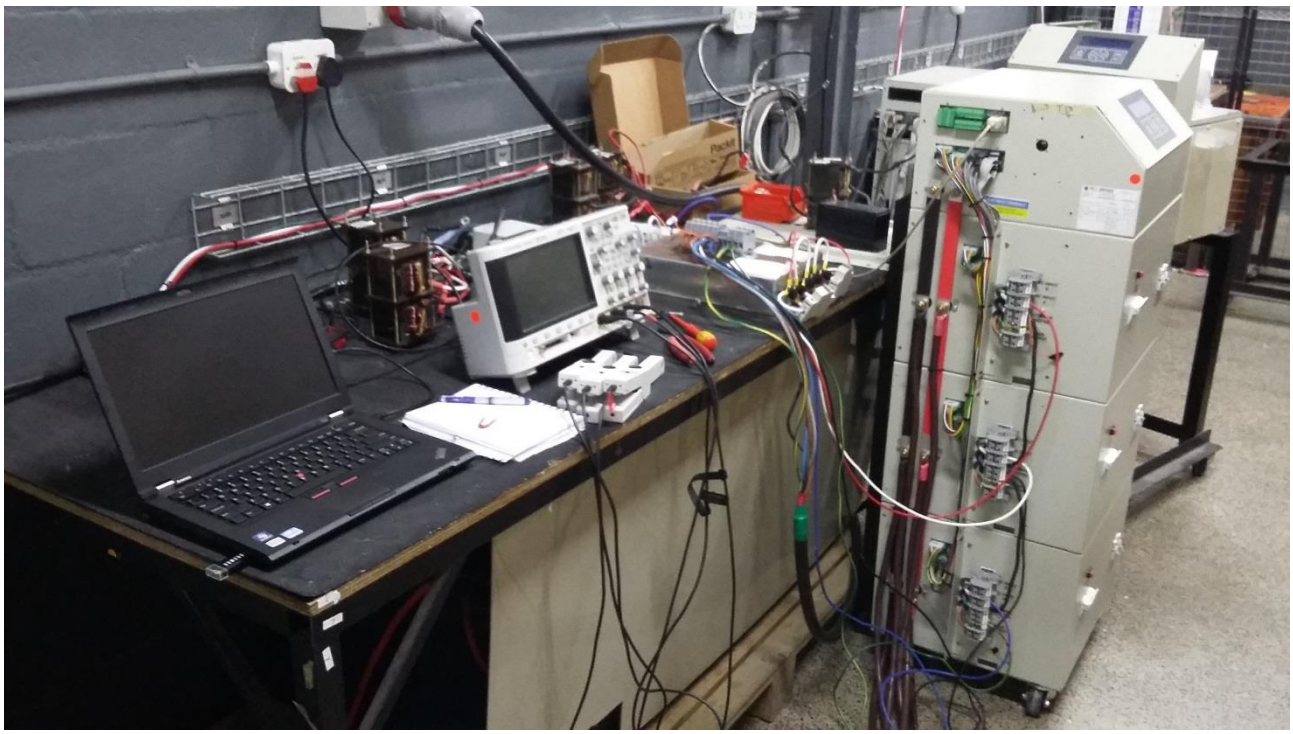

Figure 41: General setup photograph

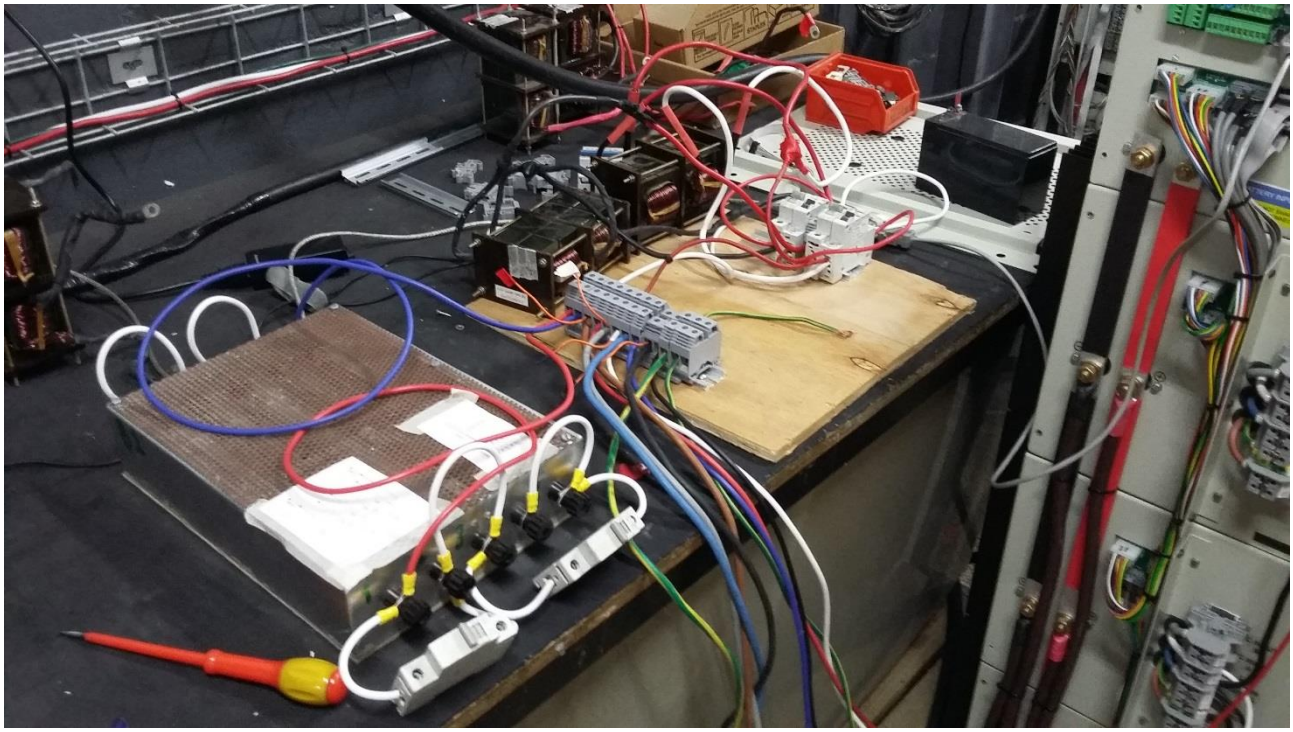

Figure 42: Resistor and inductor bank setup photograph

4.3 Setup – Stage 3

4.3.1 Testing overview

The tests performed are:

1. Evaluation of performance with optimised parameters:
    - Performed to check that the device shows high level of performance at optimised parameters.
2. Comparison of device-determined and oscilloscope-determined impedance:
    - Performed to compare the device's performance to another method that is known to be very accurate.

The results of each separate test described above are contained in Chapter 7.

4.3.2 Equipment

All equipment used is a subset of the equipment of Stage 2 (section 4.2.1)

4.3.3 Diagram

Identical to that of Stage 2 (section 4.2.3)

4.3.4 Resistor banks

Identical to that of Stage 2 (section 4.2.4)

4.3.5 Inductor banks

Identical to that of Stage 2 (section 4.2.5)

4.3.6 Oscilloscope setup

Identical to that of Stage 2 (section 4.2.6)

4.3.7 Photographs of setup

Figure 43: Photograph of testing stage 3 setup (very similar to stage 2)

5. Testing –Stage 1

5.1 Long sensing test - description

The PS is a dynamic system and it is expected that the Thévenin parameters should vary as loads and sources are connected and disconnected from the PS during normal daily operation. Few similar tests on a live PS are known to have been conducted (as discussed in the Literature review), let alone in South Africa, and thus it is not known how the PS's parameters behave and vary under normal conditions. Hence, it is important to gain a clear picture of this as our first step so that there is some understanding of what normal behaviour looks like. If there is a daily profile that can be extracted from the variation in parameters, further testing can be planned to characterise it and "normalise" our data such that the effect of this variation is taken into account.

5.1.1 Test parameters and procedure

Test date: 9/06/16 Duration: 06:00:00 Elapsed from: 09:11 – 15:11
Modulation frequency (f_m): 12.5 Hz (**standard**)
RMS injection current ($|I_{inj}|$): 12.0 A (**standard**)
Resistor banks: **Minimum resistance (≈50 mΩ)**

Controllable input factors: f_m, $|I_{inj}|$, time of day, resistance in lines
Uncontrollable input factors: ambient temperature, loading and state of PS
Responses: TEI parameter variation

The choice of injection parameter levels above is somewhat arbitrary. It is known that these parameters (12 A, 12.5 Hz) perform well in tracking line resistance changes relatively accurately, as a result of prior simple resistance bank switching trials. They may not be optimal (as further testing is likely to show) but they are good enough for obtaining a "first-look" at the PS's behaviour. We use these same parameters in several tests for ease of comparison of any potentially interesting results. These parameters remain the same for the duration of this test (are blocked) in order to focus on variation that is due to uncontrollable input factors, especially the loading and state of the PS. The resistance in each line is also kept constant.

The minimum resistance of the bank is chosen so as not to offset the PS's R_{th} value by a large amount. The duration of the test is made considerably long, so as to allow for slow variations to be visible. This large timespan gives a good idea of what can be expected in future tests. The time of day was arbitrarily chosen as a 'first look', based on the argument that if there is any significant daily variation it should become apparent from the results of this test.

5.2 Long sensing test – results

5.2.1 Parameter variation over 6h

The plot of the obtained TE resistance of each line ($R_{th\ R}$, $R_{th\ Y}$, $R_{th\ B}$) and the neutral ($R_{th\ n}$) over the six hour testing period is shown in Figure 44 below. The inverter injects current and obtains a new sample point for the resistances every 10 s.

Figure 44: Long sensing test results – Raw data

Before we consider the results in Figure 44, it should be kept in mind that the resistance parameters measured include a 50 mΩ component due to the resistor banks (which are in each line on minimum resistance setting).

Several interesting points can be made from the plot in Figure 44. Firstly, we see that the general level of the parameters is of the order of 100 mΩ. Secondly, we should notice that the resistances of the lines are not close to being balanced. There is a significant difference between the TE resistances of each line at any given point. Considering that the line's parameters are actually 50 mΩ less than what is presented in Figure 44 (RB contribution), the imbalance should actually be more severe. In fact, if we take into consideration the contribution of actual resistance of wires used locally (approx. 55 mΩ, see Appendix B) to connect to the DB in the Machines room and subtract that component, we can see that the imbalance within the PS appears to be significant.

The neutral resistance is seen to be much lower than the resistances of the lines. This is interesting, as it goes against expectation. Seeing as the neutral wire in a given PS is expected to carry considerably less current than the line wire, it has a smaller cross section and thus, greater resistance. It is expected that injection on three phases may be causing an impedance overestimate. The behaviour of the neutral resistance is also seen to have a clear link to the red phase. They both seem to vary in opposite directions simultaneously by similar amounts throughout the test.

In terms of variation, it is clear that the TE resistance of all lines and neutral did not experience large changes during the six hour period. Spikes did occur often on all lines and neutral but they appear to be inconsistent and random, suggesting that they are caused by some source of noise. Overall, there was not much deviation from the average in each plot. The higher frequency variation (noisy spikes) is interesting to consider as it is clearly not of the same degree for all lines and neutral. The blue phase appears to exhibit the largest amount of fluctuation, followed by the neutral, whilst the yellow phase exhibits least. It is also interesting that the spikes on the blue phase seem to be greater in the positive direction than in the negative.

There also appear to be slower variations, most visible in the red phase during the first hour.

Figure 44 is plotted again below as Figure 45, in this case with the averages shown for each plot as well as the standard deviations are shown as error bars at the vertical gridlines. Their numerical values are given in Table 2. The statistical parameters show that the neutral has the most significant variation of almost 5 %, followed by the blue, red and yellow phases in that order. The difference in standard deviations could possibly be due to PS behaviour or even due to the inverter not treating each phase identically (especially since each inverter is effectively 3 separate units working together). This is investigated further in the next test (subsection 5.3). The graph is shortened vertically (begins at 80 mΩ) in the interest of saving space.

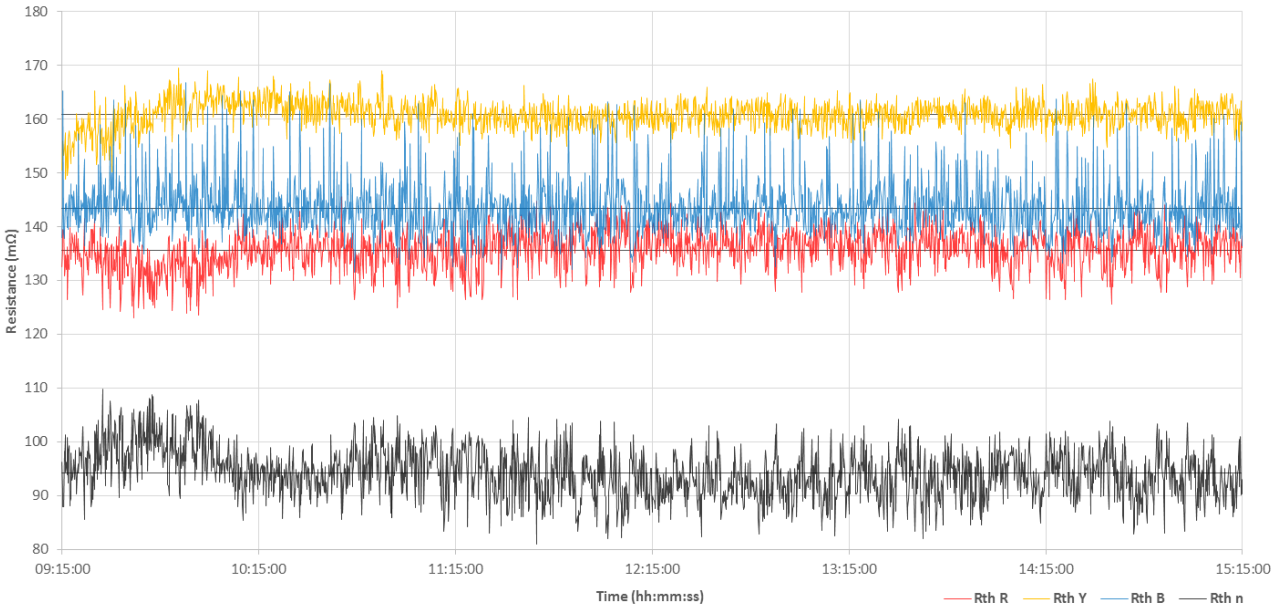

Figure 45: Long sensing test - Averages and Std. Dev. Shown

5.2.2 Parameter variation over first 20 min only

In order to get a close-up view, Figure 46 below shows only the first 20 min of the raw data. In it we can see more clearly the matching opposite behaviour of the red and neutral, as well as the large spikes on the blue phase, which seem to be unique to it and only in the positive direction.

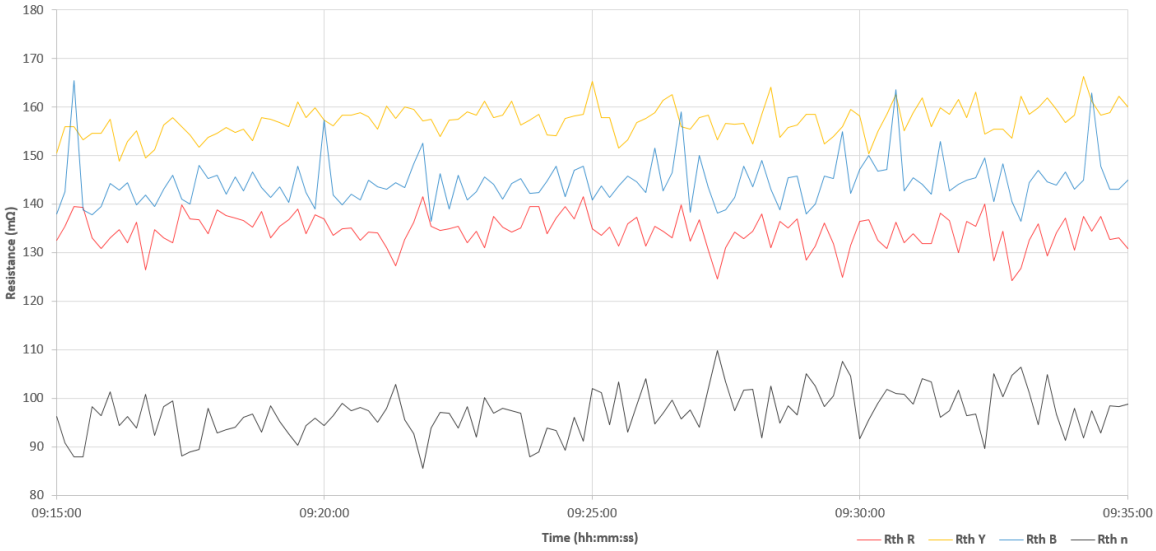

Figure 46: Long sensing test - Raw data - First 20 min only

The coupled behaviour of $R_{th\ R}$ and $R_{th\ n}$ (strong negative correlation – see

Table 3) is a direct result of the way in which the neutral's resistance is calculated, as explained in subsection 4.1.4i. In fact, if we add $R_{th\ R}$ and $R_{th\ n}$ together, effectively getting the measurement that is done with injection on only the red phase (second 5 s of 10 s period), we see a comparatively stable plot (see Appendix C) with a relatively low standard deviation of 1.09 %. This suggests that the fluctuations of $R_{th\ R}$, $R_{th\ Y}$ and $R_{th\ B}$ are due specifically to the method of symmetric injection. It would seem possible that the three phase currents are not exactly symmetrical and thus not cancelling at the common point. Indeed, if we take the Yokogawa line current data and add the three line currents, the sum is far from being zero (presented in subsection 5.6.2). This coupled behaviour also explains that the high standard deviation in Rn is mostly due to the deviation of the $R_{th\ R}$ measurement. When we 'normalise' it – divide it by the average value, it becomes much greater than that of $R_{th\ R}$ since $R_{th\ n}$'s average is small (as seen in Table 4).

5.2.3 Statistical analysis of 6h parameter data

The statistical parameters show that the neutral has the most significant variation of almost 5 %, followed by the blue, red and yellow phases in that order. The difference in standard deviations could possibly be due to PS behaviour or even due to the inverter not treating each phase identically (especially since each inverter is effectively 3 separate units working together). This is investigated further in the next test (subsection 5.3).

Table 2: Statistical parameters of long sensing test data

Colour:	Plot:	Average:	Std. dev.	Normalised Std. dev.
	$R_{th\ R}$	135.6	3.49	2.57 %
	$R_{th\ Y}$	160.9	2.48	1.54 %
	$R_{th\ B}$	143.5	5.12	3.57 %
	$R_{th\ n}$	94.2	4.62	4.91 %

The correlation between parameters is calculated and shown in

Table 3 below:

Table 3: Correlation between parameters from long sensing test data

Colours:	Parameters:	Correlation:
	$R_{th\ R}$, $R_{th\ Y}$	0.06
	$R_{th\ R}$, $R_{th\ B}$	0.37
	$R_{th\ R}$, $R_{th\ n}$	-0.85
	$R_{th\ Y}$, $R_{th\ B}$	0.16
	$R_{th\ Y}$, $R_{th\ n}$	-0.06
	$R_{th\ B}$, $R_{th\ n}$	-0.28

The most significant correlation is between the red phase and the neutral. It is strongly negative, showing that the neutral and red phase have similar behaviour that is "mirrored". Next, we see a weak positive correlation between red and blue phase, as well as weak negative correlation between blue phase and neutral. This seems to suggest that all three of these parameters are to some degree linked. The poor correlation of the yellow phase with other parameters indicates the absence of any linear association.

Figure 47 below shows a high-resolution histogram plot of the spread of each parameter about their respective means over the 6 h period, after a smoothing function is applied. This can be thought of as a representation of the "probability density function" for each parameter. It is clear from this figure that the data is spread quite symmetrically about the mean, with the exception of the blue phase which shows considerable asymmetry. Each paramter's distribution appears to be well approximated by a normal distribution. This supports the view that the TEI resistance of the grid remained quite steady over the entire period, and the use of the standard deviation in the analysis.

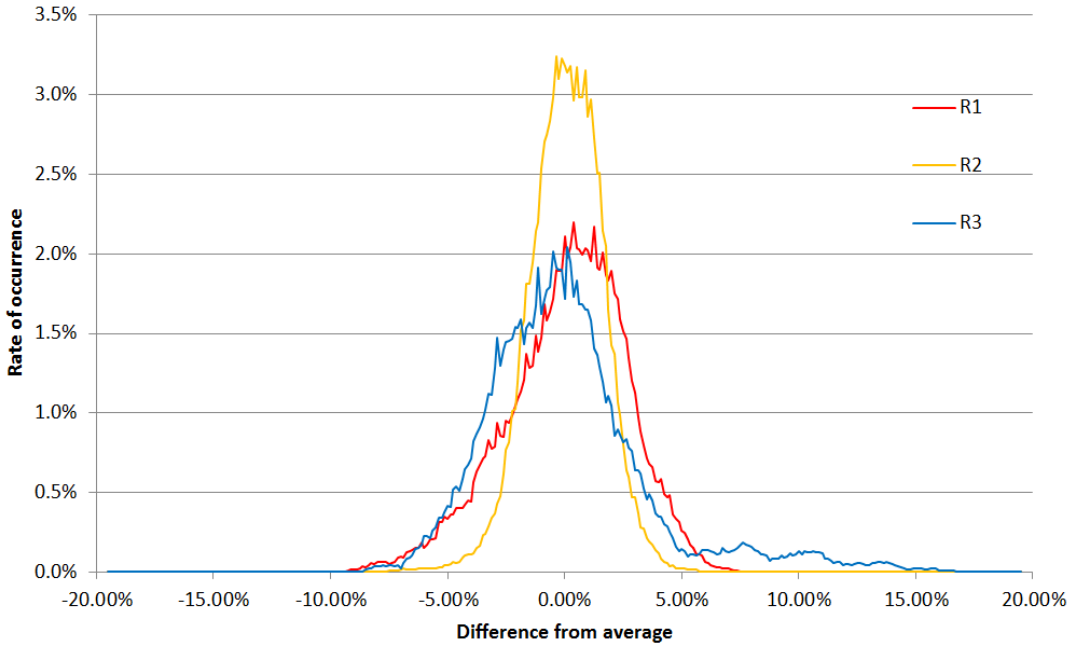

Figure 47: Distribution of parameters about mean over 6 h period

5.2.4 Recommendation for stage 2

This test was a success. Its repetition can provide data for comparison and verification of long term behaviour. A longer span of time for the test should be done if possible. It would be interesting to see whether another location would give different behaviour in the parameters and whether PS-side changes would be more pronounced. $|I_{inj}|$ and f_m should be optimised for the next long sensing test. It is also suggested that all resistor banks be removed from the lines so that only the PS's impedance itself is measured.

5.3 Changing phase rotation – description

The purpose of this test is to verify that the inverter's measurements across its three modules are consistent. That is to say, the inverter's three ports should all measure the parameters of any given line in the same way.

5.3.1 Test parameters and procedure

Test date: 17/05/16 Duration: 00:15:00 Elapsed from: 09:11 – 15:11
Modulation frequency (f_m): 12.5 Hz (**standard**)
RMS injection current ($|I_{inj}|$): 12.0 A (**standard**)
Resistor banks: **bypassed**

Controllable input factors: f_m, $|I_{inj}|$, time of day, resistance in lines, phase rotation, time delay between runs
Uncontrollable input factors: ambient temperature, loading and state of PS
Responses: TEI parameter variation

The inverter is simply left to log TEI data over a short period with no resistance in the lines. This is done once at normal phase rotation, then the next run is shortly after once the phase rotation has been moved one forward, then a third time at two phases forward. This way, each inverter port measures the TEI parameters of each PS phase for the same period. Hence, all controllable input factors are kept constant (blocked) between runs, other than the time of each test which was minimized to 5 min (unavoidable due to need for powering down and physical changing of the phase rotation between runs). From the long sensing test we have some information regarding the expected behaviour of the parameters and have an idea of how much the parameters can be expected to vary in a given time period. With this, we can take into account the separation in time between the three tests (about 5 min).

The standard test parameters are chosen - up until this point the ideal parameters for accurate TEI results are still not specifically known and 12 A, 12.5 Hz perform well according to a few trials. We use these same parameters in several tests for ease of comparison of any potentially interesting results. The test is very quick, as it is performed as a check before the next set of tests are done.

5.4 Changing phase rotation – results

The graph in Figure 48 shows the variation of the resistance of the red phase, as measured by the different inverter ports. The three plots on the graph are collected from three separate runs, as described earlier (subsection 5.3.1).

5.4.1 *R_{th} of red on each port*

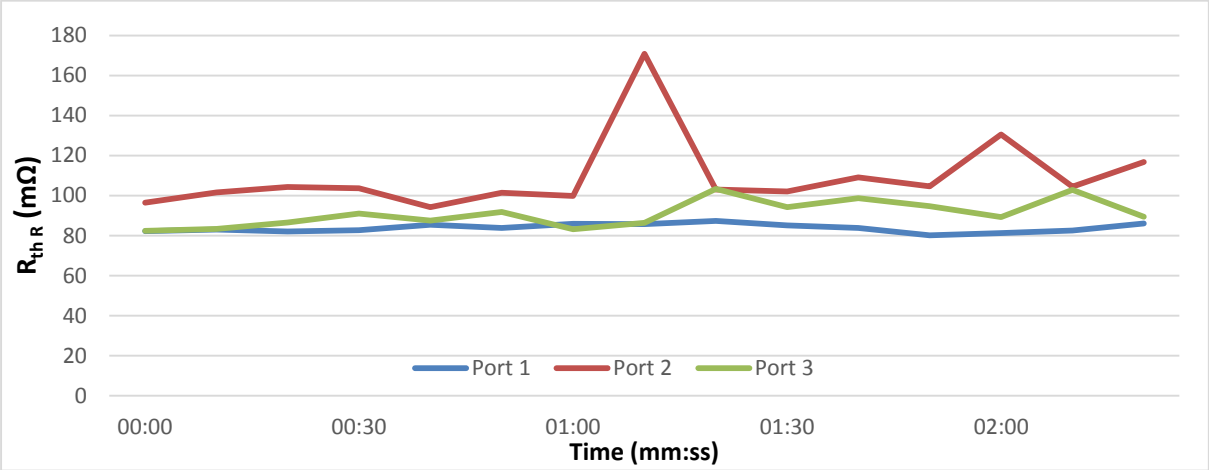

Figure 48: R_{th} of red phase measured by different inverter ports

The two upward spikes on port 2 are not accompanied by any simultaneous behaviour in the other two phases. Hence, they are considered to be anomalies that do not represent typical behaviour of the ports and are ignored.

It can be observed in the graph that the measurements taken by port 2 appear to be at a consistently higher level than that by port 3, and further by port 1. The average level of each port's measurements is, from lowest to highest: Port 2, Port 3, Port 1 and this is also consistent with measurements of the yellow and blue phase (see Appendix D). This result strongly suggests that each separate phase of the inverter has its own bias and that this may be quantifiable in a longer test, supported by other data.

5.4.2 *Recommendation for stage 2*

This test should be repeated in the next stage, with a longer duration. This would allow for comparison with those results and potentially correction for the influence of each port in skewing the measurements. Large spikes, such as that seen on port 2, should be removed if their occurrence is random and infrequent, before compensation is attempted.

5.5 Injection current analysis - description

It is important that we are able to check that the inverter is injecting current as instructed by its software. We are looking for a close match between the ideal current waveform requested from the device and the actual current waveform output measured. Measurement of current waveforms is done for all injection current ($|I_{inj}|$) levels and modulation frequencies (f_m), in order to identify any distortion or unusual behaviour that is dependent on these parameters. That way, we can insure that tests evaluating the effectiveness of frequency A or modulation current level B are impartial (A and B only relevant to example). We also are able to investigate how symmetrical the output currents are.

5.5.1 Test parameters and procedure

Test dates: 11/06/16 Duration: approx. 1h each Elapsed from: not known

Modulation frequency (f_m): **varies,** 10 Hz, 15 Hz, 20 Hz, 25 Hz
RMS injection current ($|I_{inj}|$): **varies**, 2 A, 5 A, 10 A, 20 A
Resistor banks: **bypassed**

Controllable input factors: f_m, $|I_{inj}|$, time of day, resistance in lines
Uncontrollable input factors: ambient temperature, loading and state of PS
Responses: TEI parameter variation

It is beyond the scope of this investigation to determine whether temperature, time of day and the loading and state of the PS significantly affect the injection current provided by the inverter. It is considered a reasonable assumption that the current controller's performance is independent of such factors.

Separate 'runs' are done for each $|I_{inj}|/f_m$. In each run, the inverter is set up to inject current with set parameters of $|I_{inj}|$ and f_m. Then, we measure and log the current flowing in all three phases connected to the inverter simultaneously using the Yokogawa Power Analyser. This device is set up as per subsection 4.1.6. The output is 100 ms of the three phase currents in a .csv file.

The setup of the Yokogawa is appropriate for measurement of line currents. The ranges of f_m and $|I_{inj}|$ used cover all those used in testing with the device in this phase. For justification of the use of these values, please refer to subsections 5.9.1 and 5.11.1. The duration of logged waveforms is such that we can view at least two cycles of the LF envelope easily.

5.6 Injection current analysis – results

5.6.1 *Overview*

The injection current waveforms for all three phases at every $|I_{inj}|$ (2 A-20 A) and every f_m (10 Hz-25 Hz) are shown in the figures in this section. Each figure was produced by the Yokogawa Power Spectrum Analyser and has duration of 100 ms. This allows us to see at least one cycle of the modulation envelope. The scaling of the graphs is kept constant for ease of comparison and phases are presented according to their colour (e.g. red trace is red phase current).

5.6.2 *Current waveform for long sensing test (12 A, 12.5 Hz)*

Figure 49 below shows the waveform of the typical injection currents used in all tests performed. It appears to be of a high quality – the 12.5 Hz envelope is smooth and there is little distortion present. The distortion in the signal is most visible in the troughs of the low frequency waveform (10 ms, 50 ms, 90 ms), where the inverter is attempting to produce a 0 A output. It is expected that this is due in part to high voltage distortion at the UCT machines lab connection.

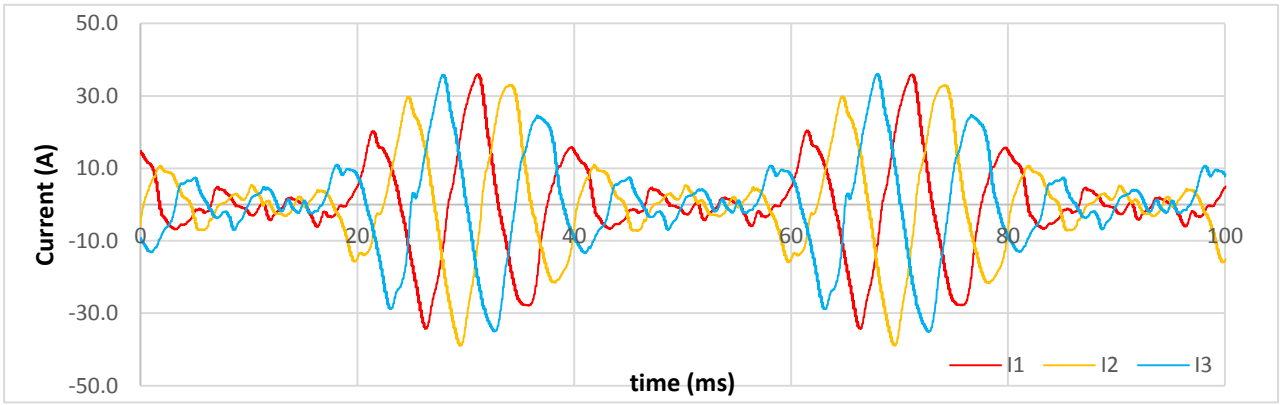

Figure 49: Current waveform measured by Yokogawa when 12 A at 12.5 Hz is requested from inverter

The envelope of the signal in Figure 49 was found to indeed be at 12.5 Hz. The peak injected current lies at around 37 A, which is considerably high. The RMS value of the waveform was calculated to be around 13 A (+- 0.5 A) for all three lines (See Appendix E).

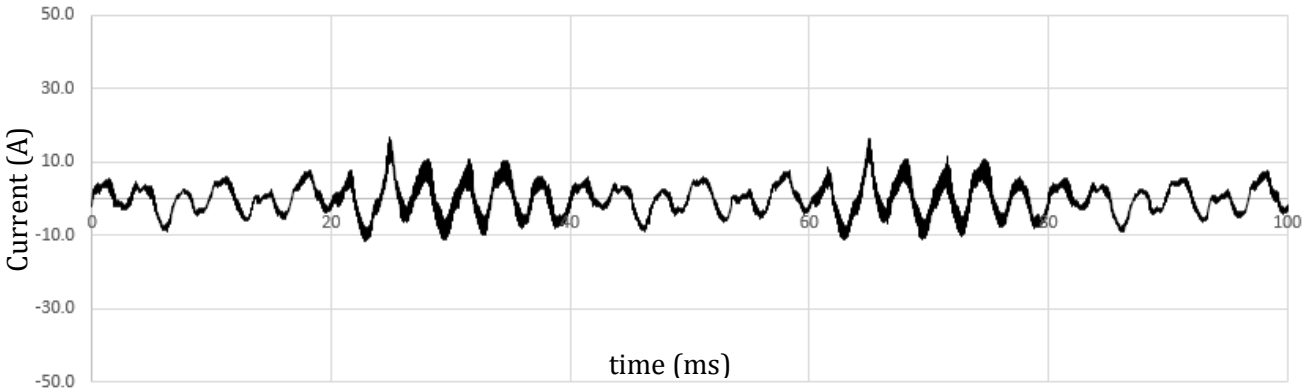

Figure 50: Sum of line currents when $|I_{inj}|$ = 12 A and f_m = 12.5 Hz

5.6.3 *Current waveforms at different $|I_{inj}|$, 12.5 Hz*

All of the waveforms shown in this section were produced by the WT-1800; they are snapshots that are not phase aligned but are all to the same scale.

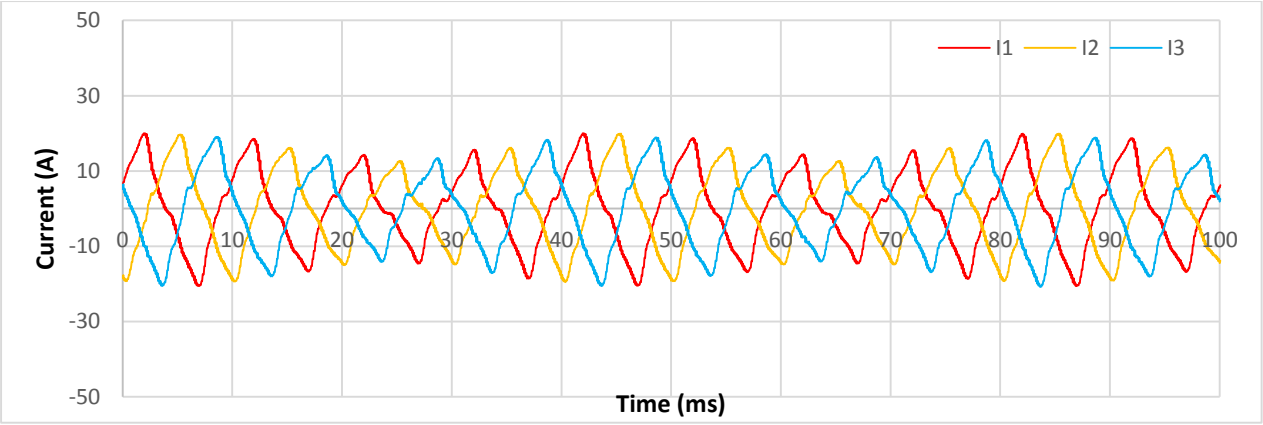

Figure 51: three-phase current, $|I_{inj}|$ = 2 A

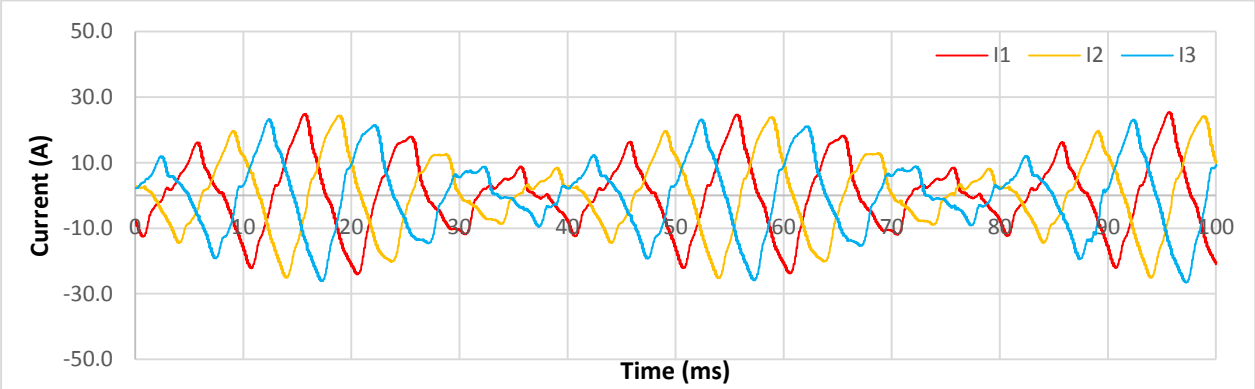

Figure 52: Three-phase current, $|I_{inj}|$ = 5 A

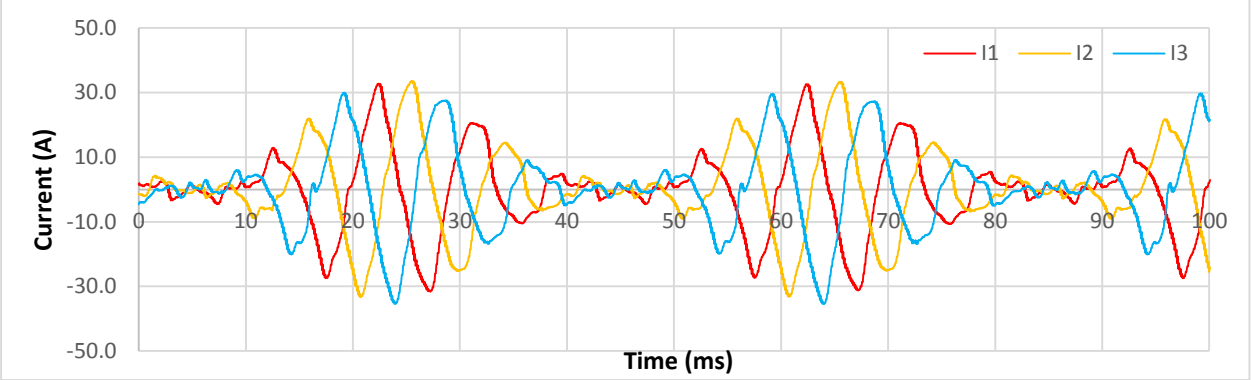

Figure 53: Three-phase current, $|I_{inj}|$ = 10 A

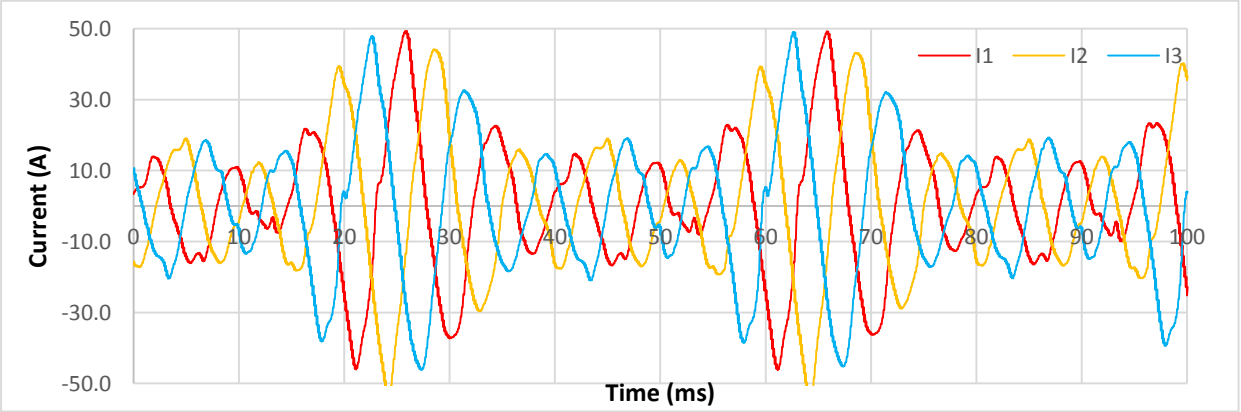

Figure 54: Three-phase current, $|I_{inj}|$ = 20 A

It is quite surprising that at 2 A requested injection magnitude we still have a massive maximum amplitude of 20 A. This is expected to be due to the voltage at the test location being significantly

distorted, making accurate current injection difficult for the PI controller to produce from the inverter. It is very interesting that, looking at the troughs of the 10 A envelope, the 10 A waveform seems to be best in terms of falling close to 0 A at these points, whereas, in the case of 2 A and 20 A we have a large component between the crests.

5.6.4 *Obtained vs. requested RMS currents*

Obtaining the RMS values of each of the waveforms shown in the previous section, the graph in Figure 55 is produced:

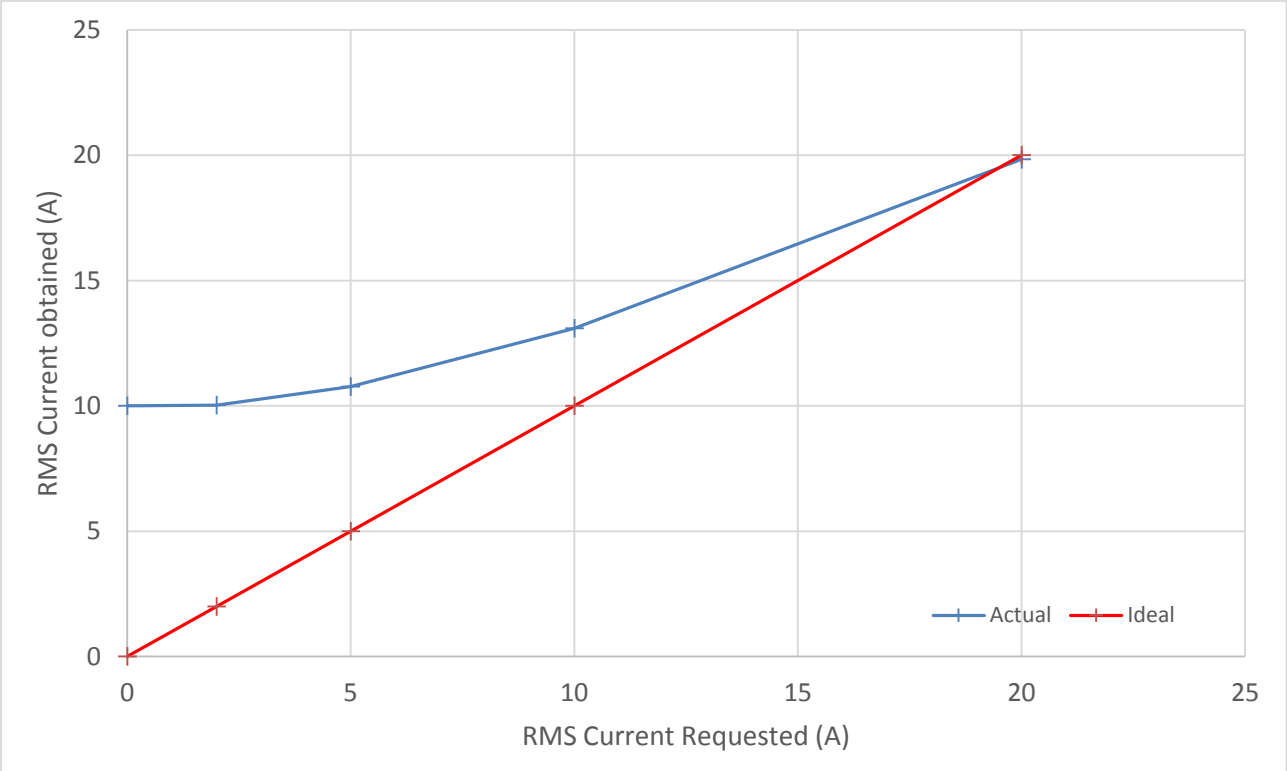

Figure 55: Obtained vs. Requested RMS current ($|I_{inj}|$)

The data used to plot the graph in Figure 55 can be found in Appendix F. The requested RMS current is the value of $|I_{inj}|$ as set in the inverter software. The obtained RMS current is calculated using measurements taken from the scope of the actual current outputted.

Here it can also be seen that uniform behaviour occurred on all lines – they all showed about the same RMS values at any requested current level.

It is clear that when low injection magnitudes are requested, the inverter provides a much greater current than requested by the software. It seems that the minimum output, when 0 A is requested, lies at 10 A. As the injection current requested increases, the inverter provides an output that is closer to that requested. This behaviour is expected to be due to aforementioned voltage distortion at the PCC.

5.6.5 *Current waveforms at different modulation frequencies (f_m), $|I_{inj}|$ = 12 A*

All of the waveforms shown in this section were produced by the Yokogawa; they are snapshots that are not phase aligned but are all to the same scale.

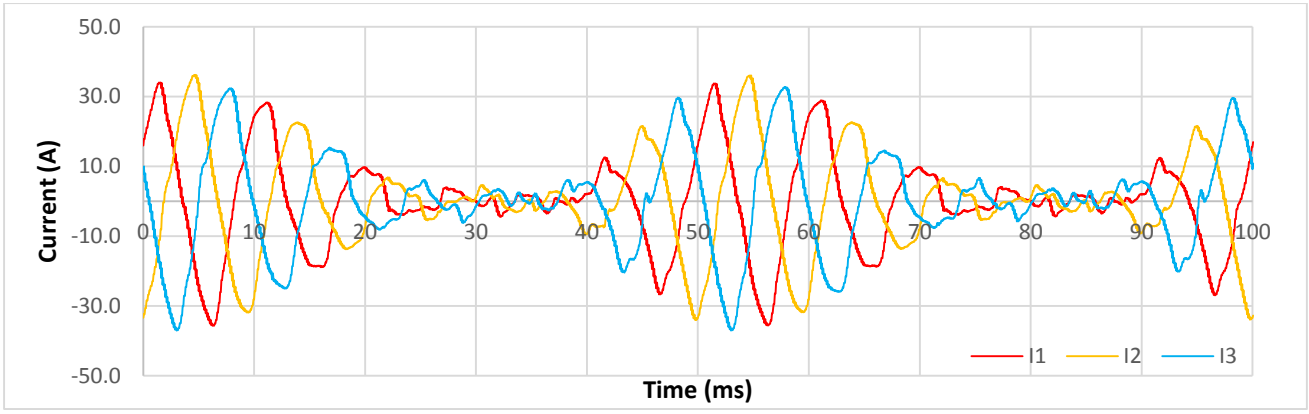

Figure 56: three phase current, f_m = 10 Hz

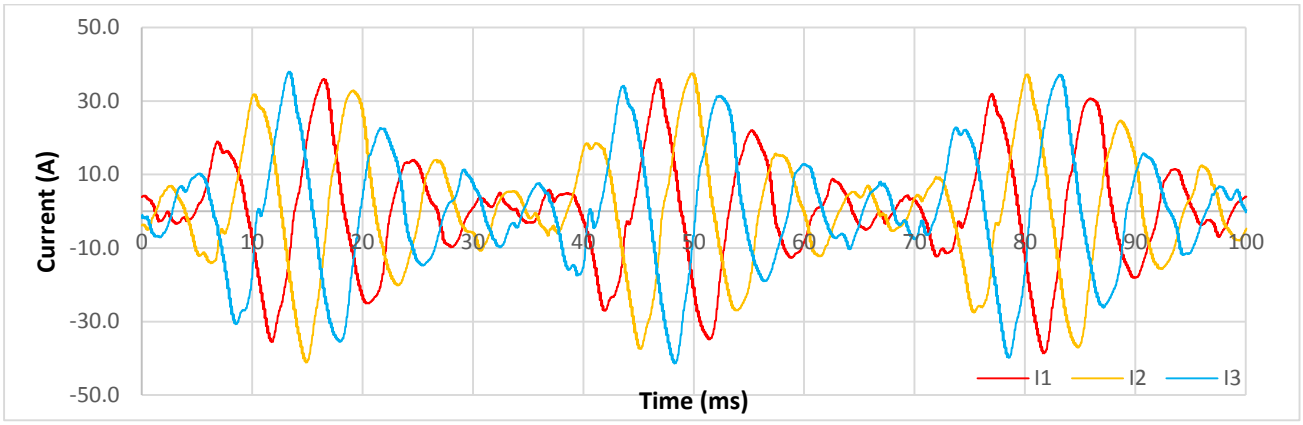

Figure 57: three-phase current, f_m = 15 Hz

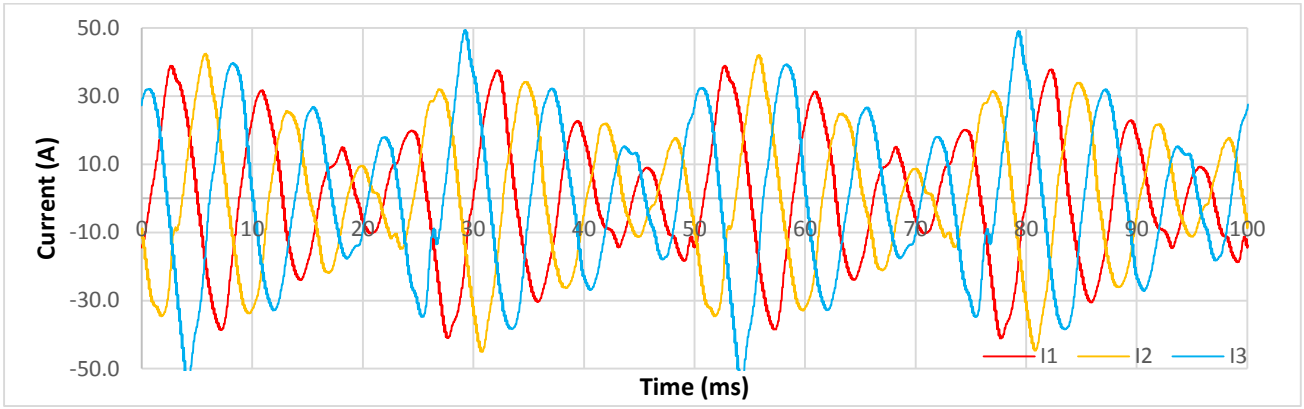

Figure 58: three-phase current, f_m = 20 Hz

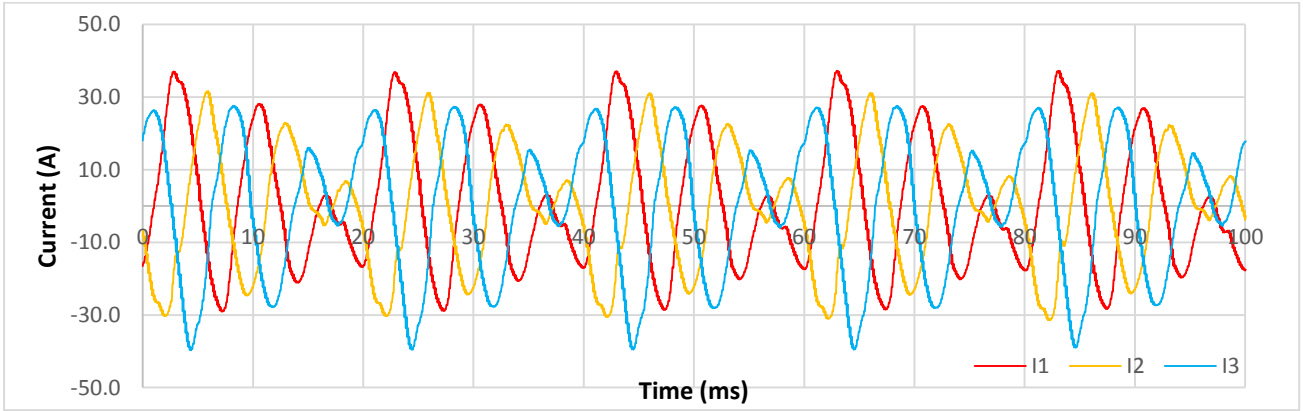

Figure 59: three-phase current, f_m = 25 Hz

Some interesting observations can be made from the above graphs. Firstly, it can be seen that the envelope frequency of the output waveforms is as requested from the inverter, to a high accuracy (See Appendix F). Secondly, we see that significant distortion occurs as f_m increases. In fact, it is quite clear that at the lowest frequency shown, 10 Hz, we have the smoothest low frequency envelope and most symmetrical injection currents. At 20 Hz and above, the distortion is very significant and the currents in each line become very different from one another. Interestingly, at 20 Hz, we have very large spikes on I3, reaching almost 50 A. The inverter is designed to perform current injection best at 50 Hz, hence, it is not surprising that the further away from 50 Hz the injection target, the less accurate injection becomes.

5.6.6 *Variation of obtained RMS current with f_m*

Figure 60 below shows how the actual RMS current measured on each phase varies as we change f_m. The $|I_{inj}|$ setpoint is always fixed at 12 A.

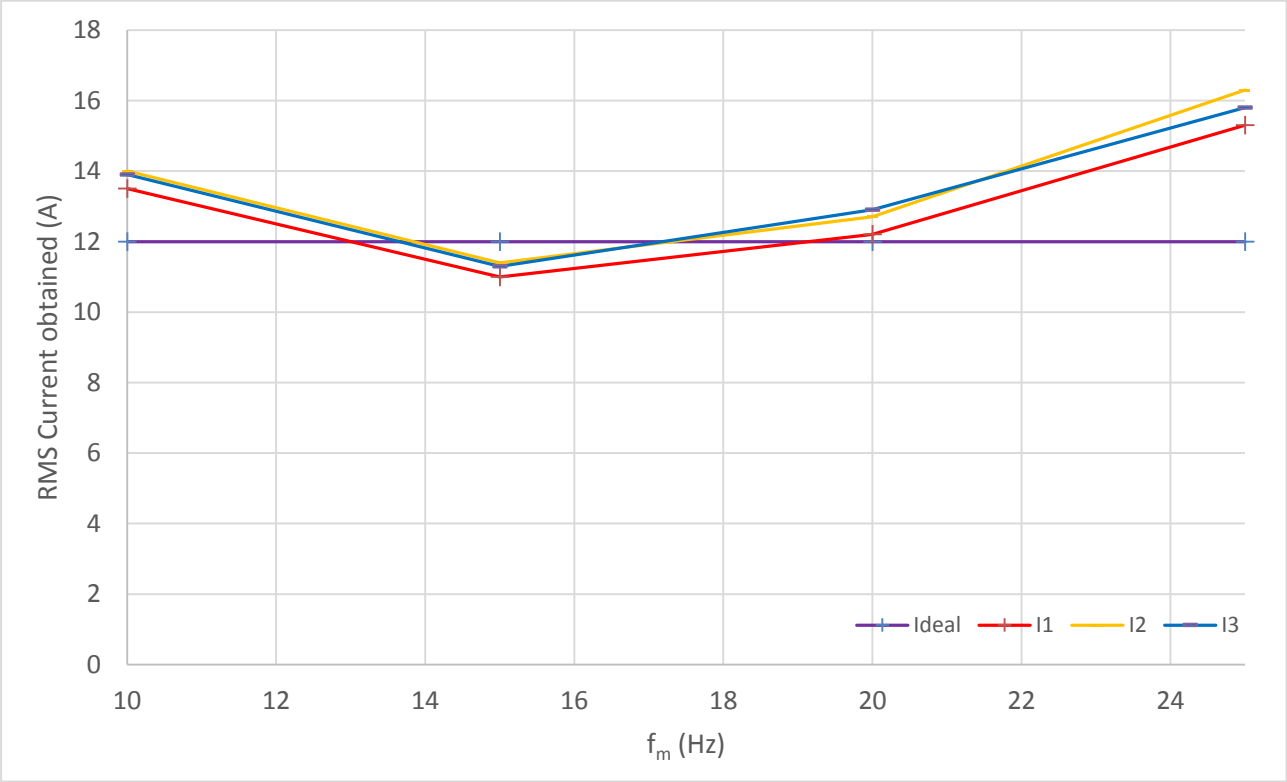

Figure 60: Actual RMS injection currents obtained for different f_m – $|I_{inj}|$ = 12 A

The variation in measured RMS current is quite uniform across all phases, again showing that the device's ability to inject a set current is significantly affected by f_m, deviating from requested values greatly above 20 Hz.

5.6.7 *Recommendation for stage 2*

From the results seen, it has become very clear that logging of current waveform data is crucial to effectively carrying out testing in future. It would be very useful for FFT data to be produced, so as to simplify analysis of the current waveforms and thereby, check whether component levels are as requested.

The range of injection current magnitudes can also be narrowed, based on the waveforms and results seen. For the 5 A case and especially the 2 A case, the output current level is very far from that requested and the waveforms do not appear to be effectively modulated.

The range of frequencies investigated may need to be narrowed down, as frequencies of 20 Hz and above seem to produce greatly distorted waveforms. It is expected that this will cause a bad performance of the device in general.

5.7 Temperature effects - description

Much of the next few sections involve tests in which resistor bank switching is done in order to evaluate the accuracy in the device's ability to track the resistance change that is effected. However, we cannot simply use the resistance values of the bank at room temp without investigating the heating effect of the currents that are being injected. If the heating effect significantly affects the resistance of the banks, it will have to be taken into account.

5.7.1 Test parameters and procedure

Test date: 8/06/16 Duration: 01:00:00 Elapsed from: 14:00 – 15:00
Modulation frequency (f_m): 12.5 Hz (**standard**)
RMS injection current ($|I_{inj}|$): 10.0 A and 20.0 A (**varies**)
Resistor banks: **Maximum resistance (**≈150 mΩ**),**

Controllable input factors: f_m, $|I_{inj}|$, time of day, resistance in line, duration of injection
Uncontrollable input factors: ambient temperature
Responses: Resistance of bank

The sensing inverter is set to inject 10 A, with all resistor banks in line at their maximum resistance. The Yokogawa is used to measure current and voltage across the banks, from which resistance is calculated every 0.5 s from ohm's law. This procedure is repeated with the inverter set to 20 A. A laser temperature gun is used to measure the temperature of RB_2 at 1 min intervals.

The duration of the two runs is simply the time taken for the resistor banks to reach a stable maximum temperature (and thereby constant resistance). 10 A and 20 A are chosen based on the injection levels to be used in subsection 5.9, with 10 A being a good mid-point for injection level and 20 A being the maximum and thereby giving the greatest possible heating effect. The same maximum resistance is used for each bank in order to have the greatest possible heating effect, and the resistance of the three resistor banks in each phase is monitored by the Yokogawa. This allows for comparison between the heating that occurs for each bank. The laser temperature gun is used to obtain information about actual bank temperature for comparison with the resistance variation. Ambient temperature is not expected to vary significantly, given that the tests are performed in a spacious, closed environment.

5.8 Temperature effects – results

5.8.1 10 A heating effect

The resistance of banks 1, 2 and 3 was calculated by dividing the voltage across each bank by the current through it using the Yokogawa. The results for 10 A RMS injection are shown in Figure 61 below.

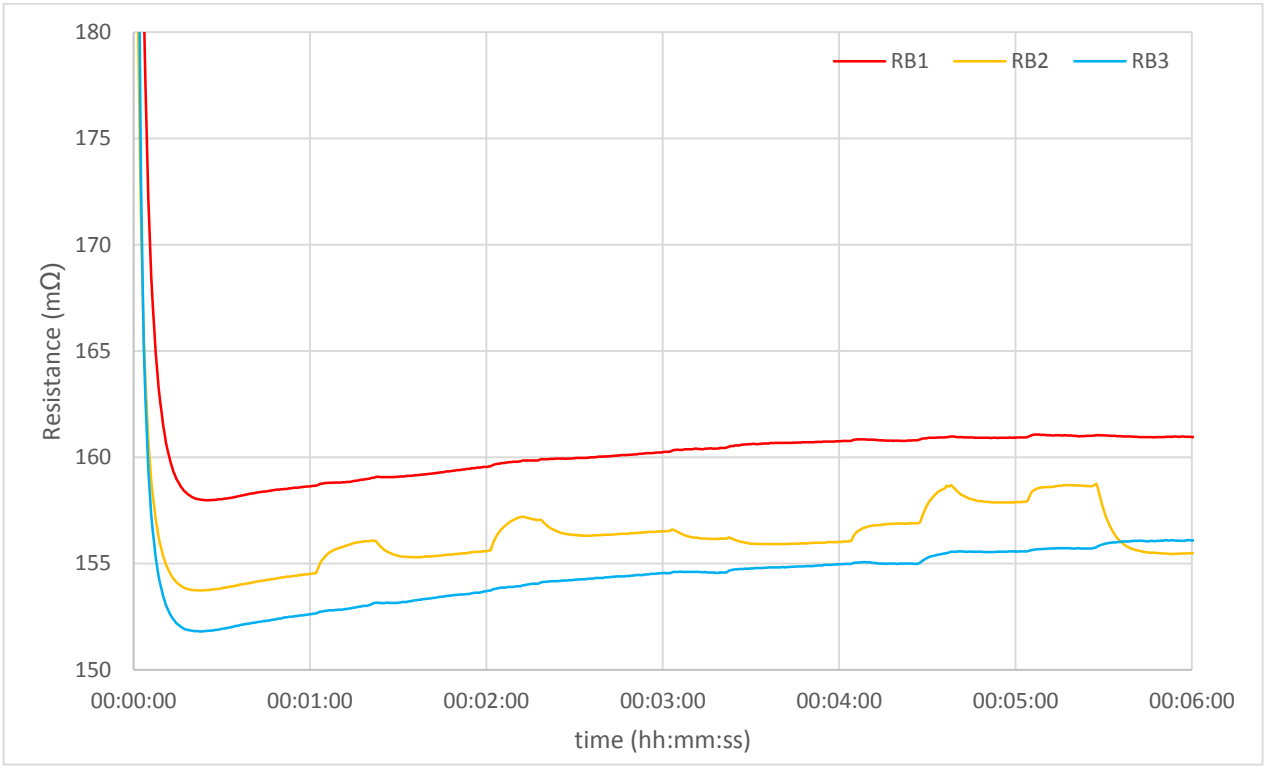

Figure 61: Resistance variation due to heating in resistor banks at 10 A RMS injection

5.8.2 20 A heating effect

The resistance variation at 20 A is shown in Figure 62 below.

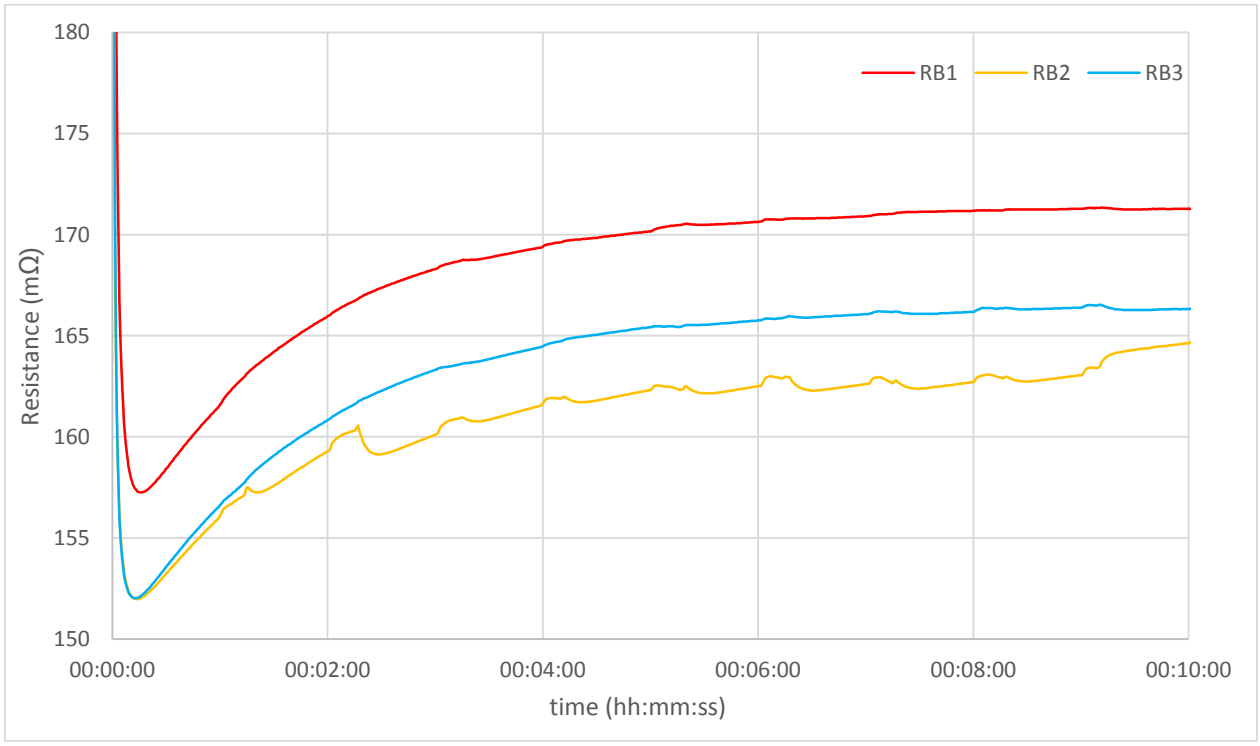

Figure 62: Resistance increase due to heating in resistor banks at 20 A RMS injection

5.8.3 Analysis

The variation in the RB_2's resistance (yellow) in Figure 61 and Figure 62 above is due to the lid of the resistor bank being opened and closed at different intervals for temperature measurements to be taken with a laser temperature gun. When the lid of the bank was opened, the resistors experienced cooling. Conversely, when the lid was closed after being opened, they continue heating up. This was done at 1 minute intervals, which produced the interesting shape in the yellow phase's graph. This has compromised the test for RB_2, although its resistance behaviour would almost certainly be of the same nature as RB_1 and RB_3 if it were left closed.

It is quite clear from the 20 A case (Figure 62) that the resistance increases considerably due to temperature over time, reaching a value about 9% greater than the resistance at the lowest point (start). However, at the 10 A level, the final resistance is only about 3% higher than at the start. The very high value of resistance at the very start in both figures is due to the fact that the inverter has yet to begin injecting current and the Yokogawa is measuring V/I, where both V and I are very small (Hence, measurement error has a high impact).

The result of the test shows that the resistance of the banks can be expected to change considerably during injection. It should be noted that, at different switch positions, the heating effect will not be the same. In this case, the maximum resistance was placed in the line and the maximum heating is caused. The results of this test will be used in future tests for compensation of resistance changes with temperature. This is of crucial importance in knowing precisely what TEI change we expect the device to track when a resistor bank is switched.

5.9 Variation of injection current magnitude ($|I_{inj}|$) - description

For the previous tests $|I_{inj}|$ was selected somewhat arbitrarily. The only known boundaries informing this selection are that the current must be large enough to cause a measurable voltage response in the PS, but not greater than the inverter is able to reliably provide. Beyond this, it is not known what current levels can be used to obtain results, or which provide more accurate results than others. Hence, the aim in this test is to get some understanding of the effect of the $|I_{inj}|$ parameter on the TEI estimation accuracy. This is a key part of the investigation as it is one of the first steps to tuning the device as well as informing the next testing stage.

5.9.1 Test parameters and procedure

Test date: 10/06/16 Duration: 00:26:00 Elapsed from: 14:32 – 14:58
Modulation frequency (f_m): 12.5 Hz (**standard**)
RMS injection current ($|I_{inj}|$): **varies during test** from 2 A to 20 A
Resistor banks: **resistance varies**

Controllable input factors: f_m, $|I_{inj}|$, time of day, resistance levels (before and after step for each line)
Uncontrollable input factors: ambient temperature, loading and state of PS
Responses: TEI parameter variation

Essentially, this test involves adding and removing known resistance into the line (through switching of resistor bank CB's) and comparing the measured changes with the known resistance to evaluate the accuracy of TE parameter determination.
Four $|I_{inj}|$ levels were chosen, based on the limitations of the sensing inverter's output. These were: 2 A, 5 A, 10 A and 20 A.

Table 4: Resistor bank setup

Change	Magnitude (mΩ)
	ΔR
'Small step' on red phase	46 (≈50)
'Large step' on yellow phase	97 (≈100)

Starting at 2 A, 20 samples are taken with all resistance banks on minimum (≈50 mΩ) setting, after which the RB_1 in red phase is increased by 50 mΩ and RB_2 in yellow phase by 100 mΩ, left for 10 samples and then changed back to 50 mΩ on each line for 10 samples. Then $|I_{inj}|$ is increased and the same process of resistor bank switching is employed. This is illustrated by Table 5.

Table 5: Variation of $|I_{inj}|$ test, resistor bank switching procedure

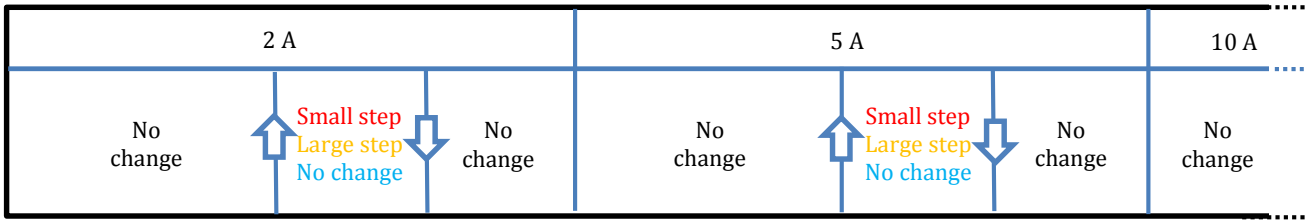

Through this procedure, we have one continuous test in which all levels of $|I_{inj}|$ are evaluated in their resistance change measurement accuracy. The other controllable input factors are held constant (blocked).

The range of currents used for injection is based on a device limit of 20 A RMS, as higher levels cause audible clicking of the automatic protection system in the inverter. As this is the first attempt, a somewhat logarithmic division of the current range is done – above a certain high level of injection, we do not expect to see any more improvement in the obtained parameters.

The switching process is chosen based on the available resistor banks, with a 'small' change that is about half of the existing resistance/reactance of the PS and a 'large' change twice as large that gives 100 mΩ ΔR. This scale of change is well suited to evaluating the effectiveness of the resistance change measurement as would be the case in a practical TEI estimation scenario. That is to say, the changes we effect are of the same order of magnitude (100 mΩ) compared to the PS's parameters at steady state. Larger changes could have been evaluated, however, these would correspond to very infrequent occurrences for normal PS operation – a 500 mΩ PS impedance change would likely be due to disconnection or a fault [22]. Such infrequent PS operating conditions are not the focus of this report. Nonetheless, any contingency could have occurred during the long sensing test.

We use a set f_m (that used in other tests before) as the signals and systems theory states that f_m and $|I_{inj}|$ should independently affect the measurement accuracy. That is to say, purely changing the amplitude of the injected current should only affect the amplitude of the voltage response.

Switching is done on two of the lines in order to produce more information while keeping the test procedure simple enough that potential for human error is minimal. Furthermore, by not changing the resistance in the blue phase, we have a 'control' that should remain steady whilst the other phases change.

5.10 Variation of injection current magnitude ($|I_{inj}|$) - results

5.10.1 TEI parameter behavior

The plot of the obtained TE resistance of each line ($R_{th\ R}$, $R_{th\ Y}$, $R_{th\ Y}$) and the neutral ($R_{th\ n}$) over the testing period is shown below in Figure 63. The plot is divided into vertical sections corresponding to the different resistor bank states described in subsection 6.11.1 Table 5. They will be referred to as "state sections".

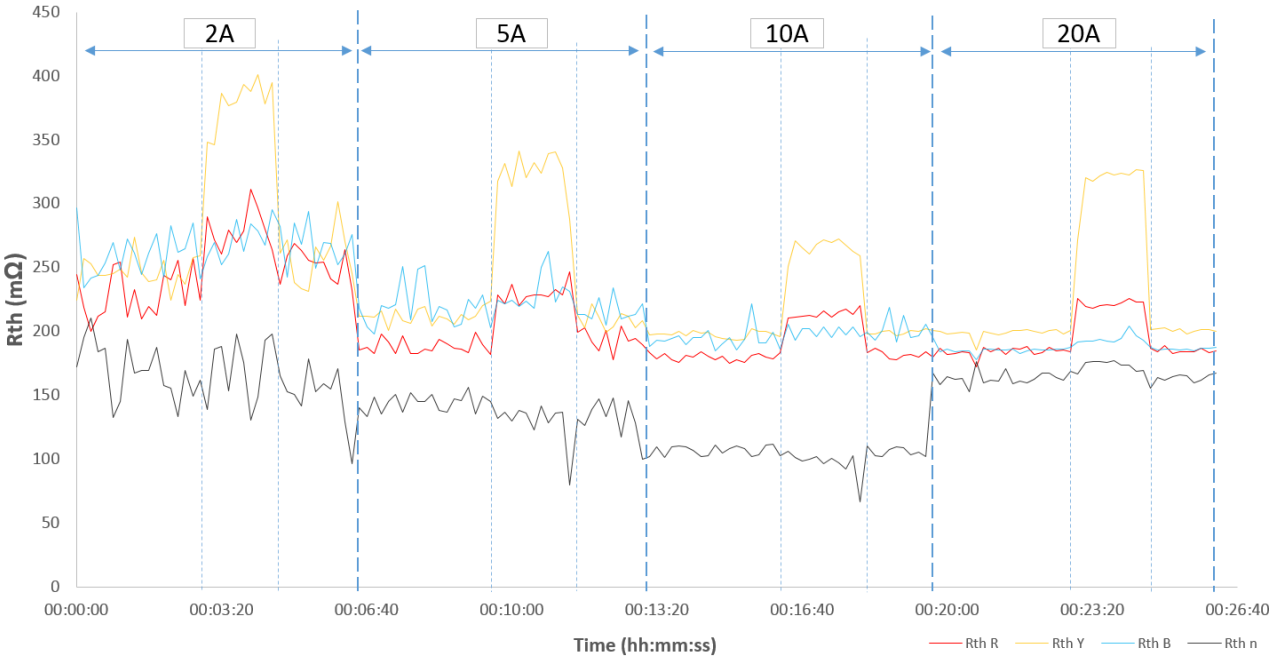

Figure 63: Variation of $|I_{inj}|$ test results - raw data (with state sectioning)

From Figure 63 it is visible that the device reacts to the line resistance changes. As is expected, the yellow phase's change seems to be about twice as large as that of the red phase. Interestingly, as the injection magnitude is increased, it appears that the rapid fluctuations in the results become much smaller. This is most likely due to the increase in SNR at higher injection levels.

Although the actual resistance 'steps' are kept constant throughout the test, it is clear that at different $|I_{inj}|$, we have very different measurements of that constant value. Finally, we see that the average level of the measured TE resistance drops whenever $|I_{inj}|$ is increased (except in the case of the neutral at the boundary between 10 A and 20 A, which increases).
By looking at the waveforms of the line currents for the different magnitude levels (see subsection 5.6.3), we are able to see a clear link to the behaviour in Figure 63. As the magnitude of current requested from the inverter increases, we see less distortion in the current waveform.

The jump in the neutral resistance at the 10 A/20 A boundary is not accompanied by any significant change in the red phase's measurement. This suggests that the injection of current on a single line (used to determine Rn) has somehow not been successful.

5.10.2 Temperature considerations

In terms of temperature considerations, we must look back to the results of subsection 5.8. For each $|I_{inj}|$, we have a different power being lost in the resistor banks as heat. We only have information about 10 A heating and 20 A heating characteristics, at full bank resistance configuration. The heating effects are of concern when we wish to compare the change in resistance measured by the device to

that of the known change as measured by the Wheatstone bridge in Appendix A. Hence, we must apply corrections to these values.

For each injection level we have a steady low resistance value, a step upward on two lines, and a step downward. For the steady low value, the resistance in the lines is at minimum (one resistor of the bank), at the high value it is at maximum for yellow phase (all five resistors of the bank) and then again at minimum. When we switch more resistance into the line, more heat is being generated due to the added resistors and the overall resistance of the bank rises, as per the two figures in subsection 5.8. At the up-step, we can assume that rise in resistance will not be more than that in subsection 5.8.1 in case of 10 A and subsection 5.8.2 in case of 20 A. It is less than this because in this case we are starting with the banks warmed by the single resistor, rather than all cold. Hence, on the up-step, at 10 A, we follow the curve in subsection 5.8.1 for the duration of 10 samples (1 min 40 s). The resistance has then, at the end of the up-step, risen by less than 1 ohm (refer to Appendix G for in-depth explanation. Corrections must be applied for the heating effect, meaning that the large upward step (on yellow phase) becomes 5 mΩ greater at 20 A and 1 mΩ greater at 10 A injection. At lower injection levels, the effects of temperature are considered negligible (<1 mΩ). For the small upward step (on red phase), the number of added resistors is halved, hence, we assume that the heating effect is halved and so are the corrections.

5.10.3 Baseline impedance variation with injected current

The relationship between the baseline impedance levels (average impedance when the resistance banks are all at equal resistance (50 mΩ)) and $|I_{inj}|$ is shown below in Figure 64. The average impedance is plotted on a p.u. basis, with the unit being the initial (2 A) average impedance for each parameter. The curves show a common decrease in the average impedance over the three phases as the injected current increases. They appear to follow a negative logarithmic curve, stabilising at an average impedance of about 0.75 p.u.
The neutral value deviates from this steady decrease significantly, especially at the high current (20 A) measurement. Based solely on the result that the values seem to tend to a common steady level at higher current, it is expected that higher current will improve the accuracy of results.

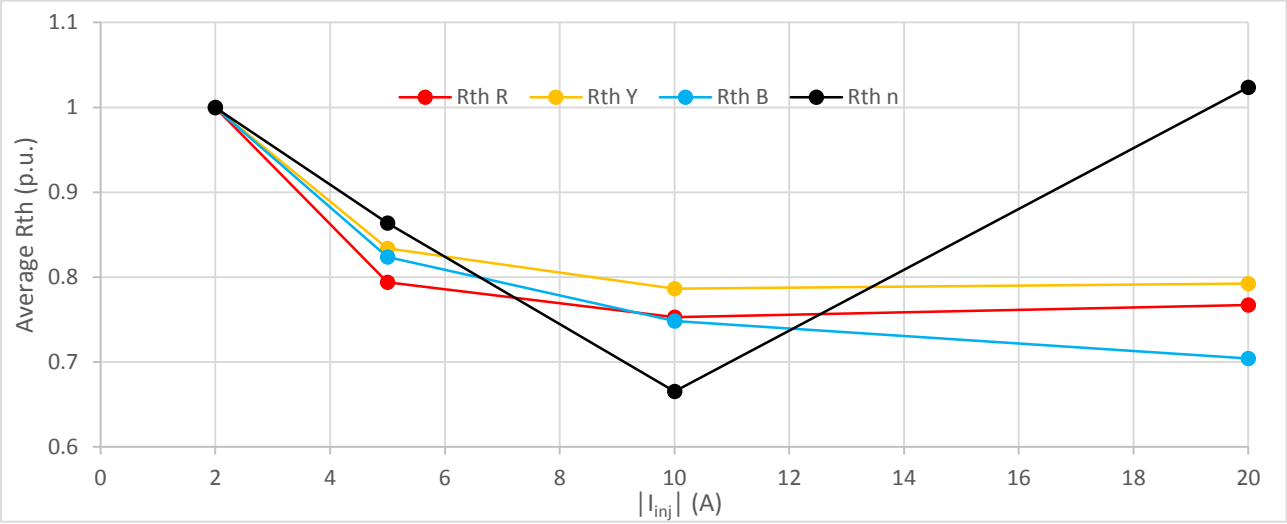

Figure 64: Baseline impedance variation with $|I_{inj}|$

5.10.4 Standard deviation variation

The standard deviation behaves in a similar way to the baseline impedance level as $|I_{inj}|$ is increased. This is seen clearly in Figure 65 below. $R_{th\ R}$ and $R_{th\ Y}$ are seen to closely match each other in a steady negative logarithmic curve, with blue deviating somewhat and neutral deviating quite significantly.

Overall, the average behaviour is well approximated by a negative logarithmic curve, as seen in Figure 65 right.

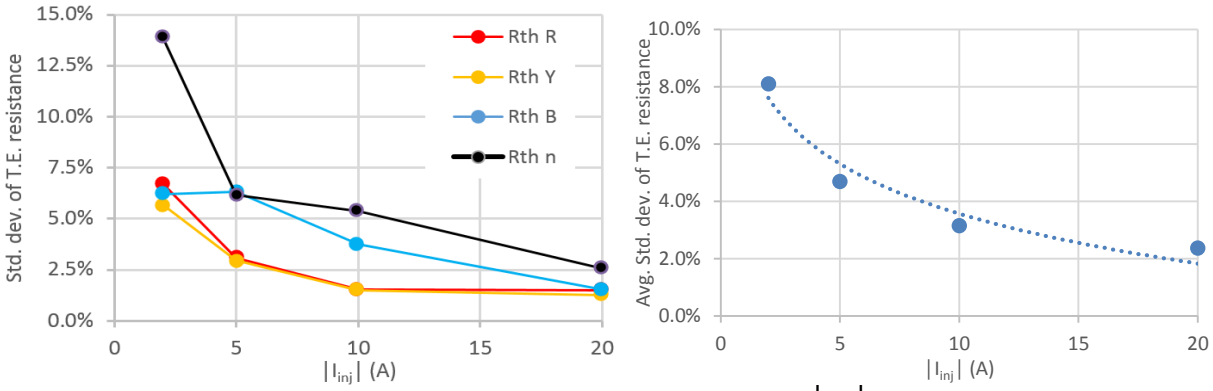

Figure 65: Variation of Std. dev. with $|I_{inj}|$:
Left: separated parameters Right: average of all four parameters

The results support the conclusion that a higher $|I_{inj}|$ will reduce unwanted fluctuations in the measured TE parameters. One possible explanation for this is that the impact of unwanted random variations and measurement noise is smaller when we have a larger resultant voltage change.

5.10.5 Resistance change measurement accuracy

The ability of the device to provide an accurate measurement of the line resistance change is now investigated. The difference in average parameter values between sections (as defined in Table 4) is used to measure the change in resistance measured and is compared with the known change. Based on this, Figure 66 is plotted.

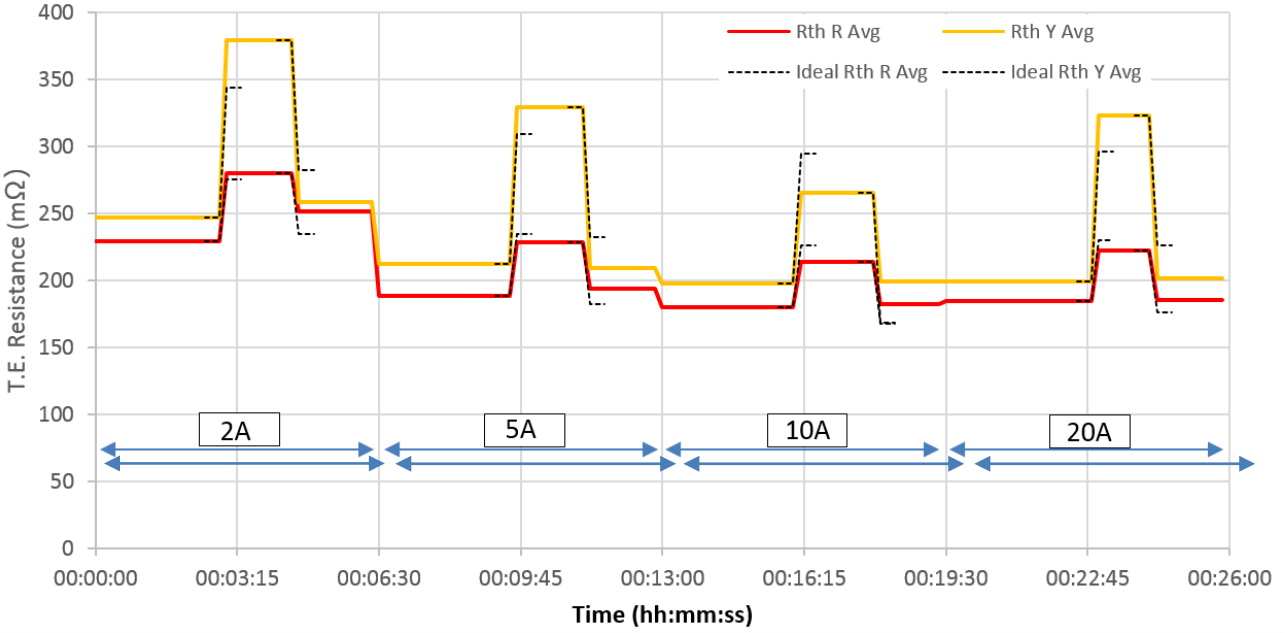

Figure 66: Comparison of ideal and measured resistance changes

In Figure 66, we see the measured values of $R_{th\ R}$ and $R_{th\ Y}$ (the parameters whose line resistance we are changing) averaged over each section and plotted. For each step change in resistance measured there is a corresponding dotted black line showing what the step change would have been if the device's measurement reflected the exact correct change in resistance. As it is clearly visible, the step changes are generally quite far off from the ideal value, suggesting that the device does not provide very accurate results. The measured change is three times out of four an overestimate of the actual change for the yellow phase, whereas, with the red phase it is an underestimate three times out of four.
The graph is seen to return to close to its original value before the change in almost all cases.

The error in measuring the known resistance change for each $|I_{inj}|$ level is shown inbelow.
Table 6 below.

Table 6: Error in measuring known resistance change

$\|I_{inj}\|$	2 A	5 A	10 A	20 A
Error in $R_{th\,R}$	-13.8 %	-19.4 %	-28.7 %	-19.9 %
Error in $R_{th\,Y}$	30.8 %	22.0 %	-30.9 %	24.8 %
Difference	44.6 %	41.4 %	2.2 %	44.7 %
Disagreement	30.4 %	7.8 %	3.1 %	1.1 %

Another interesting observation from Figure 66 is that the baseline level for the 2 A injection changes significantly before and after the resistance switching. It is much higher, especially in the case of the red phase, after switching. Looking back at the raw data in Figure 63, we see that this comes from the fact that $R_{th\ R}$ seems to be slowly increasing over the 2 A measurement interval, unlike the other parameters.below.
Table 6 also includes two indicators that should be minimized for effective TEI estimation accuracy. The "Difference" is the difference between percentage error on red phase and error on yellow phase. Ideally, this will be low, as the device should treat each phase symmetrically.
"Disagreement" is the percentage difference between the measured up-step and the measured down-step of resistance, which should ideally be zero as we are effecting the same up-step and down-step (taking temperature into consideration).

According tobelow.
Table 6, the error varies significantly for the different injection magnitudes. However, almost all of the errors lie above 20 % and it seems that the error does not vary in a predictable manner with $|I_{inj}|$. This suggests that the accuracy is not dependent on $|I_{inj}|$. It is possible that, with such high error, we are unable to see small changes in accuracy that are dependent on $|I_{inj}|$ – that is to say, there is some other factor which is limiting accuracy which needs to be addressed. However, it should be noted that the difference between errors is very high for all $|I_{inj}|$ (>40 %) except for 10 A, where it is very low (2.2 %). This strongly suggests that around 10 A, error will be consistent and therefore, easy to compensate for. Finally, disagreement between the up-step and the down-step falls greatly with increasing $|I_{inj}|$, suggesting that higher levels of $|I_{inj}|$ provide more consistency in results.

5.10.6 Recommendation for stage 2

It is quite clear that, although providing a good first look into the effects of $|I_{inj}|$ variation, the test was unable to give much information about resistance change measurement performance. A clear improvement would be to increase the duration of the test, generating more samples over each 'state section' and thus, diminishing the effects of spiky behaviour and unusual behaviour in the average value. In order for a conclusive relationship to be drawn, more points are required and, hence, the range of injection magnitudes must be divided into more levels.

The average and standard deviation of the parameters was found to be strongly dependent on $|I_{inj}|$. Repetition of this test can be used to look deeper into this behaviour.

Another improvement would be to do more than one switching event at each level for a given line, again providing more assertive results.

5.11 Variation of modulation frequency (f_m) - description

The theoretical boundaries guiding the selection of injection frequency are that it is a frequency not commonly present in the PS and that it is slow enough for the inverter to track. The fm of the currents injected by inverter 1 were chosen to be 12.5 Hz for the previous tests. The choice of this specific frequency is somewhat arbitrary – it was found that changes in line resistance could be tracked relatively well at this frequency from Testing Phase 1. Since the harmonic content of the PS is only known to us on a speculative level and there are no guidelines available for choosing the injection frequency, this parameter deserves investigation. In order for effective TEI tracking, this parameter will require tuning.

5.11.1 Test parameters and procedure

Test date: 11/06/16 Duration: 00:26:00 Elapsed from: 13:01 – 13:27
Modulation frequency (f_m): **Varies during test** from 10 Hz to 25 Hz
RMS injection current ($|I_{inj}|$): 12.0 A (**standard**)
Resistor banks: **resistance varies**

Controllable input factors: f_m, $|I_{inj}|$, time of day, resistance levels (before and after step for each line)
Uncontrollable input factors: ambient temperature, loading and state of PS
Responses: TEI parameter variation

Four f_m levels were chosen: 10 Hz, 15 Hz, 20 Hz and 25 Hz. The procedure, shown in Table 7, is essentially identical to that of the previous test. Starting at 10 Hz, 20 samples are taken with all resistance banks on minimum (50 mΩ) setting, after which the bank in line 1 is increased by 50 mΩ and line 2 by 100 mΩ, left for 10 samples, and then changed back to 50 mΩ on each line for 10 samples. Then, f_m is increased and the same process of resistor bank switching is employed.

Table 7: Variation of fm test, resistor bank switching procedure

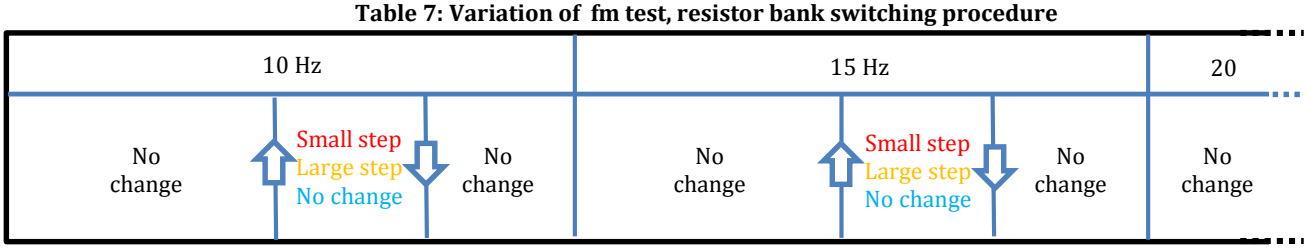

The test procedure is very similar to that in subsection 5.9.1, hence, it should be familiar. Its justification is found in the same section. The frequencies chosen are based on the limitations of the sensing inverter's output as determined by analysing the current graphs and the inverter's inability to track frequencies above 25 Hz (unpleasant sound is heard). We also assume that f_m lower than 10 Hz is undesirably close to the 50 Hz component.

5.12 Variation of modulation frequency (f_m) - results

5.12.1 TEI parameter variation

The plot of the obtained TE resistance of each line ($R_{th\ R}$, $R_{th\ Y}$, $R_{th\ B}$) and the neutral ($R_{th\ n}$) over the testing period is shown below in Figure 67. The plot is divided into sections corresponding to the different states described in Table 7.

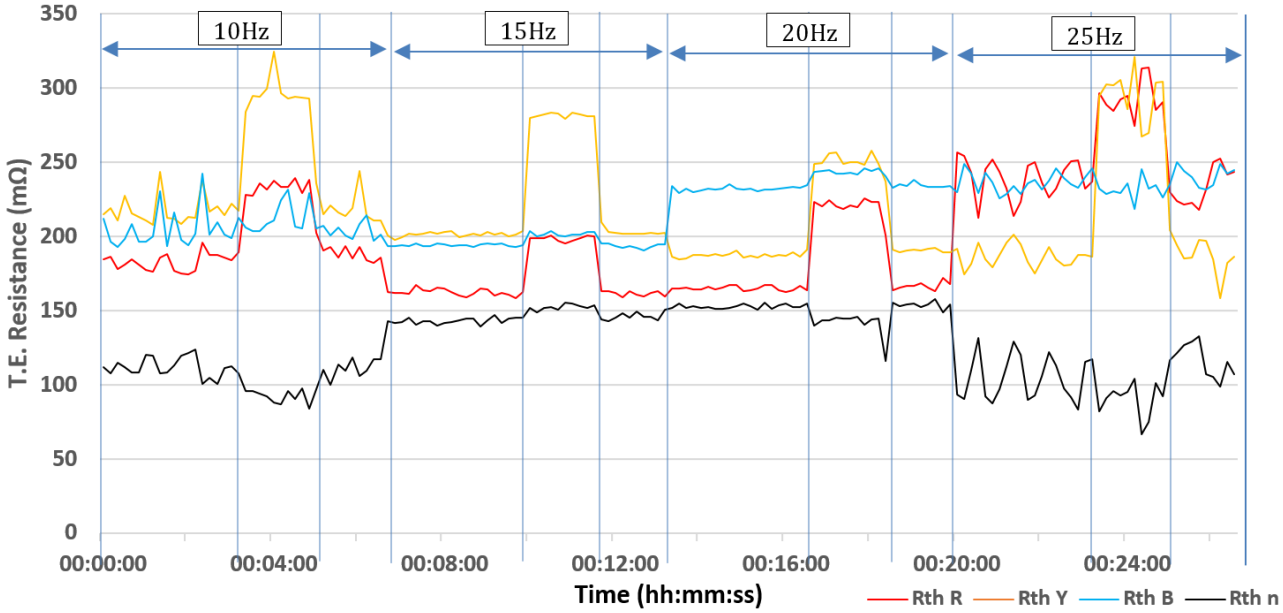

Figure 67: Variation of f_m test results - raw data (with state sectioning)

From the results in Figure 67, it is clear that varying f_m has significant effects on the TE parameters. As before, we see that the measured change in line resistance when the banks are switched is not equal for the different frequency levels.

It is interesting to note that the rapid fluctuations of the parameters are significantly attenuated at the mid-level frequencies of 15 Hz and 20 Hz, somewhat larger at 10 Hz and largest at 25 Hz.

Unusual behaviour is also visible, such as the sudden 'jump' in the baseline value of the blue phase at the 15/20 Hz boundary, as well as the large opposite behaviour in red and neutral phase at the 20/25 Hz boundary.

Much insight can be gained regarding the results if we consider the current waveforms for each frequency requested (see subsection 5.6.5). The fluctuation at 10 Hz is explained by the unusually low modulation index of the waveform. At 25 Hz, we can link the large fluctuations to the currents becoming significantly distorted. The jump of the blue phase at the 15/20 Hz boundary is clearly due to the jump in blue phase peak current from 15 to 20 Hz. A similar explanation exists for the red phase at 25 Hz, at which both red and blue phase currents are unusually high. Hence, it appears that the dependence of TE parameters estimation on f_m is related to current distortion.

These waveforms give supporting evidence to the earlier argument that the inverter's separate phase units behave differently and this is manifested in much of our results.

5.12.2 *Temperature considerations*

Given that this test is performed at 12 A, we can expect that the heating effect on resistance will be of only slightly larger degree than that described by subsection 5.8.1 for 10 A. Hence, 1 mΩ temperature correction is applied for the large change, as discussed in Appendix G.

5.12.3 *Standard deviation variation with modulation frequency (f_m)*

From looking at the standard deviation for the different frequency levels (Figure 68 below) we again see a relatively clear relationship between it and our dependent variable (f_m). The parameters all seem to follow a parabolic shape, with little difference in the mid-level frequency value but high deviations at 10 Hz and 25 Hz. As in the previous test, it is clear that the neutral experiences the most fluctuation and, hence, its graph deviates most from the average.

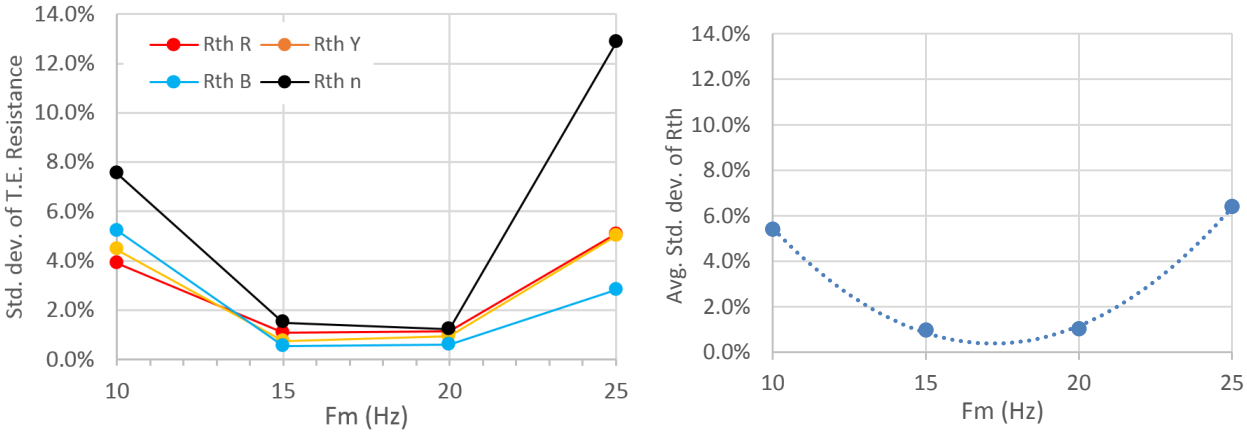

Figure 68: Variation of Std. dev. with f_m:
Left: separated parameters Right: average of parameters

Looking back at Figure 67, we notice that there are large, infrequent spikes on yellow and blue phase only for the 10 Hz case, whereas, at 25 Hz there are large deviations almost constant throughout the measurement window. This is clearly unwanted behaviour that is undermining effective TEI estimation.

5.12.4 *Resistance change measurement accuracy*

As in the previous test, the ability of the device to provide an accurate measurement of the line resistance change is now investigated.
Figure 69 shows the measured changes in average level between sections compared to the ideal.

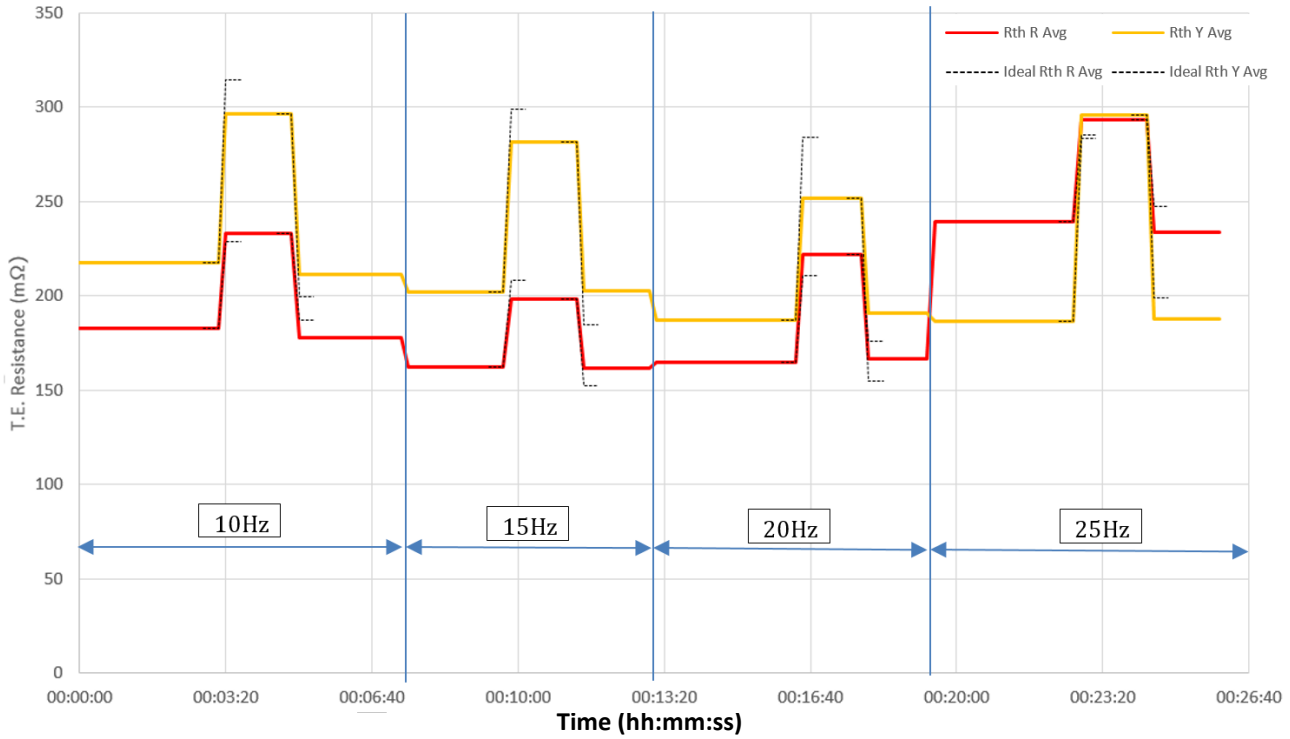

Figure 69: Comparison of ideal and measured resistance changes

As in the previous test, we see that the device is generally inaccurate in its measurement of the known change. In the case of the yellow phase, the measured change is usually less than the actual change. In the red phase, three out of four times the measured change is more than the actual change.
Again, we see the resistance before and after stepping is approximately equal, as expected.

Table 8: Error in measuring known resistance change

f_m	10 Hz	15 Hz	20 Hz	25 Hz
Error in $R_{th\,R}$	15.1%	-19.9%	21.9%	24.0%
Error in $R_{th\,Y}$	-15.7%	-18.8%	-35.7%	11.6%
Difference	30.8%	1.1%	57.6%	12.4%
Disagreement	8.8%	0.6%	2.9%	6.1%

Similar to the findings in subsection 5.10.5, we do not see large variations in error except in the case of 20 Hz which appears to be especially bad for measuring the resistance change. This may be linked to the large spikes occurring on the blue phase as seen in subsection 5.6.5. Both difference and disagreement is lowest for 15 Hz, suggesting that both resistance estimation error and change measurement is consistent at this level. The difference and disagreement performance indicators are defined in subsection 5.10.5.

5.12.5 Recommendation for stage 2

Some of the improvements listed in subsection 5.10.6 can be also be applied to this test, such as increasing the duration and dividing the range of f_m into more levels so that a better graph can be produced. Furthermore, it is seen that high fm (20 Hz and above) gives very noisy results and coupled with the current waveform distortion seen in subsection 5.6.3, the range of f_m can be reduced. f_m values lower than 10 Hz may also be investigated. In general, resistance change measurement accuracy is crucial, hence, effective results in this area should be focused on.

6. Testing – Stage 2

6.1 Power system voltage analysis - description

Up until this point, we have not actually looked at the voltage response due to the injected sensing current. The aim of this test is to:

- Gather basic information regarding the PS voltage at MLT
- Identify harmonics present in the PS
- Enable comparison of 'before' and 'during' injection, thereby measure voltage response due to injection

6.1.1 Test parameters and procedure

Test date: 25/10/16 Duration: approx. 1h Elapsed from: not known

Controllable input factors: f_m, $|I_{inj}|$, time of day, resistance and reactance in lines
Uncontrollable input factors: ambient temperature, loading and state of PS
Responses: TEI parameter variation

In 'before' case:
Sensing inverter OFF
Resistor banks: **bypassed**

In 'during' case:
Modulation frequency (f_m): 12.5 Hz (**standard**)
RMS injection current ($|I_{inj}|$): 12.0 A (**standard**)
Resistor banks: **bypassed**

Table 9: Oscilloscope setup (both cases)

Ch1, Ch2, Ch3	V_R, V_Y, V_B
Connection at	Inverter input ports
Clamps/probes	3x differential probes
Window size	20 s
Vertical scale	500 V/div
Output	.csv, .png
FFTs	Yes

We have two separate sets of data collected in this test: before injection and during injection. This way, we can attempt to isolate the voltage response specifically due to injection. The before case only involves the PS in its natural state, with no other components connected. The 'during' case involves injection of arbitrary "standard" current into the PS. Logging of the voltage statistics, such as the frequency, RMS magnitude and phase displacement, is done for 5 minutes before and after injection. This is by no means a rigorous statistical analysis, as the data is very limited. Five minutes of operation cannot be expected to characterise the potential variations fully.

We do not use resistor or inductor banks in this test. Adding any impedance in the line should cause a larger voltage response proportional to the increase in line impedance. We wish to see the 'worst case' voltage response – the small response due to the actual network's impedance only as it also gives us an idea of the SNR that can generally be expected.

6.2 Power system voltage analysis - results

6.2.1 Phase to neutral voltages before injection

A short portion of the three-phase line voltages measured directly from the PCC is shown below in Figure 70.

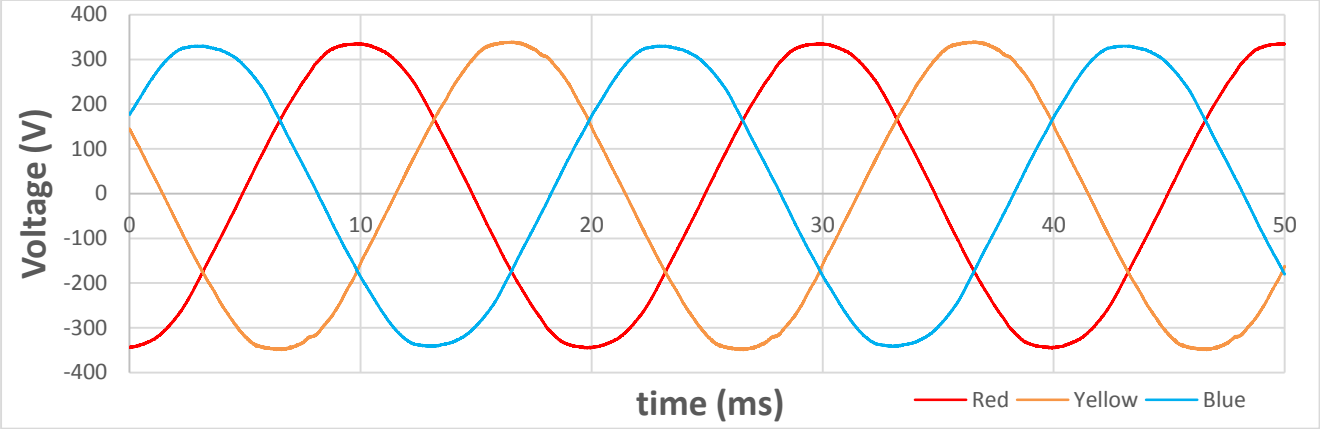

Figure 70: Phase to neutral voltages at MLT PS connection

The line voltages appear to be quite sinusoidal, symmetric, at 50 Hz and peaking at around 325 V. However, the line voltages are not quite ideal. There appears to be a negative bias, as can be seen by the fact that the negative half-cycle drops lower than the positive half. No significant distortion is visible besides for a small variation in the yellow phase near its peaks and troughs. It is also seen that the blue phase's voltage is typically a little smaller than that of the other phases. Otherwise, the waveforms appear as expected of 3-phase, 50 Hz, 230V mains.

6.2.2 RMS, Frequency and phase displacements of voltages before and after injection

We can see below statistical data gathered from the oscilloscope's 'measure' function (see subsection 4.2.6iii), based on input data taken over a longer period (50 ms/window x 6000 counts = 5 min). The mean values of RMS voltage, frequency and phase for all three lines are shown in Table 10. The voltage statistics are clearly within the expected quality of supply boundaries set out in NRS 048-2 [41], both before and after injection. The statistics show the small variations in the PS parameters that can be expected. The supply voltage is seen to be slightly higher during injection – but only on two out of three phases. This increase should be due to the inverter. However, the 'before' and 'after' measurements are separated in time by about 8 min, meaning that the voltage parameters may have naturally varied in this time. The supply voltage is actually almost 15 V higher than nominal (230 V) for all phases and the phase differences are not perfectly 120°. The implications of this may be significant, as the inverter's injection method is based on ideal 120° separated symmetric currents. The frequency is close to 50 Hz as expected.

The standard deviations for each characteristic are shown in Table 11 below – they were about the same for all lines. The low level of these shows that the PS's parameters remained steady over the 5 min period. Further statistical information taken during the 5 min period is shown in Appendix J.

Table 10: Averages of voltage characteristics over 5 min period

	BEFORE	DURING
Phase	AC RMS (V)	
Red	244.39	244.27
Yellow	244.99	245.25
Blue	242.58	242.77
	Frequency (Hz)	
Red	50.054	50.004
Yellow	50.053	50.005
Blue	50.054	50.004
	Phase difference (°)	
Red->Yellow	119.6	119.6
Yellow->Blue	120.1	120.8
Blue->Red	120.3	119.8

Due to the small size of the voltage response due to injection, the phase voltage waveforms during injection are visually indistinguishable from those taken before injection is done. Hence, they are not displayed here.

Table 11: Standard deviations of voltage characteristics over 5 min period

	BEFORE	DURING
Characteristic	Std. dev.	
AC RMS (V)	0.24	0.66
Frequency (Hz)	0.07	0.05
Phase difference (°)	0.21	0.22

The higher standard deviation in the AC RMS during injection is expected to be due to the amplitude modulated voltage components resulting from current injection.

6.2.3 Voltage FFT data, before injection

The FFT of the voltages before injection is shown below in Figure 71. These FFTs were done on 20 s of input data, using a Hamming window. Frequency range is 0 – 1 kHz, such that the horizontal scale is 100 Hz/div. The vertical scale is set to 500 mV/div. The odd-numbered harmonics are labelled on the graph.

a) Red phase

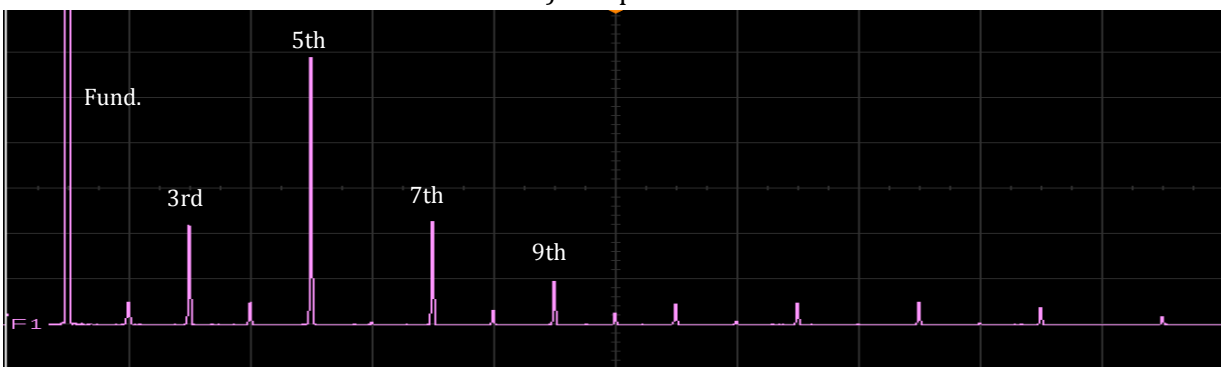

b) Yellow phase

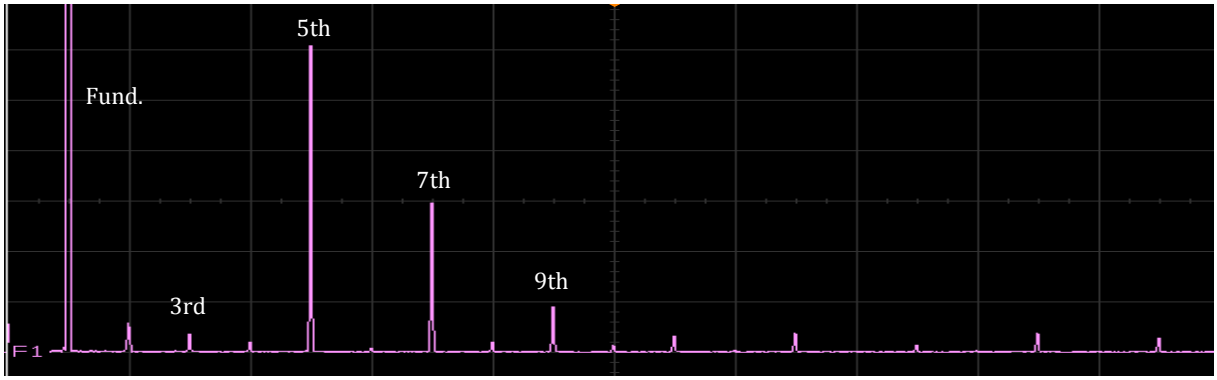

c) Blue phase

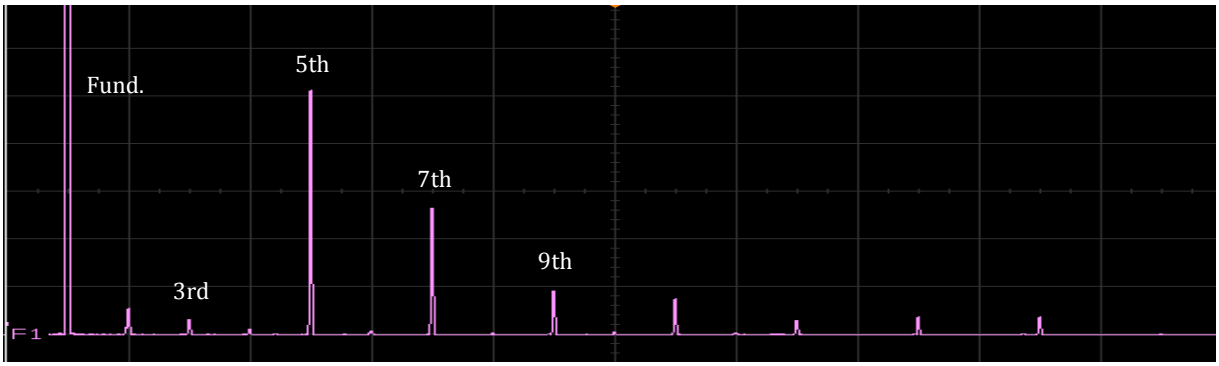

Figure 71: a-c) FFT's of phase voltages before injection

The FFTs in Figure 71 show some interesting results. The large spike to the left is, of course, the 50 Hz component present on all lines, which is not of much interest. We want to look more closely at the harmonics, which are much smaller in magnitude. As expected, we can clearly see significant odd harmonic components – the 5th, 7th and 9th harmonics are all clearly present in all phases. Their levels are slightly different on each line. The harmonic content is typical of that caused by the presence of a nearby 6 pulse drives/rectifiers, switched mode power supplies and fluorescent lights [71] – loads not uncommon for the industrial area of the location. The 3rd harmonic is generally very small, except in the red phase. Some 2nd harmonic also exists, although the higher order even harmonics are insignificant. The spaces between the harmonics where there is no existing frequency component are all available for use as injection frequencies, if no additional components arise during daily operation (this is beyond the scope).

6.2.4 Voltage FFT before and during injection

We can see the change in the voltage spectrum as increases in the voltage components at 37.5 Hz and 62.5 Hz, visible in the FFTs below in Figure 72. Only the blue phase's before and during injection FFT's are shown, together on the same plot. The span of the graph is from 25 Hz to 75 Hz. The large 50 Hz fundamental component is seen in the centre of the plot. The voltage response due to current injection is of the order of several hundred mΩ and the voltage responses are of a different size for each component. This would appear to be due to the reactive component of the impedance, but their difference is too great – linearizing the impedance would give negative impedance around the 25 Hz level. The only possible cause is that the current injection has been weaker at 37.5 Hz than 62.5 Hz. The voltage response on the other phases is seen to be almost identical.

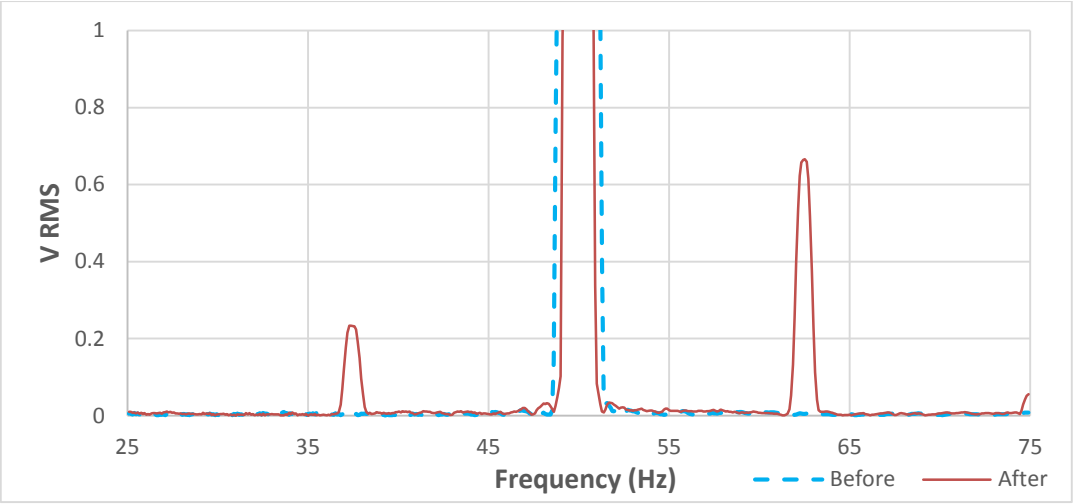

Figure 72: Voltage FFT around 50 Hz before and after injection

6.3 Injection current analysis - description

These measurements are crucial in verifying that the device is operating as expected. As seen in the last stage of testing, this is not always the case. This test is very similar to that in section 5.5.

Again, we are comparing the actual waveforms of the injection currents to those requested, according to $|I_{inj}|$ and f_m set in the software. This is done for all $|I_{inj}|$ and f_m, in order to identify any distortion or unusual behaviour that is dependent on these parameters. From the previous test, it was decided that a frequency domain analysis would be easier to conduct and more effective than a time domain one, hence, much of this test involves producing FFT data of the currents.

6.3.1 Test parameters and procedure

Test dates: 26/10/16, 07/11/16 Duration: approx. 1h each day Elapsed from: not known

Modulation frequency (f_m): **varies,** 6 – 18 Hz in 2 Hz steps
RMS injection current magnitude ($|I_{inj}|$): **varies**, 8 – 18 A in 2 A steps
Resistor/inductor banks: **bypassed**

Controllable input factors: f_m, $|I_{inj}|$, time of day, resistance and reactance in lines
Uncontrollable input factors: ambient temperature, loading and state of PS
Responses: TEI parameter variation

Table 12: Oscilloscope setup

Ch1, Ch2, Ch3	IRed, IYellow, IBlue
Connection at	Inverter input ports
Clamps/probes	3x current clamps
Window size	20 s
Vertical scale	Varies
Output	.csv, .png
FFTs	yes

Separate 'runs' are done for each $|I_{inj}|/f_m$. In each run, the inverter is set up to inject current with set parameters of $|I_{inj}|$ and f_m. Then, we measure and log the current flowing in all three phases connected to the inverter simultaneously. This is as was done in section 5.5, which this test is almost identical to in design. The differences, primarily in the levels chosen for the input factors, as well as the amount of data collected, are discussed in the following paragraphs.

The frequency range is divided so that there is a relatively good frequency resolution for a plot to be made (2 Hz) and so that we investigate the whole of the available output frequencies. The lower bound (6 Hz) is chosen so that we are closer to 50 Hz than in the previous stage but still at least 5 Hz away and hence, unlikely to be affected by spectral leakage. The higher bound is chosen based on the limits of the inverter – a higher frequency cannot be reliably provided and the clicking of the inverter's protection system is heard. In the previous testing stage, this was ignored in favour of collecting results and thoroughly checking whether higher frequencies are desirable (they are not – see subsections 5.6.5 and 5.6.7).

The amplitude range is also changed based on results and recommendations of previous testing (see subsection 5.6.7). The lower bound is 8 A and the upper bound being as high as possible before the clicking of protection is heard. The oscilloscope setup is standard, the scale chosen so that the

waveforms can take up at least 50 % of the screen. A 20 s window is the largest window possible that does not compromise on the quality of the waveform output in terms of sampling frequency, providing enough data for more confidence that random error does not affect the results.

6.4 Injection current analysis - results

6.4.1 Typical 3-phase current waveform

While the inverter is requested to inject at 12.5 Hz, 12 A, the actual measured output is the three phase current waveform shown in Figure 73 below. Only 0.2 s of the waveform are displayed, containing just over 2 cycles of the 12.5 Hz modulation envelope.

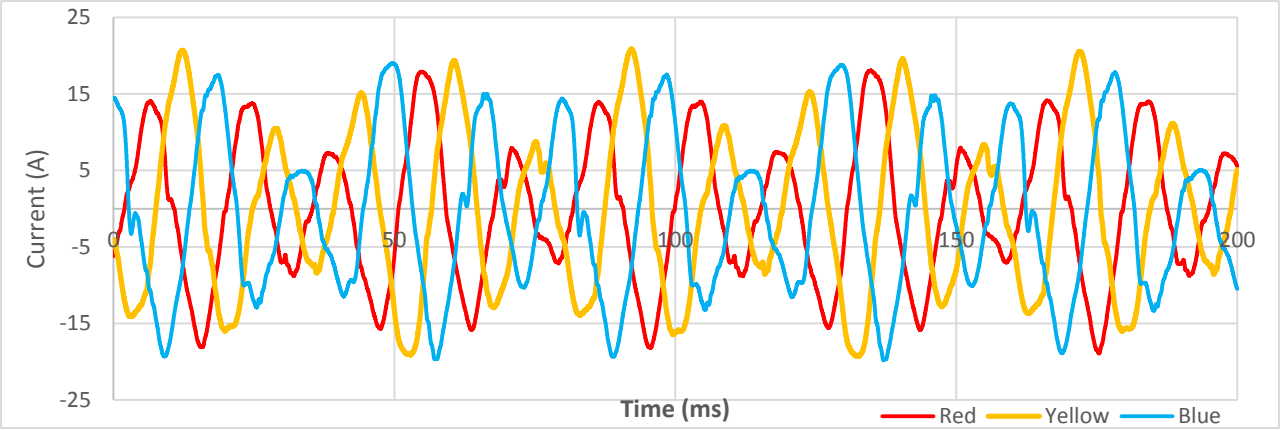

Figure 73: 3 phase injected currents at $|I_{inj}|$ = 12 A, f_m = 12.5 Hz

The current waveforms in Figure 73 are clearly far from the ideal 12 A, 12.5 Hz injection requested. The ideal 12 A, 12.5 Hz injection currents requested are shown in Figure 74 as a point of comparison.

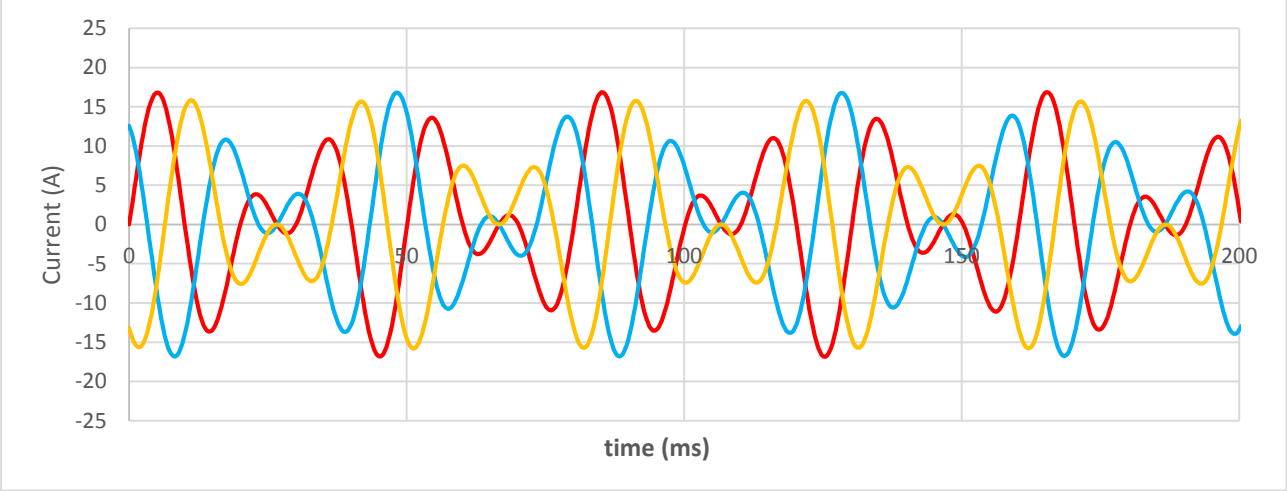

Figure 74: Ideal 3 phase injected currents at 12 A, 12.5 Hz

There are some differences between the two graphs that we can easily recognise immediately. Firstly, in the real case the amplitude of the measured current is considerably larger than that requested (12 A). Secondly, the voltage is never simultaneously zero on all phases, as it should be every 40 ms. Thirdly, we have significant distortion on the waveform, meaning that the envelope of the three waveforms does not form a nice smooth sine wave as it does in Figure 74.

6.4.2 Current FFT at 12 A, 12.5 Hz

In order to better understand the makeup of the waveforms shown in Figure 73, an FFT of the current in each line was taken. These are shown below in Figure 75:

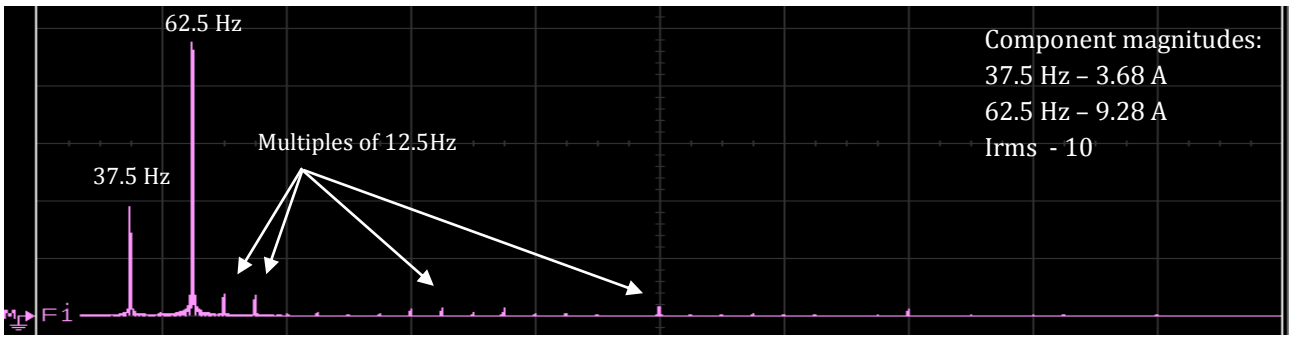

a) Red phase

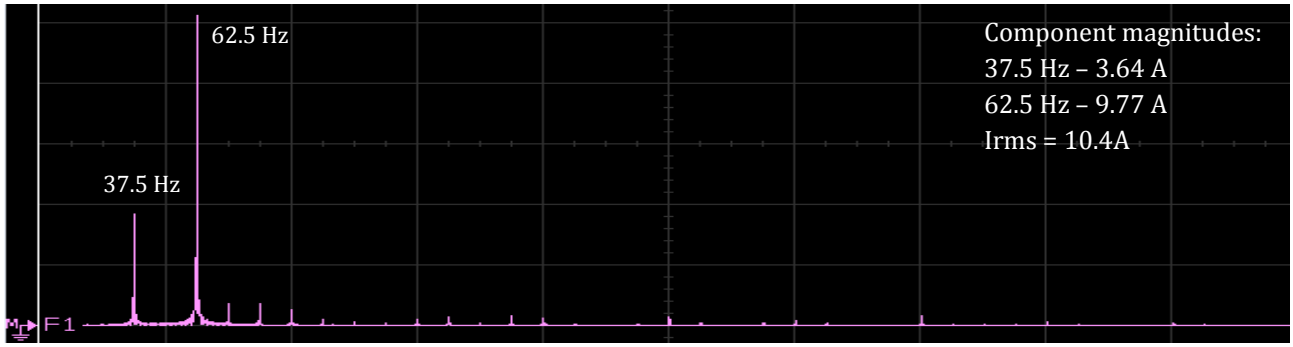

b) Yellow phase

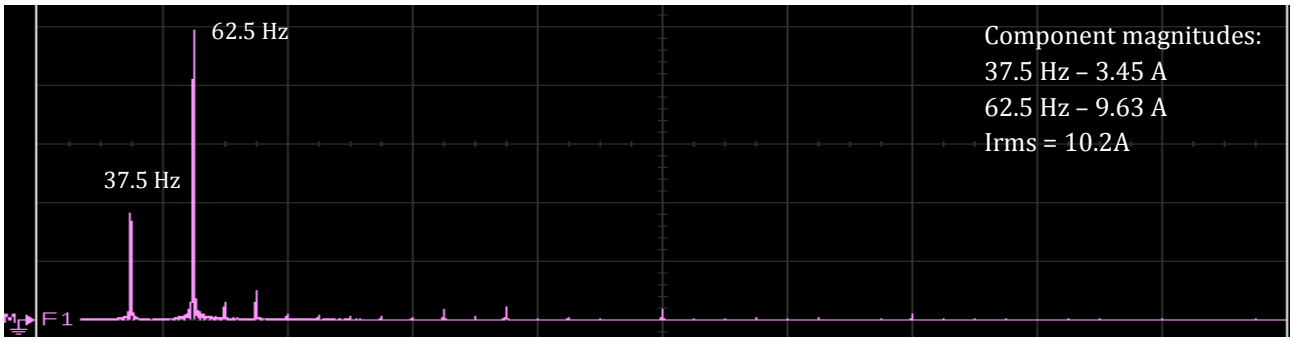

c) Blue phase

Figure 75: a-c) FFT's of line currents during injection, 2 A/div vertical scale

From the images in Figure 75 above, it is clear that the output of the inverter is quite far from the modulated sine wave that was intended. Instead of having two equal weighted components at 37.5 and 62.5 Hz, we see in all cases a 62.5 Hz component that is more than double that of the 37.5 Hz one.

A further observation is that there are many small current components above 62.5 Hz, approximately equally spaced at 12.5 Hz.

From the data on the right in Figure 75, it is clear that we have unequal currents in each line, despite having requested for a symmetric current output. Assuming that the currents are in fact symmetrical in terms of phase difference (120°), we would have a resultant current flowing through the neutral made up of 0.21 A 37.5 Hz and 0.43 A at 62.5 Hz.

Another notable observation is that the components in I2 are several hundred millihertz off of their required frequencies. This further adds to a nonzero sum at the common point.

The smaller harmonic components are at multiples of f_m away from the USB and LSB and seem to continue up past 500 Hz.

6.4.3 *Effect of varying injection level ($|I_{inj}|$)*

FFTs were taken of the output current for the red, yellow and blue phases at every value of $|I_{inj}|$ requested from the inverter. Each FFT appears as two components at 12.5 Hz, a lower sideband (37.5 Hz) and an upper sideband (62.5 Hz). The levels of these components are plotted in Figure 76 below.

The relationship between $|I_{inj}|$ and the measured LSB and USB components was linear in all cases. For the LSB, the gradient was much smaller and the ratio between the two sidebands grew from about 2 to about 2.5. The cause of this behaviour is assumed to be due to the hardware of the inverter performing worse tracking of setpoints at higher injection levels. The fast changing of the current seems to be an issue. Furthermore, there is a marked difference between the currents according to phase. It seems that the inverter module connected to the red phase was not able to match the current output of the other phases. This suggests that different TEI estimation performance will be obtained from the different ports and, thereby, the different phases. The red phase is thus expected to have a poorer SNR due to this behaviour.

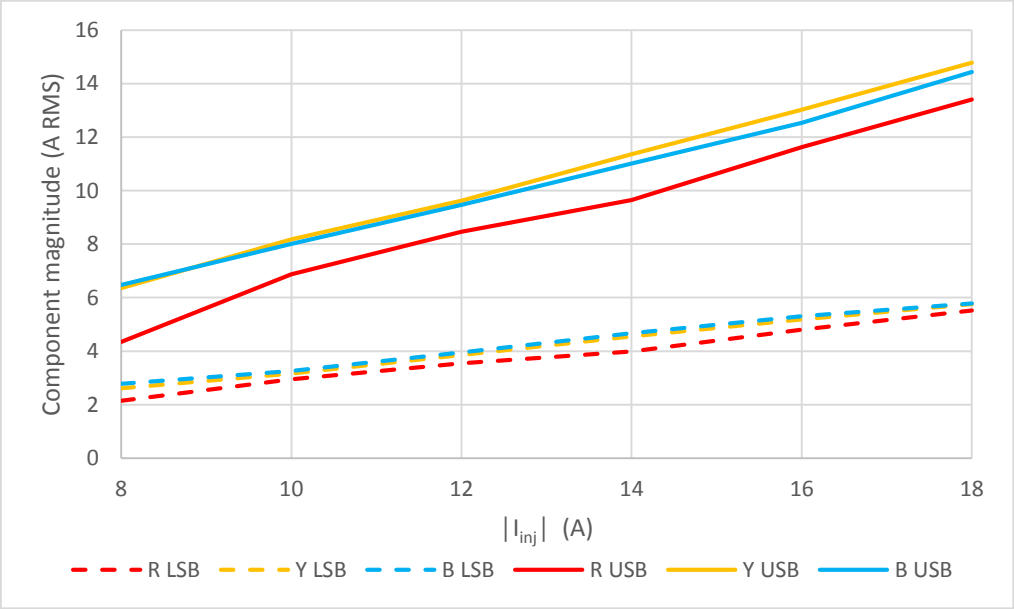

Figure 76: Measured upper and lower sideband components for varying $|I_{inj}|$

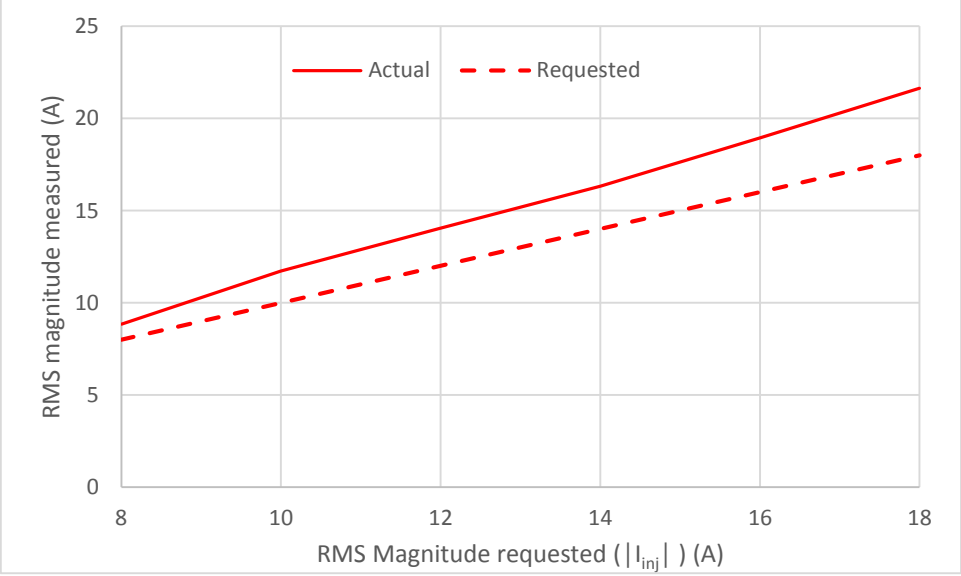

Figure 77: Average measured current output of each phase compared to that requested

Figure 77 shows the average rms current measured at the output of the inverter vs. the requested magnitude ($|I_{inj}|$) for all injection levels. In all cases, the output current is significantly higher than requested. Given that the TEI calculations performed by the inverter are not based on setpoint values but rather done with measured current and voltage information, the TEI algorithm takes the behaviour seen in Figure 77 above into account in the calculation (by using measured output currents).

6.4.4 Effect of varying modulation frequency (f_m)

The device was instructed to inject current at a constant $|I_{inj}|$ = 12 A, whilst f_m was varied. FFT data was extracted by the oscilloscope for each frequency and plotted together in Figure 78 below.

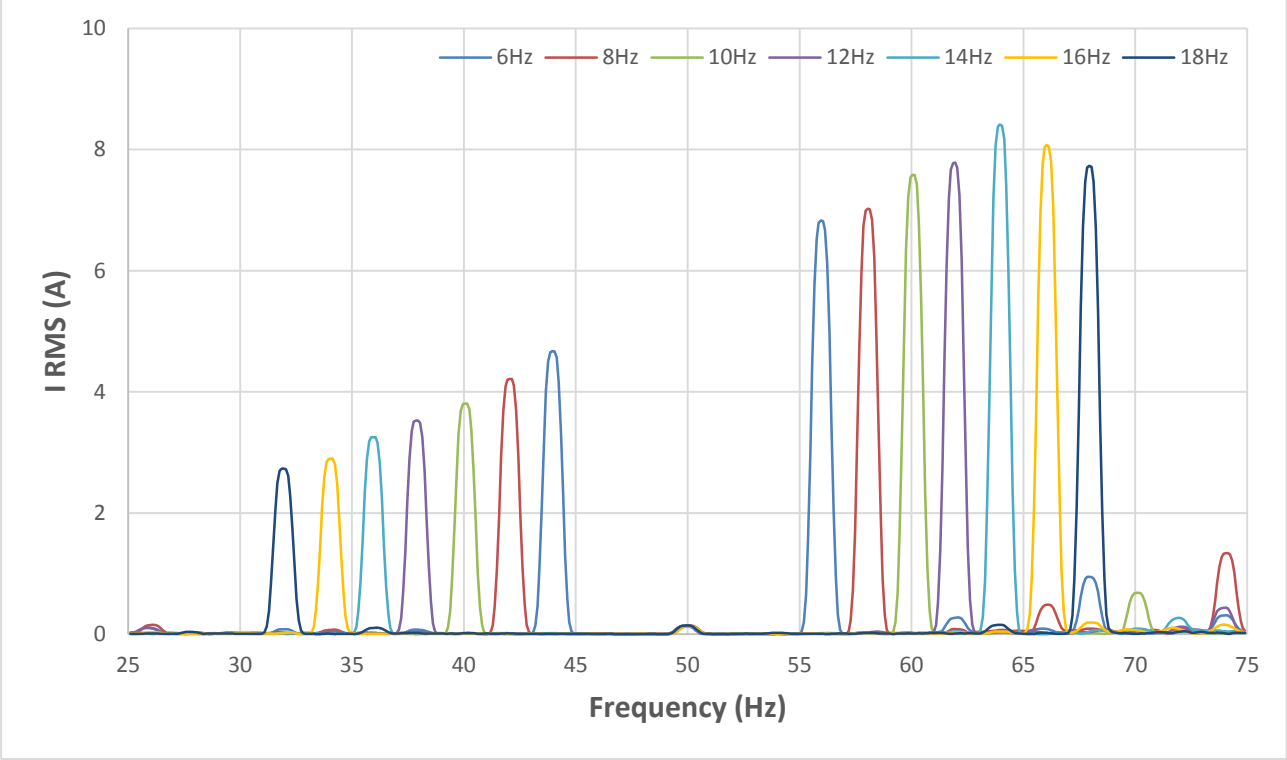

Figure 78: LSB and USB component magnitude variation with f_m

Clearly, the level of the components injected varies, depending on the modulation frequency. Closer to 50 Hz, the device injects a current that is closer to the target equal-weight components as presented in subsection 4.1.4iii. This is as expected, as the inverter's hardware was designed to perform accurate current injection at the fundamental frequency of 50 Hz. The impact of this behaviour is quite significant. The Z_{th} parameter is most independent of this current distortion, seeing as the USB and LSB values are combined to extract Z_{th}. However, calculations of X_{th} and R_{th} are expected to be inaccurate due to the difference in sideband size. This is due to the low level of the lower sideband, meaning that voltage response due to this component is more difficult to extract accurately, hence X_{th} and, thereby, R_{th} accuracy, may suffer.

Although varying $|I_{inj}|$ has no effect on f_m, the changing levels seen in Figure 78 above mean that the device is not able to maintain the requested 12 A RMS injection at high frequencies. Figure 79 shows this, as I RMS is plotted against f_m. The obtained current output increases greatly as frequency is increased. It is only at the lower levels of frequency that the output is comparable to what is requested from the inverter by its software.

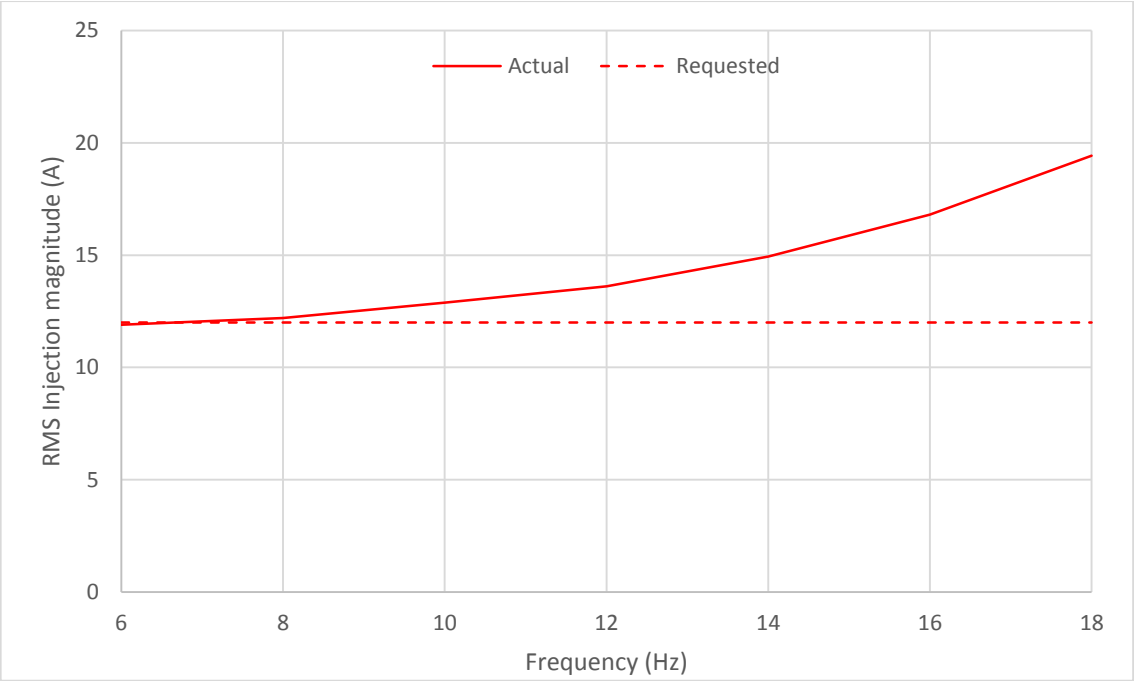

Figure 79: Unwanted injection magnitude variation with f_m

The unwanted injection magnitude variation with f_m poses a problem, as it prevents us from keeping the injection current magnitude constant to independently measure the effect of f_m variation.

6.5 Steady-state (constant impedance) measurement performance of ports - description

We are again investigating the symmetry between the different phase modules of the inverter. That is to say, we wish to see how different inverter ports measure the same line. This test allows us to potentially calibrate/correct for differences between each module and, hence, obtain more accurate levels for the impedance parameters of each phase.

6.5.1 Test parameters and procedure

Test date: 24/10/16 Duration: 00:10:20 x 3 Elapsed from: 14:34 – 15:45
Modulation frequency (f_m): 12.5 Hz (**standard**)
RMS injection current ($|I_{inj}|$): 12.0 A (**standard**)
Resistor banks: **bypassed**

Controllable input factors: f_m, $|I_{inj}|$, time of day, resistance and reactance in lines, phase rotation, time delay between runs
Uncontrollable input factors: ambient temperature, loading and state of PS
Responses: TEI parameter variation

The procedure is the same as that of the corresponding test (subsection 5.3.1) from testing stage 1, only that the duration of each of the three 'runs' is longer. Hence, the design of the tests is almost identical, the justification of which has been provided in subsection 5.3.1.

The resistor/inductor banks are bypassed simply because they are not needed for this test – they are applied in the *dynamic* impedance measurement test (section 6.7) to follow. Thus, we are directly measuring the PS's parameters at the local connection.

Three separate tests are done at separate times (consecutively with about 5 min between). This is unavoidable seeing as changing the phase rotation requires powering down of the inverter and the PS socket, which ends each test.

Only a short duration, 10:20, is taken of the PS's behaviour for each test. This is due to time restrictions in the test facility. Based on the long sensing test's results (subsection 5.2.3), it is considered very unlikely that any significant random event will occur during the test and go unnoticed to give inaccurate results.

6.6 Steady-state (constant impedance) measurement performance of ports - results

6.6.1 Red phase parameters on different ports

A small portion of the results from the changing phase rotation test are shown here. Figure 80 contains a graph of the Thévenin equivalent resistance of line 1, as measured at the three separate inverter ports. Please be aware that the red, yellow and blue lines in the graph do not refer to red, yellow and blue phases as was previously the case.

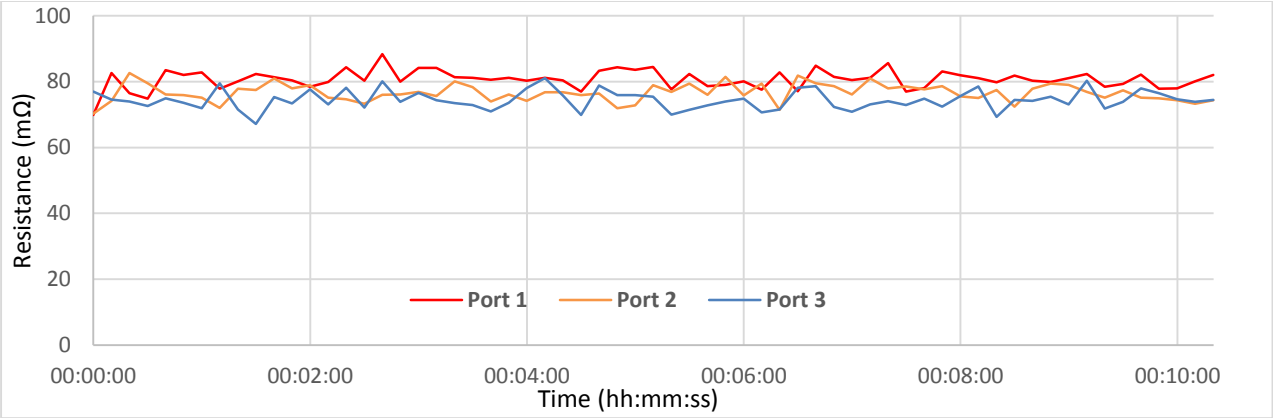

Figure 80: Red phase R_{th} parameter measured using different ports

As seen previously in the almost identical changing phase rotation test (section 5.4), the average level of the R_{th} parameter obtained with different ports shows a consistent distribution. That is, each of the three ports measures slightly offset R_{th} parameter average values compared to the others. Furthermore, the Z_{th} and X_{th} parameters show similar behaviour, as seen in Figure 81 below.

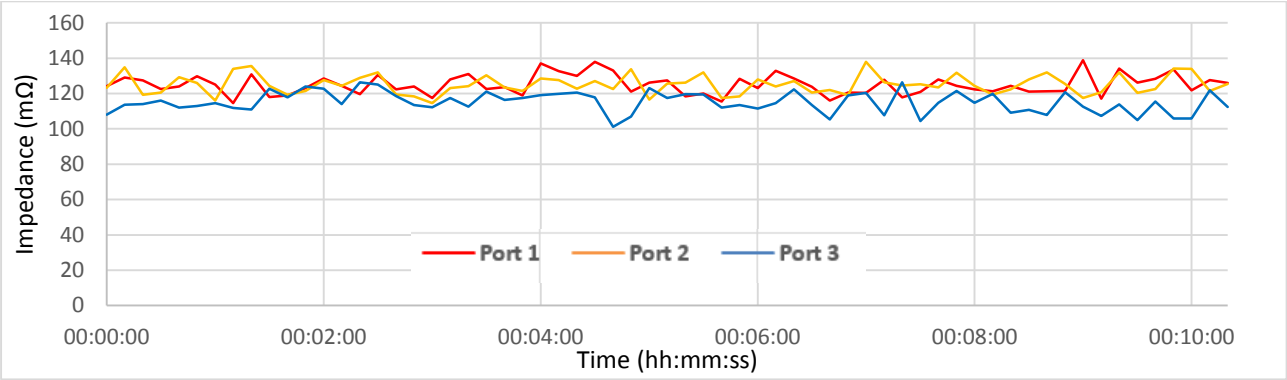

Figure 81: Yellow phase Z_{th} parameter measured using different ports

6.6.2 Analysis of port influence

There appear to be differences between the plots in Figure 80. In general, the average level of the red phase is slightly greater than that of the blue phase over a given window, regardless of the phase being measured. This trend was investigated by comparing the average levels obtained by each port for Z_{th}, R_{th} and X_{th} measuring the same line. Table 13 shows the relevant Z_{th} parameter characteristics of each line according to each port.

Table 13: Comparing differences between inverter ports - Z_{th}

	AVERAGEs				STANDARD DEVIATIONS		
	Port 1	Port 2	Port 3		Port 1	Port 2	Port 3
L1	106.4	103.0	96.4		4.27	5.17	5.66
L2	125.0	125.1	115.1		5.62	5.46	5.90
L3	111.2	105.2	100.1		4.96	4.96	4.72

It remains true that the average level of the parameters of each line may have changed from one test to the other due to their variation with time, or indeed even during the test. The results from a future test can be used to verify this assumption once more data has been collected regarding the variation of the parameters (Appendix L).

If we compare the averages done by the ports for the three lines numerically, we see that port1 on the inverter tends to overestimate the line's impedance (Z_{th}) by 4% and port 3 tends to underestimate the line's impedance by 5 %, whilst port 2 does not seem to over or underestimate much compared to the mean of the three measurements. This was quite consistent for measurement of any of the three phases. The mean of the three measurements of a phase is considered to provide the most accurate value of the phase's parameters. With these percentages, corrections can be made to any data provided by the inverter – i.e. Z_{th} measured by port 1 is decreased and by port 3 increased accordingly. The source of these differences may be related to the different levels of current injection achieved by each port of the inverter, suggesting that the red port which injects a lower current causes a lower estimate of the TEI of the line.

In terms of standard deviation, port 1's was about 5 % less than the mean and port 3's about 4 % more. This behaviour was similarly seen in R_{th} and X_{th}.

6.7 Dynamic (impedance change) measurement performance of ports – description

Following from subsection 6.5, this test goes deeper into analysing the differences between separate phase modules. In this case, we do not simply look at the steady-state level of parameters measured by each port. Here, the ability of each port to accurately measure a known change in impedance is analysed.

6.7.1 Test parameters and procedure

Test date: 03/11/16, 04/11/16 Duration: 00:10:20 x 3 Elapsed from: 14:34 – 15:45
Modulation frequency (f_m): 12.5 Hz (**standard**)
RMS injection current ($|I_{inj}|$): 12.0 A (**standard**)
Resistor/inductor banks: **RB_1 rotated between lines (1), IB_1 rotated between lines (2)**

Controllable input factors: f_m, $|I_{inj}|$, time of day, resistance and reactance levels (before and after step for each line), time delay between runs

Uncontrollable input factors: ambient temperature, loading and state of PS
Responses: TEI parameter variation

Table 14: Resistor/inductor bank setup

Change	Magnitude (mΩ)	
	ΔR (1)	ΔX (2)
'Small step'	44	31
'Large step'	93	63

We have two separate test stages, generating two sets of data, which are almost identical:

(1) – Changing phase resistance measurement

Essentially, three separate runs are done, one for each phase. For each run, we have a resistor bank (RB_1) placed in series within a single phase. In the first run this is the red phase, second run yellow and so on. The bank is switched according to the procedure in Figure 83. This switching procedure is the same for each separate run and the same bank is used. Hence, exactly the same resistance changes are effected in each line.
For this first half of the test, the small step and large step effect only a *resistance* change. The size of this change is shown in Table 14, under the ΔR column.

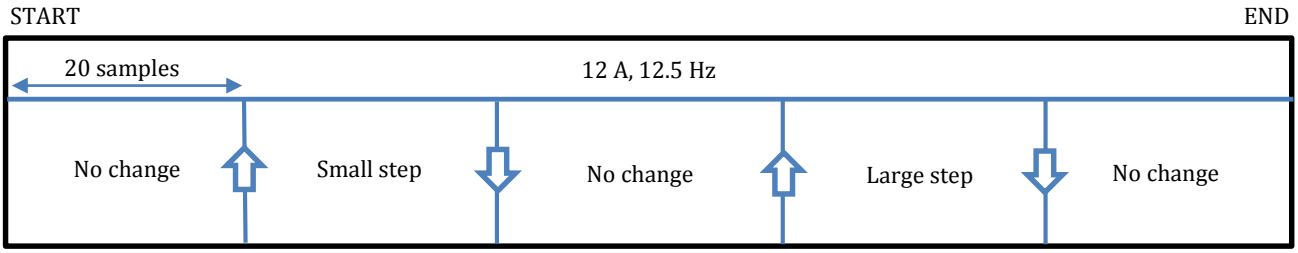

Figure 82: Bank switching procedure

(2) Changing phase reactance measurement

Part 2 involving reactance is almost identical to part 1 involving resistance. In this case we use an *inductor bank* rotated between phases (instead of the *resistor bank* in (1)) and perform the same

switching procedure. Referring back to Figure 82, the small and large change now refer to a *reactance* change whose size is shown by the ΔX column in Table 14 above.

The justification for the resistance changes used remains the same as from the previous test (see subsection 5.9.1). The reactance steps chosen here follow the same justification in terms of reactance instead of resistance.
More inductor banks could not have been used because their switching caused the inverter's protection to disconnect it from the PS. A separate test is done in which a very large amount of resistance and inductance is switched into the PS, albeit in smaller steps to avoid disconnection.

The switching procedure is somewhat similar to that in the previous stage of testing. In this stage, however, several improvements have been made. Most notably, the number of samples at each switching state is doubled (20 vs. 10) and there are now two different changes effected on the same line (small and large). This decreases the impact of any random errors, providing an increase in confidence that can be placed in the results. In this case the focus is on a single line – thereby, the processes of analysis and test procedure have been simplified, as well as the general setup.

6.8 Dynamic (impedance change) measurement performance of ports - results

Note that spikes in the data larger than 10 % of the average level were removed. These occur at a rate of about 1 in every 5 minutes and have the potential to skew the average level that is calculated over the relevant interval. This way, spikes are considered to be unusual behaviour that does not give useful information. The typical spike removal process is shown in Appendix K.

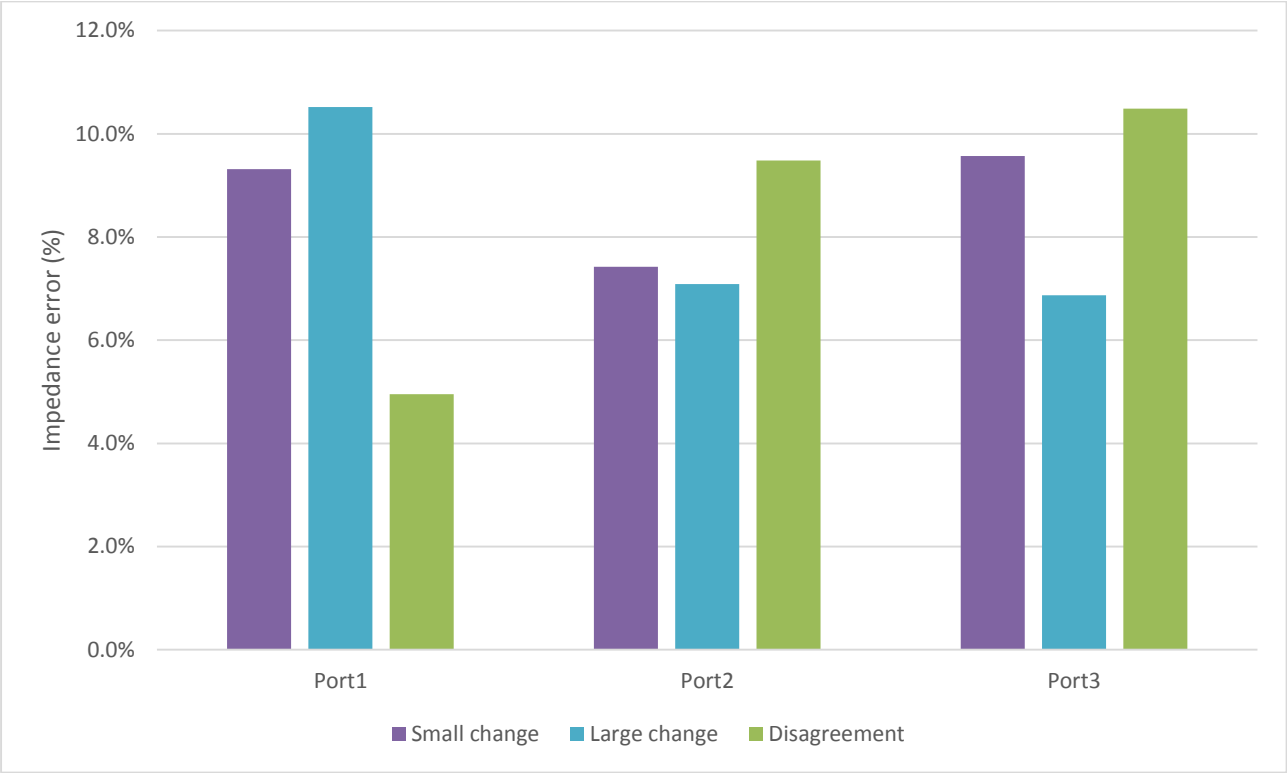

Figure 83: Impedance change measurement performance of different ports

From Figure 83 above, we see differences in the impedance change measurement performance of the different ports. At the parameters tested, the differences are almost negligible (less than 5 %). It is therefore expected that optimisation of a given port's impedance estimation accuracy will also mean optimisation of the other ports. This is a reasonable assumption based on the symmetrical nature of the process and the results shown here.

6.8.1 Temperature considerations

Given that this test is performed at 12 A, we can expect that the heating effect on the resistor banks will be greater than that described by subsection 5.8.1 for 10 A. Despite the longer duration of this test, allowing for more heating, we still only expect that 1 mΩ heating will occur (see Appendix G). Thus, 1 mΩ corrections were applied to the large changes.

6.9 Long sensing test - description

Since we have changed the location of our testing, it is expected that the PS's behaviour and parameters have also changed from before. Hence, it is important that long term behaviour is logged so that we know what to expect from the other tests. Furthermore, comparison to the previous tests will allow us to validate our results for typical PS impedance, as well as its behaviour.

6.9.1 Test parameters and procedure

Test date: 9/11/16 Duration: 08:00:00 Elapsed from: 14:24 – 22:24
Modulation frequency (f_m): 12.5 Hz (**standard**)
RMS injection current ($|I_{inj}|$): 12.0 A (**standard**)
Resistor/inductor banks: **bypassed**

Controllable input factors: f_m, $|I_{inj}|$, time of day, resistance in lines
Uncontrollable input factors: ambient temperature, loading and state of PS
Responses: TEI parameter variation

The test duration was chosen in order to obtain a large amount of data regarding variation of the PS, slightly longer than that of the previous long sensing test (6 h). The time span covers the early afternoon – late evening period, when it is expected that the most significant PS-side changes of the day would be occurring due to load variation. Thereby, the probability that they manifest themselves in the TEI obtained is maximal. No additional impedance is placed into the lines so that the focus is on only the PS itself. Normal phase rotation is used with port 1 connected to red phase and so on.

Using the standard f_m and $|I_{inj}|$ allows for results from the previous long sensing test to be compared, which is beneficial for checking the consistency of results and the testing method, as well as understanding how location affects TEI and its behaviour. There is no overlap in the time of day during which the two tests are performed. This is done in favour of sensing during the greatest change in daily loading, occurring during the evening, which has the most potential to change the PS's state and hence affect the measurements.

6.10 Long sensing test - results

6.10.1 Parameter variation over 8h

The 8 hours of TEI data was successfully obtained. Figure 84 below shows the variation in the Z_{th} parameter over this period for all three phases and neutral as measured by the inverter.

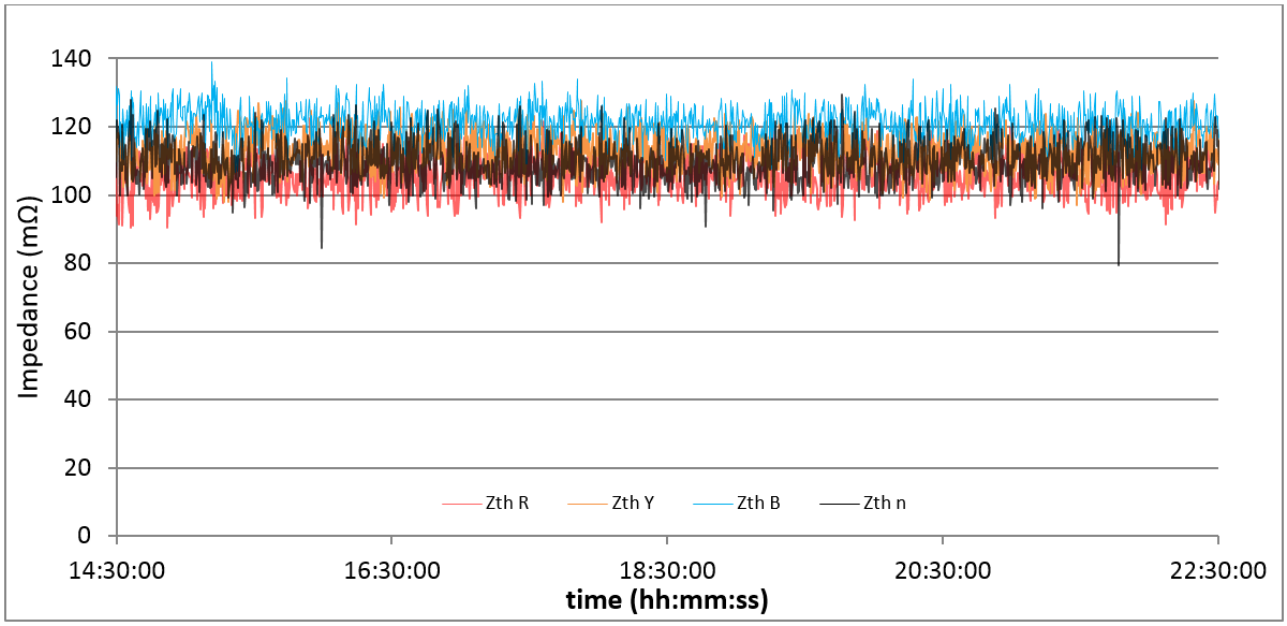

Figure 84: Long sensing test - Z_{th} parameters

Here we see some variation in the parameters, although appearing to be about an unchanging, constant mean. Similarly to the previous long sensing test (concerned instead with R_{th}) we see that the parameters are quite steady about an average, with some high and low frequency variations. The parameters all lie around 100-120 mΩ, hence the PS's impedance seems to be quite well balanced. The value of Zn is seen to be about the same level as the other lines.

In the previous testing stage, the Z_{th} parameters were logged but the R_{th} parameters were the main concern and hence they were shown. Below are shown the Z_{th} parameters from the previous test (see Figure 85), which we have not considered before. They allow us to compare the long-term Z_{th} behaviour between the two different testing locations, dates, setups and times.

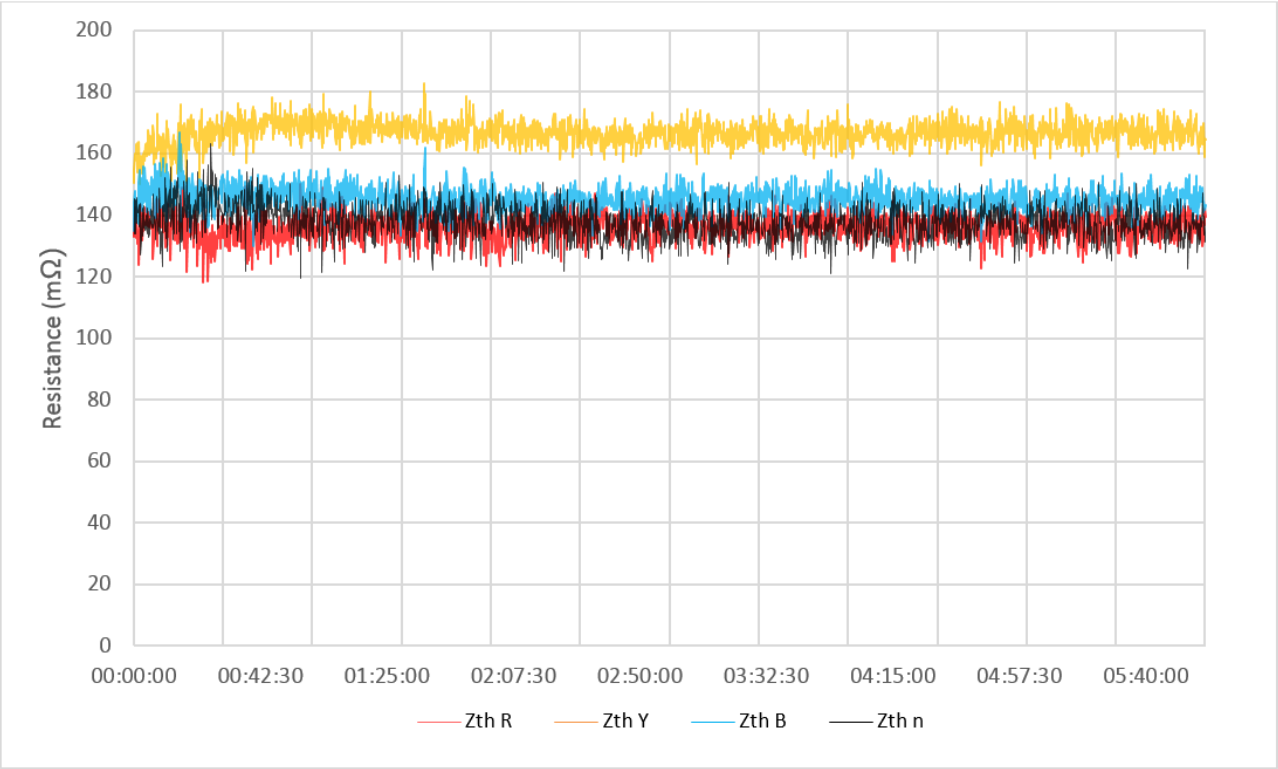

Figure 85: Previous long sensing test (Phase 1) - Z_{th} parameters

Note that, despite being carried out in different locations and at different times of the year, the results of Figure 84 and Figure 85 show a good deal of similarity. Note that the previous test involved an added ≈50 mΩ in all phases. With this in mind, the PS impedance at both locations should be similar (around 100 mΩ) and the variations are of similar magnitude. The unbalance between the lines is, however, quite different. Note also that the nature of the unbalance is different; that is to say that the blue phase is now of highest impedance, whereas in the previous test it was the yellow phase. Furthermore, the large positive spikes on blue phase seen in the previous testing stage do not seem to occur in this stage, suggesting that they are related to the local conditions at the UCT connection (see Figure 86).

The consistency in results between this testing stage and the previous strongly suggests that the nature of the local PS in terms of TEI is similar at the two locations, but by no means identical.

6.10.2 Parameter variation over first 20 min only

The fast variation of the parameters is better understood if we look at a 'close up' view – Figure 86 shows only the first 20 minutes of the data. The higher frequency variations are then more clearly visible. No unusually large spikes are occurring on the blue phase (as compared to Figure 46 in subsection 5.2.2) and the variation in the parameters is of similar size for each phase and the neutral.

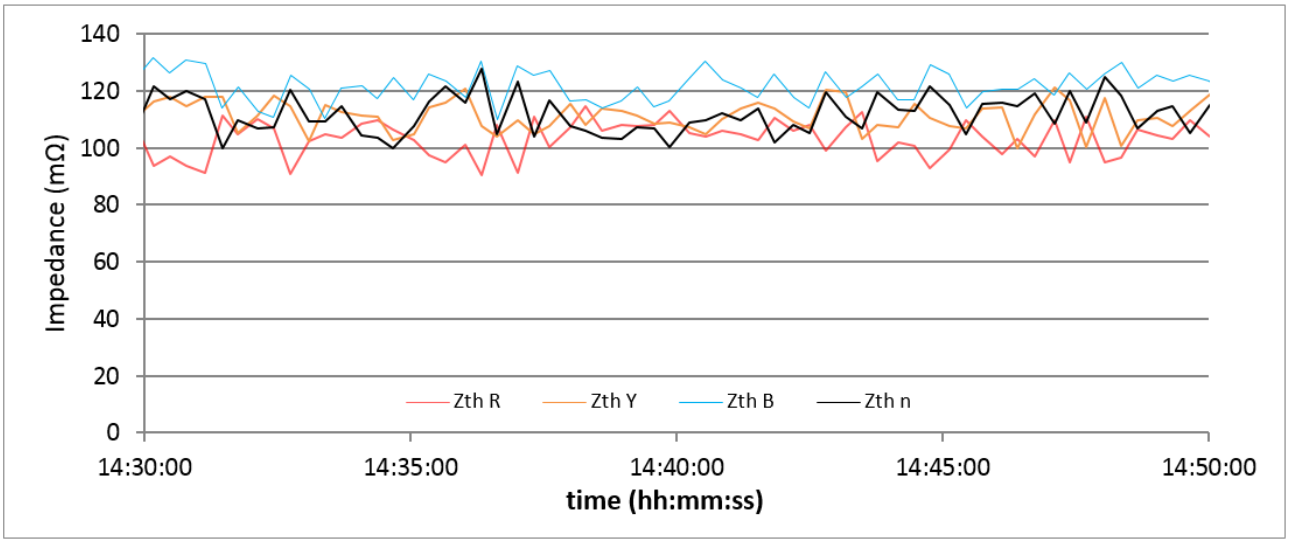

Figure 86: Long sensing test – Z_{th} parameters – first 20 min only

6.10.3 Statistical analysis of 8h parameter data

The average of each line's parameters is shown in the bar chart of Figure 87 below. The error bars in the chart show the standard deviation of each parameter. Note that the chart below is not based on the raw data – corrective factors for port influence have been applied, as determined in subsection 6.6.2.

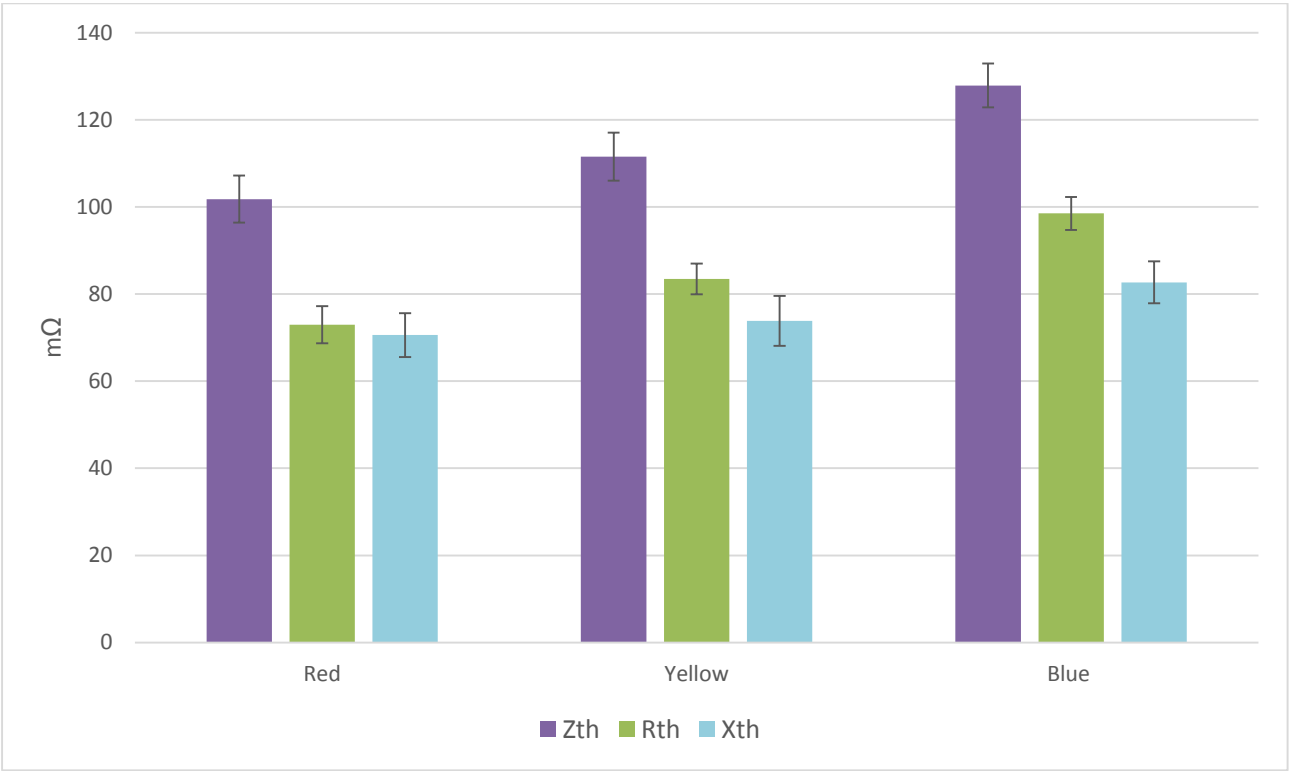

Figure 87: TE parameter averages over 8 h period, error bars are std. dev.

Compared to the previous stage of testing, we see that the resistance parameters are much less spread out than before. The lines have more even impedance levels, all within 20% of each other, suggesting that the lines are more balanced at the MLT connection. Furthermore, the standard deviation for each parameter seems to be of the same level between the three lines, reinforcing that the behaviour of the parameters is quite consistent on all phases. The standard deviations here are of similar size to those measured in testing stage 1 (subsection 5.2.3). The standard deviation of the X_{th} parameter is significantly greater than that of R_{th} for all phases, suggesting that there is more uncertainty in its estimation.

The correlation between the R_{th} parameters during the long sensing test is displayed in Table 15 below, together with the correlation obtained for the testing phase 1's long sensing test for comparison. It is clear that the correlation has changed between all parameters, with the exception of $R_{th\ R}$ and $R_{th\ n}$ which remains the same due to the same reason as described in subsection 5.2.2. The changed correlations show us that the TEI behaviour between phases has changed with the changed location and that the variations in the parameters do not appear to be tied to the inverter hardware.

Table 15: Correlation between R_{th} parameters from long sensing test data, compared to previous test

Colours:	Parameters:	Correlation:	
		Testing stage 2 (current)	Testing stage 1 (previous)
	$R_{th\ R}$, $R_{th\ Y}$	0.19	0.06
	$R_{th\ R}$, $R_{th\ B}$	-0.10	0.37
	$R_{th\ R}$, $R_{th\ n}$	-0.79	-0.85
	$R_{th\ Y}$, $R_{th\ B}$	-0.20	0.16
	$R_{th\ Y}$, $R_{th\ n}$	-0.09	-0.06
	$R_{th\ B}$, $R_{th\ n}$	0.16	-0.28

Figure 88 below contains a high-resolution histogram plot based on the entire 8 h results. This plot allows us to gain a greater understanding of the distribution of the data, and is the same type of plot as was used previously in subsection 5.2.3. As was the case in the previous testing stage, the spread of the data is quite symmetrical about the mean, loosely fitting the bell-curve shape of a normal distribution. The spread of the data is greater as compared to the corresponding results from the previous testing stage (Figure 47), and this can be partially attributed to the added 50 mΩ offset present in the previous stage.

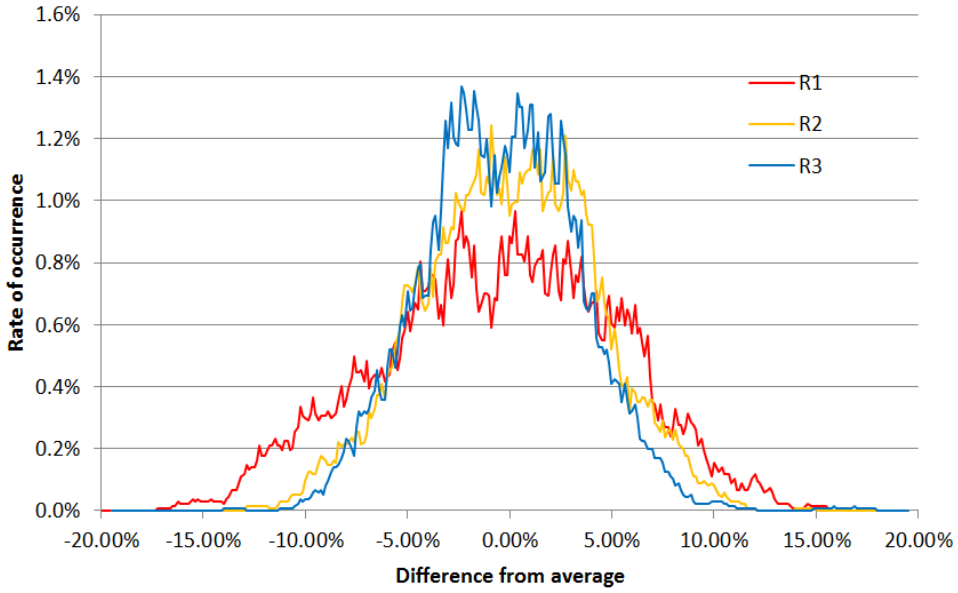

Figure 88: Distribution of parameters about mean over 8 h period

T- tests were performed to compare the results from the two long sensing tests performed during the different stages. One two-sample t-test assuming unequal variances was done for each resistance parameter, with the hypothesised mean difference set to the value of the measured resistance of the relevant bank according to Appendix H in each case (average of Yokogawa and SG+MM results). All results show that the null hypothesis is rejected – the data obtained from the different locations cannot be considered to be from the same set. This supports the postulate that the TEI is dependent on location.

6.10.4 Moving averages applied to 8h parameter data

It is of interest to separately consider the slower variations in the parameters. Whilst this kind of variation was not clearly visible in Figure 84 and Figure 85, applying a moving average to the data reveals these variations more clearly. Figure 89 and Figure 90 show the long sensing test data with an 8 minute and 25 minute moving average applied. These windows were arbitrarily chosen.

Note that the graphs do not begin at 0 mΩ. Corrective factors have been applied to this data as done before.

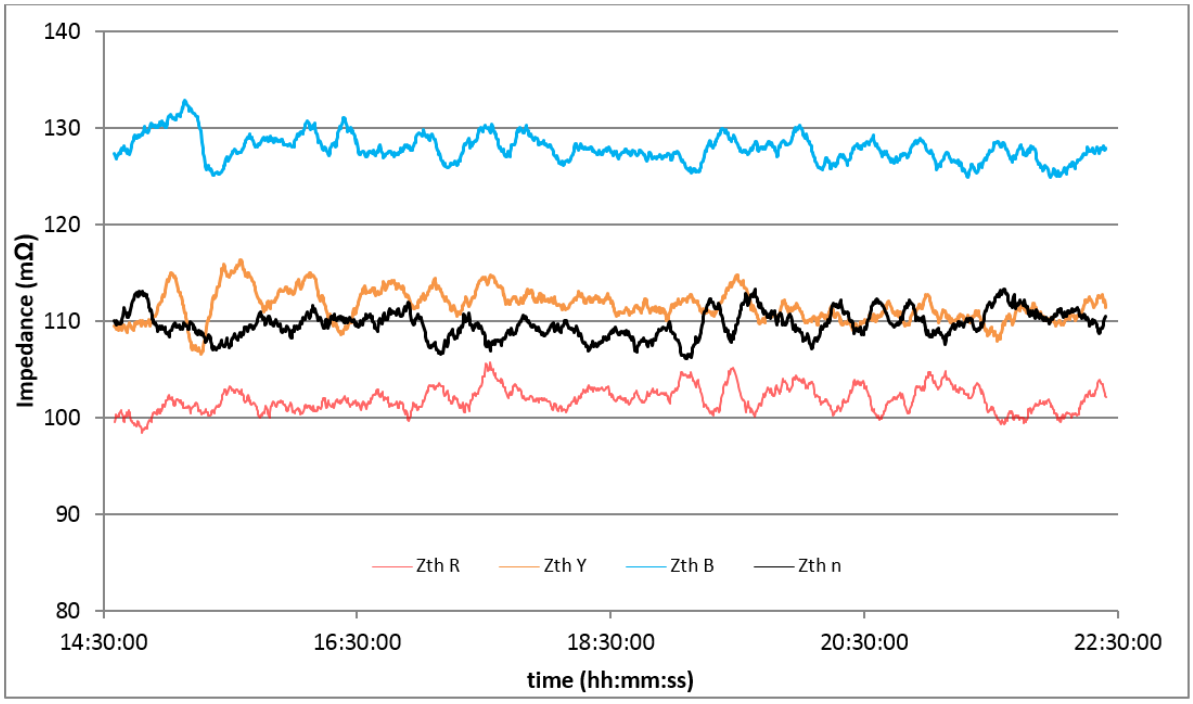

Figure 89: 8 minute moving average of long sensing test data

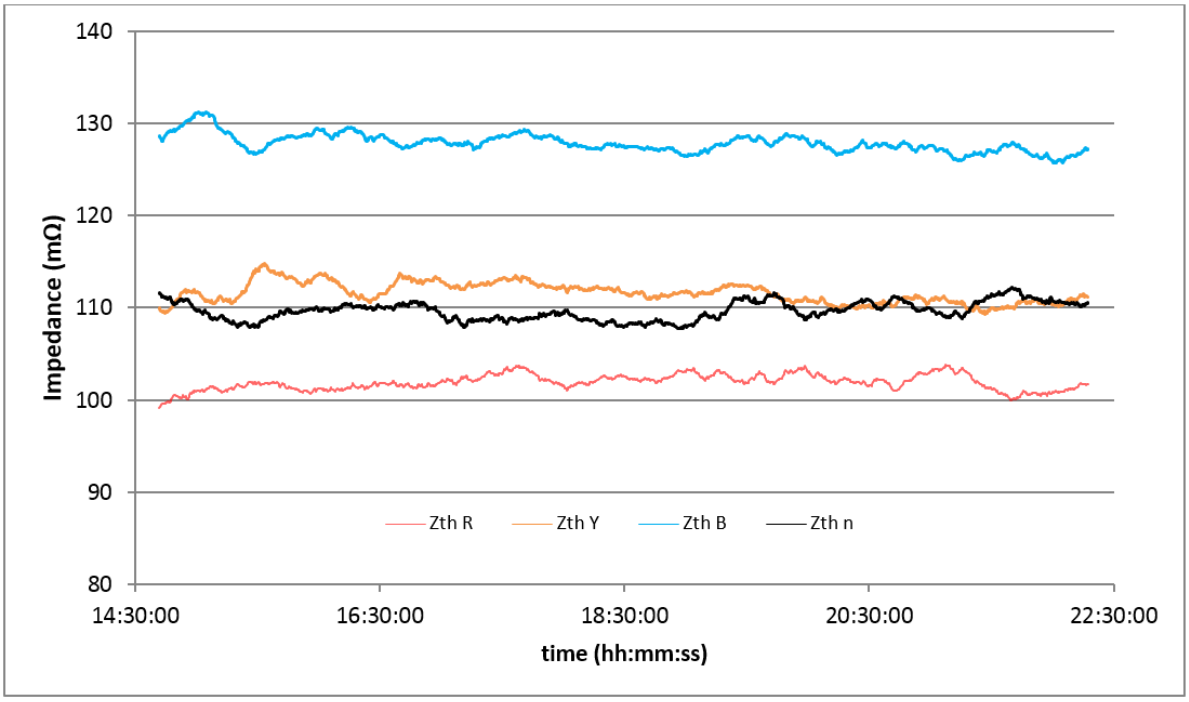

Figure 90: 25 min moving average of long sensing test data

From Figure 89 and Figure 90 above, it is clear that there is a slight slow variation in the level of the TEI of every line. Furthermore, this variation appears to be correlated between lines. The variation is small, such that the parameters always remain within about 2 mΩ of the average. Furthermore, the troughs and peaks in Figure 89 appear repetitive. It is possible that the variations may be a manifestation of three-phase load variation in the PS. There may be a cyclic heavy load connected at proximity to the PCC.

The small size and apparent randomness of variations would seems to suggest that they are noise related, however, the large timescale of the test would average out such behaviour. It is also not possible to rule out the possibility of external influences such as temperature fluctuations of the device being the cause, given the small size of the variations. The variations are seen to be very similar to results from the previous testing stage, shown in Appendix M.

6.11 Variation of injection current magnitude ($|I_{inj}|$) - description

This test is similar to that done in the previous testing stage, with some important differences. Its purpose is the same – to determine how varying $|I_{inj}|$ affects the effectiveness of the device to reliably measure the PS's TEI parameters. This is intended to directly confront the question of which value of $|I_{inj}|$ should be used for the TEI estimation.

6.11.1 Test parameters and procedure

Test date: 07/11/16 Duration: 00:20:00 x 6 Elapsed from: 12:22 – 14:47
Modulation frequency (f_m): 12.5 Hz (**standard**)
RMS injection current ($|I_{inj}|$): 8 A – 18 A (**varies**)
Resistor/inductor banks: **RB_1, IB1 and IB2 in Red phase throughout**

Controllable input factors: f_m, $|I_{inj}|$, time of day, resistance levels (before and after step for each line)
Uncontrollable input factors: ambient temperature, loading and state of PS
Responses: TEI parameter variation

Table 16: Resistor/inductor bank setup

Change	Magnitude (mΩ)	
	ΔR	ΔX
'SMALL'	50	63
'LARGE'	105	126

As in section 6.7, this test involves resistance/reactance changes.

Starting at Y = 8 A, a 20 min test is done according to the procedure shown in Figure 91. This is done for Y = 8 A, 10 A… 18 A. The exact sizes of the resistance and reactance changes effected during the test are shown in Table 16 above. In this case, both ΔR and ΔX change for each step. The large step is about twice the size of the small step.

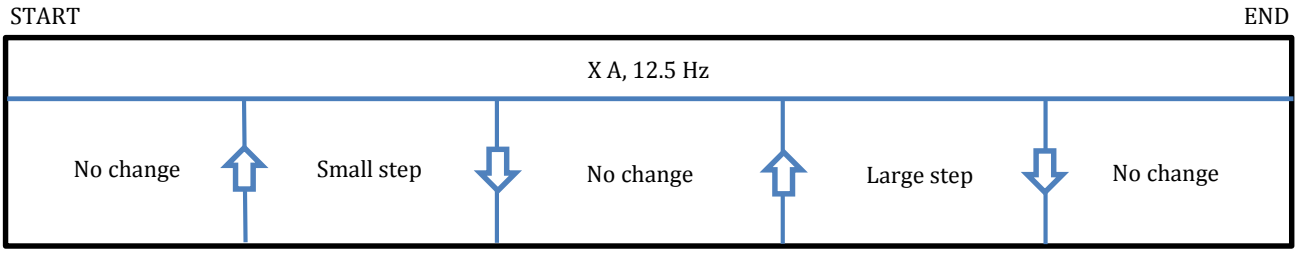

Figure 91: Bank switching procedure (for each Y $|I_{inj}|$: value)

This switching procedure is very similar to that in subsection 6.7.1, except parts '(1)' and '(2)' are combined and done simultaneously. That is, both the resistance and reactance of the line change simultaneously. This has been done to halve the time required for this test. Also, note that this test is done with banks and switching only on the red phase. That is to say, we are only effecting impedance changes on the red phase. This is a further time saving decision, as less switching is involved. The red phase (and thereby port 1) was chosen based on its poor performance as seen in subsection 6.4.3, 6.6.2 and section 6.8, with the aim that the worst performing port is easiest to optimise (due to higher error magnitude) and should improve the overall performance of the device most.

The range of $|I_{inj}|$ in this test is decided by the limitations of the device, as discussed in subsection 5.5.1. The 8 – 18 A range divided into 2 A steps gives enough points for the relationship between $|I_{inj}|$ and TEI measurement accuracy to be graphed and discerned.

The simultaneous switching of both resistor and inductor banks, rather than their separate switching, is a valid choice. The device must be able to track *impedance* changes, which will undoubtedly be complex impedances in practice. Therefore, we assume linearity in terms of resistance and reactance switching together vs. separately, which is a reasonable assumption.

6.12 Variation of injection current magnitude ($|I_{inj}|$) – results

In this section, we look at resistance change error and reactance change error separately, as they are found to behave quite differently. Spikes were also removed before this plot was generated.

6.12.1 Temperature considerations

According to Appendix G, the corrective factors to be applied are 1 mΩ at 10 A and 8 mΩ at 20 A for the large change. However, in this case we have a large range of currents used. For 8 A to 10 A, the contribution due to heating is considered negligible. For 12 A to 18 A, the 20 A heating corrective factor is scaled assuming a square law between the resistance response and the injection current. The small change is simply considered to correspond to a halved heating rate. Hence, the corrective factors are halved.

6.12.2 Resistance change measurement accuracy vs. injection level

The device was found to struggle with the large step at higher $|I_{inj}|$, causing tripping. It is expected that the device's protection system identifies this large PS-side change as something else that it is meant to be protected from. In order to circumvent this issue, the large step was staggered, making the change more gradual. This has a negligible effect on the results shown.

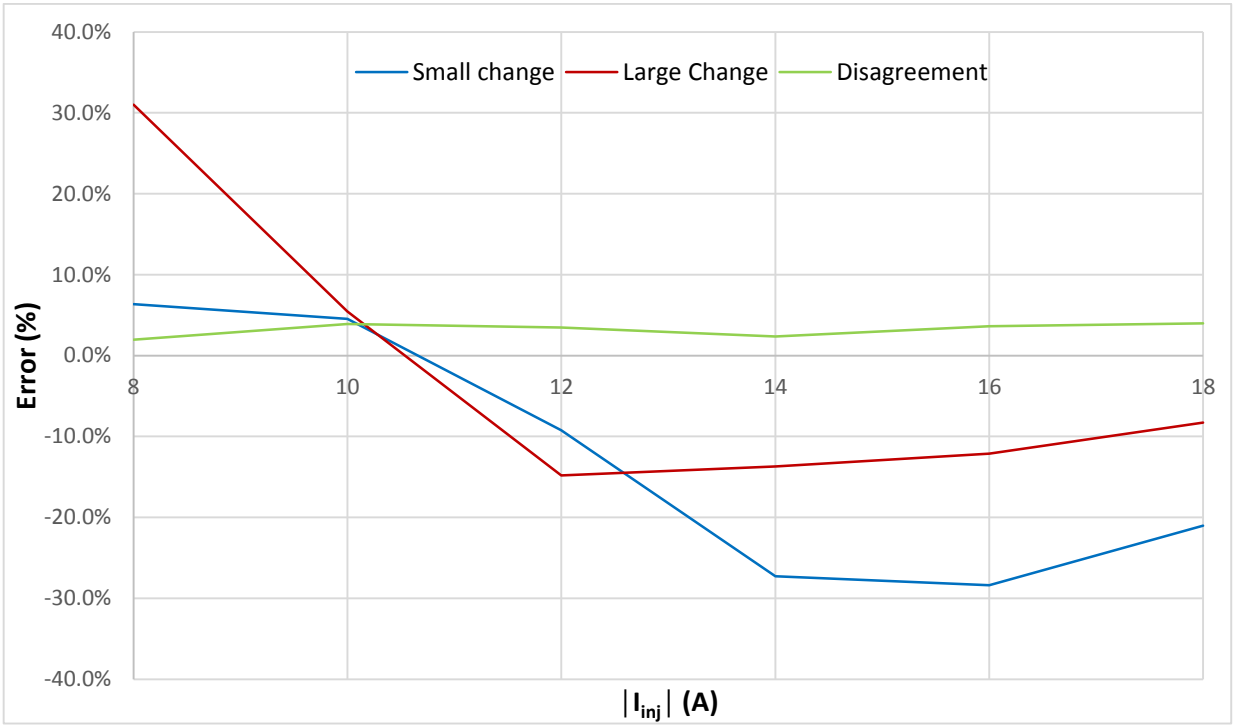

Figure 92: Error in resistance change measurement at different $|I_{inj}|$

From Figure 92, we see that resistance change measurement accuracy is heavily dependent on $|I_{inj}|$ as expected. At the low end of $|I_{inj}|$, we have both changes giving a positive error - the small change giving a relatively low error and the large change giving very large error. At the other end of the graph, we have negative error values for both small and large change, with large change giving a lower error than the small change. Both of these conditions are undesirable, as we wish to minimize the error for both small and large case, whilst having a small or negligible change in error between the large and small cases.

At around 10 A we have the ideal case of minimal total error (|small|+|large|) and almost equal percentage error for both large and small change. This is clearly the best option for accurate resistance change measurement, as the error is lowest and also seems to remain proportional to the resistance change.

In terms of disagreement, there appears to be no significant or predictable variation with $|I_{inj}|$ – it remains quite steady throughout.

Comparison to test from previous testing stage

Compared to the results of the previous testing stage, change measurement accuracy in the R_{th} parameter was considerably lower than that seen before. Due to the similarity of the test procedure, this is unexpected and cannot be attributed solely to the increase of duration of each resistor bank state from 10 samples to 20 samples. It is possible that the resistance change measurement accuracy (and thereby, impedance change measurement accuracy) is also dependent on the conditions at the PCC. The voltage waveform at UCT was seen to be significantly more distorted than that of MLT, although this result was not recorded. This may have posed difficulties for the inverter's effective current injection, deteriorating the TEI estimation performance. Nonetheless, it should be noted that there is some consistency between the two testing phases: the disagreement and error difference at 10 A is similarly low in both tests and the low disagreement at 18 A here is similar to that in the 20 A case for testing stage 1.

6.12.3 Reactance change measurement accuracy vs. injection level

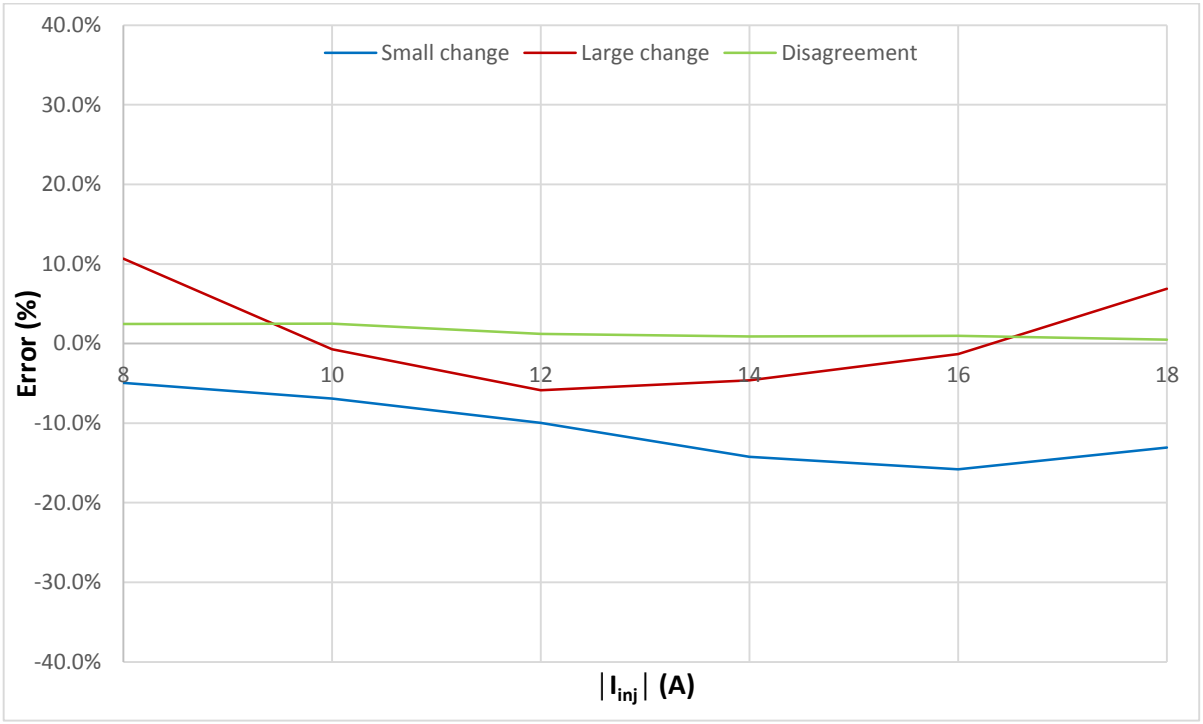

Figure 93: Error in reactance change measurement at different $|I_{inj}|$

From Figure 93 above, we see the reactance change measurement error for the same range of $|I_{inj}|$ as Figure 92. The two graphs also share the same scale; hence, they can be easily compared. One observation that can be made immediately is that the curves in this graph are much smoother than in the previous. That is to say, it is clearer that there is a predictable relationship between $|I_{inj}|$ and *reactance* change error (Figure 93) than there is between it and *resistance* change error (Figure 92). Furthermore, the percentage error is consistently lower for the *reactance* curves (Figure 93) than for the *resistance* curves (Figure 92).

Another observation from the graph is that the small change seems to have a consistently greater error (absolute) than that of the large change. This agrees with our expectations, since a small change requires higher sensitivity than a large change to detect to a low percentage error. The shape of the

graphs is also promising – we can imagine that a medium change could follow this same shape and fit between the small and large curve in terms of error, or that a larger change would follow a similar shape above the 'large' curve. If this kind of predictability exists and it is stationary, the device could be tailored to correct error over a range of impedance changes.

The disagreement between small and large change is seen to fall from about 2.5 % to 0.5 % as the injection magnitude increases.

From Figure 93, the ideal case seems to occur in the region of 10-12 A. The difference in error between small and large change is promisingly low, especially since the two graphs seem to divert from each other to either side of this interval. The falling disagreement with higher injection magnitude is too small of a benefit (about 0.8 %) to justify choosing a higher value of $|I_{inj}|$.

6.12.4 Z_{th} Standard deviation vs. injection level

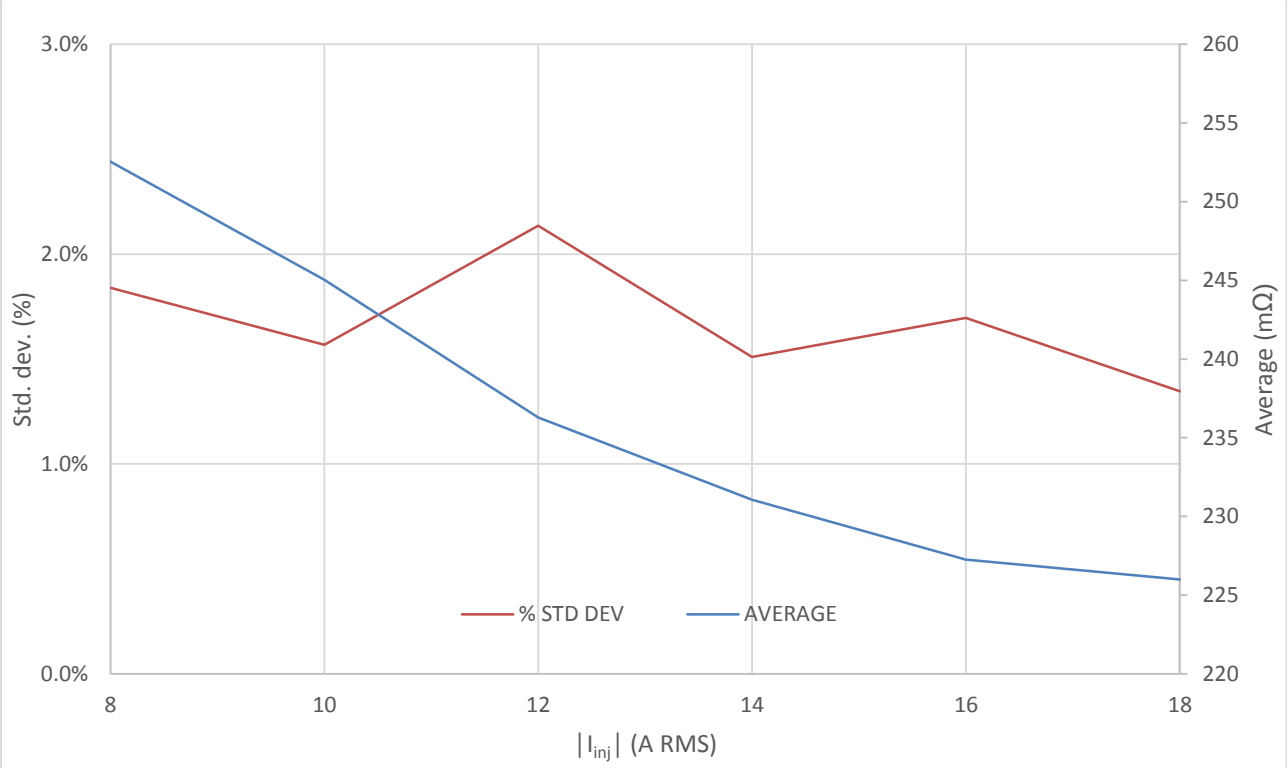

Figure 94: Average and standard deviation of Z_{th} vs. $|I_{inj}|$

Figure 94 is produced using data from the three "steady state" intervals (marked "no change in banks" in Figure 91) that occurred at each $|I_{inj}|$. It is interesting that the average level of the phase's TEI consistently drops with increasing $|I_{inj}|$. From 8 A to 18 A, we have more than a 10 % drop in the average level. The standard deviation has a very slight downward trend as well. When this graph is compared to that from the previous stage of testing, we see agreement in the average behaviour, as well as some disagreement in the behaviour of the standard deviation. The standard deviation does not follow as defined a curve as that in the previous test, dropping to low values at high $|I_{inj}|$. Instead, the behaviour is less pronounced here. This is expected to be due to the difference in the range of $|I_{inj}|$ used here (8-18 A), compared to before (2 A-20 A). Indeed, it seems that the findings from before remain consistent with these when this is considered.
Similar conclusions arise from the previous testing stage – that higher injection levels produce lower estimates of the PS TEI. Without other results for comparison, it is not known whether the steady-state impedance is more accurate at low or high injection levels.

6.12.5 Optimum injection current

The ideal injection based on the findings of subsections 6.12.2 and 6.12.3 is chosen to be at $|I_{inj}|$=10 A, at which it is expected that resistance and reactance error will be about 5 % for each parameter. In reality, the inverter output will be close to an RMS injection current of 11.7 A.

6.13 Variation of modulation frequency (f_m) - description

The theoretical boundaries guiding the selection of injection frequency are that it is a frequency not commonly present in the PS and that it is slow enough for the inverter to track. The f_m of the currents injected by inverter 1 were chosen to be 12.5 Hz for the previous tests. The choice of this specific frequency is somewhat arbitrary – it was found that changes in line resistance could be tracked relatively well at this frequency from testing stage 1. Since the harmonic content of the PS is only known to us on a speculative level and there are no guidelines available for choosing the injection frequency, this parameter deserves investigation. This is intended to directly confront the question of which f_m should be used for the TEI estimation.

6.13.1 Test parameters and procedure

Test date: 11/06/16 Duration: 00:26:00 Elapsed from: 12:40 – 15:13
Modulation frequency (f_m): **Varies** from 8 Hz to 18 Hz
RMS injection current ($|I_{inj}|$): 12.0 A (**standard**)
Resistor/inductor banks: **resistance varies**

Controllable input factors: f_m, $|I_{inj}|$, time of day, resistance levels (before and after step for each line)
Uncontrollable input factors: ambient temperature, loading and state of PS
Responses: TEI parameter variation

Table 17: Resistor/inductor bank setup

Change	Magnitude (mΩ)	
	ΔR	ΔX
'SMALL'	50	63
'LARGE'	105	126

There is a great deal of similarity between this test and the test discussed previously in subsection 6.11. Starting at Y = 6 Hz, a 20 min test is done according to the procedure shown in Figure 95. This is done for Y = 6 Hz, 8 Hz, …, 18 Hz. The exact size of the resistance and reactance changes effected during the test are shown in Table 17 above. In this case, both ΔR and ΔX change for each step. The large step is about twice the size of the small step.

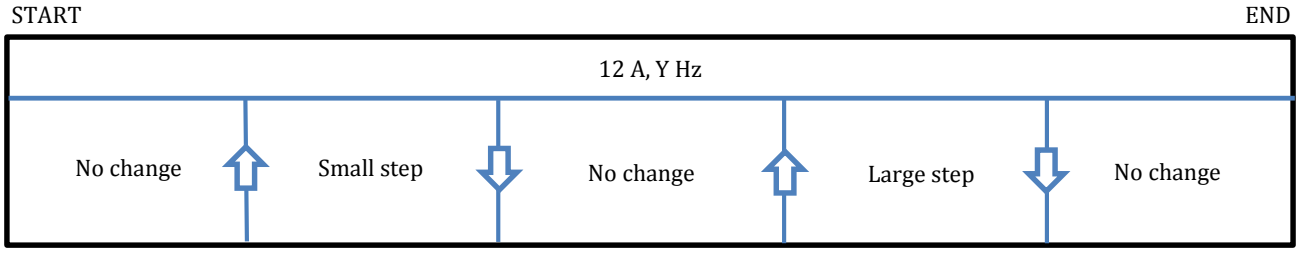

Figure 95: Bank switching procedure (for each Y f_m value)

The 6 Hz – 18 Hz range divided into 2 Hz steps gives enough points for the relationship between the f_m and TEI measurement accuracy to be graphed and discerned.

The switching procedure is identical to that in section 6.11, hence, its justification is provided in subsection 6.11.1.

6.14 Variation of modulation frequency (f_m) – results

As in section 6.12, resistance and reactance change error are treated separately and spike removal was done before this plot was generated

6.14.1 Resistance change measurement accuracy vs. modulation frequency

Figure 96 shows us the unusual relationship between resistance error and f_m and it is immediately clear that f_m greatly affects the resistance error. This effect is clearly more significant than that of $|I_{inj}|$ (see subsection 6.12.1), over the ranges investigated. The relationship is difficult to generalise or describe, although there is a clear upward trend in both small and large change error, despite an unusual deviation in the mid-range. The disagreement is also unpredictable, with an unusually high peak at 16 Hz. Thus, the selection of ideal f_m is again not straightforward.

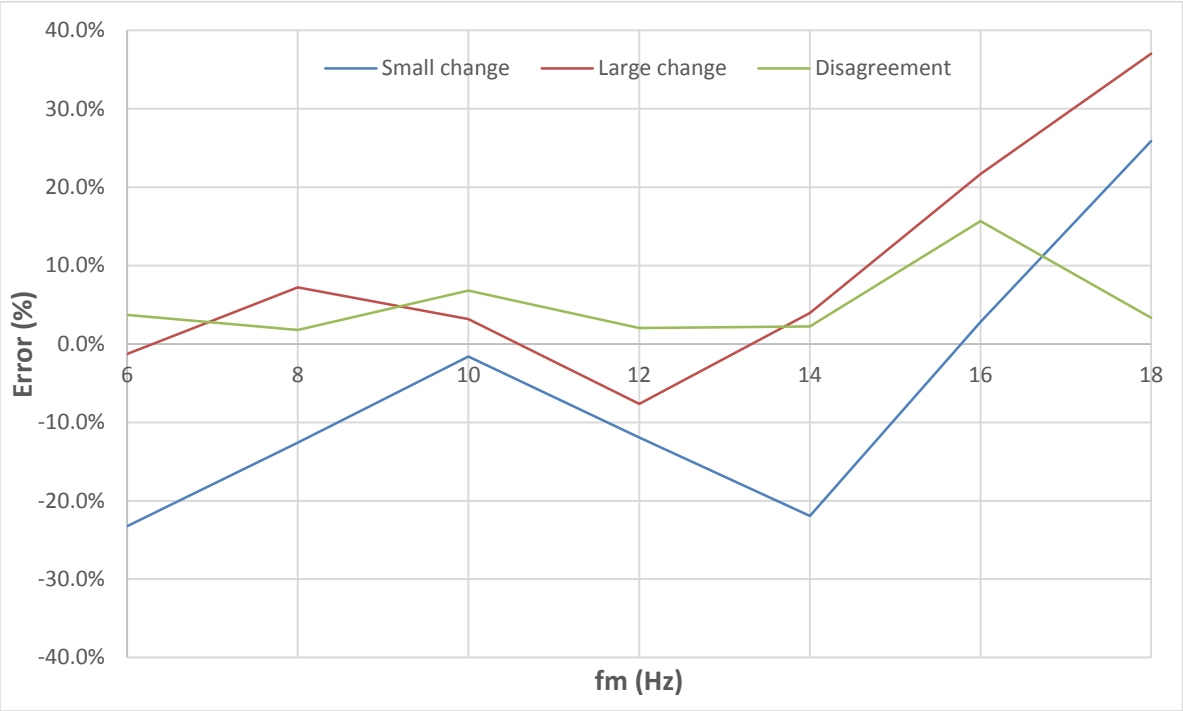

Figure 96: Error in resistance change measurement at different f_m

Following from the logic in subsection 6.12.1, the best choice of f_m should lie in the mid-range (10 Hz-12 Hz), as here we have the smallest difference between small and large change error. At these levels, the disagreement is also acceptable.

Comparison to previous testing stage results

Similar observations can be made as in subsection 5.12.4, although in this case there is generally less agreement. For example, the 15 Hz case from the previous stage was seen to have very low error difference and disagreement, which is not the case in this stage. This may be due to the current around 15 Hz being different between the two tests, due to different voltage distortion levels between the two locations.

6.14.2 *Reactance change measurement accuracy vs. modulation frequency*

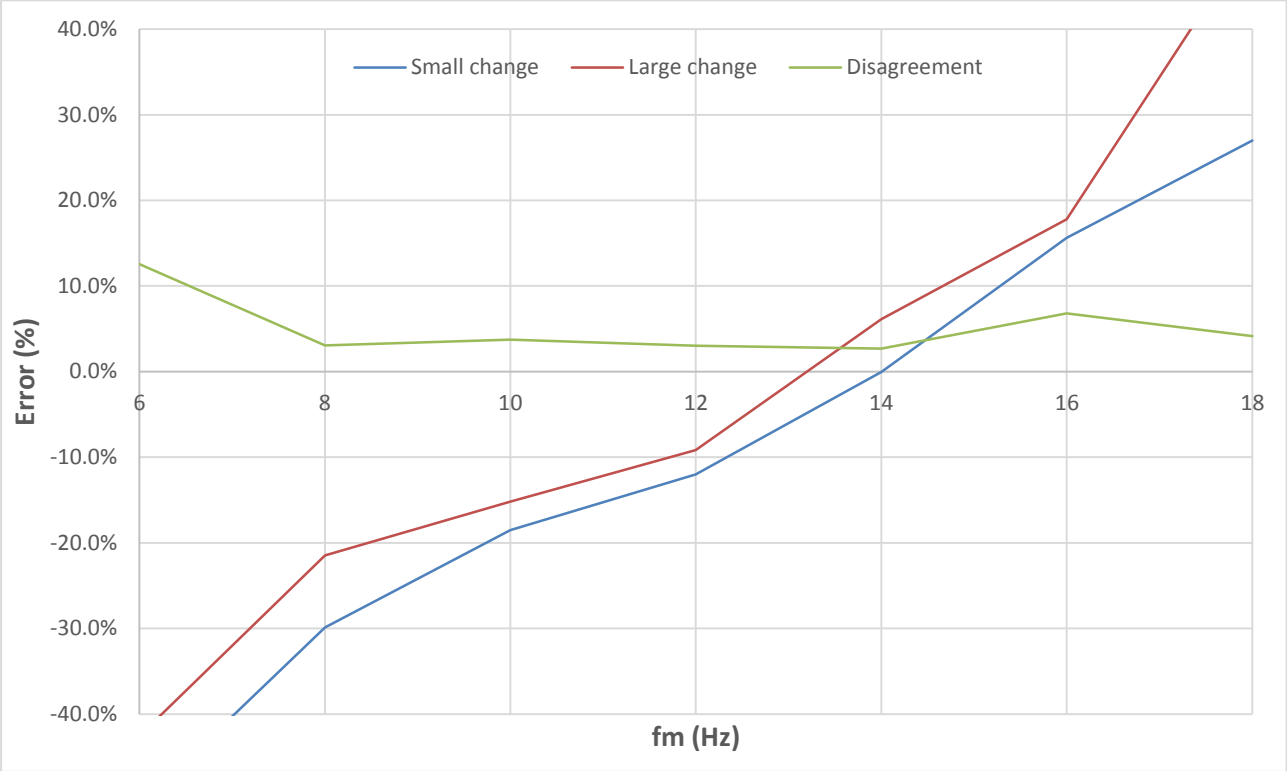

Figure 97: Error in reactance change measurement at different f_m

The effect of f_m on reactance error is clearly a defined relationship as seen in

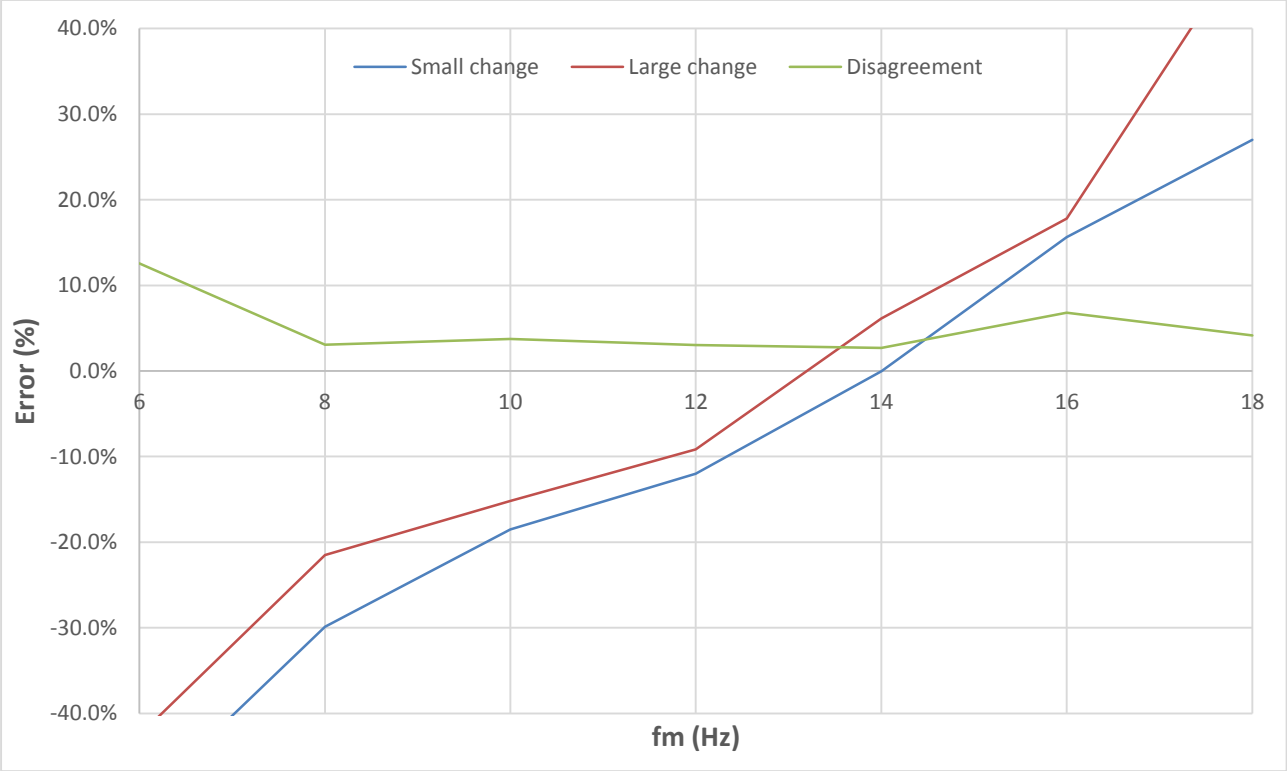

Figure 97. We see small and large change error are quite close to each other throughout, following an almost straight line. This result strongly suggests that the experimental procedure has produced real results. The error variation is extreme, from -40 % to +40 %, while the disagreement seems almost constant over the frequency range. In this case, the best f_m lies around 12-14 Hz, as this is where both the difference in small and large change error is small and the error itself is low.

6.14.3 Z_{th} Standard deviation vs. modulation frequency

Increasing the modulation frequency was found to decrease the average value of the TEI by less than 10 %, whilst no solid conclusions can be drawn about its effect on the standard deviation of the TEI. Referring back to the results of testing stage 1 (see 5.12.3), we see that the level of both average and standard deviation are as low as seen before for the 15 Hz and 20 Hz case. However, at 10 Hz and below the standard deviation is much lower in this test, due to the presence of a lot of spiky behaviour in the previous stage, which was not removed from the data and statistics.

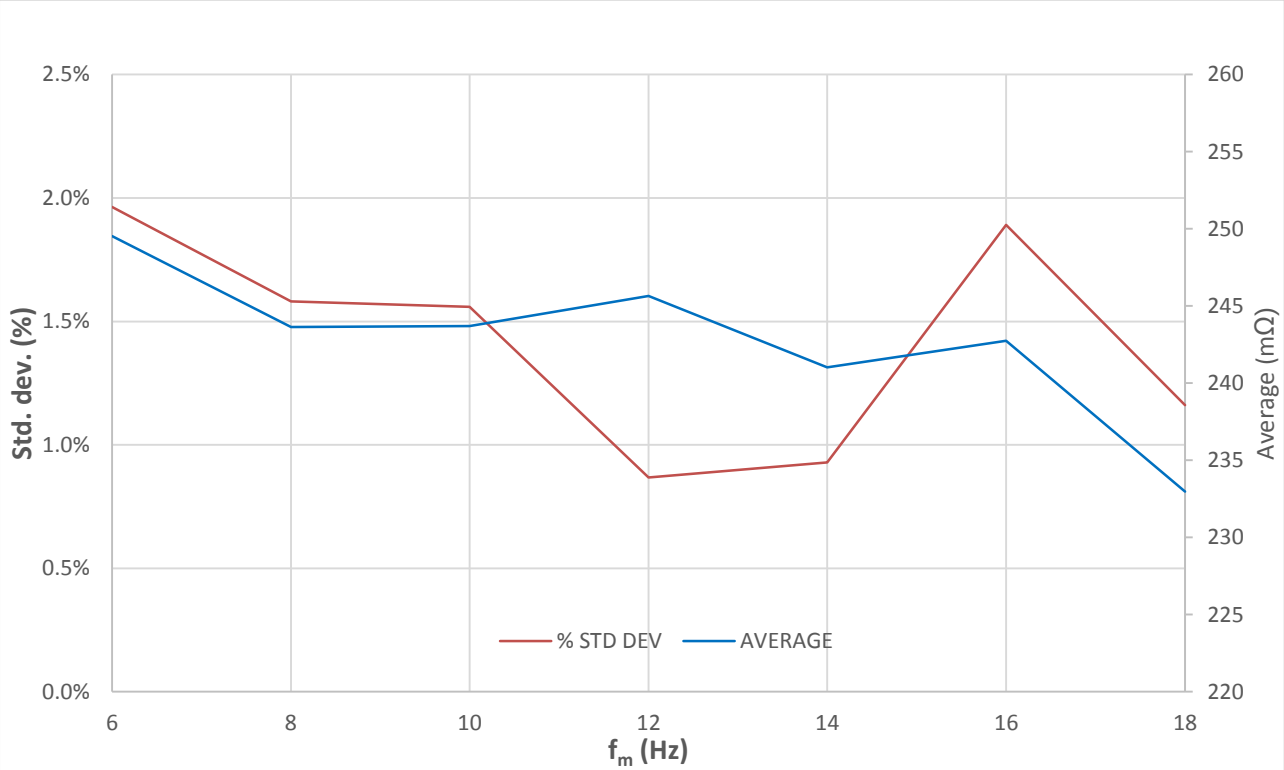

Figure 98: Average and standard deviation of Z_{th} vs. f_m

6.14.4 Optimum modulation frequency

The ideal modulation frequency, based on the findings of subsections 6.12.1, 6.14.1 and 6.14.2, is chosen to be at f_m=12 Hz. This corresponds to a real modulation frequency of the same value being provided by the inverter.

7. Testing – Stage 3

7.1 Evaluation of performance with optimised parameters - description

The previous two tests were aimed at determining optimum parameters for high TEI estimation accuracy. Based on these tests, we expect that the accuracy of the device should be higher than ever before when using the individually optimised parameters together. This test serves as a thorough evaluation of the device's performance in impedance tracking using the optimised parameters.

7.1.1 Test parameters and procedure

Test date: 16/02/17 Duration: 00:33:00 Elapsed from: 11:06 – 11:39
Modulation frequency (f_m): 10 A (**optimum according to** section 6.12)
RMS injection current ($|I_{inj}|$): 12.0 Hz (**optimum according to** section 6.14)
Resistor/inductor banks: **RB_1, RB_2, IB_1, IB_2, IB_3 and IB_4 in blue phase throughout**

Controllable input factors: f_m, $|I_{inj}|$, time of day, resistance and reactance levels
Uncontrollable input factors: ambient temperature, loading and state of PS
Responses: TEI parameter variation

Table 18: Resistor/inductor bank setup

Change	Magnitude (mΩ)	
	ΔR	ΔX
'SMALL'	50	63
'LARGE'	105	126
'VERY LARGE R ONLY'	182	0
'VERY LARGE X ONLY'	24	251
'VERY LARGE'	206	251

This test is similar to previous tests such as that described in section 6.11. However, this test involves more switching levels, includes switching of approximately 2x larger impedances as well as separate switching of resistance and reactance. This time the test is done on the blue phase rather than the red phase. The use of the blue phase, rather than the red phase, is done so as to verify that optimisation of the parameters for the red phase means that yellow and blue phases are also optimised.

The test is done according to the procedure in Table 19. Each vertical section in the figure is of 20 samples duration. The exact sizes of the resistance and reactance changes effected during the test are shown in Table 18 above. 'SMALL', 'LARGE' and 'VERY LARGE' changes involve simultaneous resistance and reactance changes, the other two tests are only resistance or reactance. The large step is about twice the size of the small step.

Table 19: Bank switching procedure

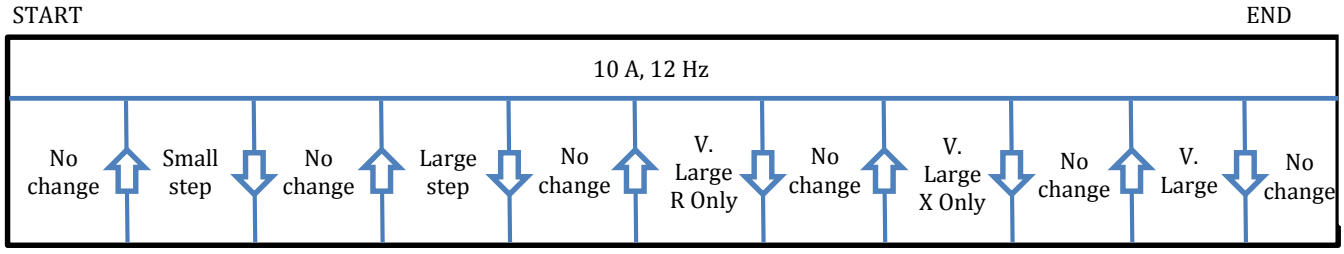

The new switching procedure is similar to that in section 6.11. The new additions to the procedure, such as the large changes and the separate R and X changes, are included to increase the thoroughness of the evaluation of the device performance. Large changes are effected to investigate whether the determination is still effective when we have a massive impedance change. Non-simultaneous changes of resistance and reactance are done so as to verify the assumption that resistance and reactance change measurement are independent of each other. Note that, although we label one change as 'VERY LARGE X ONLY', it still involves a change in resistance as our inductor banks are not of negligible resistance.

7.2 Evaluation of performance with optimised parameters – results

Data produced by the Thévenin measurement device regarding the R_{th} and X_{th} measured on the blue phase are shown in Figure 99.

7.2.1 Temperature effect considerations

As this test is performed at 10 A injection, the corrective factor used for the large step change was 1 mΩ and since the very large resistance steps involve two banks in series, the corrective factor used here was doubled.

7.2.2 Resistance and reactance plot

For each step change in resistance and reactance measured, there is a corresponding dotted black line showing what the step change would have been if the device's measurement reflected the exact correct change. The closeness between this dotted line and the actual step change is thus a visible indicator of the accuracy of resistance/reactance change measurement. This was also done in two tests during the previous testing stage (see subsections 5.10.5 and 5.12.4).

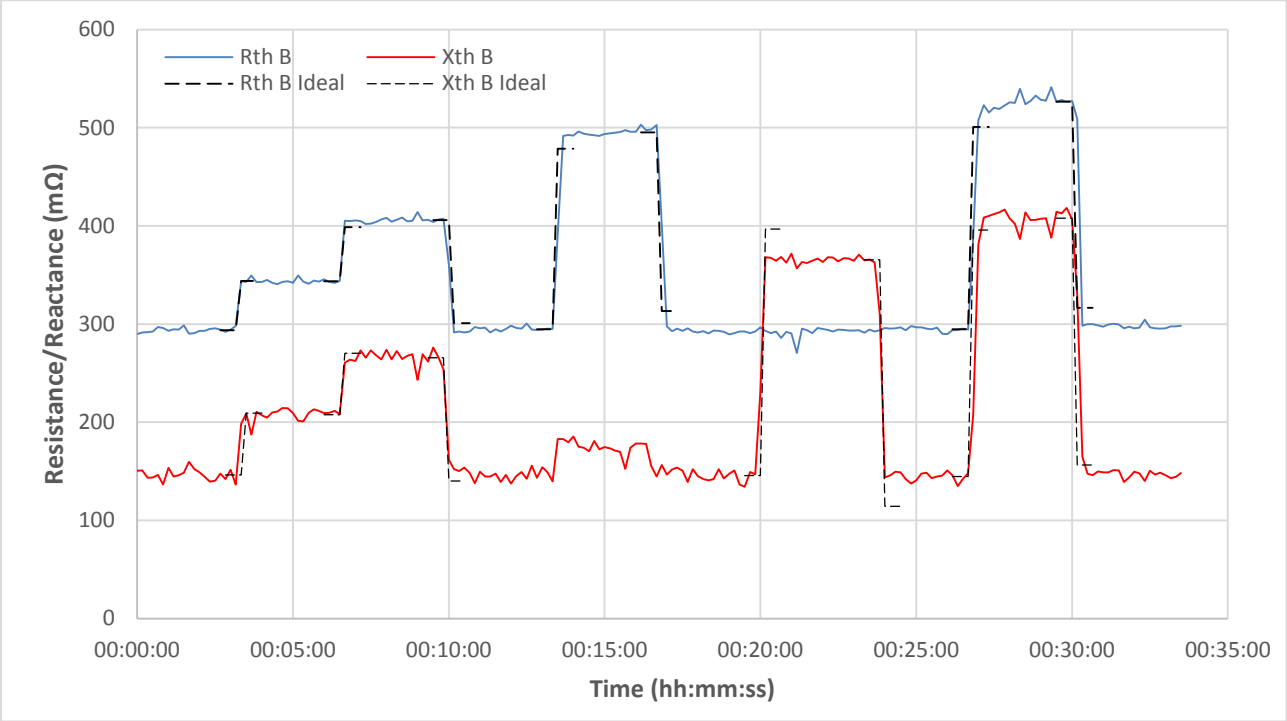

Figure 99: Resistance (blue) and reactance (red) change measurement of blue phase at optimised parameters – with ideal changes shown (black dotted lines)

Visibly, the device appears to perform considerably well in tracking the known changes correctly. The overall percentage error, averaged over all the step changes seen in Figure 99 above, is shown in Table 20 below for resistance and reactance separately.

Note that in the case of the very large R only change, there is also a perceived change in the X_{th} parameter, whereas the very large X only change does not affect the R_{th} parameter. This suggests that the measured X_{th} is dependent on R_{th}, whereas, the opposite is not true.

Table 20: Average and std. dev. of reactance and resistance change error

Parameter	Average error (%)	Error Std. dev. (%)	Disagreement (%)
Resistance	8.50	4.45	1.18
Reactance	-4.50	6.86	0.23

From the statistical parameters in Table 20, we see that the overall performance is considerably good. When compared to the performance predicted by each individually optimised parameter (I optimised – errors: R ≈5 %, X≈-5 %, f_m optimised – errors: R≈-10 %, X≈-10 %) the performance is close to as predicted. Although the values in Table 20 include very large changes which were not done in previous tests, using only the first few smaller steps as an indicator of performance gives even better results as seen in

Table 21 below.

Table 21: Average and std. dev. of reactance and resistance change error (only considering "small" and "large" steps)

Parameter	Average error (%)	Disagreement (%)
Resistance	6.18	0.83
Reactance	-5.01	0.14

Compared to the performance of port 3 as seen in section 6.8, the optimised parameters have lower error. Furthermore, the disagreement is also many times lower using the optimised parameters.

7.3 Comparison of device-determined and oscilloscope-determined impedance - description

This test is done to check that the device's measurements of the grid impedance are consistent with those taken by the oscilloscope. Essentially, the injected current and voltage response due to the device can also be measured by the oscilloscope. The high precision of the oscilloscope allows us to perform near-perfect extraction of the grid impedance. This can be done at the same time that the device performs its TEI estimation, allowing us to evaluate its performance in comparison to the oscilloscope.

7.3.1 Test parameters and procedure

Test date: 15/02/17 Duration: 05:00:00 Elapsed from: 10:00 – 15:00
Modulation frequency (f_m): **varies,** 6 Hz – 18 Hz in 2 Hz steps
RMS injection current $|I_{inj}|$: **varies**, 8 A – 18 A in 2 A steps
Resistor/inductor banks: **RB_1 and RB_2 in yellow phase throughout**

Controllable input factors: f_m, $|I_{inj}|$, time of day, resistance and reactance levels, duration of FFTs
Uncontrollable input factors: ambient temperature, loading and state of PS
Responses: TEI parameter variation

Table 22: Resistor bank setup

Change	Magnitude (mΩ)	
	ΔR	ΔX
'VERY LARGE R ONLY'	184	0

Essentially, this test involves simultaneous use of the oscilloscope and the device. The oscilloscope's FFT function is used to measure the current harmonics and voltage harmonics on the yellow phase at the relevant injection frequencies and these are logged as .csv files. Since only one FFT may be done at a time, there is a delay between the voltage and current FFT logging of a few seconds. At the same time, the device performs its own parameter determination, on all phases.

The banks are used to effect a large resistance change on the yellow phase. Logging V and I FFTs before and after this change gives us an accurate measure of the change according to the oscilloscope, while the device is left to log parameter data over the same period.

The entire range of f_m and $|I_{inj}|$ is used, with the resistance change in Table 22 being effected for each level. 20 samples are taken by the device before and after the change.

Table 23: Bank switching procedure

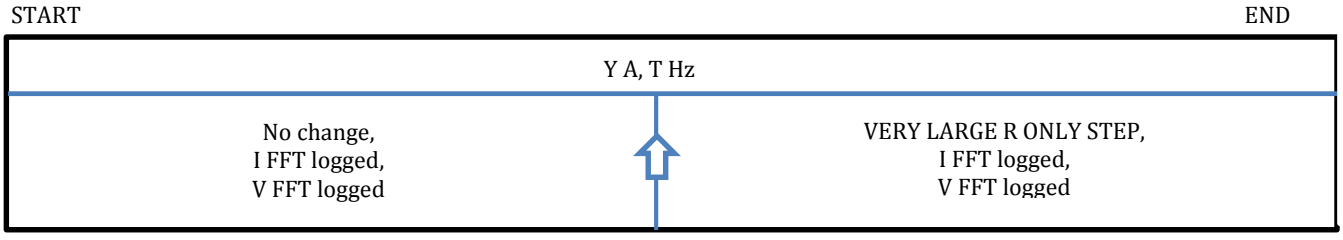

The use of the blue phase, rather than the red phase, is done so as to verify that optimisation of the parameters for the red phase means that yellow and blue are also optimised.

The new switching procedure is similar to that in section 6.11. The new additions to the procedure, such as the large changes and the separate R and X changes, are included to increase the thoroughness of the evaluation of the device performance. Large changes are effected to investigate whether the determination is still effective when we have a massive impedance change. The separate changes are done so as to verify the assumption that resistance and reactance change measurement are independent of each other. Note that, although we label one change as 'VERY LARGE X ONLY', it still involves a change in resistance, as the inductor banks are not of negligible resistance.

7.4 Comparison of device-determined and oscilloscope-determined impedance – results

7.4.1 FFT data for 10 A, 12 Hz

As a first look, the FFT result for the standard injection and f_m parameters is shown below in Figure 100. The current before and after the large resistance change is effected is shown. The current does not change much, except for a small reduction in the upper sideband component. This is probably due to the inverter being unable to keep the current output steady with the higher impedance in the line, which necessitates that it outputs a higher voltage on that line.

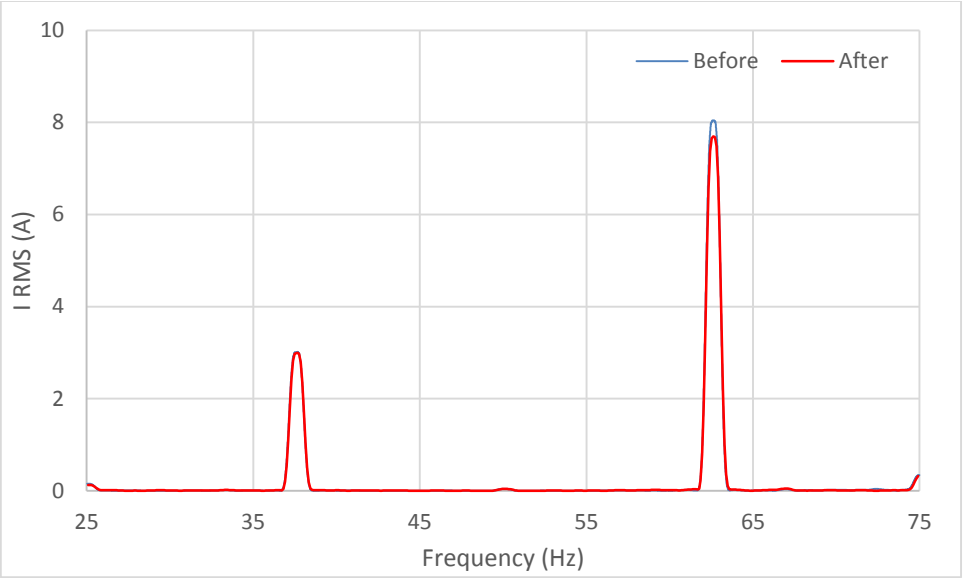

Figure 100: Yellow phase current FFT before and after large resistance change

The voltage responses before and after are shown below in Figure 101. They were of the order of a few volts. The impedance is found using the oscilloscope by dividing the voltage component at each sideband by the current component at the same sideband, giving Z_{th} at 37.5 Hz and 62.5 Hz. The reactance and resistance are then extracted simply by assuming a constant inductance and simultaneously solving equations as set out in subsection 2.5.3.

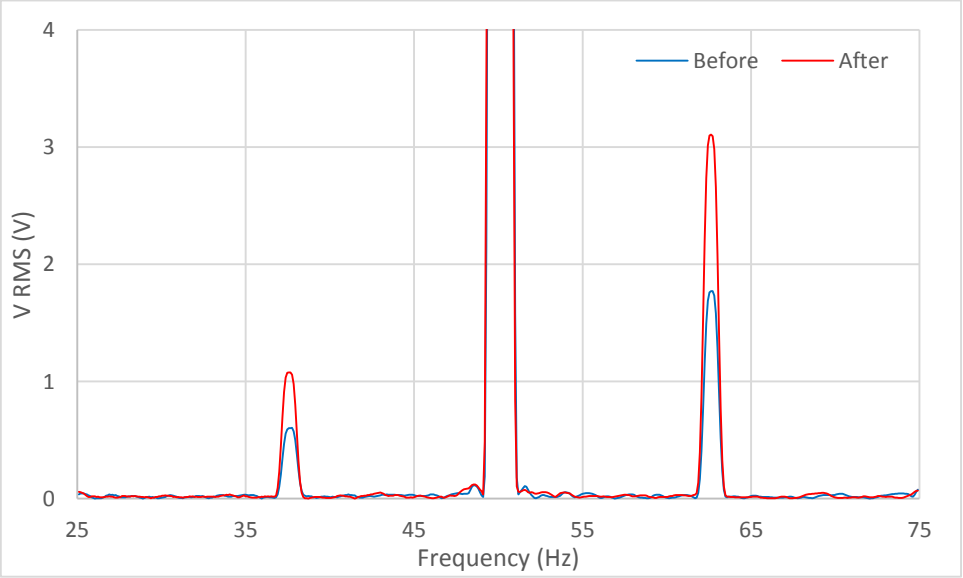

Figure 101: FFT of voltage before and after large resistance step, yellow phase

The resulting Z_{th}, X_{th} and R_{th} parameters are shown in the bar graph in Figure 102, where they are compared to the parameters obtained by the Thévenin device. The 'ideal' change - the known value of the resistance change – is also shown.

The oscilloscope-determined values of R_{th} and X_{th} are calculated based on a linearization of the X_{th} parameter, assuming a constant L, then using the impedance found at the two harmonic frequencies to calculate L.

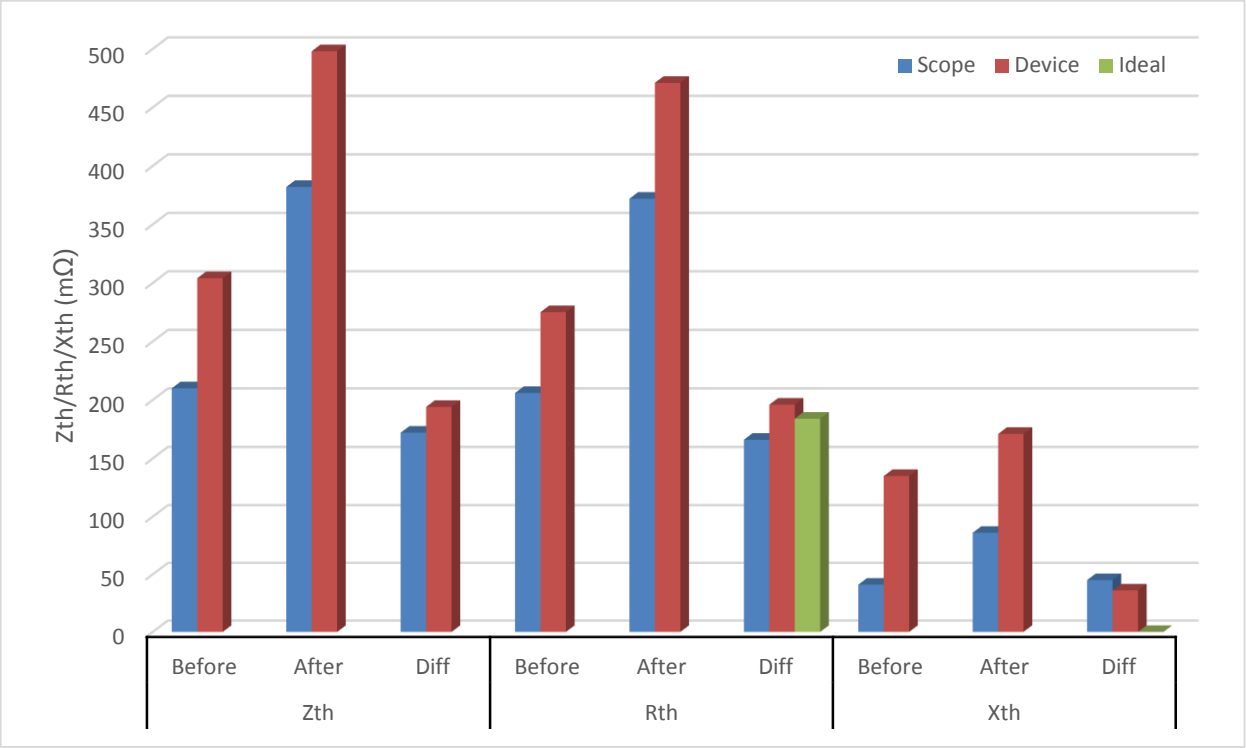

Figure 102: Z_{th}, R_{th} and X_{th} according to: Oscilloscope (blue), Thévenin device (red), before and after resistance change (ideal - green), at 10 A, 12 Hz

From the graph, several observations can be made. Firstly, we see that the measurements of Z_{th}, R_{th} and X_{th} by the Thévenin device are greater than that of the oscilloscope by a near-constant amount in each case. Despite this, the difference in the measured parameters appears to be quite close together and to the ideal value. That is to say, the Thévenin device seems to estimate impedance changes accurately, but gives an imprecise estimate of the steady parameters. It is also strange that the oscilloscope, although having such a high measurement accuracy, did not perform very well in measuring the change in resistance (difference between green bar and left hand side blue bar in Figure 102).

Finally, it is strange to see that both the oscilloscope and device measured a change in the reactance parameter, where there was none. It is not possible that this is due to random PS variation, as such large deviations in X_{th} were not observed during the long sensing test (subsection 6.10.1). This behaviour is explained in two parts. Firstly, the PS's inductance estimate before and after the change according to the oscilloscope was considerably different. Secondly, it is known from the previous test (subsection 7.2.1) that the Thévenin device seems to perceive small reactance increases when only the resistance of the line is increased.

This analysis, as applied to the 10 A, 12 Hz case, is also done for every $|I_{inj}|$ and f_m. It was found that the inductance estimate according to the oscilloscope varied significantly at each $|I_{inj}|$ and f_m, with no

predictable relationship appearing. Given that R_{th} is calculated using X_{th} and thereby L, this variation may have caused the relatively high discrepancy between the ideal resistance change and that measured by the oscilloscope in Figure 102. It was indeed found that, when the average of L calculated from all the oscilloscope measurements combined was used instead of just the individual L values at each level, the oscilloscope's result was much closer to the ideal difference. In this case, the average resistance difference estimate was 183 mΩ, almost exactly the ideal 184 mΩ value. This closeness shows that the oscilloscope is accurate when used in this way. Averaging the inductance measured before and after the change gives a reactance change of 8 mΩ, which is also very close to the ideal value of 0 mΩ.

This brings the conclusion that, for an accurate TEI estimate using the oscilloscope, several measurements of V and I must be taken at different times. This averages out variations in the component heights, which may be being caused by noise or time-variation of the injection current/voltage between measurements.

Figure 103 and Figure 104 show the levels of parameters before and after the resistance change, measured by the Thévenin device at all the $|I_{inj}|$ and f_m tested previously. They are compared to the results obtained from the oscilloscope, after appropriate averaging as described in the previous paragraph. These oscilloscope results are deemed the most accurate estimates of the grid's TEI parameters available, verified by their high precision in resistance change measurement. As a result, its results are the "ideal" results that the device is intended to approach.

It is seen that the variation of $|I_{inj}|$ and f_m affect the average level of the parameters. Generally, higher levels of f_m and $|I_{inj}|$ decrease the overestimation of the PS TEI, consistent with results seen in subsections 6.12.4 and 6.14.3. It is interesting that the offset decreases in size for all parameters. The offset is also seen to grow in size after switching is performed and the impedance level increases, in all cases.

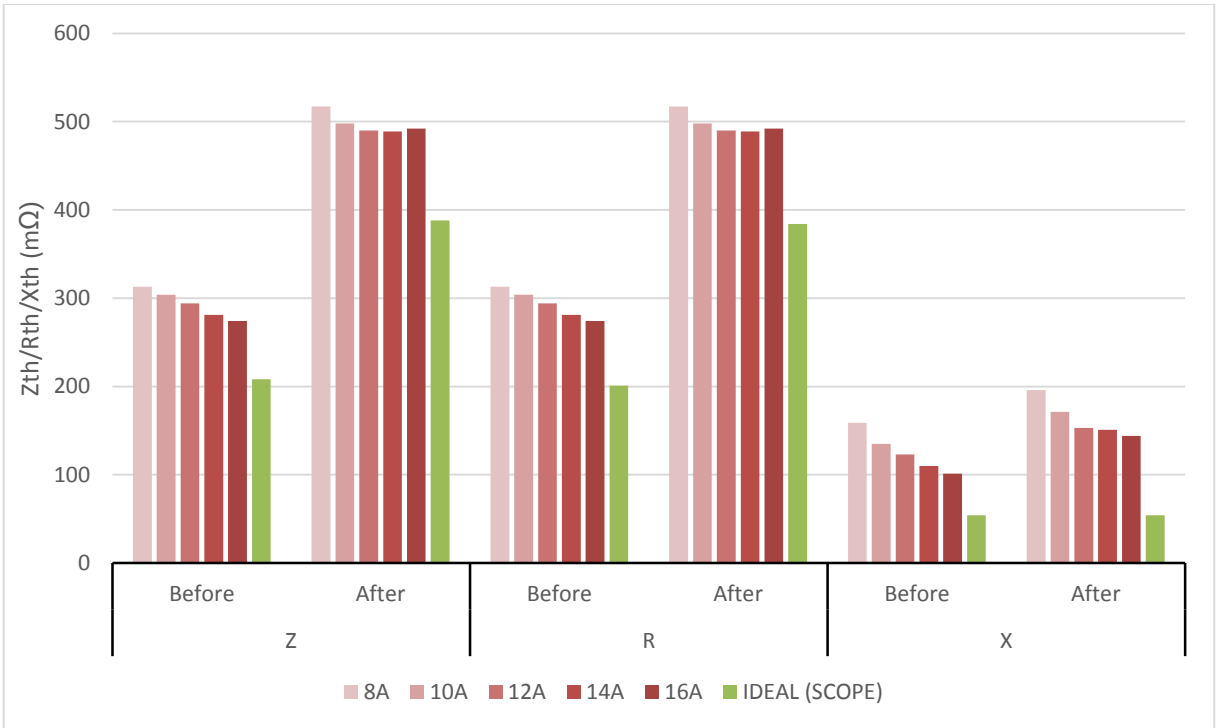

Figure 103: Levels of Z_{th}, R_{th} and X_{th} before and after resistance change at different $|I_{inj}|$. Oscilloscope-determined levels provided for 'ideal' comparison

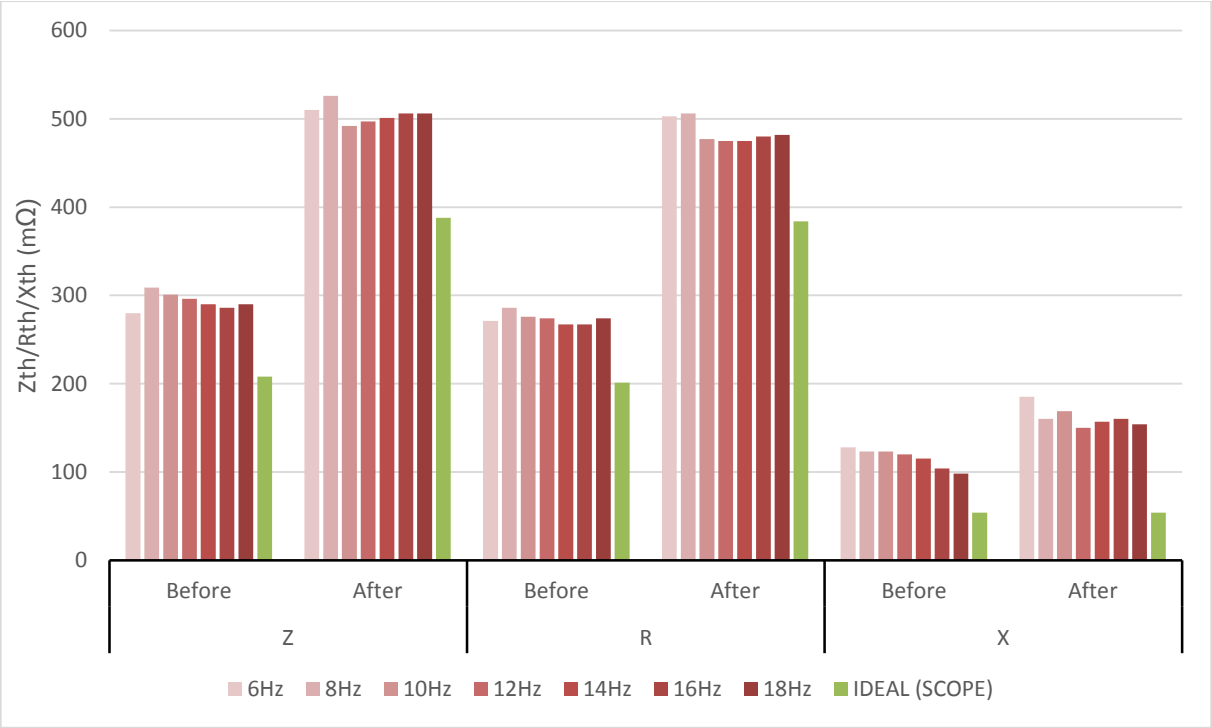

Figure 104: Levels of Z_{th}, R_{th} and X_{th} before and after resistance change for various f_m. Oscilloscope-determined values provided for 'ideal' comparison

A by-product of this test is verification of the results of subsections 6.12 and 6.14, regarding resistance change measurement accuracy and its variation with f_m and $|I_{inj}|$. The resistance change measured by the device is in agreement with the findings of these previous tests – at $|I_{inj}| = 10$ A and at f_m=12 Hz the resistance change is closest to the ideal, as seen in Figure 105. Thereby, it is seen that optimisation of parameters using red phase is also optimisation of the blue phase.

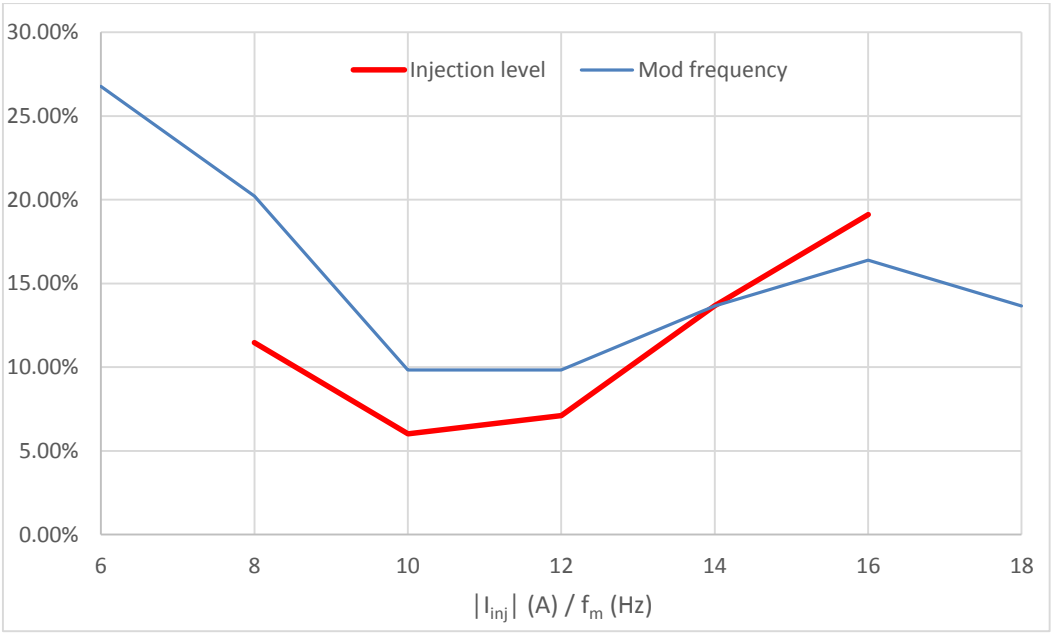

Figure 105: Resistance change measurement error variation with $|I_{inj}|$ (red) and f_m (blue)

8. Conclusions and recommendations

8.1 Conclusions

The two principal methods of online TEI measurement were discussed in depth and prominent results analysed and compared. It was found that both methods require more study in crucial areas. For the active method, no authors were found to have provided convincing reasoning behind their choice of the specific frequency and magnitude of current injection used, or thoroughly considered the effects of these parameters. Finally, the extent of practical testing and evaluation of implementation of both methods has been limited.

An active method using dual-harmonic injection through a unique amplitude modulation scheme was implemented in a three-phase PV-inverter and thoroughly tested on the live South African national PS at two locations. The system was found to be effective in TEI estimation due to its accurate tracking of known changes effected in the PS impedance. Investigations revealed:

- The implementation was effective in obtaining the TEI of all three phases of the PS over long time periods.
- The PS's impedance was found to be of the order of 100 mΩ at both locations, on all three phases as well as the neutral conductor.
- Tests of several hours duration show the variation in the grid's impedance was found to be minimal, with standard deviation of less than 5% and weak low-frequency behaviour. Hence the impact of daily load variation and PS-side changes was found to be minimal.
- Varying the injection current magnitude has a significant effect on TEI estimation accuracy, with resistance accuracy and reactance accuracy being affected in different ways (see section 6.12). The same is said for variation of modulation frequency (see section 6.14).
- The most preferable current injection magnitude is 11.7 A RMS, achieved with a target injection level of 10 A RMS instructed to the inverter. At this level, impedance change estimation error of the order of 5% can be expected (with 12.5 Hz injection) for impedance variations of the order of the typical LV PS impedance (100 mΩ).
- The most preferable modulation frequency is 12 Hz. At this value, impedance change estimation error of the order of 10% can be expected (with 12 A injection) for impedance variations of the order of the typical LV PS impedance (100 mΩ).
- Using both optimised parameters, impedance, reactance and resistance change error of about 5 % can be expected for impedance changes of the order of the typical LV PS impedance (100 mΩ).
- Increasing the injection current magnitude causes the average level of all TEI parameters to fall toward the value obtained with calibration equipment. The same is true for the modulation frequency. Thus, optimising TEI change measurement does not necessarily mean that steady-state TEI estimation accuracy is optimised.

In terms of the equipment and methods used, it was found that:

- The inverter hardware used limited the possible injection current levels and modulation frequency levels to the ranges of 0 – 20 A and 0 – 25 Hz, respectively.
- The tracking of a known impedance change in series with the PS impedance has proven to be an easy, effective way of evaluating the accuracy of TEI estimation in terms of dynamic measurement performance. However, static measurement performance must be evaluated by other means, such as comparison to calibration equipment.

- Asymmetry between the device's three phase modules in parameter measurement was present, requiring compensation.
- The device's ability to inject the desired current was highly dependent on the frequency and injection current magnitude chosen. Distortion in the form of unequal component weight for the two harmonics injected was found in all cases.
- It is difficult to vary the inverter's modulation frequency setpoint without also affecting the injection current magnitude. However, varying the injection current magnitude setpoint does not affect the modulation frequency.

The results of the extensive practical testing entailed in this research have shown that this specific PV-inverter implementation is more robust than any other seen to date. TEI estimation was successful despite non-ideal current injection. The algorithm's processing and data-handling requirements are minimal, such that accurate real-time TEI estimation is achieved with existing hardware. Furthermore, the device tested in this thesis retains its full existing inverter functionality. That is to say, the device can sense the TEI of the grid at set intervals, and perform as a normal inverter when not sensing the TEI. Compatibility with other models of power inverter has yet to be investigated but the algorithm itself can be implemented in any similar hardware.

The long sensing tests performed provide confidence in the effectiveness of the device's prolonged operation, as well as a view of the grid's TEI parameter variations at the LV level over several hours duration. This is a unique result.

Optimisation of current injection based on thorough testing and evaluation of the accuracy of TEI estimation for a specific range of impedances has not been done before. Because of this, the design of the test protocol can be used as guidance for further work. If any other implementation is to approach the stage of widespread deployment, similarly thorough dynamic impedance change testing would be required. In future, the entire testing process could be streamlined to have duration of about two weeks, requiring only a single lab operator with minimal training.

8.2 Recommendations for further study

Areas for further study should include:

- Investigation of the cause and minimization of steady-state TEI error in this implementation
- Simulation of PV-inverter based PS TEI estimation for a typical LV network, for comparison
- Analytical investigation into effects of load changes on TEI seen from the PCC
- The degree of linearity of the PS at LV level (where NLLs are common) and its impact on TEI estimation applicability
- Investigation of the effect of injection magnitude and rate of repetition of injection on the power quality of the PS
- How to overcome the issue of interference between devices in the active method

For effective further study, the following points should be considered:

- Measurement and evaluation of injected current waveform purity is very important when optimising waveform parameters
- Asymmetry between the device's modules can have an effect and should be compensated for
- The tracking of a known impedance change in series with the PS impedance should be used for easy evaluation of dynamic TEI estimation accuracy
- Small resistors are difficult to build and, together with small inductors, can introduce added resistance if any loose connection exists. Care should be taken to accurately measure and handle such components.

- If such testing is to be repeated, use of switching relays to perform switching of impedances would simplify the test procedure significantly and allow for the lab operator to concentrate on other aspects of their work.

9. List of references

[1] V. D. Toro, *Electrical Engineering Fundamentals*, 2nd ed.: Prentice-Hall, 1986.

[2] M. Ciobotaru, R. Teodorescu, and F. Blaabjerg, "On-line grid impedance estimation based on harmonic injection for grid-connected PV inverter," in *2007 IEEE International Symposium on Industrial Electronics*, 2007, pp. 2437-2442.

[3] M. Ciobotaru, R. Teodorescu, P. Rodriguez, A. Timbus, and F. Blaabjerg, "Online grid impedance estimation for single-phase grid-connected systems using PQ variations," in *2007 IEEE Power Electronics Specialists Conference*, 2007, pp. 2306-2312.

[4] H. Zhou, X. Zhao, D. Shi, H. Zhao, and C. Jing, "Calculating sequence impedances of transmission line using PMU measurements," in *2015 IEEE Power & Energy Society General Meeting*, 2015, pp. 1-5.

[5] S. M. Abdelkader and D. J. Morrow, "Online Thevenin Equivalent Determination Considering System Side Changes and Measurement Errors," *IEEE Transactions on Power Systems,* vol. 30, pp. 2716-2725, 2015.

[6] S. Corsi and G. N. Taranto, "A Real-Time Voltage Instability Identification Algorithm Based on Local Phasor Measurements," *IEEE Transactions on Power Systems,* vol. 23, pp. 1271-1279, 2008.

[7] J. R. Massing, M. Stefanello, H. A. Gründling, and H. Pinheiro, "Adaptive current control for grid-connected converters with LCL-filter," in *2009 35th Annual Conference of IEEE Industrial Electronics*, 2009, pp. 166-172.

[8] F. Gubina and B. Strmcnik, "Voltage collapse proximity index determination using voltage phasors approach," *IEEE Transactions on Power Systems,* vol. 10, pp. 788-794, 1995.

[9] G. Verbic and F. Gubina, "A new concept of protection against voltage collapse based on local phasors," in *Power System Technology, 2000. Proceedings. PowerCon 2000. International Conference on*, 2000, pp. 965-970 vol.2.

[10] B. Milosevic and M. Begovic, "Voltage-stability protection and control using a wide-area network of phasor measurements," *IEEE Transactions on Power Systems,* vol. 18, pp. 121-127, 2003.

[11] M. H. Haque, "On-line monitoring of maximum permissible loading of a power system within voltage stability limits," *IEE Proceedings - Generation, Transmission and Distribution,* vol. 150, pp. 107-112, 2003.

[12] M. M. El-Kateb, S. Abdelkader, and M. S. Kandil, "Linear indicator for voltage collapse in power systems," *IEE Proceedings - Generation, Transmission and Distribution,* vol. 144, pp. 139-146, 1997.

[13] J. Zhang, M. Liu, Y. Yin, W. Lin, Q. Wang, L. Liu*, et al.*, "A transient voltage stability index based on critical equivalent impedance," in *2014 International Conference on Power System Technology*, 2014, pp. 25-29.

[14] J. Lavenius, L. Vanfretti, and G. N. Taranto, "Performance assessment of PMU-based estimation Methods of Thevenin Equivalents for real-time voltage stability monitoring," in *2015 IEEE 15th International Conference on Environment and Electrical Engineering (EEEIC)*, 2015, pp. 1977-1982.

[15] X. Wang, F. Blaabjerg, and P. C. Loh, "An impedance-based stability analysis method for paralleled voltage source converters," in *2014 International Power Electronics Conference (IPEC-Hiroshima 2014 - ECCE ASIA)*, 2014, pp. 1529-1535.

[16] M. N. Islam and W. Ongsakul, "Thevenin equivalent parameter tracking for on-line voltage stability assessment," in *2015 IEEE Innovative Smart Grid Technologies - Asia (ISGT ASIA)*, 2015, pp. 1-7.

[17] W. Xuran, H. Sun, B. Zhang, W. Wu, and G. Qinglai, "Real-time local voltage stability monitoring based on PMU and recursive least square method with variable forgetting factors," in *IEEE PES Innovative Smart Grid Technologies*, 2012, pp. 1-5.

[18] A. H. Al-Mohammed and M. A. Abido, "A Fully Adaptive PMU-Based Fault Location Algorithm for Series-Compensated Lines," *IEEE Transactions on Power Systems,* vol. 29, pp. 2129-2137, 2014.

[19] F. Chunju, D. Xiuhua, S. Li, and Y. Weiyong, "An Adaptive Fault Location Technique Based on PMU for Transmission Line," in *2007 IEEE Power Engineering Society General Meeting*, 2007, pp. 1-6.

[20] P. Yazdkhasti and C. P. Diduch, "An islanding detection method based on measuring impedance at the point of common coupling," in *2015 IEEE 28th Canadian Conference on Electrical and Computer Engineering (CCECE)*, 2015, pp. 57-62.

[21] N. Liu, A. Aljankawey, C. Diduch, L. Chang, and J. Su, "Passive Islanding Detection Approach Based on Tracking the Frequency-Dependent Impedance Change," *IEEE Transactions on Power Delivery,* vol. 30, pp. 2570-2580, 2015.

[22] N. Liu, C. Diduch, L. Chang, and J. Su, "A Reference Impedance-Based Passive Islanding Detection Method for Inverter-Based Distributed Generation System," *IEEE Journal of Emerging and Selected Topics in Power Electronics,* vol. 3, pp. 1205-1217, 2015.

[23] K. Jia, H. Wei, T. Bi, D. W. P. Thomas, and M. Sumner, "An Islanding Detection Method for Multi-DG Systems Based on High-Frequency Impedance Estimation," *IEEE Transactions on Sustainable Energy,* vol. 8, pp. 74-83, 2017.

[24] G. Shen, J. Zhang, X. Li, C. Du, and D. Xu, "Current control optimization for grid-tied inverters with grid impedance estimation," in *Applied Power Electronics Conference and Exposition (APEC), 2010 Twenty-Fifth Annual IEEE*, 2010, pp. 861-866.
[25] M. Liserre, F. Blaabjerg, and R. Teodorescu, "Grid Impedance Estimation via Excitation of LCL -Filter Resonance," *IEEE Transactions on Industry Applications,* vol. 43, pp. 1401-1407, 2007.
[26] M. A. Elgendy, D. J. Atkinson, M. Armstrong, and S. M. Gadoue, "Impact of grid background harmonics on inverter-based islanding detection algorithms," in *2015 IEEE 11th International Conference on Power Electronics and Drive Systems*, 2015, pp. 67-72.
[27] L. Asiminoaei, R. Teodorescu, F. Blaabjerg, and U. Borup, "A new method of on-line grid impedance estimation for PV inverter," in *Applied Power Electronics Conference and Exposition, 2004. APEC '04. Nineteenth Annual IEEE*, 2004, pp. 1527-1533 Vol.3.
[28] F. D. Mango, M. Liserre, and A. Dell'Aquila, "Overview of Anti-Islanding Algorithms for PV Systems. Part II: ActiveMethods," in *2006 12th International Power Electronics and Motion Control Conference*, 2006, pp. 1884-1889.
[29] W. Cai, B. Liu, S. Duan, and C. Zou, "An Islanding Detection Method Based on Dual-Frequency Harmonic Current Injection Under Grid Impedance Unbalanced Condition," *IEEE Transactions on Industrial Informatics,* vol. 9, pp. 1178-1187, 2013.
[30] Z. Shen, M. Jaksic, P. Mattavelli, D. Boroyevich, J. Verhulst, and M. Belkhayat, "Three-phase AC system impedance measurement unit (IMU) using chirp signal injection," in *Applied Power Electronics Conference and Exposition (APEC), 2013 Twenty-Eighth Annual IEEE*, 2013, pp. 2666-2673.
[31] B. Palethorpe, M. Sumner, and D. W. P. Thomas, "System impedance measurement for use with active filter control," in *Power Electronics and Variable Speed Drives, 2000. Eighth International Conference on (IEE Conf. Publ. No. 475)*, 2000, pp. 24-28.
[32] P. Garc, J. M. Guerrero, J. Garc, R. Navarro, and M. Sumner, "Low frequency signal injection for grid impedance estimation in three phase systems," in *2014 IEEE Energy Conversion Congress and Exposition (ECCE)*, 2014, pp. 1542-1549.
[33] M. Sumner, D. W. P. Thomas, and P. Zanchetta, "Power System Impedance Estimation for Improved Active Filter Control, using Continuous Wavelet Transforms," in *2005/2006 IEEE/PES Transmission and Distribution Conference and Exhibition*, 2006, pp. 653-658.
[34] Eskom. (2017, 10th February). *Palmiet Pumped Storage Scheme*. Available: http://www.eskom.co.za/Whatweredoing/ElectricityGeneration/PowerStations/Pages/Palmiet_Pumped_Storage_Scheme.aspx
[35] IEEE, "IEEE Recommended Practice for Electric Power Distribution for Industrial Plants," *IEEE Std 141-1993,* pp. 1-768, 1994.
[36] M. Rycroft. (2015, 10/03/17). Eskom's power transmission development plan. *Energize*. Available: http://www.ee.co.za/article/eskoms-power-transmission-development-plan.html
[37] Siemens. (2nd February 2017). *Planning of Electric Power Distribution - Technical Principles*. Available: http://w3.siemens.com/powerdistribution/global/EN/consultant-support/download-center/tabcardpages/Documents/Planning-Manuals/Planning_of_Electric_Power_Distribution_Technical_Principles.pdf
[38] X. Mou, W. Li, and Z. Li, "A preliminary study on the Thevenin equivalent impedance for power systems monitoring," in *Electric Utility Deregulation and Restructuring and Power Technologies (DRPT), 2011 4th International Conference on*, 2011, pp. 730-733.
[39] NER, "Electricity Supply Statistics for South Africa 2001," 2001.
[40] (2016, 30/08). *Frequency Response | National Grid* [Website]. Available: http://www2.nationalgrid.com/uk/services/balancing-services/frequency-response/
[41] NERSA, "NRS 048-2," ed, 2003.
[42] Enerdata. (2016, 10th February). *Global Energy Statistical Yearbook 2016 - Electricity domestic consumption*. Available: https://yearbook.enerdata.net/#electricity-domestic-consumption-data-by-region.html
[43] C. Reis, A. Andrade, and F. P. Maciel, "Voltage stability analysis of electrical power system," in *2009 International Conference on Power Engineering, Energy and Electrical Drives*, 2009, pp. 244-248.
[44] M. H. Bollen, *Integration of Distributed Generation in the Power System*: John Wiley & Sons, 2011.
[45] EIA. (2012, 10th February). *Primary Energy Consumption by Source and Sector, 2012*. Available: http://www.eia.gov/totalenergy/data/monthly/pdf/flow/primary_energy.pdf
[46] E. D. Research and Group, "Failure to act: The economic impact of current investment trends in electricity infrastructure," American Society of Civil Engineers, Washington, DC2011.
[47] I. Smon, G. Verbic, and F. Gubina, "Local voltage-stability index using tellegen's Theorem," in *Power Engineering Society General Meeting, 2007. IEEE*, 2007, pp. 1-1.

[48] M. Iftakhar, "Thevenin Equivalent Circuit Estimation and Application for Power System Monitoring and Protection," Master of Science in Electrical Engineering, Department of Electrical Engineering, University of Kentucky, 2008.
[49] A. Ghanem, M. Rashed, M. Sumner, M. A. El-sayes, and I. I. I. Mansy, "Grid impedance estimation for islanding detection and adaptive control of converters," in *8th IET International Conference on Power Electronics, Machines and Drives (PEMD 2016)*, 2016, pp. 1-6.
[50] R. Teodorescu, M. Liserre, and P. Rodriguez, *Grid Converters for Photovoltaic and Wind Power Systems*: Wiley, 2011.
[51] P. S. Georgilakis and N. D. Hatziargyriou, "Optimal Distributed Generation Placement in Power Distribution Networks: Models, Methods, and Future Research," *IEEE Transactions on Power Systems,* vol. 28, pp. 3420-3428, 2013.
[52] M. Sumner, B. Palethorpe, and D. W. P. Thomas, "Impedance measurement for improved power quality-Part 2: a new technique for stand-alone active shunt filter control," *IEEE Transactions on Power Delivery,* vol. 19, pp. 1457-1463, 2004.
[53] R. A. Walling and N. W. Miller, "Distributed generation islanding-implications on power system dynamic performance," in *IEEE Power Engineering Society Summer Meeting*, 2002, pp. 92-96 vol.1.
[54] N. Jenkins, J. Ekanayake, and G. Strbac, *Distributed Generation*: Institution of Engineering and Technology, 2010.
[55] IEEE Power Engineering Society, *Voltage Stability of Power Systems: Concepts, Analytical Tools, and Industry Experience*: IEEE, 1990.
[56] Z. Wang, H. Sun, and D. Nikovski, "Static voltage stability detection using local measurement for microgrids in a power distribution network," in *2015 54th IEEE Conference on Decision and Control (CDC)*, 2015, pp. 3254-3259.
[57] A. Woyte, K. De Brabandere, D. Van Dommelen, R. Belmans, and J. Nijs, "International harmonization of grid connection guidelines: adequate requirements for the prevention of unintentional islanding," *Progress in Photovoltaics: Research and Applications,* vol. 11, pp. 407-424, 2003.
[58] N. Hoffmann, F. W. Fuchs, and L. Asiminoaei, "Online grid-adaptive control and active-filter functionality of PWM-converters to mitigate voltage-unbalances and voltage-harmonics - a control concept based on grid-impedance measurement," in *2011 IEEE Energy Conversion Congress and Exposition*, 2011, pp. 3067-3074.
[59] J. A. Suul, S. D. Arco, P. Rodríguez, and M. Molinas, "Impedance-compensated grid synchronisation for extending the stability range of weak grids with voltage source converters," *IET Generation, Transmission & Distribution,* vol. 10, pp. 1315-1326, 2016.
[60] VDN, "Technische Regeln zur Beurteilung von Netzruckwirkungen (Technical Rules for System Peturbation Assessment)," ed. Frankfurt, 2007.
[61] C. T. G. R. Herman, G.S. Raubenheimer, "Negative Effects of Energy-Saving, Non-Linear Loads on LV Systems: Causes and Recommendations," *SAIEE Africa Research Journal,* vol. 99, 2008.
[62] M. Sumner, B. Palethorpe, and D. W. P. Thomas, "Impedance measurement for improved power quality-Part 1: the measurement technique," *IEEE Transactions on Power Delivery,* vol. 19, pp. 1442-1448, 2004.
[63] Y. He, K. w. Wang, and H. S. h. Chung, "Utilization of proportional filter capacitor voltage feedforward to realize active damping for digitally-controlled grid-tied inverter operating under wide grid impedance variation," in *2014 IEEE Energy Conversion Congress and Exposition (ECCE)*, 2014, pp. 4450-4457.
[64] M. J. B. Ghorbal, W. Ghzaiel, I. Slama-Belkhodja, and J. M. Guerrero, "Online detection and estimation of grid impedance variation for Distributed Power Generation," in *2012 16th IEEE Mediterranean Electrotechnical Conference*, 2012, pp. 555-560.
[65] B. Palethorpe, M. Sumner, and D. W. P. Thomas, "Power system impedance measurement using a power electronic converter," in *Ninth International Conference on Harmonics and Quality of Power. Proceedings (Cat. No.00EX441)*, 2000, pp. 208-213 vol.1.
[66] Y. Sun, C. Dai, and J. Li, "Thevenin equivalent circuit parameter estimation for the PCC upstream system," in *2015 5th International Conference on Electric Utility Deregulation and Restructuring and Power Technologies (DRPT)*, 2015, pp. 2299-2303.
[67] R. Rubesa, V. Kirincic, and S. Skok, "Transmission line positive sequence impedance estimation based on multiple scans of Phasor Measurements," in *Energy Conference (ENERGYCON), 2014 IEEE International*, 2014, pp. 644-651.
[68] CERTS. (2nd Februrary). *Phasor Advanced FAQ*. Available: http://www.phasor-rtdms.com/phaserconcepts/phasor_adv_faq.html
[69] S. M. Abdelkader and D. J. Morrow, "Online Tracking of Thevenin Equivalent Parameters Using PMU Measurements," *IEEE Transactions on Power Systems,* vol. 27, pp. 975-983, 2012.
[70] B. Alinejad and H. K. Karegar, "On-Line Thevenin Impedance Estimation based on PMU data and Phase Drift Correction," *IEEE Transactions on Smart Grid,* vol. PP, pp. 1-1, 2016.

[71] E. Electrical. (2005, 12/03/17). *Harmonic Distortion from Variable Frequency Drives*. Available: https://ewh.ieee.org/r3/nashville/events/2005/Harmonics_MCPQG_IEEE_2005.pdf
[72] J. H. Neher and M. H. McGrath, "The calculation of the temperature rise and load capability of cable systems," *Transactions of the American Institute of Electrical Engineers. Part III: Power Apparatus and Systems,* vol. 76, pp. 752-764, 1957.

10. Appendices

10.1 Appendix A: Resistor bank specifications (Testing stage 1)

The resistance of each resistor bank for every possible switching state is shown in Table 24. The resistance of leads (9 mΩ) used to connect the bridge to each bank was taken into consideration and subtracted from the measurements.

Table 24: Measurements of bank resistance states according to Yokogawa Wheatstone Bridge

Switch position		Resistance (mΩ) at 24°C			
S1	S2	RB_1	RB_2	RB_3	RB_4
ON	ON	52	44	46	50
OFF	ON	98	92	93	94
ON	OFF	102	94	95	98
OFF	OFF	145	141	142	141

Although each resistor in the banks is of the same length and material, there is considerable difference between the different banks in each switch position. This is due to the high sensitivity of the resistance to the nature of the connections used and impurity in the resistor material meaning that even small differences in geometry of connectors can have a significant effect on bank resistance.

10.2 Appendix B: Calculation of approximate resistance of local connection (Testing stage 1)

The local connection is defined as the physical 3-phase 4-wire cable connecting the inverter device to the DB in the Machines Lab. The resistance of each line (excluding resistor bank resistance) is roughly calculated below, based on measurements of cable lengths and cross section.

5.2 m of 6 mm^2 cable to patch panel[1]:

$$5.2\ m\ x\ 3.3\ m\Omega/m = 17.16\ m\Omega$$

8.5 m of 5 mm^2 cable to resistor banks:

$$Resistance\ of\ 5\ mm^2 = 3.3\ m\Omega/m\ x\ 6\ mm^2/5mm^2\ = 3.96\ m\Omega/m$$

$$8.5\ m\ x\ 3.96\ m\Omega/m\ = 33.66\ m\Omega$$

1 m of 5 mm^2 cable to inverter 1:

$$1.0\ m\ x\ 3.96\ m\Omega/m\ = 3.96\ m\Omega$$

Total per phase resistance of connection:

$$17.16\ m\Omega +\ 33.66\ m\Omega +\ 3.96\ m\Omega = 54.78\ m\Omega$$

[1] Taken from Page 19, Aberdare LV Cable Catalogue, **http://tinyurl.com/aberdare14**

10.3 Appendix C: $R_{th\,R} + R_{th\,n}$ for long sensing test (Testing stage 1)

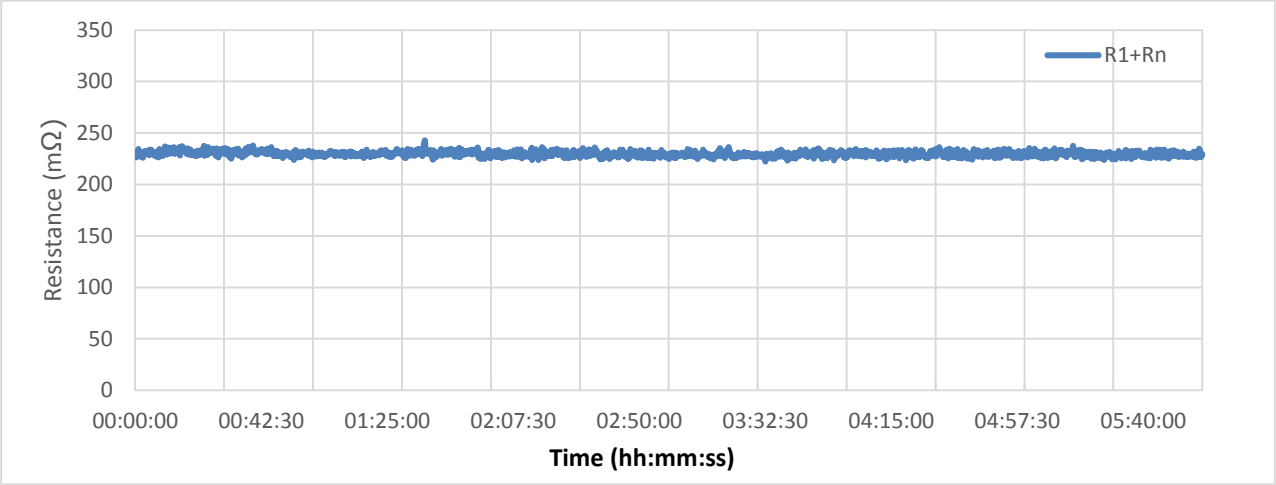

Figure 106: $R_{th\,R} + R_{th\,n}$ for long sensing test (Testing phase 1)

Standard deviation: 1.09 %

10.4 Appendix D: Changing phases test, additional graphs (Testing stage 1)

10.4.1 R_{th} of yellow on each port

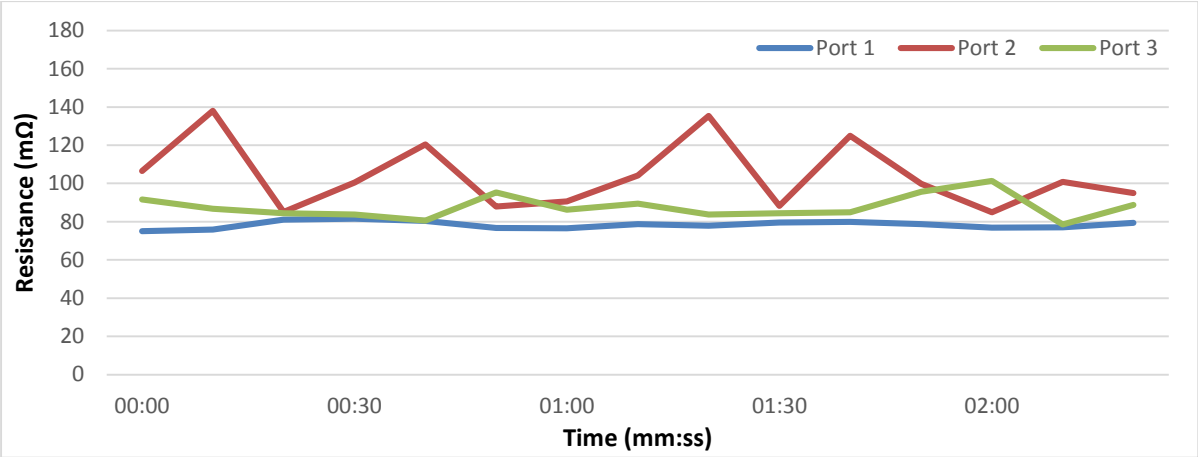

10.4.2 R_{th} of blue on each port

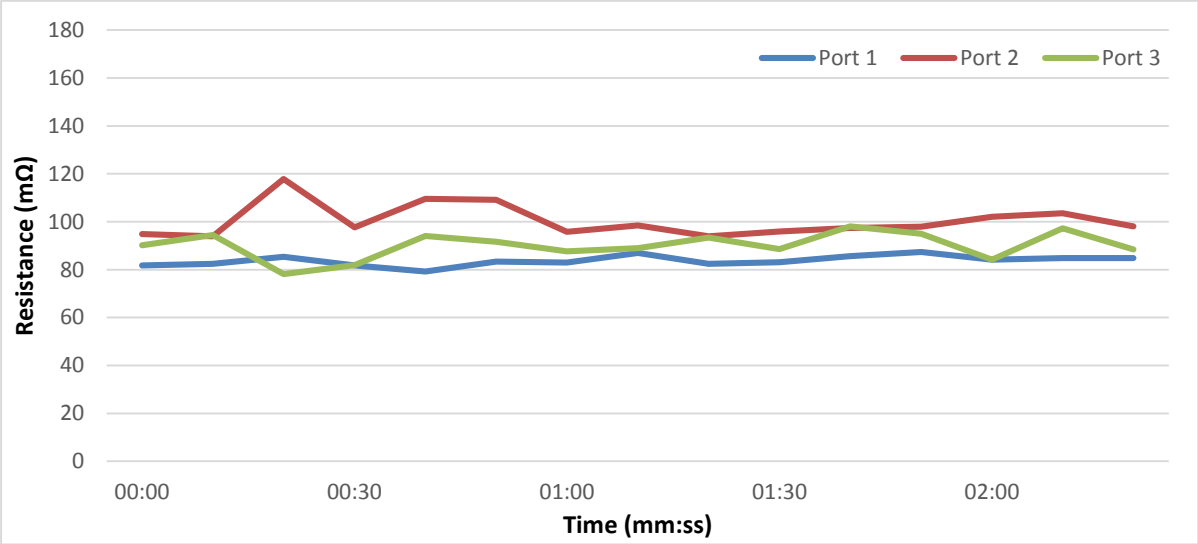

10.5 Appendix E: RMS Values and envelope frequencies for current (Testing stage 1)

10.5.1 Standard 12 A, 12.5 Hz waveform

Table 25: RMS Values and envelope frequencies for current (Testing Phase 1)

	RMS Current (A)			Envelope frequency (Hz)
	I1	I2	I3	
Requested:	12			12.5
Actual	14.0	14.8	14.6	12.5

10.6 Appendix F: Current statistics (Testing stage 1)

10.6.1 RMS currents, requested vs. actual, for Figure 55

Table 26: RMS currents, requested vs. actual, for Figure 55

RMS Currents (A)			
Requested (all phases)	Actual		
	I1	I2	I3
0	10.0	10.0	10.0
2	10.0	10.1	10.0
5	10.5	10.9	10.9
10	12.7	13.3	13.3
20	19.1	20.4	20.0

10.7 Appendix G: Temperature considerations

10.7.1 Phase 1: variation of injection test

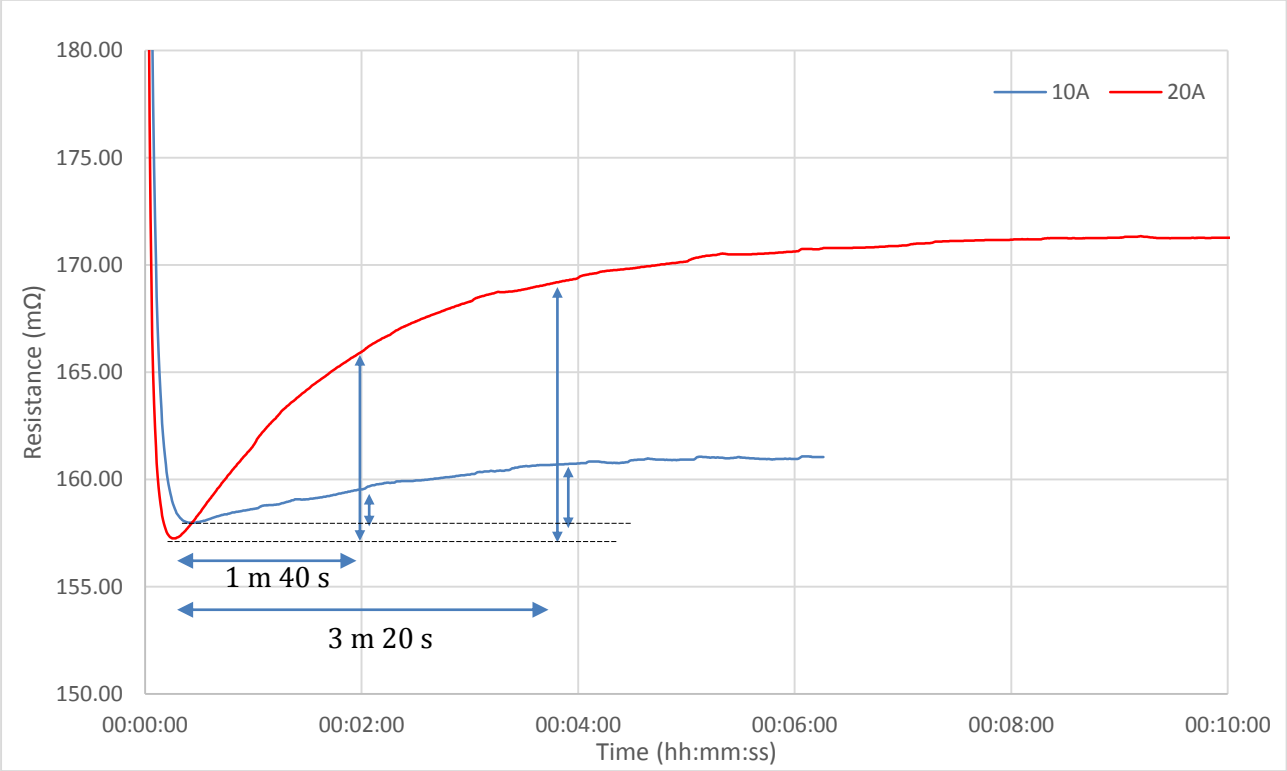

Figure 107: Resistance of B1 change for 10 A, 20 A. Arrows for case of Phase A

As seen in Figure 107, the up-step of 10 samples corresponds to 1 min 40 sec of heating, after which the resistors would have had an increase of less than 2 mΩ for 10 A and 9 mΩ for 20 A. However, in the resistance change measurement process, the average value of the level is taken. This means that the contribution to the resistance change calculation is more complex than single values. We have to average over the heating period to obtain the true increase in resistance that heating has added onto that measured. Averaging the resistance increase 10 A for 1 min 40 s gives 1 mΩ and 20 A gives 4 mΩ. Hence, the real resistance changes will be not more than 1 mΩ and 4 mΩ greater than the 23 °C values in each case. Another consideration must be made, which is the downward step. Since no experiments were done on the effect of cooling, we assume that after the down-step the cooling process will be the inverse of the heating process and that the same offsets will occur again, meaning that over 10 samples the resistance change will be almost the same as at 23°C as the heating contributions almost cancel out.

10.7.2 Phase 2: dynamic change test, variation of injection test

Here we use the same curve in Figure 107, except the duration has become 3 min 20 s (20 samples). Hence, the heating effect is more significant. In the case of 10 A, we have an average contribution (over 20 samples) of maximum 1 mΩ at 10 A and 8 mΩ at 20 A. However, we have more levels of current to consider, which we do not have individual heating tests for. From Figure 107, supported by theory (Fourier heat transfer equation/Neher-McGrath equation [72]), we see that the change in temperature is proportional to the square of the RMS current injected. Resistance is, in turn, proportional to change in temperature. This was verified by comparing the 10 A and 20 A graph, finding a ratio of 4.28 in resistance change compared to 4 in current squared. Hence, we simply apply a correction factor (CF) appropriately scaled according to this relationship. For example, for 18 A:

$$CF_{18} = \frac{(18)^2}{20^2}\ x\ CF_{20} = 8m\Omega\ x\ 0.81 = 6.48m\Omega$$

10.8 Appendix H: Resistor bank specifications (Testing stage 2)

In order to verify that the resistor banks' resistances have not changed since the previous testing stage, they are measured again. Unavailability of the Yokogawa Wheatstone Bridge used previously for resistance measurement necessitates a new method.

10.8.1 Signal generator + multimeters (SG+MMs) resistance measurement method

This method simply involves passing 10 A of DC current through each bank and measuring the DC voltage that results across them in each switching state. The diagram for this setup is shown in Figure 108.

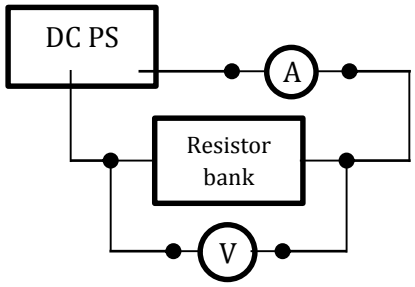

Figure 108: Diagram of SG+MMs resistance measurement method

10.8.2 Bank resistance at different switching states measured by two methods

Table 27 below shows measurements of resistor bank resistances according to:

a) Yokogawa wheatstone bridge method - taken in previous testing stage
b) Multimeter method – taken in this second testing stage

Table 27: Measurements of bank resistance states according to a) Yokogawa WB b) SG+MMs method

Switch position		Bank Resistance (mΩ) at 24°C								
S1	S2	Expected	RB_1		RB_2		RB_3		RB_4	
			Yoko.	SG+MMs	Yoko.	SG+MMs	Yoko.	SG+MMs	Yoko.	SG+MMs
ON	ON	50	52	60	44	54	46	55	50	58
OFF	ON	100	98	102	92	103	93	94	94	100
ON	OFF	100	102	105	94	104	95	106	98	106
OFF	OFF	150	145	153	141	155	142	146	141	147

10.8.3 Bank resistance changes measured by two methods

Table 28: Measured relevant bank resistance changes according to Table 27

Switching	Bank Resistance change (mΩ) at 24°C								
	Expected	RB_1		RB_2		RB_3		RB_4	
		Yoko.	SG+MMs	Yoko.	SG+MMs	Yoko.	SG+MMs	Yoko.	SG+MMs
Small change (ON,ON -> OFF,ON)	50	46	42	48	49	47	42	44	41

Large change (ON,ON -> OFF,OFF)	100	93	93	97	100	96	93	91	89

10.8.4 Comparison of results from different methods

From the tables in the previous section, it is clear that there is some discrepancy between measurements obtained by the two methods. Although this discrepancy is not very large, it deserves some attention due to the criticality of accurate measurements of the small change and large change.

The below statistics are of interest:

1. Average error between two resistance measurements – This is 4.08 %
2. Average error between two resistance change measurements – this is -1.74 %

The errors are measured based on the difference between two measurements divided by the average of the two measurements. Resistance measurement errors are all positive, meaning that the SG+MMs method seemingly overestimates resistance.
The errors were greatest at the lowest level of resistance measurement (50 mΩ expected).
The overestimate in the SG+MMs method was found to be predictable, having an average of 7.56 and a low standard deviation of 3.3. It is unfathomable that an added 7.56 mΩ of resistance has been added to the banks in any way, hence it must be a measurement error.

The final decision was made that the average be taken of the corrected results from Yokogawa and SG+MMs methods and this value used as the comparison value throughout the data analysis.

10.8.5 Correcting for error

Correcting for the error described earlier by simply subtracting 7.56 mΩ from all relevant measurements brings the error between measurements down to 0.5 %. The error between change measurements, however, does not change.

10.9 Appendix I: Inductor bank specifications (Testing stage 2)

Each inductor bank is made up of two inductors whose ratings are:

ACCORDING TO PROVIDED LITERATURE
Rated peak current: 50 A
Rated DC current: 40 A
Turns: 14
Strands: 18
Wire diameter each: 1.03 mm (of which 0.2 mm insulation)
Total wire area: 14.94 mm^2
Inductance: 0.109 mH
Resistance: 3 mΩ

ACCORDING TO MEASUREMENT AND CALCULATION

Wire diameter each: 1.07 mm (of which 0.2 mm insulation)
Turns: Unknown
Strands: 19
L1 = 33 mm
L2 = 82 mm
Total length: 33x2 + 82x2 = 230 mm
Resistance of 1 m copper at 1 mm^2 = 17 mΩ
Calculated resistance: 14 x 0.23 m x 17 mΩ x 1/(0.87 x 19) = 3.3 mΩ
Measured resistance: 5 mΩ[1] (not entirely accurate)
Impedance according to T48: 0.101 mH

10.10 Appendix J: Additional voltage statistics (Testing stage 2)

Table 29: Complete voltage statistics over 5 min period, before and during injection

	Mean		Min		Max		Std. Dev.	
	Before	During	Before	During	Before	During	Before	During
AC RMS (V)								
Red	244.4	244.3	243.8	242.5	244.9	245.9	0.18	0.60
Yellow	245.0	245.3	244.3	243.3	245.7	247.1	0.28	0.80
Blue	242.5	242.8	241.9	241.4	243.2	244.3	0.25	0.60
Frequency (Hz)								
Red	50.054	50.004	49.90	49.89	50.18	50.13	0.066	0.045
Yellow	50.053	50.005	49.90	49.89	50.18	50.15	0.066	0.050
Blue	50.054	50.004	49.90	49.89	50.19	50.13	0.066	0.046
Phase (°)								
Red->Yellow	119.6	119.8	119.0	118.9	120.2	120.4	0.22	0.22
Yellow->Blue	120.4	119.6	119.8	119.6	121.1	121.1	0.23	0.25
Blue->Red	120.0	119.4	119.5	119.4	120.5	120.7	0.19	0.20

[1] Obtained by SG + MM method (Appendix X) applied to each inductor. The average is shown

10.11 Appendix K: Spike removal process (Testing stage 2)

10.11.1 Process

Find number of data points that are more than 10% greater/smaller than average level over the relevant period. If the percentage of data points that fit that criterion was smaller than 10%, then they can be considered sufficiently uncommon 'spikes' that they can be removed. Data points more than 20% greater/smaller than the average were also removed, given they were also of less than 10% incidence rate.

10.11.2 Example

Figure 109 below shows the graph of the $R_{th\ R}$ parameter taken from one of the tests in section 6.14. The spikes to be removed according to the process described above are indicated by the arrows in the graph.

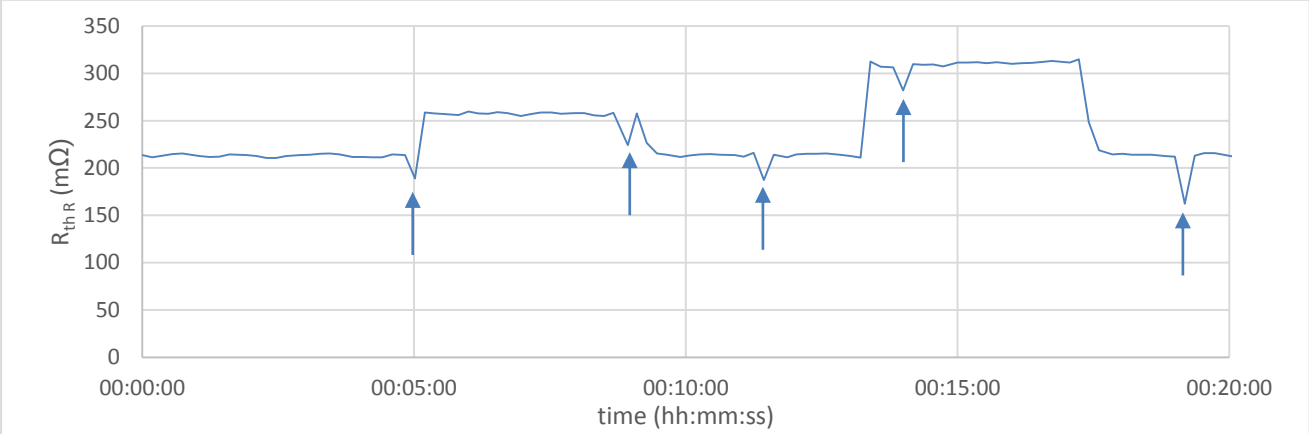

Figure 109: $R_{th\ R}$ during 12 A, 12 Hz resistance change test - arrows show unwanted spikes to be removed

10.12 Appendix L: Changing phases informed by long sensing test

Taking the long sensing test data, we produce a 10 min 10 s (61 pt) moving average, which represents our changing phase test result. Then the difference between two points in this moving average (two hypothetical tests) separated by 30 min in time is taken for all possible points. The maximum absolute difference is recorded for each parameter and it is expected that the contribution to skewing of the changing phases averages will not be greater than this maximum difference.

These maximum differences are shown for all relevant parameters below. The average difference is also shown.

Table 30: Average and max absolute difference between 10 min average separated by 30 min

	$Z_{th\ R}$	$Z_{th\ Y}$	$Z_{th\ B}$	$Z_{th\ n}$	$R_{th\ R}$	$R_{th\ Y}$	$R_{th\ B}$	$R_{th\ n}$	$X_{th\ R}$	$X_{th\ Y}$	$X_{th\ B}$	$X_{th\ n}$
AVERAGE	0.04	-0.11	-0.29	0.19	0.11	-0.06	-0.29	0.03	-0.06	-0.08	-0.09	0.26
Abs Max	3.73	4.98	2.67	3.67	3.6	4.13	2.3	3.6	2.7	3.1	2.5	2.9

10.13 Appendix M: Moving averages of Z_{th} parameters from stage 1 long sensing test

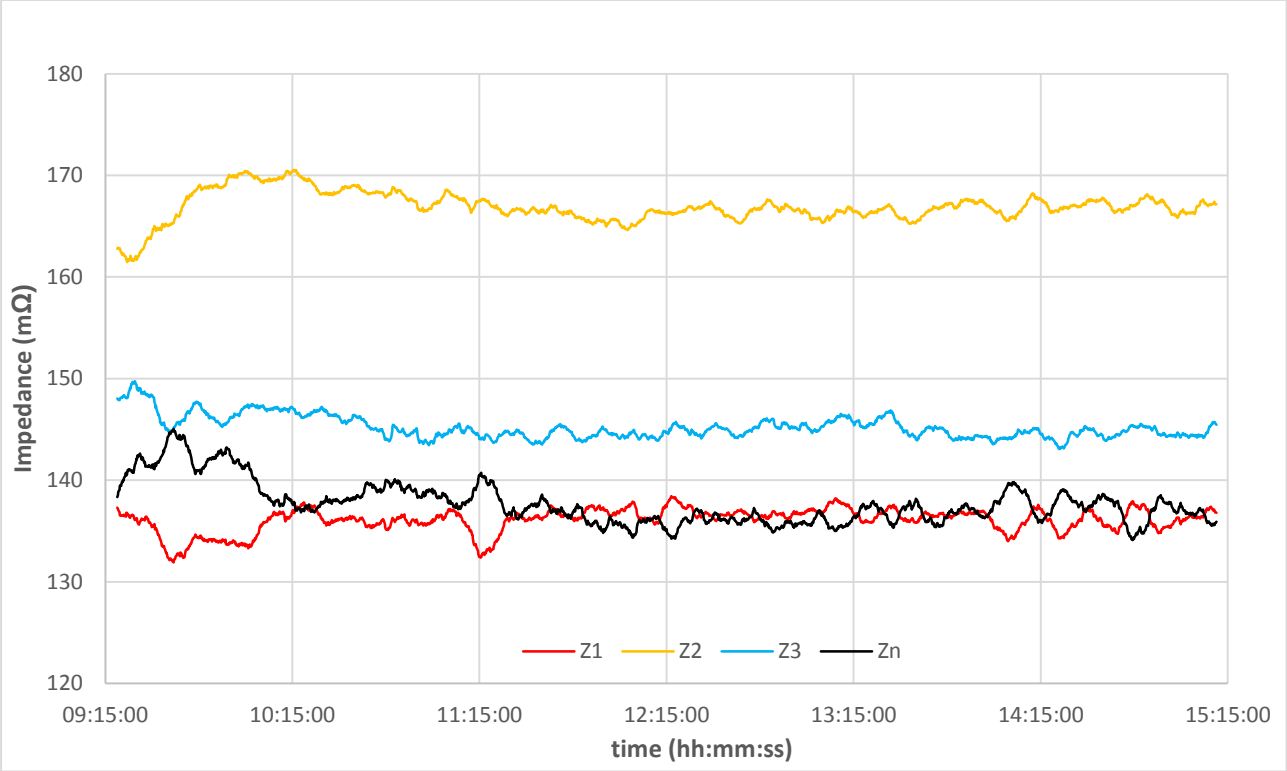

Figure 110: 8 min moving average of long sensing test data – testing phase 1

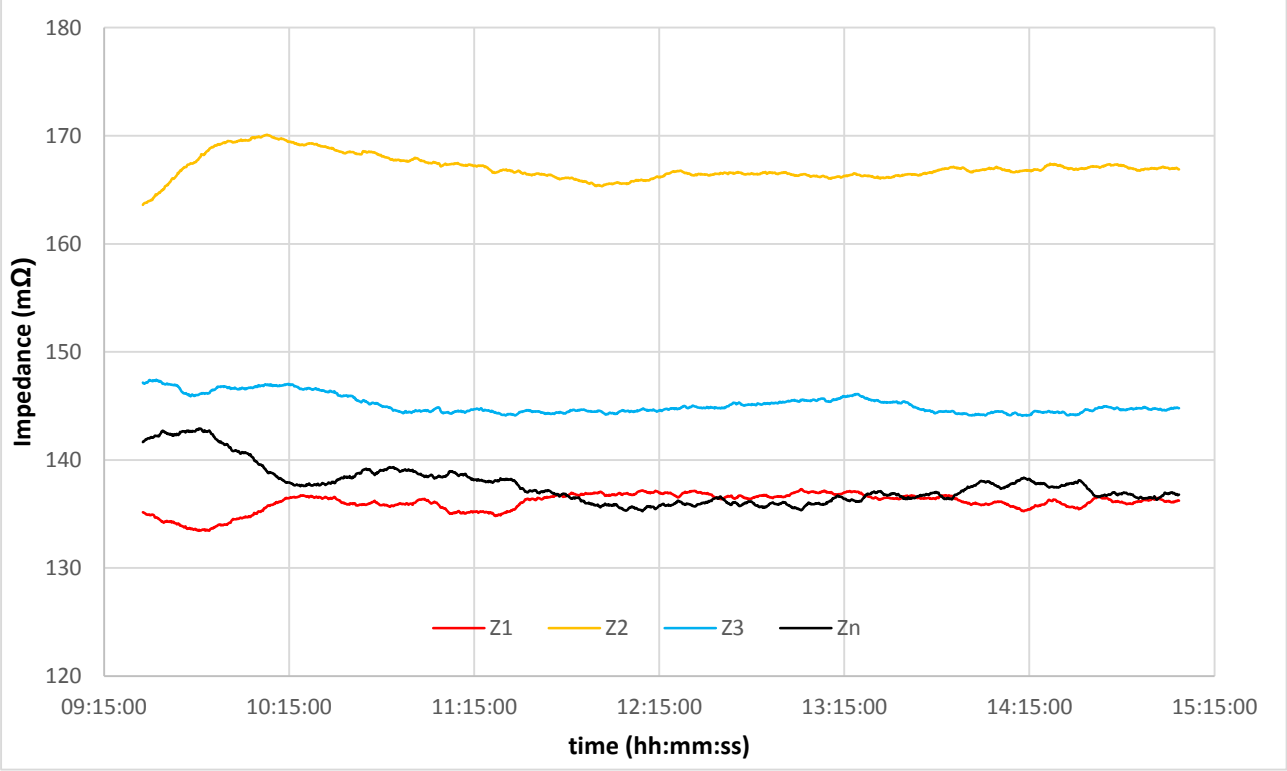

Figure 111: 25 min moving average of long sensing test data – testing phase 1